



HAL
open science

The role of Huntington protein in two models of stem cells : The Glioblastoma and the stem cells of the sub-ventricular zone

Rayane Kassem

► **To cite this version:**

Rayane Kassem. The role of Huntington protein in two models of stem cells : The Glioblastoma and the stem cells of the sub-ventricular zone. *Neurons and Cognition [q-bio.NC]*. Université Grenoble Alpes [2020-..], 2023. English. NNT : 2023GRALV101 . tel-04559355

HAL Id: tel-04559355

<https://theses.hal.science/tel-04559355>

Submitted on 25 Apr 2024

HAL is a multi-disciplinary open access archive for the deposit and dissemination of scientific research documents, whether they are published or not. The documents may come from teaching and research institutions in France or abroad, or from public or private research centers.

L'archive ouverte pluridisciplinaire **HAL**, est destinée au dépôt et à la diffusion de documents scientifiques de niveau recherche, publiés ou non, émanant des établissements d'enseignement et de recherche français ou étrangers, des laboratoires publics ou privés.

THÈSE

Pour obtenir le grade de

DOCTEUR DE L'UNIVERSITÉ GRENOBLE ALPES

École doctorale : CSV- Chimie et Sciences du Vivant

Spécialité : Neurosciences - Neurobiologie

Unité de recherche : Grenoble Institut des Neurosciences

Le rôle de la protéine Huntingtin dans deux modèles de cellules souches: Les glioblastomes et les cellules souches de la zone sous-ventriculaire

The role of Huntington protein in two models of stem cells: The Glioblastoma and the stem cells of the sub-ventricular zone

Présentée par :

Rayane KASSEM

Direction de thèse :

Sandrine HUMBERT

Professeure, Université de Grenoble Alpes

Directrice de thèse

Fabienne AGASSE

Maîtresse de conférences, Université Grenoble Alpes

Co-directrice de thèse

Rapporteurs :

Emmanuelle HUILLARD

CHARGÉE DE RECHERCHE HDR, CNRS délégation Paris Centre

Jean-Phillipe HUGNOT

PROFESSEUR DES UNIVERSITÉS, Université de Montpellier

Thèse soutenue publiquement le **16 novembre 2023**, devant le jury composé de :

Catherine GHEZZI,

PROFESSEURE DES UNIVERSITÉS, Université grenoble alpes

Présidente

Sandrine HUMBERT,

DIRECTRICE DE RECHERCHE, INSERM délégation Auvergne-Rhône-Alpes

Directrice de thèse

Fabienne AGASSE,

MAITRESSE DE CONFÉRENCES HDR, Université grenoble alpes

Co-directrice de thèse

Emmanuelle HUILLARD,

CHARGÉE DE RECHERCHE HDR, CNRS délégation Paris Centre

Rapporteuse

Jean-Phillipe HUGNOT,

PROFESSEUR DES UNIVERSITÉS, Université de Montpellier

Rapporteur

Ahmed IDBAIH,

PROFESSEUR DES UNIVERSITÉS - PRATICIEN HOSPITALIER, Sorbonne Université

Examinateur

Valérie CORONAS,

PROFESSEURE DES UNIVERSITÉS, Université de Poitiers

Examinatrice



الحمد لله حتى يبلغ الحمد مُنتهاه



DEDICATION

In the depths of my heart, I dedicate the culmination of countless hours, sleepless nights, and unwavering determination in my thesis to the brave souls battling the relentless adversary, glioblastoma. Throughout this journey, each face, every story etched in my memory, has shone a light on the importance of finding better treatments, seeking potential cures, and pushing the boundaries of medical science.

To the glioblastoma fighters, you are the true heroes of this work. Your resilience and tenacity in the face of adversity inspire me beyond measure. your faces were never far from my thoughts.

To the families who stand by your loved ones, your unwavering support and love are a testament to the power of human connection. Your presence, your sacrifices, and your hope have motivated me to strive for breakthroughs that can bring relief and comfort to those who matter most to you. In every breakthrough, I see the faces of your dear ones, and my determination is further kindled.

To the caregivers, your selfless dedication and tireless efforts have not gone unnoticed. The burden you bear, the sacrifices you make, and the love you shower upon your patients are the cornerstones of the strength. As I delve into the complexities of this disease, I am acutely aware of the vital role you play in the lives of those you care for.

Your faces, your stories gave my research meaning and purpose. As I reach for new discoveries and potential breakthroughs, I do so with the hope that my efforts may contribute, even in the smallest way, to easing the burden and improving the lives of you.

With every word, every chart, and every conclusion, I pour my heart into this work, knowing that it is all dedicated to you.

Together, we fight, and together, we hope for a brighter future.

REMERCIEMENT

Sandrine, thank you for being a mother for the team before being a director, your belief in my abilities gave me the courage to push beyond my limits and explore new horizons, I am forever grateful.

Fabienne, you have played an indelible role in shaping this moment, and I stand humbled by the profound impact you've had on my life and my work. Thank you for always being there when I need you. I owe so much of my growth and success to you. As I reach the end of this journey, my heart overflows with gratitude and emotions that words can barely express.

To my colleagues, you have been more than just colleagues; you have become my second family. The camaraderie, the shared struggles, and the triumphs we celebrated together have made these years memorable and meaningful. Your collaborative spirit and support have been instrumental in my achievements. Sophie, you'll always be my best Wiki. Thank you for the unconditional love you gave. Camille and Lethy, thank you for being my partners in crime. Toff, thanks for the support and the coffee breaks we had all along this journey. Leslie, thank you for the support and motivation you gave me. Eric, thank you for the "Bonne nuit and n'oublie pas de rentrer chez toi" you said to me. To all of you, your constant encouragement has been a source of strength throughout this endeavor. I cherish the bonds we share and the memories we've created together.

To my Favorite person, my Papitto, you are the epitome of resilience, wisdom, and unconditional love. Your unwavering belief in my potential has given me the confidence to pursue my passions fearlessly. Your guidance and encouragement have been a beacon of hope in times of doubt.

To my Queen, my Mamitto, you have been my pillar of strength, my source of comfort, and my guiding light. Your boundless love and selflessness have been a constant source of inspiration that encourage me to build my dreams.

To my Guiding Backbone sister, through life's ups and downs, you've stood by my side, offering an assurance that no matter what, we would face it together. We've shared laughter, tears, and a bond that time and distance could never break. I want you to know that you've played an integral role in shaping the person I am today and have inspired me to be a better person and to never give up on my dreams. In you, I have found a sister, a friend, and a soulmate. Thank you for being the constant source of love, laughter, and joy in my life. I am forever grateful for your love and for the precious bond we share.

To my Brothers, thank you for always standing by my side, your love, support, and unwavering presence have been the anchor that kept me grounded through life's storms

To my Beloved Fiancé, you are my rock, my anchor, and my constant source of love and support. With you by my side, I know I can conquer any challenge that comes my way.

To my Nieces and Nephews, you bring immeasurable joy and light into my life. Your innocent laughter and boundless energy remind me of the beauty and wonder in the world. You

are the reason I strive to make a difference and leave a positive impact on the world. I want you to know that I carry your love and values with me in every step I take.

To my best friends, Yara and Farah, you have been my confidants, my partners in crime, and my rocks in times of need. I treasure the bond we share and the memories we've created together.

To all of you, my family, thank you for providing me with a safe haven, a place where I could grow, learn, and flourish. Thank you for the love, support, and the greatest gift you gave me, the gift of a loving family. Thank you for the moments we've shared, the laughter we've echoed, and the love that binds us together, **forever and always**.

With boundless love and gratitude, Rayane.

FOREWORD

Sandrine Humbert's team, where I conducted my doctoral research, explores how the mutant form of the protein huntingtin (HTT) affects the biology of neural stem cells. The team showed that mutant HTT impairs several steps of cortical brain development such as proliferation of neuroepithelial stem cells, neuroprogenitor polarization, axonal growth and synaptogenesis. In the adult mouse brain where neural stem cells reside, mutant HTT diminishes also neurogenesis by decreasing the maintenance of subventricular zone (SVZ) stem cells. Regarding its role in neural stem cells and considering recent evidences showing that glioblastoma may originate from deregulated SVZ cells, I asked whether wild-type HTT might be involved in glioblastoma stem cells (GSC) biology and notably in their ability to resist to anticancer treatments.

Conventional therapeutic approaches have generally proven inadequate in effectively treating glioblastoma multiforme (GBM). The alkylating agent temozolomide (TMZ) remains the most potent anticancer drug to date, significantly increasing the median survival of patients. However, the development of resistance to TMZ, and notably the expression of the enzyme *O*⁶-methylguanine-DNA methyltransferase (*MGMT*) by tumor cells, poses a significant challenge. Here, I tested whether decreasing HTT levels in GSC would sensitize them to TMZ. I used antisense oligonucleotides (ASO) to target HTT mRNA and showed that decreasing HTT protein levels sensitizes glioma cell lines to TMZ as lower concentrations of TMZ exacerbates DNA damage and cell death. The same results were obtained when treating highly resistant patient-derived GSC that express *MGMT*. In Nude mice injected with human GSC, co-treatment with the ASO and TMZ was able to reduce brain tumor growth. An *in vivo* survival assay is currently ongoing. This work represents the main part of my thesis (**Part I**) and will be submitted for publication by the end of the year.

During the first year of my PhD, I studied the role of HTT in the progression through the neural stem cells lineage of the subventricular zone cells and found that HTT is a key intrinsic regulator of the quiescent and activated stem cell states. I showed that HTT downregulation is necessary to promote the transition from the activated stem cell state to the progenitor state.

Preliminary experiments showed that HTT is degraded at the progenitor stage. Moreover, in HD SVZ cells, HTT is maintained at the progenitor stage. I also showed that differentiation of HD SVZ cells is directed towards the glial fate at the expense of the neuronal fate. Further work has to be done to determine how downregulation of HTT at the progenitor stage affects differentiation. This work is presented in (**Part II**).

In parallel to the first and second research projects, I had the pleasure of collaborating with other members of my team, notably Mariacristina CAPIZZI, on a project focused on the role of NUMA1 in the microtubule and axonal growth. For instance, suppressing NUMA1 in wild-type cells recapitulates the microtubule and axonal growth defects of HD, whereas raising NUMA1 levels restores microtubule organization and rescues axonal growth (Capizzi et al., 2022). In a second collaboration, this time with Monia BARNAT, I worked on embryonic development defects in a murine model of MH and contributed to demonstrating that these defects are present in the brains of human fetuses carrying the mutation (Barnat et al., 2020). These studies are published and I added the manuscripts in (**Part III**).

ABSTRACT

Glioblastoma multiforme (GBM) is a deadly brain tumor with limited treatment options. The alkylating agent temozolomide (TMZ) significantly increases the median survival of patients. However, tumor cells develop resistance to TMZ. In this study, we explored a novel therapeutic approach to sensitize cells to TMZ. Huntingtin (HTT), which mutated form causes Huntington disease, is a prosurvival protein widely expressed by neurons. HTT is also expressed in glioblastoma. We downregulated the huntingtin (HTT) protein using an antisense oligonucleotide (ASO) that directs the HTT mRNA for RNase degradation. We treated ASO-transduced glioma cell lines with TMZ and found that HTT-depletion exacerbates TMZ-induced DNA double-strand breaks, poly(ADP-ribose) polymerase 1 (PARP1) cleavage, cell cycle arrest in G2 and eventually cell death by apoptosis. ASO-mediated HTT downregulation also sensitizes patient-derived glioma stem cells (GSCs) that express the DNA repair enzyme O6-methylguanine-DNA methyltransferase (MGMT). Moreover, HTT-downregulation decreases stem cell properties namely expression of the proneural stem cell marker DLL3 and self-renewal. *In vivo*, in immunocompromised mice injected subcortically with MGMT expressing GSCs, a single intracerebroventricular administration of ASO followed by oral TMZ treatment delayed significantly proliferation, expression of DLL3 and tumor growth as compared to mice receiving a scramble oligonucleotide. The ASO-mediated HTT downregulation strategy to sensitize GSCs to TMZ holds promise for the treatment of glioblastoma.

Keywords: glioma stem cells, temozolomide, glioblastoma, huntingtin, antisense oligonucleotide, MGMT.

RESUME

Les glioblastomes sont des tumeurs cérébrales létales pour lesquelles les options thérapeutiques sont limitées. L'agent alkylant témozolomide (TMZ) augmente significativement la durée de vie des patients. Cependant, les tumeurs deviennent résistantes au traitement anticancéreux. Dans cette étude nous proposons une nouvelle approche consistant à sensibiliser les cellules cancéreuses au TMZ. La huntingtine (HTT) est une protéine connue pour causer la maladie de Huntington lorsqu'elle est mutée. C'est une protéine impliquée dans la survie des neurones. HTT est exprimée par les cellules de gliomes. Nous avons diminué les niveaux protéiques de HTT en traitant des lignées cellulaires de gliomes avec un oligonucléotide antisens (ASO) ciblant l'ARNm de la HTT ce qui induit sa dégradation par la RNase H1. La diminution des niveaux de HTT exacerbe les effets toxiques du TMZ, augmentant les cassures double-brins de l'ADN, le clivage de la poly(ADP-ribose) polymérase 1 (PARP-1), l'arrêt du cycle en G2 et la mort cellulaire par apoptose. La diminution des niveaux de HTT par traitement à l'ASO sensibilise également des cellules souches de gliome (GSCs) issues d'un patient et exprimant l'enzyme méthylguanine méthyltransférase, une enzyme de réparation de l'ADN. De plus, la diminution des niveaux de HTT diminue les capacités d'autorenouvellement des GSCs et l'expression du marqueur de cellules souches proneurales DLL3. *In vivo*, des souris immunodéficientes ont été greffées avec ces GSCs en sous-cortical pour former des tumeurs et l'injection d'ASO dans le ventricule latéral suivi du traitement oral avec du TMZ retarde significativement la pousse tumorale comparé à des souris traitées avec un oligonucléotide contrôle (non dirigé contre un ARNm). Ce ralentissement tumoral est associé à une diminution de la prolifération des cellules tumorales ainsi qu'à la perte d'expression du marqueur DLL3.

L'utilisation d'ASO pour diminuer la HTT sensibilise les tumeurs au TMZ et semble une stratégie prometteuse dans la lutte contre les glioblastomes.

Mots-clefs : cellules souches de gliome, témozolomide, glioblastome, huntingtine, oligonucléotide antisens, MGMT.

ABBREVIATIONS

2-cET -	2'-O-(2-carboxyethyl)
2-MOE -	2'-O-methoxyethyl
2-OMe -	2'-O-methyl
5-ALA -	5-Aminolevulinic acid
5-MeG -	5-Methylcytosine
Gy -	Gray (unit of ionizing radiation dose)
ABC transporter	ATP-binding cassette transporter
ABCG2 -	ATP-binding cassette subfamily G member 2
APE1 -	Apurinic/aprimidinic endonuclease 1
AKT -	Protein kinase B
ALDH1 -	Aldehyde dehydrogenase 1
AMP -	Adenosine monophosphate
APC -	Adenomatous polyposis coli
ATM -	Ataxia telangiectasia mutated
ATXN3 -	Ataxin-3
ATRX -	Alpha-thalassemia/mental retardation syndrome X-linked
ASOs -	Antisense oligonucleotides
BCRP1 -	Breast cancer resistance protein 1
BCNU -	Carmustine
BER -	Base excision repair
BMP4 -	Bone morphogenetic protein 4
BDNF -	Brain-derived neurotrophic factor
BBB -	Blood-brain barrier
BLBP -	Brain lipid-binding protein
CA3 -	Cornu Ammonis 3 (region of the hippocampus)
CAG -	Cytosine-adenine-guanine (repeat sequence)
CBP -	CREB-binding protein
CCNU -	Lomustine
CD133 -	Cluster of Differentiation 133
CD44 -	Cluster of Differentiation 44
CD80 -	Cluster of Differentiation 80
CD86 -	Cluster of Differentiation 86
CDK -	Cyclin-dependent kinase
CNS -	Central nervous system
CREB -	cAMP response element-binding protein
CT -	Computed tomography
CTC -	Circulating tumor cell
DCVax -	Dendritic cell vaccine
DED -	Death effector domain
DES -	Diethylstilbestrol
DG -	Dentate gyrus
DMR1 -	Differentiation of Multiple Organs and Tissues Overlapping Transcript 1
DNA -	Deoxyribonucleic acid
DSBs -	Double-strand breaks
DTI -	Diffusion tensor imaging
EGFR -	Epidermal growth factor receptor
EGF -	Epidermal growth factor
ENTH -	Epsin N-terminal homology
EphB2 -	Ephrin type-B receptor 2

FEN1 -	Flap endonuclease 1
FGFR-2 -	Fibroblast growth factor receptor 2
FLAIR -	Fluid-attenuated inversion recovery
FOXO3A -	Forkhead box O3A
GFAP -	Glial fibrillary acidic protein
GCSs -	Glioblastoma stem cells
GBM	Glioblastoma
GLAST -	Glutamate aspartate transporter
HER2 -	Human epidermal growth factor receptor 2
HIP1 -	Huntingtin-interacting protein 1
HGF -	Hepatocyte growth factor
HIF2 -	Hypoxia-inducible factor 2
HTT -	Huntingtin gene
IGF-1 -	Insulin-like growth factor 1
IKK -	IκB kinase
IL6 -	Interleukin 6
IL10 -	Interleukin 10
JHD -	Juvenile Huntington's disease
LC3A/B -	Microtubule-associated proteins 1A/1B light chain 3A/3B
LC3B -	Microtubule-associated protein 1A/1B light chain 3B
LOH -	Loss of heterozygosity
MAPK -	Mitogen-activated protein kinase
MDM2 -	Mouse double minute 2 homolog
MGMT -	O6-methylguanine-DNA methyltransferase
MLH1 -	MutL homolog 1
mTORC2 -	Mammalian target of rapamycin complex 2
MSH2 -	MutS homolog 2
MSH6 -	MutS homolog 6
MSN -	Medium spiny neuron
MRI -	Magnetic resonance imaging
MTIC -	5-(3-methyl-1-triazeno) imidazole-4-carboxamide
mHTT -	Mutant huntingtin
N17a -	N-terminal fragment of huntingtin exon 1
NADPH -	Nicotinamide adenine dinucleotide phosphate
NF1 -	Neurofibromin 1
NfκB -	Nuclear factor kappa-light-chain-enhancer of activated B cells
NOD-SCID -	Non-obese diabetic/severe combined immunodeficiency
NOTCH -	Notch receptor
NSCs -	Neural stem cells
O6Me -	O6-methylguanine
OLIG2 -	Oligodendrocyte transcription factor 2
PAR3 -	Partitioning defective 3
PARP1 -	Poly(ADP-ribose) polymerase 1
PDGFRA -	Platelet-derived growth factor receptor alpha
PEST -	Proline (P), glutamic acid (E), serine (S), and threonine (T) rich
PIP3 -	Phosphatidylinositol-3,4,5-trisphosphate
PKC -	Protein kinase C
p62 -	Sequestosome-1
PRD -	Proline-rich domain
PTEN -	Phosphatase and tensin homolog
RAS -	Rat sarcoma
ROS -	Reactive oxygen species
Rb -	Retinoblastoma

RNA -	Ribonucleic acid
RTK -	Receptor tyrosine kinase
S100 -	S100 calcium-binding protein
SDMT -	Symbol Digit Modalities Test
SH2 domain -	Src homology 2 domain
SH3 domain -	Src homology 3 domain
SOX2 -	SRY-box transcription factor 2
STAT3 -	Signal transducer and activator of transcription 3
SVZ -	Subventricular zone
TCGA -	The Cancer Genome Atlas
TERT -	Telomerase reverse transcriptase
TMZ -	Temozolomide
TNF -	Tumor necrosis factor
TOP2A -	DNA topoisomerase 2-alpha
TP53 -	Tumor protein 53
TRC102 -	Methoxyamine
TrKB -	Tropomyosin receptor kinase B
VEGF -	Vascular endothelial growth factor
WHO -	World Health Organization
WT -	Wild type
XRCC1 -	X-ray repair cross-complementing protein 1
ZnT3 -	Zinc transporter 3
Zo-1 -	Zonula occludens-1

TABLE OF CONTENT

DEDICATION _____	3
REMERCIEMENT _____	4
FOREWORD _____	6
ABSTRACT _____	8
RESUME _____	9
ABREVIATIONS _____	10
TABLE OF CONTENT _____	13
INTRODUCTION _____	18
CHAPTER.1 The GLIOBLASTOMA MULTIFORM _____	18
1.Generalities _____	18
1.1-Epidemiology.....	18
1.2-Etiology of GBM and risk factors.....	18
1.3-Symptoms and diagnosis.....	19
2-Classification of GBM _____	20
2.1-Historical facts.....	20
2.2-WHO classification of gliomas.....	21
2.2.1-Primary GBMs.....	22
2.2.2-Secondary GBMs.....	23
2.3-Other mutations.....	26
2.3.1-PDGFR α amplification.....	26
2.3.2-Mutations or deletion of the Ras antagonist <i>NF1</i>	26
2.3.3-1p/19q co-deletion.....	26
2.3.4-Homozygous deletion of CDKN2 (cyclin-dependent kinase inhibitor 2) A and B (CDKN2A/B).	26
2.3.5-O6-Methylguanine-DNA Methyltransferase (MGMT) expression.....	27
3- Glioma cancer stem cells _____	27
3.1-Tumor growth relies on GCSs.....	27
3.2-Markers of stem cells.....	28
3.3-Molecular Classification.....	30
4-Are tumor originating from deregulated NSCs? _____	31
4.1-NSCs and neurogenesis in the adult brain.....	32
4.2-Transformation.....	34

5- Treatment	36
5.1- Surgical Resection	36
5.2- Radiotherapy	37
5.3- Temozolomide	38
5.4- Other chemotherapies	40
6- Resistance to anticancer therapies	41
6.1-Tumor microenvironment	41
6.2- Mechanisms of resistance to radiotherapy	42
6.3- Mechanisms of resistance to TMZ	43
6.3.1- TMZ concentration in the deep brain parenchyma	43
6.3.2- O6-Methylguanine-DNA Methyltransferase (MGMT) expression	43
6.3.3-MMR deficiency	44
6.3.4- BER proficiency	45
CHAPTER 2. THE HUNTINGTIN PROTEIN	46
1.Huntington's Disease (HD)	46
1.1-Introduction to HD	46
1.2-HD symptoms	47
1.3- Neurobiological characteristics	49
2-Huntingtin Protein	51
2.1-Structure of HTT	51
2.2-Diversity of HTT proteins: variants, isoforms, oligomers and post-translational modifications	53
2.2.1-Shorter forms of HTT	53
2.2.2- HTT oligomers	54
2.2.3- post-translational modifications	54
2.3-HTT interactions	55
2.4-HTT and membrane trafficking	55
2.5-HTT and autophagy	56
2.6-HTT and vesicular transport	56
2.7-HTT and Development	57
Does abnormal brain development contribute to disease onset?	59
2.8-HTT and DNA Damage Response	59
2.9-HTT and Apoptosis	60
2.10-HTT and Cancer	61
CHAPTER 3. THE ANTISENSE OLIGONUCLEOTIDES	63
1-Generalities	63
2-Chemistry	63
2.1-Backbone modifications	63
2.2-Stereochemistry	65

2.3-2'Ribose substitution	66
2.4-Other modifications	67
3.Mode of action	67
3.1-Degradation of a target RNA	68
3.2-Splice-switching ASOs	68
3.3-Other mechanisms of action.....	71
4.Delivery	71
5.Cellular uptake.....	73
6.ASO in HD	73
6.1-Tominersen	73
6.1.1-Description.....	73
6.1.2-Preclinical data.....	74
6.1.3-Clinical Trials.....	74
6.1.4-Stereopure ASOs.....	75
7.ASO in cancer.....	76
4- THESIS OBJECTIVES	78
I. Are glioma/glioblastoma cells lines more sensitive to TMZ when depleted of HTT?	79
II. How does downregulation of HTT induce cell death?.....	79
III. Is the MGMT status relevant to sensitization by HTT depletion?.....	79
.....	81
PART I	81
ABSTRACT	83
Highlights	83
INTRODUCTION	84
MATERIAL AND METHODS	86
RESULTS	94
FIGURES	100
DISCUSSION AND PERSPECTIVES	111
I-Significance of RG6042 in Downregulating HTT and Sensitizing GBM Cells to TMZ.	112
II-HTT Downregulation Reduces MGMT Protein and mRNA Levels.	118
III-HTT Depletion's Impact on Glioma Stem Cells and Proliferation.	121
IV-The Role of HTT in Stem Cell Proliferation and Implications in Glioma.....	122
V-Promising Potential of RG6042 and TMZ Co-Treatment for GBM.....	123
.....	125
PART II	125
INTRODUCTION	127
MATERIALS AND METHODS	129
RESULTS	134

Establishment of a differentiation protocol.....	134
Expression of stem cells and progenitors' markers along the lineage.....	134
Expression of HTT varies along WT and Q111 SVZ lineage.....	135
HTT protein is degraded at the progenitor stage.	135
HUWE1 is expressed in SVZ WT progenitor cells.....	136
mHTT reduces neuronal differentiation	136
DISCUSSION _____	136
FIGURES	140
_____	145
PART III _____	145

INTRODUCTION

INTRODUCTION

CHAPTER.1 The GLIOBLASTOMA MULTIFORM

1.Generalities

1.1-Epidemiology

Glioblastoma (GBM) are tumors from glial origin and is considered a grade IV glioma based on the WHO classification (Louis et al., 2016). GBM is the most common and most aggressive brain tumor with an average annual incidence of 3.23 per 100 000 persons in the United States (Miller et al., 2021). In 2018 in France, 3481 patients were newly diagnosed for GBM (Defossez et al., 2021). While the average annual age-adjusted incidence rate of primary malignant brain and other CNS tumors was 7.08 per 100 000, GBM accounts for half of all malignant brain tumors (Miller et al., 2021; Ostrom et al., 2020). GBM is uncommon in children and affects people age 45 to 75 with a median age at diagnosis of 64 (Tamimi and Juweid, 2017). The incidence of GBM is 1.6 times higher in men than women (Colopi et al., 2023). Extracranial metastases of GBM are rare due to the fast-growing nature of the tumor and the short overall survival.

To date, there is no effective treatment to cure GBM. The standard of care consists of maximal resection of the tumor followed by radiotherapy. Concomitant and adjuvant chemoradiotherapy with temozolomide (TMZ) increases the median survival by 2.5 months that reaches 15 months after diagnosis ((Stupp et al., 2005). Despite treatments, the five-year survival rate is of only 7.2% and the disease remains 100 % lethal (Ostrom et al., 2020).

1.2-Etiology of GBM and risk factors

Most of the GBM occurs sporadically and their origin remains elusive. There is no evidence supporting environmental causes for developing glioma with the exception of exposure to ionizing radiation due to prior radiotherapy during childhood (Braganza et al., 2012).

There is an ongoing debate on whether cell phone use can increase the risks of developing brain tumors. A recent study led in UK on more than 700 000 women followed-up for 14 years concluded that there was no association between cell phone use and brain tumors (Schüz et al., 2022).

An aggregation of cases of gliomas was reported several years ago in the Isère department in France, in a small village of 1600 inhabitants. Seven cases of brain tumors including glioblastomas were reported between 2002 and 2016, which is 7 times more than expected. Nevertheless, the inquiry failed to elucidate a cause and attributed this aggregation of cases to the random distribution of the disease in a small population.

Regarding genetic factors, a higher risk of GBM was found in patients with hereditary tumor syndromes, such as Li-Fraumeni and Turcot syndromes. The Li-Fraumeni syndrome is a hereditary genetic condition caused by germline mutations in the tumor suppressor gene TP53 that predispose patients to the development of cancer and notably to low grade and high grade gliomas (Orr et al., 2020). Turcot syndrome is characterized by the formation of multiple benign growths (polyps) in the colon that occur in association with a primary brain tumor. This is an extremely rare disease with only 150 cases reported worldwide. Turcot syndrome is due to mutations in DNA mismatch repair genes such as MLH1 and PMS2 or in the tumor suppressor gene APC (“adenomatous polyposis coli”). Other inherited familial tumor syndromes that increase the risk for malignant gliomas include germline mutation of the tumor suppressor gene NF1 encoding for neurofibromin, a GTPase activating protein that inactivates Ras proteins (Reuss and von Deimling, 2009).

Interestingly, the incidence of glioma is reduced in patients suffering from asthma, allergies and atopic diseases probably because of the exacerbation of immune surveillance mechanisms (Tamimi and Juweid, 2017).

1.3-Symptoms and diagnosis

GBMs are commonly located in the supratentorial regions of the brain: namely the frontal, temporal, parietal and occipital lobes, and rarely in the cerebellum and brainstem. According to GBM localization, symptoms include headache, alterations in mental status, speech and language difficulties, gait alteration, sensory abnormalities and seizures (Tamimi and Juweid, 2017).

Magnetic resonance imaging (MRI) is the modality of choice for diagnosis and is also used to plan the surgery and assess the treatment response. T2-weighted, fluid attenuated inversion

recovery (FLAIR) and pre- and post-gadolinium T1-weighted MRI exams capture detailed images of the tumors and associated features such as tumor volume, peritumoral edema, necrosis, degree of enhancement, and presence of cysts. MRI provides better pictures of soft tissue organs than X-rays-based computerized tomography (CT). However, as MRI is contraindicated for patients with a pacemaker or an implantable cardiac defibrillator, CT scan is prescribed alternatively to these patients. Advanced MRI techniques provide more detailed information about the tumor, which is essential to make an informed decision about tumor management. As an example, diffusion tensor imaging (DTI) uses anisotropic diffusion to reconstruct the white matter tracts in the peritumoral regions, enabling surgeons to assess tumor infiltration (Bernstock et al., 2022). When removed, the tumor tissue is sent to histopathology for histological diagnosis.

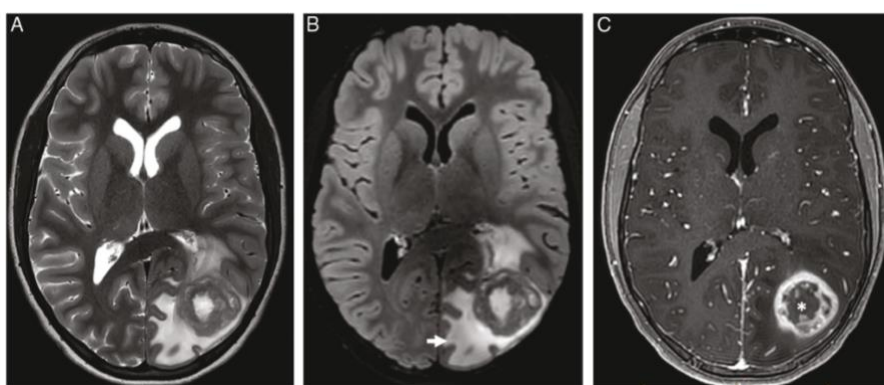


Figure.1| Typical imaging findings of glioblastoma in a 12-year-old male patient. In the axial T2-weighted(A) and fluid-attenuated inversion recovery (FLAIR) images (B), there is a tumor located in the left occipital lobe that appears as a heterogeneous T2 hyperintense area. Additionally, there is noticeable peritumoral edema surrounding the tumor (indicated by an arrow). On the axial post-contrast T1-weighted image, the tumor exhibits a characteristic heterogeneous rim enhancement. Furthermore, the color-coded fractional anisotropy image shows disruption of the brain structure at the necrotic core of the tumor (C). *Adapted from (Bernstock 2022).*

2-Classification of GBM

2.1-Historical facts

The first recorded reports of non-metastatic primary central nervous system (CNS) tumors were reported by Berns in 1800 and by Abernety in 1804. Their reports were based on autopsy materials and gross morphological observations lacking information about the origin of the cells and their structural features. They defined tumors as being infiltrate malignant cells growing in the CNS, distinctly different from healthy tissues (Scherer, 1940). In 1865, Rudolf Virchow gave the

first description of a glioma based on its cellular organization: it is a tumor from glial origin, which organization contrasts with the healthy surrounding tissue. He noticed differences at the histological levels between tumors and therefore proposed the first classification into groups based on the cellularity and general contrast when compared to normal brain tissue. The two distinct groups correspond to low-grade gliomas (LGGs, Grade I and II) and high-grade gliomas (HGGs, grade III and IV) as defined now in the WHO classification.

Later, Percival Bailey and Harvey Cushing introduced the base of modern glioma classification based on histological observations. Bailey and Cushing introduced the term « Spongioblastoma multiforme » to the most malignant glioma tumor. Multiform refers to the polymorphic appearance of the tumor within the same tissue sample. Bailey discovered tumors originating from astrocytic glia termed astrocytoma according to their microscopic similarities with astrocytes. After, spongioblastoma term was replaced by glioblastoma (GBM).

In the 30s, the German pathologist Hans-Joachim Scherer proposed a diagnosis based on the histopathological observations of the whole tumor sample rather than individual cells and conclude that GBM and astrocytoma share the same precursor origin cell and that astrocytoma can progress to GBM along the course of the disease. These secondary GBM arising from previous astrocytoma share similar histomorphological features with *de novo* primary GBM however, they respond differently upon clinical treatments. Primary GBM are more aggressive than secondary GBM.

In 20th century, the immunohistochemistry technique was introduced and GBM tumors were characterized as being positive for glial markers such as S100, GFAP and Vimentin. Later, the introduction of genetic studies and progress in DNA sequencing refined the classification according to the presence of key mutations (Stoyanov and Dzhenkov, 2018). Nowadays, the World Health Organization (WHO) proposes a classification based on histopathological features of the tumor, the cell of origin and genetic mutations and epigenetic alterations.

2.2-WHO classification of gliomas

There are two main groups of gliomas: the diffuse and the non-diffuse ones. Non-diffuse glioma has a more circumscribed growth pattern, pilocytic astrocytomas and ependymal tumors being the most frequent representatives. Diffuse gliomas extensively infiltrate the healthy CNS parenchyma and therefore are difficult to treat. Diffuse gliomas are the most frequent and comprise astrocytomas, glioblastomas, oligodendrogliomas and oligoastrocytomas (Figure 2).

According to the mitotic pattern of the tumor, the presence of necrosis and neovascularization, a grade ranging from I to IV is assigned. The grading correlates with aggressiveness, with LGG (grades II and I) being less aggressive as compared to HGG such as anaplastic astrocytomas (grade III) and glioblastoma (grade IV).

Primary and secondary GBM previously characterized by Scherer based on histological observations are distinguishable genetically according to their isocitrate dehydrogenase (IDH) status: primary tumors are IDH wild type whereas secondary GBM are mutated for this enzyme (Louis et al., 2016).

2.2.1-Primary GBMs

Primary GBM develops *de novo* in patients at the median age of 62 years old and represent 90% of the GBMs. These tumors are highly necrotic and are very aggressive as the median overall survival time with the Stupp protocol is about 15 months. Among the mutations (Table 1) that characterized these tumors:

- **TERT:** alterations in the promoter region of the *telomerase reverse transcriptase (TERT)* gene occur predominantly in *IDH* wild-type glioblastoma (70% of cases). TERT are nucleoprotein complexes located at the end of chromosomes and are required to repair and maintain telomere length in cycling cells, avoiding replicative senescence or cell death. Mutations at locations upstream the translation start site result in the upregulation of *TERT* gene expression (Meyerson et al., 1997).
- **EGFR:** the epidermal growth factor receptor (EGFR) is a tyrosine kinase receptor belonging to the ERBB family of receptors. Once activated by EGF binding, two receptors dimerize and their intracellular domains auto-phosphorylate at tyrosine residues that serve as docking sites for adaptor proteins with SH2 domains. These adaptor proteins activate pro-proliferative and pro-survival pathways such as the Ras/MAPK kinases and the phosphoinositide 3-kinase (PI3K)-AKT pathways. In primary GBM, exacerbated proliferation is associated with the amplification of the EGFR gene or the expression of an oncogenic receptor with constitutive activity (35% of cases). The oncogenic receptor EGFRvIII is caused by an in-frame exons 2-7 deletion, resulting in a receptor with a lack of cysteine rich region in N-terminal. Thus, EGFR is continuously activated in a ligand-fixation

independent manner promoting GBM cell growth and tumorigenesis (Guo et al., 2015). EGFRvIII expression is frequently enhanced in GBM due to its promoter demethylation (Del Vecchio et al., 2013). In addition, it was shown that the co-expression of EGFR WT and EGFRvIII promotes oncogenicity. In fact, activated EGFR WT phosphorylates EGFRvIII triggering nuclear transport of EGFRvIII that binds and phosphorylates STAT3, which drives transformation (Fan et al., 2013). Despite exacerbating proliferation, EGFR amplification does not correlate with poor outcomes (Quan et al., 2005),(Hsu et al., 2022).

- **PTEN:** loss of the tumor suppressor gene “phosphatase and tensin homologue” (PTEN) results from the deletion or mutation of the 10q23 locus and is found in 37% of cases. PTEN is a phosphatase that regulates the PI3K-AKT pathway associated with cell survival. PTEN removes the phosphate from the phospholipid second messenger phosphatidylinositol-3,4,5-trisphosphate (PIP3) impeding the activation of the pro-survival serine/threonine kinase AKT. When PTEN is lost, apoptotic pathways are inhibited. Loss of PTEN is associated with poor prognosis in glioma patients (Han et al., 2016).

2.2.2-Secondary GBMs

Secondary GBM arise in younger patients at the median age of 44 years old and represent 10% of the GBMs. They develop from previous tumors such as anaplastic or diffuse astrocytoma. Secondary GBMs are found in equal proportion between males and females while primary GBM are more frequent in males. Necrosis is limited in these tumors. The prognosis is better as compared to primary GBMs as the median overall survival time with the Stupp protocol reaches 31 months. Among the mutations (Table 1) that characterized these tumors:

	IDH-wildtype glioblastoma	IDH-mutant glioblastoma
Synonym	Primary glioblastoma, IDH-wildtype	Secondary glioblastoma, IDH-mutant
Precursor lesion	Not identifiable; develops de novo	Diffuse astrocytoma Anaplastic astrocytoma
Proportion of glioblastomas	~90%	~10%
Median age at diagnosis	~62 years	~44 years
Male-to-female ratio	1.42:1	1.05:1
Mean length of clinical history	4 months	15 months
Median overall survival		
Surgery + radiotherapy	9.9 months	24 months
Surgery + radiotherapy + chemotherapy	15 months	31 months
Location	Supratentorial	Preferentially frontal
Necrosis	Extensive	Limited
<i>TERT</i> promoter mutations	72%	26%
<i>TP53</i> mutations	27%	81%
<i>ATRX</i> mutations	Exceptional	71%
<i>EGFR</i> amplification	35%	Exceptional
<i>PTEN</i> mutations	24%	Exceptional

Table 1 | Key characteristics of IDH-wildtype and IDH-mutant glioblastomas. Adapted from (Louis et al 2016).

- IDH:** the enzyme isocitrate dehydrogenase (IDH) is key enzyme of the Krebs cycle that catalyzes the oxidative decarboxylation of isocitrate, resulting in α -ketoglutarate, carbon dioxide and NADPH release. Point mutations in *IDH1* (R132) and *IDH2* (R172) results in the loss of the IDH native enzymatic activity and gain of alternative enzymatic activity producing the oncometabolite D-2-hydroxyglutarate from α -ketoglutarate. NADPH is consumed during the reaction, which increases the oxidative burden of the cell that may potentiate the cytotoxicity of Stupp treatment. D-2-hydroxyglutarate is a competitive inhibitor of α -ketoglutarate -dependent enzymes such as DNA and histone demethylases. This inhibition modifies the epigenetic status of histones and DNA, resulting in increased levels of DNA and histone methylations. IDH-mutant gliomas exhibit a cytosine-phosphate-guanine (CpG) island methylator phenotype (G-CIMP) characterized by a genome-wide hypermethylation induced directly by mutant IDH1 (Turcan et al., 2012). The two mutated isoforms are found in secondary GBM but also in grade II astrocytoma and grade III oligodendrogliomas. IDH-mutant GBMs respond better to therapy with longer survival as compared to IDH wild-type patients (SongTao et al., 2012).
- ATRX:** loss-of-function mutations of the genes coding for the histone chaperone alpha thalassemia/mental retardation syndrome X-linked (ATRX) or for the cofactor death-

domain associated protein (DAXX) have been found to be mutually exclusive with TERT promoter mutations. In these cells, lengthening of the telomeres during replication is independent of telomerase activity and rely on hyperactive homologous recombination. It has been shown that loss of ATRX or DAXX activates the alternative lengthening of telomeres (ALT) mechanisms in cancer cell (Li et al., 2019).

- TP53:** TP53 deficiency invariably co-occurs with mutations in *ATRX* and *IDH1/2*. The *TP53* gene encode the p53 protein that plays a critical role in cellular responses to DNA damage. Activation of p53 triggers cell cycle arrest to allow for DNA repair or directs cellular senescence or apoptosis. Mutations in the p53 pathway are found in 80% of cases of secondary GBMs. P53 is a tumor suppressor and its inactivation in GBM (mutation, homozygous depletion, 35% of cases) promotes tumor formation by enabling damaged cells to survive and grow. Overexpression (gene amplification) of the MDM2 oncoprotein, an E3 ubiquitin ligase promoting p53 proteasomal degradation, is found 14% of the GBM (Cancer Genome Atlas Research Network, 2008),(Phillips et al., 2013).

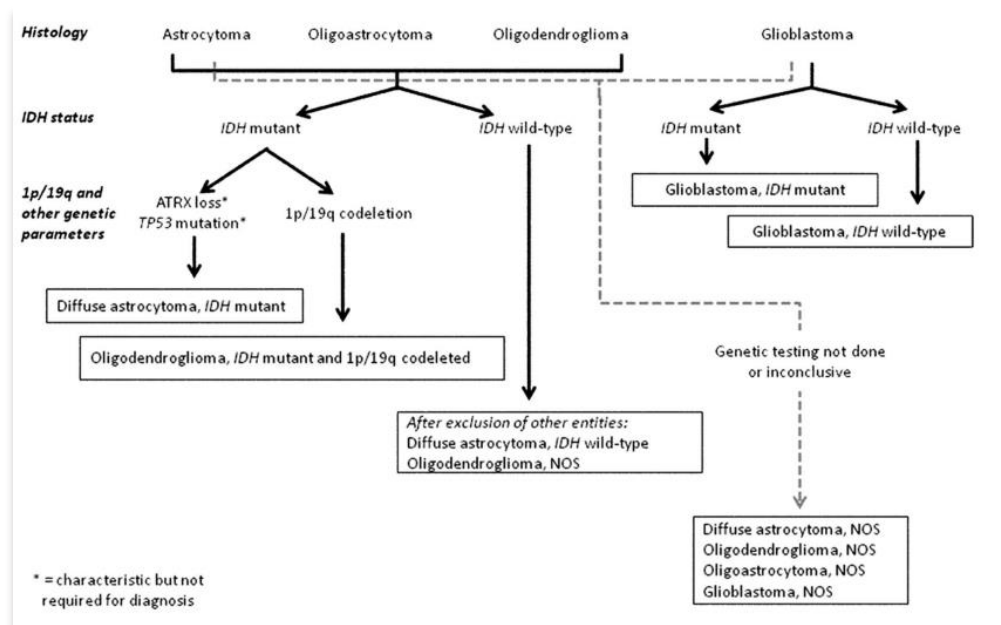


Figure.2 | A simplified algorithm for classification of the diffuse gliomas based on histological and genetic features, adapted from (Louis et al 2016).

2.3-Other mutations

2.3.1-PDGFR A amplification

Platelet-derived growth factor receptor A (PDGFR A) is the second most frequently mutated tyrosine kinase receptor following EGFR in GBM. The PDGFR A gene is amplified in 10% of GBM. In the CNS, activation of PDGFR A by PDGF induces the proliferation of oligodendrocyte precursors. PDGFR A amplification is associated with worse overall survival in IDH-mut GBM (Phillips et al., 2013).

2.3.2-Mutations or deletion of the Ras antagonist *NF1*

The Neurofibromatosis type 1 (*NF1*) gene encodes the neurofibromin 1 protein. Neurofibromin 1 transduces signals from receptor tyrosine kinases to the Ras-MAPK pathway. Neurofibromin 1 possesses a GTPase-activating domain related domain that promotes the hydrolysis of active Ras-GTP to the biologically inactive form of Ras-GDP. Neurofibromin 1 negatively regulates the Ras/MAPK pathway. *NF1* is mutated in approximately 13–14% of GBM patients. When *NF1* is mutated, Ras is hyperactivated (Scheer et al., 2021)(Eckel-Passow et al., 2015)

2.3.3-1p/19q co-deletion

Loss of heterozygosity (LOH) due to partial or total deletion of the p and q arms of chromosomes 1 and 19 respectively is mostly found in of low-grade oligodendroglioma, anaplastic astrocytoma, anaplastic oligodendrogliomas and in secondary GBM (or IDH mutant grade 4 astrocytoma). Patients with this co-deletion have a better favorable outcome with longer survival when treated. 1p/19q co-deletion is frequently associated with TERT and IDH1 mutations (Eckel-Passow et al., 2015).

2.3.4-Homozygous deletion of CDKN2 (cyclin-dependent kinase inhibitor 2) A and B (*CDKN2A/B*).

CDKN2A/B homozygous deletion is a strong adverse prognostic factor. It is found in about 45% of primary GBM and 20% of secondary GBM (Hsu et al., 2022; Huang, 2022; Ohgaki and Kleihues, 2013). The *CDKN2A/B* genes are located on chromosome 9p21 locus and encode for the

tumor-suppressor proteins p14(ARF), p16(INK4A) and p15(INK4B). P15 and p16 are cyclin-dependent kinase (CDK) inhibitors, which form a complex with CDK4 or CDK6, limiting their activating interaction with the CDK cyclin D1. Progression through the G1 phase of the cell cycle is therefore stopped as CDK4/cyclin D1 or CDK6/cyclin D1 cannot phosphorylate the retinoblastoma protein RB that sequesters the transcription factor E2F. p14(ARF) triggers p53-mediated cell-cycle arrest or apoptosis by inactivating MDM2 (mouse double minute 2), an E3 ubiquitin-protein ligase targeting p53 for degradation.

2.3.5-O6-Methylguanine-DNA Methyltransferase (MGMT) expression

The expression of MGMT will be treated in a following chapter (5-3.2)

3- Glioma cancer stem cells

3.1-Tumor growth relies on GCSs

Malignant solid tumors are heterogeneous neoplasms composed of different types of cells in different states of incomplete differentiation. It was proposed that any differentiated cells of the adult brain that undergo oncogenic transformation could de-differentiate, proliferate unrestrictedly and become tumorigenic. In line with this stochastic model, within a tumor, any given cells would be capable of initiating tumor growth and recreating the cellular heterogeneity of the original tumor. This hypothesis was challenged by observations that not all cells of the tumor mass can reinitiate a tumor when grafted in immunodeficient mice. Historically, Bonnet and Dick found that only a subpopulation of acute myeloid leukemia cells (as few as 0.2% in one patient) purified from a human patient sample were able to transfer the disease to NOD-SCID mice (Bonnet and Dick, 1997). Therefore, tumor initiation and growth rely on a subpopulation of cells endowed with stem cells capacities: cells capable of proliferating, self-renewing and giving rise to pseudo-differentiated cells constituting the heterogeneous population of the tumor mass. In accordance with this hierarchical cancer stem cell model, glioma cancer stem cells (GSCs) i) are able to reinitiate a tumor after sequential transplantations in immunodeficient mice (Galli et al., 2004) and ii) transplantation of as few as 10 GSCs is sufficient to generate a tumor (Richichi et al., 2016).

Glioma stem cells (GSCs) have been originally isolated from tumor biopsies using the functional sphere-forming assay. Culture methods used to culture neural stem cells from the

mouse subventricular zone (SVZ) were applied to tumor biopsies (Galli et al., 2004; Singh et al., 2004; Vescovi et al., 2006; Yuan et al., 2004). Neural stem cells are grown in culture in free-floating: after mechanic and enzymatic dissociation of freshly dissected SVZ explants, SVZ cells are cultured in serum-free medium completed with epidermal growth factor (EGF) and basic fibroblast growth factor (FGF-2). SVZ neural stem cells were originally cultured using this protocol in the seminal work of Reynolds and Weiss in 1992 (Reynolds and Weiss, 1992). Four to 6 days later, the clonal proliferation of stem cells generates free-floating neurospheres containing both progenitors endowed with a limited proliferation capacity, and stem cells with an unlimited capacity to self-renew. To assess self-renewal, spheres are dissociated and single cells are re-plated in the same conditions: capacity to regenerate neurospheres is indicative of self-renewal (Weiss et al., 1996). A clonal sphere derived from a neural stem cell give rise to neurons, astrocytes and oligodendrocytes when adhered and upon growth factor withdrawal as a neural stem cell is multipotent. The differentiated cell progeny of neural stem cells is therefore postmitotic cells. In contrast, the progeny of GSCs never terminally differentiate and can reenter the cell cycle. Caren and collaborators differentiated GSCs by long-term exposure to BMP4. This treatment decreased cell proliferation and stem cells expression of *OLIG2* and *EGFR* genes while differentiating cells in GFAP astrocytes and O4 oligodendrocytes. However, when re-exposed to EGF and FGF2, astrocytes and oligodendrocytes re-entered the cell cycle indicating that were not driven to a terminally differentiated cell-cycle arrested state by BMP4 treatment. Moreover, despite long-term BMP4 treatment, the cells were able to initiate tumors when orthotopically grafted in immunodeficient mice. This failure in inducing complete differentiation and cell-cycle arrest is due to inappropriate chromatin remodeling and an incomplete DNA methylation associated with downregulation of oncogene pathway silencing (Carén et al., 2015).

3.2-Markers of stem cells

One of the main challenges for studying GSCs was to identify a *bona fide* marker. Several markers have been described such as the transcription factors Sox2 and Olig2, the intermediary filament nestin, the RNA-binding protein musashi-1 and others. However, these intracellular markers are not found in all tumorigenic cell derived from GSCs cultures. Moreover, identifying a cell-surface marker is of better interest in the prospective of sorting these cells from the cells constituting the tumor mass or from GSC cultures. Sorting for CD133 (prominin1) expressing cells was for a time the gold standard for GSCs isolation. CD133 is a cholesterol-binding membrane

protein of unknown biological function expressed by haemopoietic stem cells as well as by fetal brain cells. It was reported that only CD133+ cells isolated from GBM derived stem cell cultures can initiate tumors after xenotransplantation and only as few as 100 CD133+ cells could do so in a NOD-SCID mouse brain while CD133- are non-tumorigenic (Singh et al., 2004). Nevertheless, CD133 negative cells from primary tumor-derived adherent cultures were also able to reinitiate a tumor (Beier et al., 2007). Percentage of CD133+ cells were reported to vary from 30 % to 5% in tumor-derived culture which questions CD133 as a reliable marker for GSC. Indeed, CD133 has been shown to increase with hypoxia (Rosenberg et al., 2018).

The cell surface marker stage-specific embryonic antigen 1 (SSEA-1/LeX) is a trisaccharide highly expressed on embryonic stem cells in the developing brain and adult SVZ (Capela and Temple, 2002) SSEA-1+ cells isolated from GSC cultures are highly tumorigenic *in vivo*. This marker seems to be more reliable than CD133 as it is expressed in 96% of GBM tumors analyzed in Son et coll whereas CD133+ cells are found in 54% of these tumors (Son et al., 2009).

GSCs can also be identified and isolated with functional assays. GSCs exhibit a high activity of the enzyme aldehyde dehydrogenase 1 (ALDH1). ALDH1 catalyzes the oxidation of retinol to retinoic acid (RA) and RA contributes to the maintenance of an undifferentiated stem cell phenotype. ALDH1 has been described as a marker of cancer stem cells in numerous solid tumors including glioma (Rasper et al., 2010). The ALDEFLUOR™ was developed by the firm STEMCELL Technologies to sort cells with high ALDH1 activity, i.e., GSCs.

The tumorigenic capacity was shown to be retained by a side population of cells able to pump out the Hoechst 33342 dye, due to the expression on their surface of ABC transporters such as the multidrug resistance transporter 1 and the ABCG2 (also known as BCRP1). In the rat C6 glioma cell line, 0.4% of cells have this capacity and only these cells display tumorigenic potential (Kondo et al., 2004). However, brain endothelial cells express also these pumps (Golebiewska et al., 2013) therefore, this functional assay does not allow the isolation of a pure population of stem cells. All these markers (antigenic and functional) are still used to date, none of them is considered indisputably.

The search for a universal marker for GSCs main in fact be senseless as molecular profiling showed that GBMs may originate from different tumor initiating cells.

3.3-Molecular Classification

Histopathology ambiguity and tumor heterogeneity challenges GBM diagnosis and prognosis. Molecular classification of GBM based on transcription profile complements the traditional pathology based description. Gene expression profiling initially used microarray technology, then large-scale high-throughput next-generation sequencing technology. In the seminal work of Phillips and collaborators, microarray expression profiling of high-grade glioma samples identified 3 GBM subtypes according to a set of 35 signature genes (Phillips et al., 2006). Each subtype is characterized by an over-expression of signature genes. The pro-neural (PN) subtypes which affects younger patients, express genes associated with neurons (e.g., Neural cell adhesion molecule (NCAM) and Gamma-aminobutyric acid B receptor 1 (GABBR1)). The proliferative subtype presents mRNA associated with proliferation (e.g., proliferating cell nuclear antigen (PCNA) and DNA topoisomerase II α (TOP2A)), a gene signature that resembles the one of stem cells. The mesenchymal (MES) subtype displays overexpression of angiogenesis markers such as PECAM1 (Platelet endothelial cell adhesion molecule) gene and VEGF (Vascular endothelial growth factor).

Subtypes of GBM have been further characterized by combining transcriptomic analyses to the Cancer Genome Atlas (TCGA) Research Network TCGA catalog of genomic abnormalities in GBM (Verhaak et al., 2010). The PN stem cells overexpress PDGFR α due to focal amplification of its locus at 4q12. In addition, point mutations in the isocitrate *IDH1/2* genes are characteristic of the pro-neural (PN) subclass of GBM as well as mutations in *TP53*. Classical (CL) tumors were characterized by EGFR overexpression (gain on chromosome 7), deletion of PTEN (chromosome 10 loss), focal 9p21.3 homozygous deletion (loss of *P16INK4A*, *P14ARF*) and over-activation of NOTCH pathway (Verhaak et al., 2010). The Mes subtype is characterized by the focal hemizygous deletion of a region at 17q11.2 containing the gene *NF1*. Genes in the tumor necrosis factor super family pathway and NF-kB pathway are highly expressed in this particularly necrotic and inflammatory subtype (Verhaak et al., 2010). Finally, Neural subclass was characterized by the expression of neural markers. Among the four subtypes of GBM, the PN one shows longer survival. Patients with CL subtype shows a significant reduction in mortality with aggressive radiotherapy and chemotherapy. Although responsive to aggressive radiotherapy and chemotherapy, the prognosis of MES subtypes is the worst among all subtypes. The 2016 WHO classification proposes a simpler classification based on IDH mutation status (Louis et al., 2016) (Table 1).

In addition, the methylation profile of GBM is altered as compared to the normal brain which probably mediates tumorigenesis and the DNA methylation states in GBM has been shown to correlate with survival. Brennan and collaborators (Brennan et al., 2013) identified a subtype of glioma carrying hypermethylation in cytosine-phosphate-guanine (CpG) island: the G-CIMP (glioma-CpG island methylator phenotype). Most of the PN tumors displays the G-CIMP phenotype that confers the survival advantage over the non-G-CIMP tumors.

The methylation status of the MGMT promoter is used as a predictive biomarker for TMZ response (see 5-3-2). The MGMT promoter is methylated in 79% of G-CIMP versus 46% for non-G-CIMP. However when correlated with outcome, MGMT status distinguished responders from non-responders only amongst samples classified as classical (Brennan et al., 2013).

Detecting molecular markers specific for each GSCs population is valuable for accurate diagnosis and stronger prognosis. However, despite the classification, there is no targeted therapy based on molecular characteristics of GBM subtypes.

Phillips et al. (2006)	Proneural	Proliferative	Mesenchymal	
Signature	NCAM, GABBR1, SNAP91	PCNA, TOP2A, EGFR	VEGF, VEGFR1, VEGFR2, PECAM1	
Chromosome Gain/loss	None	Gain on Chr.7, loss on Chr.10	Gain on Chr.7, loss on Chr.10	
Biological process	Neurogenesis	Proliferation	Angiogenesis	
Verhaak et al. (2010)	Proneural	Neural	Classical	Mesenchymal
Signature	PDGFRA, OLIG2, DDL3, SOX2, NKX2-2	MBP/MAL, NEFL, SLC12A5, SYT1, GABRA1	EGFR, AKT2, SMO, GAS1, GLI2, NOTCH3, JAG1, LFNG	YKL40, MET, CD44, MERTYK, TRADD, RELB, TNFRSF1A
Mutated genes	TP53, PI3K, IDH1, PDGFRA		PTEN, CHKN2, PDGFRA	NF-κB, NF1

Table.2 | GBM stem cells classification, adapted from (Zhang et al 2020).

4-Are tumor originating from deregulated NSCs?

Evidences suggest that CSCs may originate from the deregulation of neural stem cells (NSCs) located close to the lateral ventricles. NSCs are slowly dividing cells in the brain capable of generating new neurons in rodents. As dividing, these cells are more prone to accumulate DNA damages and mutations than postmitotic cells and are therefore more susceptible to oncogenic transformation.

4.1-NSCs and neurogenesis in the adult brain

Neurogenesis persists in the brain of adult rodents throughout life. The first evidence was reported in the sixties: using a tritiated-thymidine uptake assay, it was shown that a population of cells in the adult rodent brain retains the capacity to cycle. The new generated cells are found in the anterior forebrain in the subventricular zone (SVZ), the olfactory bulb and the sub-granular zone of the hippocampus (SGZ) of rats (Altman and Das, 1965a) Since then, many studies have shown that constitutive neurogenesis in the SVZ and SGZ of adult rodents produces neurons that add to the olfactory bulb and to the granule cell layer of the dentate gyrus respectively (Ming and Song, 2011). In the olfactory bulb, the new neurons differentiate into inhibitory interneurons that integrate into the pre-existing circuitry and modulates the processing of sensory information by the olfactory bulb's projection neurons, regulating odor discrimination (Lledo et al., 2006). In the DG, these newly born neurons mature into new granule cell neurons, extending axonal projections to area CA3 and dendritic arbors into the molecular layer. These newly generated neurons are the cellular substrate to memory, learning and stress regulation (Braun and Jessberger, 2014). The magnitude of neurogenesis has been estimated to 30 000 neuroblasts exiting daily the SVZ while 9000 new granule cells are produced in the rodent DG over the course of a day (Lledo et al., 2006).

NSCs in the SVZ have been identified as a subpopulation of astrocytes. In the adult rodent brain, the SVZ is localized in the walls bordering the lateral ventricle. This region contains slowly dividing astrocyte-like NSCs termed astrocytes B1, expressing glial fibrillary acidic protein (GFAP), glutamate-aspartate transporter (GLAST), brain lipid binding protein (BLBP) and CD133 (prominin1) but are negative for the mature astrocyte marker S100 β . Astrocytes B1 extend a single cilium to contact the cerebrospinal fluid of the lateral ventricle and have a long basal process ending on blood vessels (Obernier and Alvarez-Buylla, 2019).

The majority of NSCs divisions in the SVZ are symmetric "consuming" divisions where NSCs generate C cells or progenitors that differentiate into A neuroblasts. These consuming divisions represent 80% of NSCs divisions. The pool of NSC is maintained in the SVZ by 20% of symmetric self-renewing divisions giving rise to two NSCs (Obernier et al., 2018) NSCs are found in two different states in the SVZ, in an activated (a) proliferative state and a quiescent (q) state. qNSCs extend a cilium at their apical surface and do not express the EGFR while aNSCs do no longer present the cilium and express EGFR. It has been shown that qNSCs and aNSCs can interconvert between more quiescent and activated states (Codega et al., 2014). C cells are transit amplifying

prognitors expressing the transcription factors Dlx2 that give rise to neuroblast or type A cells. A neuroblasts express the surface marker polysialylated neuronal cell adhesion molecule (PSA-NCAM) and the microtubule-associated protein doublecortin (DCX), both expressed by migrating and immature neurons (Doetsch et al., 1997; Garcia et al., 2004).

In the human SVZ, NSCs persist in the adult however, neurogenesis is largely extinguished in the adult. Extracted from the adult brain, cultured NSCs are able to generate multipotent neurospheres (Sanai et al., 2004). In vivo, migration of PSA-NCAM and DCX positive neuroblasts born in the SVZ has been observed till the 18th month of postnatal life. Interestingly, these neurons migrate toward the olfactory bulb but also to the ventromedial prefrontal (Sanai et al., 2011) via the RMS and the medial migratory stream respectively (MMS). Beyond 18 months of age, both proliferative activity and chains of migrating immature neurons are largely depleted (Sanai et al., 2011). The adult SVZ in humans has a different cyto-architecture organization as compared to rodents. It is composed of four distinct layers. Layer I is an ependymal monolayer that borders the lateral ventricles. Layer II consists of a hypocellular gap that separates the layer I from the ribbon of astrocytes of the layer III. This gap is very rich in processes from astrocytes and ependymal cells that interacts through gap junctions (between astrocytes only) and desmosomes and tight junctions. Some of the astrocytes found in layer III continue to divide in the adult SVZ. Layer IV is a transitional zone that contains myelin and separates layer III from the brain parenchyma. Unlike in rodents, no chains of migrating neurons in observed in the human SVZ.

There is a relative consensus that SVZ neurogenesis is extinguished in the adult human brain and there is no proof that proliferating astrocytes observed in layer III generate neurons. However, Ernst and collaborators found immature neurons expressing DCX and PSA-NCAM in the SVZ and the nearby striatum in adult human brains. It is easy to speculate that these immature neurons may originate from NSCs in the SVZ, which would suggest that neurogenesis is still active in the adult (Ernst et al., 2014).

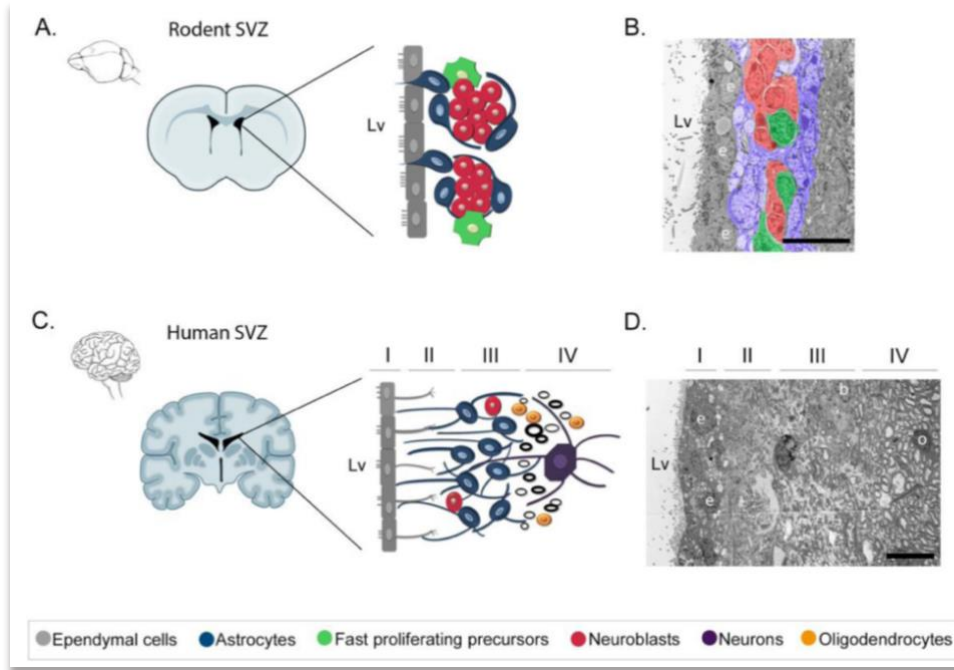


Figure.3 | illustrates the cellular arrangement of the neurogenic niche in the SVZ (subventricular zone). In panel A, a schematic diagram provides a coronal view of the mouse brain, with a specific focus on the neurogenic niche's cytoarchitecture. Panel B presents an electron microscopy image of the rodent SVZ, corresponding to the depiction in panel A. Moving on to panel C, a schematic representation of the SVZ in a coronal view of the human brain is shown, highlighting the four layers where the SVZ cells are organized. Panel D complements this with an electron microscopy image of the human SVZ, corresponding to the depiction in panel C. The key elements labeled in the figures include astrocyte-like cells (b), ependymal cells (e), oligodendrocytes (o), and the lateral ventricle (Lv). The scale bar indicates a length of 10 μm. *Adapted from (Capilla-Gonzalez et al.2006).*

4.2-Transformation

A growing body of evidences suggest that brain tumors may originate from the oncogenic transformation of SVZ NSCs. Many tumors are indeed either periventricular or contiguous with the SVZ and experimental exposure to oncogenic viruses or administration of carcinogens results in the formation of tumors in the SVZ. For instance, the loss of p53 associated with fetal exposure to the mutagen N-ethyl-N-nitrosourea, results in the formation in adult mice, of periventricular areas of cellular hyperplasia, characterized by clusters of GFAP positive cells, mature glia and neuroblasts (Gil-Perotin et al. 2006, *J. Neurosci.*, 26(4):1107–1116). The combine ablations of key tumor suppressors such as p53, PTEN and the protein retinoblastoma (Rb), specifically in GFAP proliferating cells, i.e., NSCs of the SVZ, leads to the growth of infiltrating gliomas with similar features to the ones observed in humans (Jacques et al 2010, *EMBO J* 29:222–235). Specific loss of heterozygosity of PTEN, NF1 and p53 in nestin expressing NSCs resulted in the spontaneous development of malignant gliomas with 100% penetrance (Alcantara Llaguno et al., 2009). These

transformed SVZ NSCs disseminate in the brain to proliferate and the more quiescent cells are spared by TMZ treatment, reinitiating tumor growth (Chen et al., 2012). The *INK4a-ARF* tumor suppressor locus encodes two proteins p16^{INK4} and p14^{ARF} that inhibits cell cycle progression. Deletion of this locus is frequent in human GBMs. The experimental loss of *INK4a-ARF* in NSCs expressing activated form of AKT and K-Ras induces gliomagenesis in mice (Uhrbom et al., 2002) Similarly, the constitutive activation of K-Ras in NSCs results in the formation of infiltrating glioma in adult mice (Abel et al., 2009). The overexpression of Rictor, a scaffolding protein of the mTORC2 complex, in GFAP proliferating cells of the SVZ, results in the growth of infiltrating tumor in adult mice. The features of the tumor were aggravated when both Rictor overexpression and EGFRVIII expression were induced in SVZ stem cells with overall survival of mice decreasing by 50% (Bashir et al., 2012) In humans, comparisons of somatic mutations found in the healthy SVZ samples and tumor mass of glioblastoma patients showed that both tissue harbor driver mutations in *TERT* promoter or cancer-driving genes such as *EGFR*, *PTEN* and *TP53*. In addition, some mutations are only found in the tumor tissue. This suggests that oncogenic transformation occurs first in SVZ NSCs that clonally evolve to glioblastoma (Lee et al., 2018).

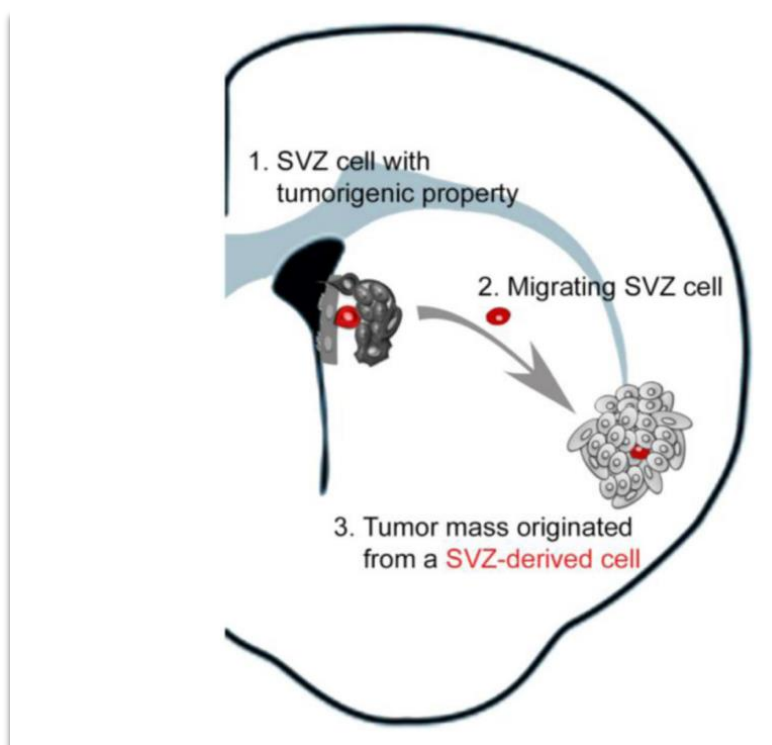


Figure.4 | A diagram illustrating a coronal hemisection of the rodent brain highlights the involvement of the subventricular zone (SVZ) in tumor development. The SVZ contains neural stem cells (NSCs) that have the ability to initiate tumor growth. It is hypothesized that these SVZ cells can migrate to different regions of the brain and give rise to a tumor mass. Adapted from (Capilla-Gonzalez et al. 2006)

5- Treatment

The Stupp protocol (Stupp et al., 2005) has become the standard of care for the treatment of glioblastoma. After maximally safe surgical resection of the tumor, the patient is treated by radiotherapy plus concomitant and adjuvant chemotherapy with temozolomide. Radiotherapy consists of fractionated focal irradiation at a low dose of 2 Gy per fraction given once daily from Monday through Friday over 6 weeks, for a total dose of 60 Gy. Temozolomide is taken orally concomitantly with radiotherapy at a dose of 75 mg/m² of body surface/day, 7 days per week. After a 4-week break, the patient receives up to 6 cycles of adjuvant temozolomide at a dose of 150-200 mg/m² of body surface per day for 5 days during each 28-day cycle. This therapy resulted in a significant survival improvement at 2 years with 26.5% survival as compared to 10.4% with radiotherapy alone (Stupp et al., 2009). However, the five-year survival rate is of only 7.2% and the disease remains 100% lethal (Ostrom et al., 2020). This is in part due to the heterogeneity and the highly infiltrative nature of GBM but also to the development of mechanisms of resistance. In this part, we will first detail the different steps of the Stupp protocol and the mode of action of radiotherapy and chemotherapy with TMZ. We will then present a non-exhaustive list of alternative therapies to GBM. Mechanisms of resistance will be addressed later.

5.1- Surgical Resection

Maximal safe surgical resection prolongs survival of patient with GBM. This procedure consists of removing the tumor mass by excising the margins without damaging the surrounding healthy tissue and causing neurological deficits. Besides removing tumor cells, tumor resection helps to reduce intracranial pressure due to the tumor and provides biopsies for histological analysis. It also provides a cavity for application of local therapies for destruction of residual tumor cells responsible for recurrence (Jain, 2018). The neurosurgical procedures have improved to maximize tumor resection. As an example, fluorescence guided surgery consists of the application of an exogenous fluorescent marker in order to label cancer cells. The 5-aminolevulinic acid (5-ALA) is a photosensitive substance that turns into a red fluorescent emission signal when metabolized by mitochondria. Its uptake by tumor cells improves the visualization of the tumor tissue in the operating room (Lara-Velazquez et al., 2017). Intraoperative mass spectrometry methods are used during surgeries in order to understand the tumor's molecular spatial arrangement. Based on specific tumor molecules, surgeons can discriminate between the tumor

tissue and the healthy tissue and better circumscribe the excision margins (Pirro et al., 2017). Cortical mapping is used to precisely locate the tumor. Functional MRI before the surgery and direct electrical stimulation (DES) of the cortex during surgery on an awake patient allow the surgeons to delineate the tumor margins, avoiding damaging the healthy tissue and increasing the extent of resection. During the procedure, the electrodes are placed directly in contact with the cortex. By stimulating the cortex and subcortical structures, neuronal networks are depolarized, activating or inhibiting the patient's corresponding neurological function (speech, movement etc...) (Qiao et al., 2021),(Lara-Velazquez et al., 2017) .

Despite all the innovations, a complete resection of the tumor is inachevable. Indeed, GBM infiltrates normal parenchyma and can reform tumors centimeters away from the resection site. In the case of butterfly glioblastoma, cells migrate along the corpus callosum white matter tract and disseminate to the contralateral hemisphere rendering the tumor inoperable (Opoku-Darko et al., 2018). Radiotherapy and chemotherapy are therefore the only way to target disseminated cancer cells.

5.2- Radiotherapy

Radiation therapy uses high-energy particles or waves, such as x-rays, gamma rays, electron beams, or protons, to induce cancer cell death. Ionizing radiations remove electrons from atoms. It can directly damage the DNA or indirectly by generating reactive oxygen species (ROS) from the radiolysis of water in the extracellular environment. Massive oxidative stress causes lipid peroxidation, protein misfolding, and DNA strand breaks (W. Kim et al., 2019).

Radiotherapy is administered in fractions to enable normal cells surrounding the tumor to recover between sessions of treatment. In GBM patients, a postoperative dose of radiotherapy of 60 Gy divided in 30 fractions of 2Gy is given over 6 weeks. New procedures have been developed that deliver radiation to the tumor while sparing the nearby healthy tissues. As examples, during intensity-modulated radiotherapy (IMRT), the intensity of radiation x-ray beams is controlled so that a higher dose is delivered to the tumor while the healthy tissue receives minimal doses of radiations. Stereotactic radiosurgery consists in the administration of radiations of high intensity to a small tumor in a single session while in stereotactic radiotherapy, radiations of lower intensities are delivered to larger tumors over several sessions of treatment. In both cases, the head of the patient is immobilized in a rigid frame and high gamma ray or x-ray beams from different angles are focused on the tumor. The surrounding healthy tissue is spared from

radiations. In brachytherapy, radioactive isotopes such as iodine-125 or iridium-192 are placed directly inside or next to the tumor and are a source of ionizing radiations (Barbarite et al., 2017). Particle therapy uses heavy ion beams to target tumors. In the case of carbon ion radiotherapy, the carbon ions are concentrated on the tumor site where they deliver ionizing radiations and induce cell death (Pompos et al., 2022).

Despite the improvement of the radiation delivery techniques, there is no clear evidence of a benefit in terms of overall survival over conventional external beam radiotherapy (Cantidio et al., 2022).

Another noninvasive technique but non-based on radiotherapy has been developed: the tumor-treating fields (TTFs). The patient wears on his shaved head, a portable device that continuously delivers low-intensity electric fields that produce antimetabolic effects by disrupting mitotic spindle formation (Burri et al., 2018). TTFs therapy has been shown to improve both progression-free (56% versus 37% at 6 months) and overall survival (13% versus 5%) when administered during maintenance therapy with temozolomide after standard radio chemotherapy, as compared with temozolomide alone (Stupp et al., 2017).

5.3- Temozolomide

TMZ (brand names: Temodar® in north America and Temodal® in UE) is an imidazotetrazine alkylating agent belonging to the group of triazene compounds. TMZ is a small molecule of 194 Dalton. It is a lipophilic prodrug able to cross the blood brain barrier and to reach the tumor site in therapeutically relevant concentrations. TMZ is administered orally and is robustly stable at the acidic pH of the stomach. Once in the blood and tissues, TMZ undergoes spontaneous hydrolysis to convert to the active metabolite 5-(3-dimethyl-1-triazenyl) imidazole-4-carboxamide (MTIC), which rapidly breaks down to form the reactive methyl diazonium ion. As an alkylating agent, TMZ transfers its electrophilic alkyl group to ring nitrogen and extra cyclic oxygen atoms of the DNA bases (Strobel et al., 2019), (Agarwala and Kirkwood, 2000). Its active metabolite, the methyl diazonium ion, methylates purine bases (figure 3). Upon TMZ treatment, 60–80% of the DNA adducts are formed at the N7 position of guanine and about 10–20% are formed at the N3 position of adenine. Only 5% of total DNA methylation occur at the O6 position of guanine (figure 3). N7-methylguanine and N3-methyladenine are easily repaired *via* the base excision repair (BER) pathway that excises these adducts without damaging the DNA. These N-alkylation adducts are therefore less toxic than the O6-methylguanine (O6mG) adducts that are

mainly responsible for the cytotoxicity of TMZ. During DNA replication, the O6mG mispairs with thymine, which is recognized by the DNA mismatch repair (MMR) system that reinserts the thymine opposite the O6mG. These futile cycles of DNA repair are repeated along 2 to 3 cell cycles and eventually leads the formation of single- and double-stranded DNA breaks resulting in cell cycle arrest at G2/M, senescence and apoptosis (Hirose et al., 2001),(Strobel et al., 2019),(Wang and Edelman, 2006).

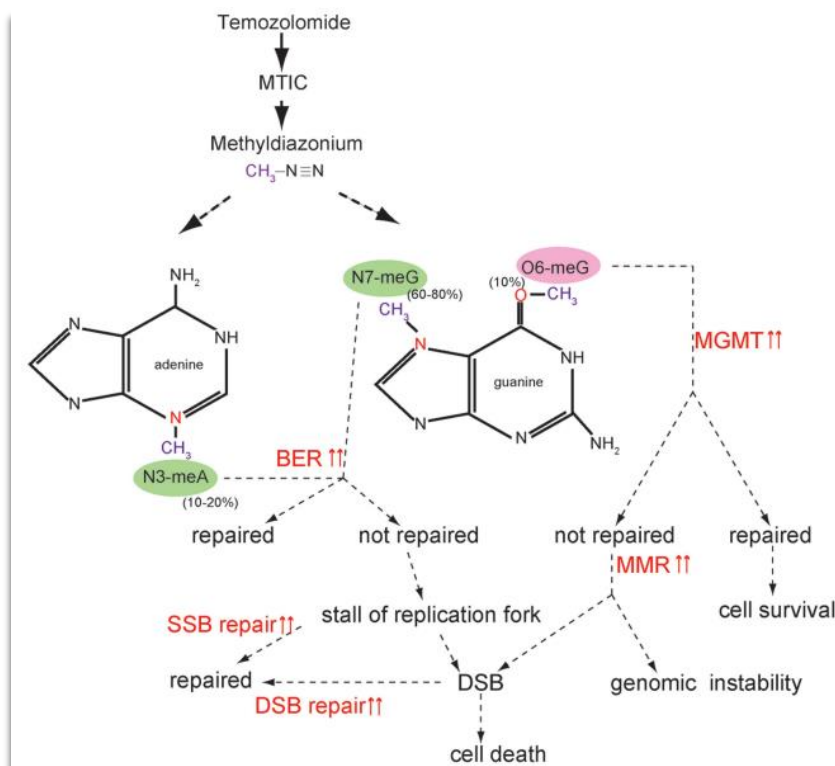


Fig.3| Illustration of the function of Temozolomide (TMZ) on the DNA repair pathway. Under physiological conditions, TMZ undergoes a chemical conversion to MTIC (5-3-(methyltriazene-1-yl) imidazole-4-carboximide) and degrades into a methyl diazonium cation. This cation transfers a methyl group to DNA. The primary sites of methylation are N7-MeG (60-80%), followed by N3-MeA (10-20%) and O6-MeG (5-10%). When the enzyme MGMT is active, it can repair O6-MeG without causing harm to the cell. However, if MGMT is inactive or unable to fully repair O6-MeG, the unrepaired O6-MeG undergoes continuous repair through the futile cycle of MMR (mismatch repair), leading to the induction of double-strand breaks (DSB) and cell death. When MMR malfunctions, it amplifies genomic instability. N7-MeG and N3-MeA are repaired by the BER (base excision repair) pathway. If these bases are not repaired, they can cause replication stalls and collapse of the replication fork, resulting in the generation of single-strand breaks (SSBs) that ultimately induce DSB. It is possible that the repair pathways for SSBs and DSBs are activated, thereby reducing the cytotoxic effects of TMZ. *Adapted from (Yoshimoto et al,2012).*

5.4- Other chemotherapies

Other chemotherapeutic agents are used concomitantly to the Stupp protocol or to treat recurrent GBM. Lomustine (also known as CCNU for chloroethyl-cyclohexyl-nitrosourea), is an alkylating agent of the nitrosourea family. Lomustine alkylates DNA and RNA and inhibits enzymatic functions by carbamylating of amino acids. The most relevant lesions induced by lomustine is the formation of O6-chloroethylguanine. However, this modification be reverted by MGMT which may explain the low activity of lomustine in patients with tumors lacking MGMT promoter methylation. Lomustine is used in second intention at recurrence. A major limitation to the use of lomustine in chemotherapy for recurrent glioblastoma is due to the drug inducing thrombocytopenia (Weller and Le Rhun, 2020).

Carmustine (also known as BCNU for bischloroethyl nitrosourea) is a nitrosourea alkylating that causes cross-links in DNA and RNA, inhibiting DNA synthesis. Due to its high toxicity when administered systemically, carmustine-impregnated wafers (Gliadel®) are inserted into the resection cavity, which allows the local delivery of the drug into the tumor bed. This treatment was reported to provide survival benefits for GBM patients (Xiao et al., 2020). However intracranial infections consequent to Gliadel® insertion were reported (Juratli et al., 2013). Inhibitors of kinases are currently tested in clinical trials. Among them, Regorafenib showed promising results in phase 2 clinical trial: regorafenib improved the overall survival of recurrent patients as compared to lomustine trial (Lombardi et al., 2019). Another clinical trial with regorafenib is ongoing of relapsed GBM (ClinicalTrials.gov Identifier: NCT04810182). Paxalisib, a PI3K/mTOR inhibitor is currently tested in phase 2 clinical trial together with a ketogenic diet and metformin to assess what effects it has on glioblastoma in patients with either newly diagnosed MGMT unmethylated glioblastoma or patients with recurrent glioblastoma regardless of MGMT promoter methylation status (ClinicalTrials.gov Identifier: NCT05183204).

Immunotherapeutic strategies were also tested to treat GBM. Bevacizumab (Avastin®) is a monoclonal antibody against the vascular endothelial growth factor A (VEGF-A). VEGF-A stimulates endothelial cell proliferation and vascularization of tumors. The purpose of treating patients with bevacizumab is to inhibit the neovascularization of tumors. In a phase 3 clinical trial, bevacizumab was administered intravenously in newly diagnosed GBM patients treated with the Stupp protocol: progression-free survival, but not overall survival was improved with bevacizumab (Chinot et al., 2014).

DCVax[®]-L is an immunotherapy treatment for newly diagnosed GBM. It uses a patient's own tumor lysate and precursors of the dendritic cells. The dendritic cells are instructed to present at their surface the tumor antigens which will trigger an immune response and the destruction of the tumor cells. This strategy is currently in phase 3 clinical trial for testing (ClinicalTrials.gov Identifier: NCT00045968).

6- Resistance to anticancer therapies

The addition of TMZ to radiotherapy has increased the overall survival as compared to radiotherapy alone. However, the prognostic remain grim in 100% of the cases (Ostrom et al., 2020; Stupp et al., 2009). Indeed, patient eventually relapses as the tumor recurs. The tumor microenvironment promotes resistance and sustain GSCs. Moreover, tumor cells develop mechanisms of resistance and escape DNA damaged induced by the therapy.

6.1-Tumor microenvironment

The highly hypoxic tumoral environment sustains stemness in GSCs. Hypoxia inducible factor 2 α (HIF2 α) is upregulated in hypoxic GSCs together with the glucose transporter type 1 (*Glut1*) and *VEGF*. HIF2 α sustains growth, stemness and survival of GSCs. The experimental downregulation of HIF2 α *in vivo* decreases the tumorigenicity of GSCs (Li et al., 2009). Hypoxia expands the pool of CD133 positive GSCs by upregulating HIF1 α (Soeda et al., 2009) One of the mechanism proposed is that, at hypoxia, the intracellular domain of the CD44 glioma stem cell marker is released *via* the cleavage by ADAM and γ -secretase. CD44 intracellular domain binds hypoxia inducible factor 2 α (HIF2 α) to enhance the transcription of genes that maintain stemness such as SOX2 (Johansson et al., 2017).

Glioma cancer cells fuel their metabolism with glucose to meet the bioenergetic and biosynthetic demands of proliferation. Pyruvate, the end product of glycolysis, is converted into lactate by the lactate dehydrogenase. Released in the microenvironment, the lactate is up taken by endothelial cells via the monocarboxylate transporter 1 (MCT1) transporter inducing the reprogramming of quiescent endothelial cells that proliferate, sprout and migrate to vascularize the tumor (Miranda-Gonçalves et al., 2017).

GSCs are found close to the vasculature in highly vascularized primary tumors and endothelial cells secrete factors that support the propagation of GSCs: Depletion of brain tumor

vessels by bevacizumab eradicates the self-renewal of cancer stem cells (Calabrese et al., 2007) Therefore, the maintenance of the tumor vasculature sustain GSCs. The tumor vasculature itself is resistant to chemotherapy. Glioma derived tumor brain endothelial cells overexpress the anti-apoptotic factor surviving and the endoplasmic reticulum chaperone GRP78/BiP that allows them to resist to temozolomide toxicity (Virrey et al., 2008).

Non-malignant cells of the brain support tumor growth and aggressiveness. As an example, pericytes are hijacked by glioblastoma cell to facilitate tumor progression. Pericytes lie on the abluminal vessel wall of brain capillaries and contribute to the maintenance of the blood–brain barrier integrity. In contact with glioblastoma cells, pericytes secrete the anti-inflammatory cytokines IL-10 and TGF- β and show decreased expression of the costimulatory molecules CD80 and CD86 and of histocompatibility complex molecules, MHC-II. The reduction of surface expression of co-stimulatory molecules and major histocompatibility complex molecules in correlated with a failure of antigen presentation to T cells providing an immune tolerance that favors glioma progression (Valdor et al., 2017). In addition to pericytes, reactive astrocytes and microglia secrete cytokines such as IL6 and the matrix metalloproteinase 2 that favor the parenchymal infiltration by glioma cells (Guan et al., 2018).

6.2- Mechanisms of resistance to radiotherapy

The overall outcome of radiotherapy in GBM remains far from optimal as tumor cells inevitably develop resistance to radiation. Non-tumoral cells from the microenvironment such as reactive astrocytes have been show to promote tumor cell survival and stemness after radiation (Berg et al., 2021). Moreover, GSCs are particularly resistant to radiation as they show greater checkpoint activation in response to DNA damage. This allows a more efficient DNA repair as compared to non-tumoral cells (Bao et al., 2006). Also, as access to oxygen decreases in the tumor due to its rapid growth and to an inadequate vascular system, the IR-induced generation of reactive oxygen species is reduced leading to less DNA damages that are caused by ROS in nonnormoxic conditions (Rey et al., 2017) When exposed to low oxygen concentration, the transcription of the hypoxia inducible factor 1 α (HIF1 α) is increased in cancer cells and HIF1 α sustains GBM radio resistance (Marampon et al., 2014).

6.3- Mechanisms of resistance to TMZ

6.3.1- TMZ concentration in the deep brain parenchyma

The bioavailability of TMZ is of 100 % meaning that TMZ is completely absorbed by the gastrointestinal tract when taken orally. The maximum concentration of TMZ in the plasma is achieved 30 to 90 minutes after oral administration and the concentration in the plasma is about 13–14 mg/L when administered at the concentration of 200 mg/(m² daily) for 5 days (Brada et al., 1999). In the cerebrospinal fluid (CSF), the concentration of TMZ have been reported to be approximately 20% of the one measured in the systemic circulation (Ostermann et al., 2004) In the brain parenchyma, measures of TMZ have been done in the brain by micro dialysis: a catheter was placed in the peritumoral brain tissue at the time of surgical resection of the tumor. Patients received a single oral dose of TMZ (150 mg/m²) the day following the surgery. TMZ concentrations in brain reached 1.55–4.64 μM in 2.0 ± 0.8 hrs. (Portnow et al., 2009) These concentrations are far under the relevant clinical concentration necessary to induce glioma cell death. *In vitro*, the IC₅₀ of TMZ on MGMT negative glioma cell lines is comprised between 10 to 100 μM while in cells with high MGMT expression, IC₅₀ values are beyond 350 μM (Perazzoli et al., 2015).

TMZ passes the BBB and the BBB remains mainly intact in the peritumoral region where infiltrative glioma cells disseminate. In order to increase TMZ penetration in the brain, a recent clinical trial investigated the effect of the temporary disruption of the BBB by magnetic resonance-guided focused ultrasounds (clinical trial registration no. NCT03712293). The procedure was performed on the first or the second day of the 4-week TMZ chemotherapy cycle. The first-year patient's follow up showed that the procedure increased time to recurrence as compared to TMZ treatment alone. Whether the procedure succeeded in increasing TMZ concentration in the brain parenchyma has to be determined. Further studies are warranted to assess the benefit on the overall survival (Park et al., 2020).

Sensitization of cancer cells to TMZ may prove a good strategy to increase TMZ therapeutic properties.

6.3.2- O6-Methylguanine-DNA Methyltransferase (MGMT) expression

O6-Methylguanine-DNA Methyltransferase (MGMT) is a DNA repair enzyme. MGMT transfers the methyl group present on the O6-methylguanine to its own cysteine residue thus removing the cytotoxic lesion induced by TMZ. After, alkylated MGMT is ubiquitinated and

degraded by the proteasome (Marchesi et al., 2007). Therefore, a high level of MGMT in GBM is a poor prognosis for patient survival as MGMT expressing cancer cells are resistant to TMZ. MGMT gene expression is regulated through the methylation of its promoter and MGMT promoter methylation status has emerged as a biomarker of the response to the treatment.

Methylation of the promoter is a major mechanism of gene silencing. However, discordance between methylation status and protein expression levels are reported: methylation of the promoter assessed by methylation-specific PCR, high-resolution melting PCR (HRM) or pyrosequencing, does not always correlate with low labelling of MGMT assessed by immunohistochemistry. Two genomic regions situated in the MGMT promoter and within exon 1 are enriched in CpG dinucleotides and have been identified as being the most concordant with transcriptional repression when methylated: differentially methylated region 1 and 2 (DMR1 and 2 respectively). However, in some cases, methylation in these regions does not correlate with gene silencing. For instance, hypermethylation of gene body cytosines has been shown to increase gene expression despite promoter methylation. Also decrease gene expression and mRNA levels are reported in cells with an unmethylated promoter and a hypomethylated gene body. Therefore assessing the methylation status of both the promoter and the gene body is necessary to characterize MGMT gene expression (Butler et al., 2020). Along with the treatment, the MGMT status of a tumor is susceptible to change the treatment selects cells with unmethylated MGMT promoter.

6.3.3-MMR deficiency

Antitumoral activity of TMZ requires a functional DNA mismatch repair (MMR). The O6MeG mispairs with thymine during the S phase and this thymine is replaced by another thymine by MMR enzymes. DNA strand breaks that result from the MMR futile cycles of repair induce cell cycle arrest in G2M and cell death. However, when cells are deficient in MMR enzymes, the cytotoxicity of TMZ is cancelled. Inactivation of mismatch repair (MMR) genes, *MSH2*, *MSH6*, *MLH1* and *PMS2*, has been identified in both IDH mutant and IDH wild-type recurrent gliomas that have been previously treated notably with TMZ. The MMR genes are rarely altered in primary tumors (Choi et al., 2018), (Hunter et al., 2006). For instance, mutation in the mismatch repair protein MSH6 favors tumor progression in recurrent GBM (Yip et al., 2009), (Cahill et al., 2007).

6.3.4- BER proficiency

Base excision repair (BER) is a cellular mechanism responsible for repairing damaged single nucleotide. TMZ-induced the methylation of N7-guanine and N3-adenine and these modifications are repaired within hours by the BER enzymes. N7meG and N3meA are removed by the N-methylpurine DNA glycosylase (MPG, also known as alkyl-adenine glycosylase: AAG) creating a basic sites recognized and filled up by the concerted actions of apurinic endonuclease, DNA polymerase- β (pol-B) and the XRCC1/LIG3 DNA ligase complex (Strobel et al., 2019). Therefore, N7meG and N3meA are only toxic when the BER is inactive or defective which is rare. On the contrary, *MPG* gene expression and protein levels have been shown to increase in human glioma as compared to normal brain tissue and its expression increases with tumor grading which worsen the prognosis (Liu et al., 2012).

Inhibitors of BER have been tested to enhance sensitivity to TMZ. Among them, methoxamine covalently binds to basic sites and inhibits BER. Methoxamine (TRC102) was administered with TMZ to recurrent glioblastoma patients in a phase 2 clinical study (ClinicalTrials.gov Identifier: NCT02395692). No results were communicated so far.

Another protein of the BER pathway is poly (ADP-ribose) polymerase 1 (PARP1). PARP-1 is a nuclear protein that participates in initiating base excision repair (BER). At the basic sites, PARP1 facilitates the recruitment of the downstream BER proteins DNA polymerase- β (pol-B) and the XRCC1/LIG3 DNA ligase complex. PARP1 binds to DNA strand breaks and produces a poly (ADP-ribose) chain from NAD⁺ substrate, which signals the cell to initiate DNA damage repair. PARP1 is overexpressed in glioblastoma (Murnyák et al., 2017). Inhibitors of PARP1 have been tested to increase the toxicity to TMZ and clinical trials are still undergoing (Hanna et al., 2020).

TMZ is to date the best anti-cancer chemotherapeutic agent to treat GBM due to its cytotoxic capacities, its ability to cross the BBB and its bioavailability. Finding a way to overcome TMZ resistance of GBM i.e., to restore the efficiency of the drug may prove to improve the treatment. I targeted the protein huntingtin to sensitize glioma cells and glioma stem cells.

CHAPTER 2. THE HUNTINGTIN PROTEIN

This chapter introduces the different biological functions of the Huntingtin (HTT) protein, that is mutated in Huntington's disease (HD). The physiopathology of HD is discussed. The general structure and functions of wild type (WT) HTT is explored. The role of HTT in DNA damage repair is detailed, together with the role of the protein in cancer and cell death. Lastly, the role of the antisense oligomer RG6042 is briefly addressed in the downregulation of WT HTT in GBM cells.

1. Huntington's Disease (HD)

1.1-Introduction to HD

Huntington's Disease (HD) was first discovered in 1872 by an American physician, Georges Huntington, who noticed the dramatic motor symptoms (choreiform movements) on adult patients from the same family, with symptoms worsening with age and a fatal outcome after a period of up to 20 years from motor symptoms onset.

Later, HD was characterized as a rare cortical and striatal neurodegenerative disorder, with a mean age of 40 years at onset and a prevalence of 5 to 10 cases per 100 000 (Sandrine humbert, 2016) and less than 5% of the cases occurring before the age of 20 years (juvenile form of the disease).

In 1993, the genetic cause of HD was discovered: it is due to an abnormal expansion of the cytosine–adenine–guanine (CAG) trinucleotide repeats in the exon 1 of the IT15 gene (chromosome 4p), encoding for an abnormal expansion of polyglutamine stretch at the N-terminal of the HTT protein (The Huntington's Disease Collaborative esearch Group 1993). The wild type HTT gene contains 9 to 35 CAG repeats when the CAG repeat length is comprised between 35 and 39, the CAG is unstable and there is a risk to develop the disease. Beyond 39 repeats, the mutation is fully penetrant and the patient will inexorably develop the disease (Kremer et al., 1994),(Rubinsztein et al., 1996) (figure 1). The length of CAG expansion is inversely proportional to the onset age of the disease with juvenile Huntington's disease (JHD) associated with more than 60 CAG repeats.

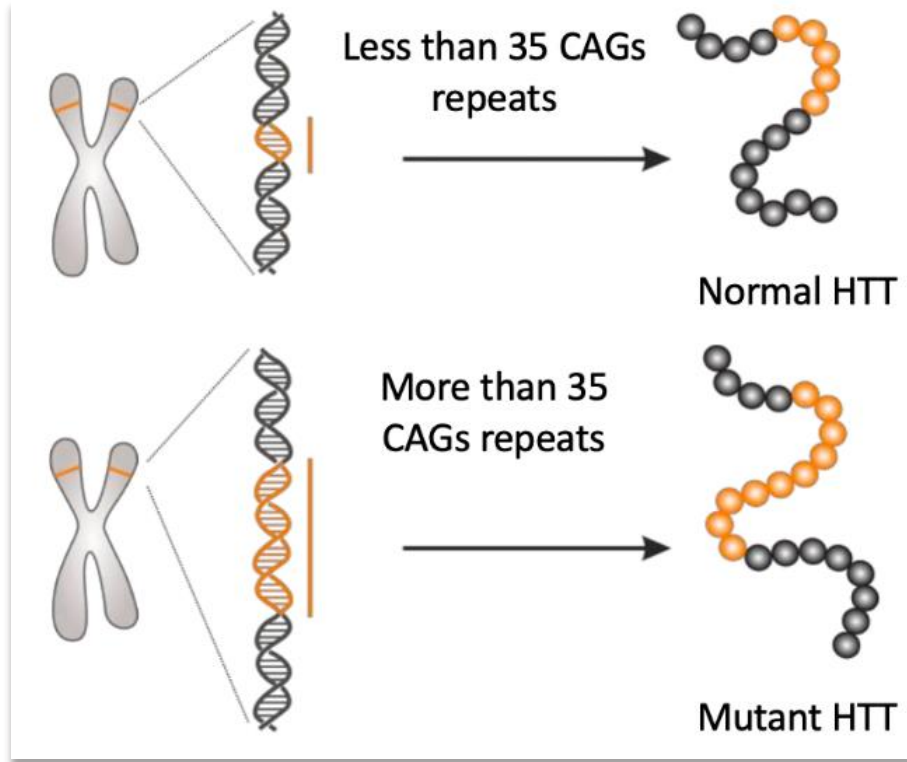


Fig.1 | Huntingtin protein and its mutation. Huntington's disease (HD) is caused by an abnormally long repetition of CAG triplets (beyond 35 repetitions) in the coding sequence of the huntingtin protein (HTT) gene. As a result, a poly-glutamine (polyQ) tail forms at the N-terminal end of the mutated HTT, altering its conformation and affecting its function.

HTT mutation is transmissible to the next generation in an autosomal dominant way meaning that most patients carry one wild-type and one mutant allele.

1.2-HD symptoms

HD is characterized by a triad of cognitive, psychiatric and motor symptoms. Cognitive and psychiatric symptoms that face HD patients are among the first symptoms to appear in patients. They are often present as early as 20 years, before the onset of motor symptoms (Eddy and Rickards, 2015),(Unmack Larsen et al., 2015). In fact, 40% of the pre-symptomatic patients develop cognitive disorders associated with facial recognition problems and a decrease in memory and attention flexibility (Epping and Paulsen, 2011), (Epping et al., 2016)Cognitive problems tend to worsen over time, ultimately leading to dementia.

HD patients are also frequently subjected to psychiatric disorders such as depression, apathy, anxiety, irritability or social disinhibition (McColgan and Tabrizi, 2018)and Tabrizi 2018).

Although chorea is the most prominent and characteristic motor symptom in HD, motor disabilities such as bradykinesia, dystonia and akinesia are observed later in the course of the disease. Historically, HD patients were divided into two clinical classes mostly based on the severity of their motor symptoms. The pre-manifest class group that refers to the pre-symptomatic patients with no symptoms that progress through the prodromal stage with an exhibition of moderate motor and cognitive symptoms. Eventually, the disease evolves to the manifest class that refers to the patients displaying marked motor dysfunctions as well as severe cognitive impairment (Bates et al., 2015)(figure 2).

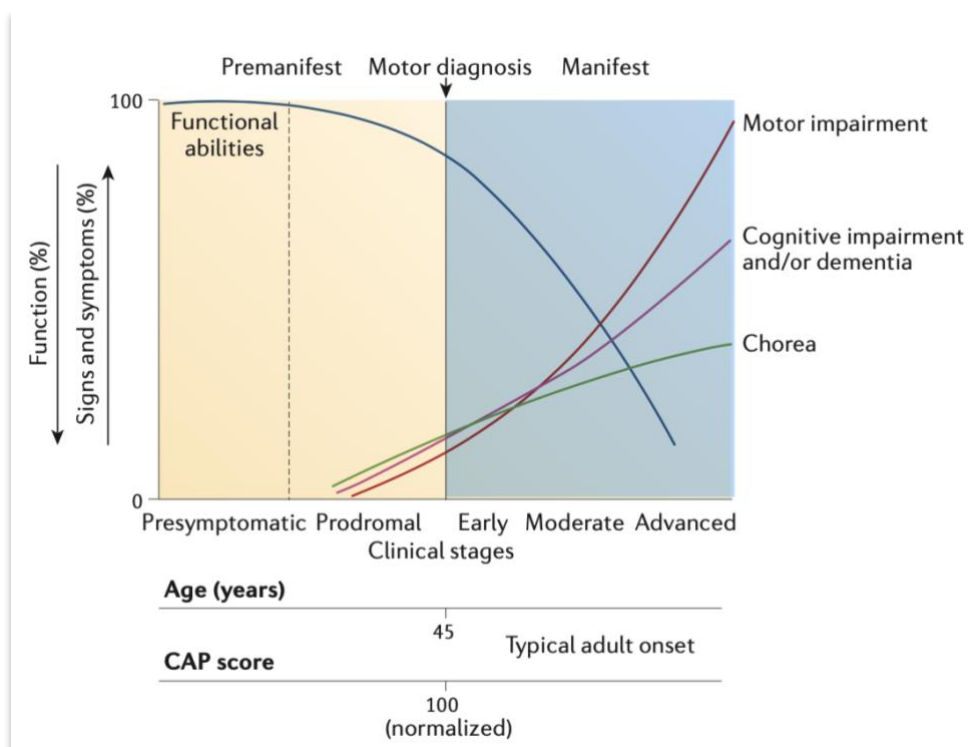


Fig.2 | The symptoms of Huntington's disease (HD). HD is characterized by a triad of motor, cognitive, and psychiatric symptoms. Motor diagnosis is typically made around the age of 45, although cognitive and psychiatric symptoms may be detected earlier during a phase known as the "pre-symptomatic" phase. All these symptoms worsen over time, leading to the progressive loss of the patient's functional abilities. Adapted from Bates et al., 2015.

As the community realized that changes occur decades before the onset of motor diseases, there was a crucial need to consider biomarkers of these changes to stage HD gene carriers and patients. Therefore, a new staging system of the course of the disease has been recently proposed: the Huntington's Disease Integrated Staging System (HD-ISS) (Tabrizi et al., 2022). The HD-ISS categorizes the disease period between birth and clinical motor diagnosis. This

classification is based on distinct stages defined by specific landmark measures including CAG track length, detectable pathological biomarkers, signs or symptoms, or functional changes attributable to HD. This staging system is applicable to individuals with 40 or more CAG repeats, ie bearing a fully penetrant allele. Stage 0 characterizes gene carriers bearing the diseased allele with no clinical symptoms or neurodegeneration. At stage 1, gene carriers show a decreased volume of the caudate and putamen by MRI. Patients in stage 2 of the disease display cognitive and motor dysfunctions evaluated through the symbol digit modalities test (SDMT) (the patient has to decipher a text in which numbers are randomly substituted for letters or geometric symbols: the test measures the subject's information procession speed and attention) and a full total motor score that assesses for the presence and severity of motor features ("Unified Huntington's Disease Rating Scale," 1996). At stage 3, changes in a patient's functional ability, such as difficulties in performing daily tasks, is observed.

Bringing all together, HD is a progressive pathology, that starts with cognitive and psychiatric symptoms followed by motor ones. It evolves into an increasing decline of patients' conditions suggesting that aging is a key component of the disease.

As discussed before, HD patients develop symptoms during mid-adulthood. However, young patients with severe symptoms have been reported; in most cases this correlates with an extremely high number of CAG repeats, reaching up to 175 Glutamines in juvenile forms of HD (Duyao et al., 1993), (Myers, 2004) (Johnson et al., 2021) The juvenile form of Huntington's disease (HD) is a rare variant of HD that affects individuals who are under the age of 20 ,sharing many similarities with the adult-onset form of the disease, but there are some distinct features and differences in symptom presentation.

The symptoms onset is generally earlier than the typical adult-onset form of HD, which typically occurs in mid-adulthood. The progression of the juvenile form of HD is often faster than the adult-onset form. Symptoms may worsen more rapidly, leading to more severe disability in a shorter period.

HD patients usually die 20 years after diagnosis, suffering from fatal pneumonia. There is no treatment at the current time to cure the disease or to delay disease onset.

1.3- Neurobiological characteristics

Brain from HD patients are severely atrophied as a nearly 20% reduction in the brain volume is observed on post-mortem brains (figure 3) with a regional specificity of brain atrophy.

Over a decade of HD progression, the highest total volume reduction was seen in the striatal, with a reduction of 18 regions; the putamen and caudate showed 18.7% and 15.4% of volume reduction respectively as compared to less than 3% for both regions in control subjects (Johnson et al., 2021). Neurodegeneration of striatal medium spiny neurons accounts mostly for the loss of volume in the striatum. Medium spiny neurons are GABAergic neurons (MSNs) that project to the substantia nigra (SN) and globus pallidus. These neurons are the first to die in early-stage of HD, and they die in the greatest numbers compared to the other neuronal populations (Vonsattel and DiFiglia, 1998). In addition, the cortex is also affected. The occipital, frontal temporal and parietal areas of the cortex exhibit the highest loss of volume among cortical regions). It has been shown that there is a significant loss of pyramidal neurons in layers III, V, and VI. Thus, the two frequent cerebral structures affected in HD are the striatum and the cortex with a loss of striatal and cortical neurons in in post-mortem HD patients (Tabrizi et al., 2009) followed by intra-nuclear inclusions generating the pathogenic aggregations of HTT N-terminal fragment (Rosas et al., 2008) All these pathogenic features are preceded by a striatal reduction and cortical thinning before even the symptoms appear.

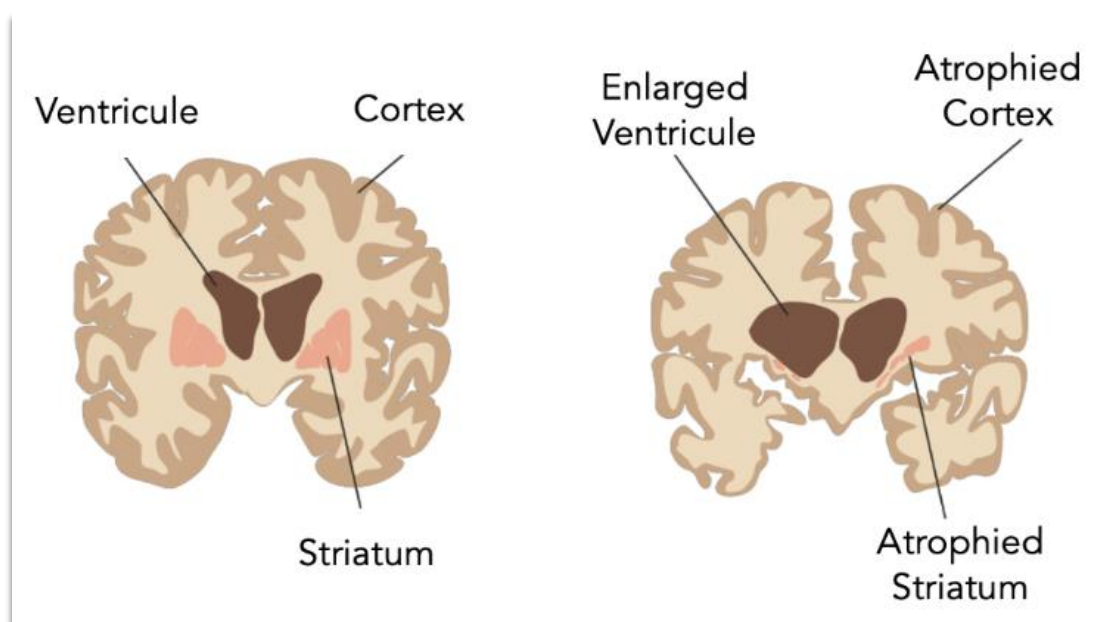


Fig.3| Brain atrophy in Huntington's disease HD. HD brain is characterized by extensive neurodegeneration of the striatum and cortex, accompanied by an enlargement of the cerebral ventricles. On the left: a healthy brain; On the right: a brain affected by HD.

In addition to the CNS alterations of HD, patients also suffer from immune and metabolic perturbation in addition to the muscle atrophy and cardiac failure (Vanderburg et al., 2009). These defects are not the result of the neuronal dysfunction but caused by the expression of the mutant gene in the tissue of interest.

Altogether this suggest that multiple cellular signalling is disturbed in HD in and outside the CNS. This could be linked to HTT presence in several tissues. Indeed, as we will see, in addition to the toxic functions of mutant HTT, the HD mutation also interferes with the ubiquitous native roles of HTT in the organism.

2-Huntingtin Protein

HTT is a scaffold protein of 350 kDa that is ubiquitously present in the organism with a high expression in both, the testis and the brain tissues (Marques Sousa and Humbert, 2013). Several studies show that the abnormal polyQ expansion in HTT contributes to a general neuronal dysfunction by gaining toxic functions but also by losing native functions of the wild-type protein.

Homozygous inactivation of the wild-type HTT in mouse is embryonic lethal as early as day 8 (E8). A massive cell death is observed in the ectoderm showing that HTT is essential for development (Duyao et al., 1995, Zeitlin et al 1995). This does not look like HD signs in patients; therefore, most studies have focused on the toxic functions of mutant HTT while much less described the role of the native HTT. The current view of HTT biology is described as a scaffold protein that interacts in direct or indirect ways with multiple proteins to generate complexes involved in a large variety of cellular processes.

2.1-Structure of HTT

HTT is composed of 3144 amino-acids divided into three main domains: the N-HEAT, the Bridge and C-HEAT domains. The first and last domains correspond respectively to the first 1-1684 amino-acids and the last 2092-3144 amino-acids of HTT linked together by the Bridge domain (Guo et al., 2018). Both domains contain several pairs of anti-parallel alpha-helices termed HEAT domains (Andrade and Bork, 1995),(Palidwor et al., 2009) such domains are known to mediate protein-protein interactions. In line with this, HTT interacts with more than 125 different partners (Harjes et Wanker 2003) (Harjes and Wanker, 2003)and is a multi-conformational protein that can reach approximately 100 different conformations (Seong et al., 2010).

The N-terminal domain of HTT was for long a focus point of study as it contains the HD mutation. HTT N-HEAT domain contains a proline rich domain (PRD) and the N-17 region, a sequence of 17 amino-acids followed by the polymorphic poly-glutamine repeats that is abnormally expanded in HD. Deletion of the poly-glutamine stretch promotes autophagy and increases the mouse lifespan (Zheng et al., 2010). Deletion of the PRD of HTT in mouse induces learning and memory impairments without affecting motor functions (Neveklovska et al., 2012). However, when both the poly-glutamine (polyQ) stretch and the proline-rich domain (PRD) are deleted in the HTT, several mitigations have been observed in mice such as a reduced aggregation propensity of polyQ stretch, an altered protein-protein interactions involving The PRD of HTT and an improved cellular viability.

Overall, the deletion of both the polyQ stretch and PRD in huntingtin has been shown to mitigate the pathological consequences associated with Huntington's disease, including reduced protein aggregation, improved cellular viability, and restoration of normal huntingtin function André 2017(André et al., 2017).

HTT N-17 region has an amphipathic α -helix structure, however, the polyglutamine stretch is flexible which makes it more susceptible to adopt different conformations such as α -helix, coiled coil or extended loop conformation (Atwal et al., 2007; Kim et al., 2009). Due to the presence of the PRD in the N-terminal region of HTT, the last can interact with proteins containing SH3 domain named after its identification in the Src tyrosine kinase protein and WW initially identified in the human dystrophin protein and is named after two conserved tryptophan residues within the domain (Gao et al., 2006),(Harjes and Wanker, 2003).

Interestingly, the N-17 can also interact with the PRD, forming a folded protein, which is impeded by pathogenic poly-glutamine stretch (Caron et al., 2013). In addition, N-terminal and C-terminal domains are refolded on the central domain of HTT by interacting with this central domain(Palidwor et al., 2009).

The 3-D structure of HTT was recently described as spherical structure containing an internal cavity capable to host the Huntingtin associated protein 40 (HAP40) to form the HTT/HAP40 complex (Vijayvargia et al., 2016),(Guo et al., 2018).These conformations are altered when HTT is mutated, where a rotation of the C-HEAT domain is observed (Vijayvargia et al., 2016), (Jung et al., 2020).

2.2-Diversity of HTT proteins: variants, isoforms, oligomers and post-translational modifications

HTT is modified by cellular processes that generate several forms of the protein. For instance, shorter forms of HTT are generated by alternative splicing or cleavage, HTT dimers are obtained consequently to HTT oligomerization. HTT is also the target of a large number of post-translational modifications which generate a diversity of HTT molecules. One can speculate that all these variants will carry different physiological functions.

2.2.1-Shorter forms of HTT

Alternative splicing of HTT mRNA were shown to generate shorter HTT isoforms (Ruzo et al., 2015),(Hughes et al., 2014) such as HTT Δ 10 and HTT Δ 12, HTT Δ 29: HTT Δ 10 lacks exon 10 encodes a stretch of glutamine residues (polyQ tract) of the HTT protein, which contains a CAG repeat region and a CDK5 phosphorylation site that reduces caspase-dependent cleavage of the protein. HTT Δ 12, on the other hand, lacks exon 12 encodes a portion of the N-terminal region of the HTT protein that contains a caspase cleavage site(Luo et al., 2005),(Wellington et al., 2002). Finally, HTT Δ 29 is missing a binding site to several proteins that are necessary to promote nucleocytoplasm transport (Hughes et al., 2014).

Cleavage of HTT also generates shorter forms of the protein. HTT sequence contains several PEST regions that are proteolysis-sensitive domains (amino acids proline (P), glutamic acid (E) or aspartic acid (D), serine (S), and threonine (T) (Warby et al., 2008). These PEST are the target of a variety of proteases members belonging to the caspase family, the Ca²⁺-dependent Calpain and the metalloproteinase MMP10 (Goldberg et al., 1996),(DiFiglia, 2002),(Miller et al., 2021),(Tebbenkamp et al., 2012).The proteolysis of mutant HTT generates small N-terminal fragments that accumulate and are prone to form the nuclear aggregates observed in HD (Benn et al., 2005; Graham et al., 2006; Saudou et al., 1998).

In addition to the N-terminal aggregation toxicity, it was shown that C-terminal fragment generated by HTT cleavage also alters the normal functions of the endoplasmic reticulum (El-Daher 2015).(El-Daher et al., 2015)

2.2.2- HTT oligomers

Originally, HTT was described to behave as a homodimer. However, HTT potentially functions under oligomeric forms such as dimers, trimers and higher-order oligomers that are increased with the aggregated forms in the HD pathological condition (Huang et al., 2015). HTT oligomerization is induced by the N-terminal part encoded by the exon1 of the protein consistent with the N-terminal aggregation observed in HD.

In fact, in HD heterozygous mice, a specific silencing of the mutated allele was sufficient to compensate HD phenotype (Drouet et al., 2014, 2009).

2.2.3- post-translational modifications

Post-translational modifications such as SUMOylation, acetylation, palmitoylation, phosphorylation and ubiquitylation, modulate HTT functions and localization in different ways (Saudou and Humbert, 2016a), (Ehrnhoefer et al., 2011). Acetylation and ubiquitination of HTT contribute to its degradation (Cong et al., 2011), (Jeong et al., 2009). The acetylation promotes HTT degradation and the SUMOylation assures its stabilization and nuclear re-localization (Steffan et al., 2004). Additionally, HTT palmitoylation by HIP14, Huntingtin Interacting Protein 14, controls HTT subcellular localization allowing the its attachment to membranes.

For all, the most studied HTT post-translational modifications are the multiple phosphorylation of the protein. HTT is phosphorylated by multiple kinases such as Akt, CDK5, EphB2, IKK, or PKC (Schilling et al., 2006; Watkin et al., 2014), (Huang et al., 2015) implying HTT in a wide range of cellular processes.

The phosphorylation of serine 421 (S421) by Akt and the S1181 and S1201 CDK5-mediated phosphorylations, alter HTT vesicular transport function by favouring the anterograde transport or stimulating the transport in both directions, respectively (Ben M'Barek et al., 2013; Colin et al., 2008; Humbert et al., 2002) CDK5-mediated phosphorylations of HTT are involved in response to DNA damages induced by the oxidative stress, suggesting a role of HTT in the DNA repair pathway (Anne, Saudou et al. 2007 (Anne et al., 2007)). S13 and S16 phosphorylations of the HTT N-terminal by casein kinase 1 (CK1) and glycogen synthase kinase 3 beta (GSK3 β) re-localize the protein in nucleus, or towards the mitotic spindle and mitotic furrow (Atwal et al., 2011; Maiuri et al., 2013).

However, In HD, HTT protein undergoes several post-translational modifications that are believed to contribute to the pathogenesis of the disease: Aberrant phosphorylation of HTT by casein kinase 2 (CK2) and cyclin-dependent kinase 5 (CDK5) particularly in the N-terminal region, is

thought to modulate its function and contribute to disease pathology. In addition, mutant HTT undergoes increased ubiquitination, leading to its proteolytic cleavage, resulting in the generation of toxic protein fragments. The proteolytic cleavage of HTT produces N-terminal fragments that have increased aggregation propensity and contribute to the formation of intracellular protein aggregates called inclusion bodies, a hallmark of HD.

2.3-HTT interactions

As a scaffold protein, HTT promotes the formation of multi-protein complexes, interacting with up to 400 interactors (HIPPIE ref) and this is mainly due the presence of the PRD in the N-terminal of the protein, that hosts the binding of other proteins containing WW and SH3 domains which are the most frequent HTT interactors (Faber et al., 1998; Gao et al., 2006; Liu et al., 1997; Tourette et al., 2014). For instance, WW-containing proteins are involved in multiple cellular processes such as stem cell maintenance, tissue homeostasis and tumorigenesis (Passani et al., 2000; (Passani et al., 2000)Proteins that contain SH3 domains are involved in the signalling of the transmembrane receptors to small G proteins (Liu et al., 1997; Pawson and Gish, 1992). Interestingly, different sets of interactors were characterized between wild-type and mtt HTT (Culver et al., 2012; Ratovitski et al., 2012; Shirasaki et al., 2012, 2012; Zhao et al., 2018) as the conformational change induced by the polyglutamine stretch modulates the binding affinity of its interactors.

Other than N-terminal, the internal and C-terminal domains also specifically interact with some proteins such as Dynamin1, LC3B, GABARAP11, Atgs, NfκB and Kalirin (Ochaba et al., 2014). Altogether, the different nature of HTT interactors prove that HTT is involved in a wide range of cellular functions including membrane trafficking, cellular metabolism and gene expression (Harjes and Wanker, 2003).

2.4-HTT and membrane trafficking

HTT interactions with HIP1, HIP12 and Dynamin1 involve HTT in clathrin-dependent endocytosis (El-Daher et al., 2015) and its interactions with Rab5 and HAP40, in the trafficking of endosomes (Pal et al., 2006).HTT also targets the Rab8 and Rab11 cargoes to the plasma membrane and thus participates in the polarized recycling of endosomes (Elias et al., 2015; Hattula and Peränen, 2000; Li et al., 2008).

2.5-HTT and autophagy

HTT plays roles in both the early and late stages of autophagy by binding to its biological partners, p62 and LC3A/B (Rui et al., 2015). Additionally, HTT interactions with HAP1 and dynein, mediates the autophagosomes transport. The loading of cargos to autophagosomes is defective in HD but the autophagy is abnormally activated (Kegel et al., 2000; Martin et al., 2015; Ravikumar et al., 2004).

2.6-HTT and vesicular transport

HTT scaffolds molecular motors to promote microtubule-based transport of vesicles in neurons (Vitet et al., 2020). HTT interacts with Dynein intermediate chain (Caviston et al., 2007), and can also bind indirectly through HAP1 to the p150glued dynactin subunit and Kinesin-1. Specify that these are anterograde and retrograde motors. Thus, by contributing to the assembly of molecular motor complexes on microtubules, HTT participates to the anterograde and retrograde transport in the axonal shaft of several cargoes:

For instance, HTT mediates the anterograde transport of the brain derived neurotrophic factor BDNF-containing vesicles (Gauthier et al., 2004) in the cortico-striatal connection that refers to the neural pathway connecting the cerebral cortex (specifically, the motor and prefrontal areas) to the striatum (Figure 4). This pathway consists of two main components: the cortico-striatal projections that send excitatory glutamatergic signals to the striatum forming synapses onto the dendritic spines of medium spiny neurons (MSN), which are the principal neurons in the striatum, and the striatal output that integrates the input from different cortical areas. Thus, the cortico-striatal pathway is involved in a wide range of functions, including motor planning and execution, habit formation, reward processing, and cognitive flexibility. Dysfunctions in this pathway have been implicated in various neurological and psychiatric disorders, such as Huntington's disease.

In HD, because the binding of mutant HTT to the molecular motor proteins is modified, BDNF transport in cortical axons and its release from cortical neurons to striatal neurons is decreased leading to striatal dysfunction and death (Gauthier et al., 2004; Virlogeux et al., 2018). In addition, Huntingtin (HTT) protein has been implicated in the retrograde trafficking of the TrkB receptor, which is a receptor for brain-derived neurotrophic factor (BDNF).

Through its HAP1 binding domain, HTT interacts with the HAP1 protein. HAP1 acts as an adapter protein that links HTT to TrkB-containing vesicles. Through this interaction, HTT serves as

a scaffold protein that facilitates the retrograde transport of TrkB vesicles along the microtubule tracks within the neuron.

The retrograde trafficking of TrkB mediated by HTT is crucial for the transport of BDNF signaling from the axon terminals to the cell body. BDNF-TrkB signaling is involved in various neuronal processes, including neuronal survival, differentiation, and synaptic plasticity. Thus, the HTT-mediated retrograde transport of TrkB ensures that the BDNF signals are properly delivered and reach the appropriate target sites within the neuron.

Similarly, the HTT mediated reduction of BDNF release at cortico-hippocampal synapses contributes to a decrease of hippocampal adult neurogenesis, resulting in an anxiety/depression-related behavior in mouse (Ben M'Barek et al., 2013).

Through the regulation of intracellular dynamics, HTT is also required for ciliogenesis of the ependymal cells (Keryer et al., 2011; Liu and Zeitlin, 2011). During ciliogenesis, HTT is required for the dynein-based transport of PCM-1 to the centrosome, forming the basal body (Keryer et al., 2011). Consistently, the absence of wild-type HTT or the presence of its mutation result in aberrant number of primary cilia (Barnat et al., 2020; Haremakei et al., 2015; Keryer et al., 2011; Maiuri et al., 2013).

Additionally, HTT expression is not restricted to the brain and as such, HTT participates to the of trafficking of the polarity complex PAR3-aPKC in mammary cells (Elias et al., 2015).

2.7-HTT and Development

Expression of both wild-type and mutant HTT starts in early development (Bhide et al., 1996). In line with this, even though symptoms of HD are emerging during mid-adulthood, several studies suggest a role of wild-type HTT in early embryogenesis that is altered in HD (Reiner et al., 2003; Wiatr et al., 2018). The inactivation of *HTT* gene induces lethality in mice at the embryonic day 7.5 (E7.5) due to a defect in iron transport (Dragatsis et al., 1998; Duyao et al., 1993; Nasir et al., 1995; Zeitlin et al., 1995). In addition, the absence of HTT at E7.5 triggers chromatin dysregulation leading to a failure in the expression of growth factors required for early patterning (Seong et al., 2010; Woda et al., 2005). Thus, the loss of HTT or its mutation impair the differentiation of stem cells into the germ mouse embryonic layers.

In addition to the embryonic development overall, HTT is important for the central nervous system development. The downregulation of HTT in Zebra fish showed that HTT is required for the formation of neural tube as it is required for maintaining cell-to-cell adhesions (Henshall et al., 2009; Lo Sardo et al., 2012). In addition, HTT downregulation in mice induces perinatal death and abnormal central nervous system development

For instance, expressing low levels of mutant HTT displays ventricles enlargement, and agenesis or misrouting of white matter tracts. In fact, during brain development, mutant HTT can interfere with normal neuronal processes, including cell migration, axon guidance, and synapse formation. This disruption in neurodevelopment can contribute to the abnormal organization of white matter tracts and ventricular enlargement observed in affected individuals. In addition, mutant HTT has a toxic effect on neurons. It can lead to neuronal dysfunction and cell death through various mechanisms, including protein misfolding, impaired mitochondrial function, excitotoxicity, and dysregulation of cellular signaling pathways. These neurotoxic effects can disrupt the normal architecture of the brain, including the white matter tracts and ventricular system. Thus, mutant HTT can disrupt the process of myelination, leading to abnormalities in the white matter tracts. This disruption can result in misrouting or incomplete development of these tracts. As Huntington's disease progresses, there is a progressive loss of neurons, particularly in specific brain regions such as the striatum. The loss of neurons can disrupt the connectivity within the brain, affecting white matter tracts and leading to their misrouting or agenesis. Additionally, the loss of neuronal cells can cause atrophy and shrinkage of brain structures, which can further contribute to ventricular enlargement.

Our laboratory has addressed the role of HTT during cortical development where HTT regulates every step: HTT controls the neuronal division of neuronal progenitors, their multipolar-bipolar transition, the migration of newly generated neurons and the maturation of their somato-dendritic compartment. In early corticogenesis stages, HTT participates to the organization of the neuro-epithelium formed by radial glial cells: junctions at the apical end foot of radial glial cells are disrupted in HD, displaying a mis-localization of ZO1, PAR3, B-catenin and N-cadherin (Barnat et al., 2020). HTT also belongs to the molecular machinery that controls the neurogenic divisions of radial glial cells by properly assembling their spindle poles (Godin et al., 2010; Lopes et al., 2016; Molina-Calavita et al., 2014).

Loss of wild-type HTT and expression of mutant HTT disturb the orientation of the mitotic spindle and the subsequent cell fate of the progeny, favouring neurogenic divisions at the expense

of maintenance of the stem cell pool. HTT is required for the distribution of the mitotic spindle proteins NuMA1 and Dynein, between spindle poles and the cell cortex through the astral microtubules. HTT loss of function decreases the cortical localization of NuMA1 and dynein localization on astral microtubules. In the contrary, NuMA1 is enriched at the spindle poles. HTT functions as a scaffold of the kinesin molecular motor, which then promotes the transport and cortical localization of NUMA1 and Dynein (Capizzi et al., 2022). In post-mitotic neurons, HTT is required for the bipolar-multipolar transition and the migration of newly generated neurons during later stages of corticogenesis: HTT promotes the recycling of endosomes of N-cadherin required for the cell-to-cell adhesion necessary for the radial migration of newborn neurons along glial fibers (Barnat et al., 2017; Tong et al., 2011). Finally, HTT participates to the maturation of post-mitotic neurons. Morphologic analysis of HTT-depleted layer II/III neurons reveal a reduced dendritic arborization complexity (Barnat et al., 2017; McKinstry et al., 2014), together with an alteration of the excitatory synapses number and the subsequent excitatory glutamatergic cortical transmissions (Braz et al., 2022; McKinstry et al., 2014).

However, all the functions of wild-type HTT are altered in HD.

Does abnormal brain development contribute to disease onset?

In mouse, the expression of mutant HTT during a developmental window triggers HD phenotypes in adulthood such as motor deficits (Molero et al., 2016). Similarly, transient downregulation of wild-type HTT during embryonic development until post-natal day P21, is sufficient to cause alteration of cortical layers and striatal structures (Molero et al., 2016). These studies suggest that HTT depletion or mutant HTT expression during embryonic stages are sufficient to cause alterations at adult stages (Braz et al., 2022)

In conclusion, HTT is necessary for the development of the central nervous system and ensures proper corticogenesis. Loss of HTT expression or expression of mutant HTT modifies the development of the central nervous system and this contributes-at least in part- to the adult disease onset.

2.8-HTT and DNA Damage Response

HTT when phosphorylated at N17 α , a domain located at the N-terminus of the protein and characterized by the presence of a repeated sequence of the amino acid glutamine (Q),

colocalizes with ATM at nuclear puncta at the DNA damage sites, suggesting a role of HTT in oxidative DNA damage repair pathways. However, ATM is required for HTT nuclear localization but does not influence the phosphorylation of HTT at N17. In HD patients' fibroblasts, a dysfunction of HTT in the DNA repair leads to an accumulation of DNA oxidative lesions due to an increase of reactive oxygen species (Maiuri et al, 2017).

HTT also participates in the base excision repair pathway. For instance, in the presence of ROS species, HTT translocate into the nucleus through the oxidation of methionine 8 in the N17 α domain, in an ATM-dependent manner and colocalizes with APE1 et the euchromatin regions. Indeed, under stress, N17 α undergoes a conformational change that releases HTT from the ER, enhancing its phosphorylation at S13 and S16 and its nuclear translocation. Thus, HTT localizes to sites of base excision repair and interacts with DNA repair protein such as XRCC1, FEN1, APE1 and phosphorylated ATM suggesting a scaffolding role of HTT of the DNA repair machinery (Maiuri et al., 2017).

HTT acts as a scaffold factor that assembles various components of the Transcription-Coupled Repair complex such as RNA polymerase II subunit A (POLRA2), Ataxin-3, DNA repair enzyme polynucleotide-kinase-3-phosphatase (PNKP) and cyclic AMP-response element binding CREB protein CBP. The formation of this complex senses DNA damage during transcriptional elongation and stimulates the DNA end-processing activity to facilitate neuronal DNA repair and maintain the transcription of specific neuronal genes. This contributes to the maintenance of neuronal genome integrity. Similarly, interfering with PNKP activity results in the accumulation of persistent DNA breaks leading to an altered activation of ATM in HD transgenic mouse. This cascade of events disrupts DNA repair and induces neuronal dysfunction and neurodegeneration (Gao et al., 2019).

2.9-HTT and Apoptosis

Early studies, focused on the anti-apoptotic properties of HTT. Rigamonti et al showed that wild-type HTT protects clonal striatal derived cells from apoptotic stimuli downstream Bcl-2 and upstream from Caspase 3 activation. Also, the inactivation of HTT in mice leads to neuronal degeneration. However, the protective effect of wild-type HTT is lost when it encompasses an abnormal polyglutamine expansion in HD as in this condition, mutant HTT leads to selective neurodegenerative loss of spiny striatal neurons (Gervais et al., 2002). This can be illustrated by the HIP1-Hippi cascade: HIP1 (HTT-interacting protein 1) is a pro-apoptotic protein which

overexpression induces a rapid caspase 3-dependent cell death. A conserved phenylalanine residue within the death effector domain (DED) of HIP1 is responsible for HIP1 apoptotic activity independently of caspase 8. HIP1 activates caspase 3 suggesting that HIP1 is active downstream from the formation of DISC (Hackam et al., 2000).

In HD, the interaction of Hip1 with mutant HTT is weaker than with wild-type HTT. Thus, mutant HTT releases HIP1 which in turn binds to Hippi (Hip1-Protein interactor) through the talin- and myosin-like domains, forming together a pro-apoptotic Hippi-Hip1 heterodimer. The heterodimer recruits pro-caspase 8, launching by this apoptosis through extrinsic cell death components such as TNF receptor or Fas receptor (Gervais et al., 2002). In contrast, wild-type HTT binds Hip1 and reduces cellular toxicity by inhibiting the formation of Hip1-Hippi heterodimer (Gervais et al., 2002).

2.10-HTT and Cancer

HD patients have lower cancer incidence than non-HD people. Sorensen et al showed that only 5% of death in HD patients were associated to cancer. Later in 2012, Ji et al described similar decrease in cancer incidence in most HD individuals. In fact, HTT can act as a tumor suppressor by modulating the apoptosis of neoplastic cancer cells (Ji et al 2012).

Whereas CAG long length has a protective role in breast and ovarian cancer, it could be paradoxically associated with tumor progression and metastasis. In fact, metastasis is increased by a factor of 11.1 in patients with sporadic HER2 breast cancer with every 10 additional HTT CAG repeats. Mutant HTT interacts with dynamin 2 and impairs HER2 recycling by inhibiting its endocytosis thus, provoking HER2 accumulation and enhancing cancer severity (Moreira Sousa et al., 2013; Thion and Humbert, 2018). Another mechanism could involve cellular junctions: loss of wild-type HTT in breast cancer promotes metastasis by altering tight junctions (Thion et al., 2016). Similar to the loss of wild-type HTT, the dephosphorylation of HTT at S421 accelerates cancer progression (Thion et al., 2015). In line with this, FK 506, an inhibitor of Calcineurin that dephosphorylates HTT at S421, inhibits the migration of breast cancer cells and decreases mammary tumor growth in vivo (Thion et al., 2015).

In addition, HTT decreases metastatic breast cancer cells through its interaction with CREB-binding protein (CBP), which mediates the CREB-dependent transcription of ZO1, a protein involved in maintaining cellular tight junctions.

Altogether, this suggests an anti-tumor role of wild-type HTT and S421-phosphorylated HTT in breast cancer cells.

Another pathway of HTT in cancer involves the HTT associated protein 1 (HAP1). This cytoplasmic protein is less expressed in breast cancer cells compared to normal tissues in contrast to Huntingtin interacting protein (HIP1) that is overexpressed in breast cancer cells. HAP1 expression in ER positive and triple negative breast cancer cells in culture reduces the proliferation, invasion and migration of both cell types enhancing the apoptotic activity of caspase 3 in the ER positive cells and not the triple negative cells.

Another HTT interacting protein, HTT interacting protein 1 (HIP1) is associated with other human cancers such as prostate cancer. An aberrant (over or decreased) expression of HIP1 is found in prostate and colon tumor cells but not in benign epithelial corresponding cells (Rao et al., 2002). In the TRAMP transgenic adenocarcinoma mouse model, HIP1 is overexpressed in prostate tumor. Depletion of HIP1R in prostate tumors decreased metastasis by reducing the mesenchymal-like cell morphology (Rice et al., 2016), suggesting that HIP1R positively regulates the transition from prostatic hyperplasia to carcinoma. Moreover, HIP1 modulates the function of several Glutamate receptors such as EGFR (describe), PDGFR (describe) and transferrin receptors (Bradley et al., 2005). The lipid binding domain of HIP1 directly extends the EGFR expression and half-life (Bradley et al., 2007). miR23b-27b targeting HIP1 is downregulated in human metastatic prostate tumors. In orthotopic prostate xenograft transduced with miR23b-27b, seminal vesicle invasion and distant metastases supporting the role of HIP1R expression as a metastasis suppressor (Rice et al., 2016). Controversially, other studies suggest that HIP1 promotes apoptosis in a caspase-8 independent way. The differences observed in these studies may come from the use of different HIP1 cDNAs: one of the cDNA lacks the N-terminal sequence containing the ENTH, the Epsin N-terminal homology domain that is critical to maintain HIP1 roles in cellular survival or death pathways (Rao et al., 2002).

Finally, Simeone et al described four major network hubs in Glioblastoma, composed of HTT, HNF4 α , c-Myc and 14-3-3 ζ that cross talk with p53 and EGFR pathways. In this study, HTT was found in the cytoplasm of high-grade GBM and in the nucleus of low-grade GBM (Simeone et al., 2014).

CHAPTER 3. THE ANTISENSE OLIGONUCLEOTIDES

1-Generalities

Antisense oligonucleotides (ASOs) are short, single stranded oligonucleotides, typically around 20 nucleotides in length, which bind to the RNA through standard Watson-Crick base pairing.

ASOs interfere with gene expression by altering RNA function. In 1978, Zamecnik and Stephenson used ASOs for the first time to inhibit the replication of the Rous sarcoma virus in vitro (Stephenson and Zamecnik, 1978). Two decades after, the first FDA approved ASO was launched to treat cytomegalovirus (CMV) retinitis, an inflammation of the retina that can lead to blindness. The ASO fomivirsen was administered by intravitreal injection. Fomivirsen is a synthetic 21-nucleotide ASO designed to be complementary to a sequence in CMV mRNAs encoding proteins that are essential for CMV replication (Perry and Balfour, 1999).

2-Chemistry

The first ASOs that have been developed were composed of synthetic, short single stranded oligodeoxynucleotides of 8-50 nucleotides with unmodified phosphoribose backbone that bind by base pairing complementary to a target mRNA and induce its knockdown by endogenous endonuclease-mediated degradation, reducing the levels of deleterious proteins.

Unfortunately, the first generation ASOs showed limited clinical potential in vivo due to their rapid degradation by endonucleases and exonucleases (Rinaldi and Wood, 2018). Second and third generations of ASOs with modified backbones have an increase resistance to nucleases.

2.1-Backbone modifications

The phosphodiester backbone of unmodified oligonucleotides is highly susceptible to degradation by nucleases in vivo. The phosphorothioate (PS) bond substitutes a sulfur atom for a non-bridging oxygen in the phosphate backbone. This modification renders the internucleotide linkage resistant to nuclease degradation (Figure1). Moreover, the negative charge of the sulfur at physiological pH increases the lipophilicity of ASOs, facilitating binding to plasma proteins, to cell-surface proteins and uptake into cells (Crooke et al., 2021a),(Kandasamy et al., 2022).

Others second and third generation ASOs lack the phosphoribose backbone, such as the phosphorodiamidate morpholino oligomers (PMOs) in which morpholino rings replace the ribofuranose rings and the backbone is linked by phosphorodiamidates instead of phosphates (Figure 2). These ASOs are particularly resistant to nucleases. Neutral at physiological pH, they do not bind to proteins with significant affinity, meaning that high doses are needed for in vivo activity and that they are rapidly eliminated from the body. These ASOs are used in splicing modulation or translation inhibition (see 3- Mode of action). Other modifications of the backbone include peptide nucleic acids (PNAs) and locked nucleic acids (LNAs) modifications (Figure 2). PNAs have a charge-free polyamide scaffold of repeating N-(2-aminoethyl) glycine units, with the nucleobases attached via methylene carbonyl linkers, in place of the negatively charged ribose-phosphate backbone found in other oligonucleotides. Despite binding with great affinity to DNA or RNA sequences, PNAs show poor cellular penetration and they have fallen out of favor as a treatment modality. In locked nucleic acids (LNAs), the ribose 2'-O- and 4'-C-atoms of sugar moieties are connected via a methylene bridge. The effects of LNAs are mediated primarily through RNase H (see 3- Mode of action). Due to high specificity of binding and lower immunostimulatory potential as compared to PS ASOs, LNAs ASOs are currently in trials for therapies.

Recent ASOs were developed with phosphoryl guanidine (PN) backbones (Figure 1). PN linkages are neutral and more stable to nuclease degradation and have improved pharmacology and efficacy compared to PS-modified oligo nucleotides in a model of DMD (Kandasamy et al., 2022).

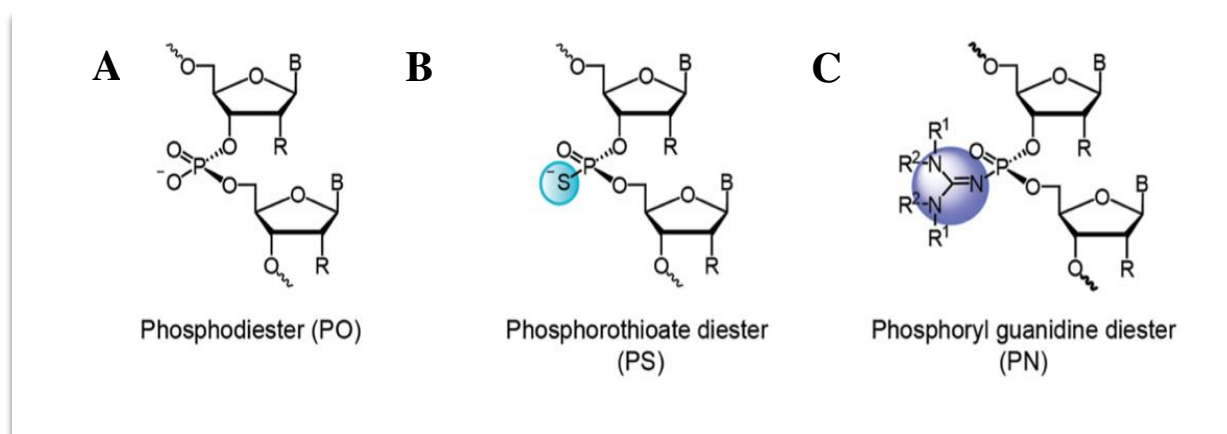


Fig. 1 | The distinct structural modifications of ASO's backbone. These include the phosphodiester (PO) backbone in (A), the phosphorothioate (PS) backbone where a sulfur atom replaces a non-bridging oxygen in (B) and the phosphoryl guanidine diester (PN) backbone where a phosphoryl guanidine-containing moiety or derivative replaces a non-bridging oxygen in (C). Adapted from (Kandasamy et al,2022)

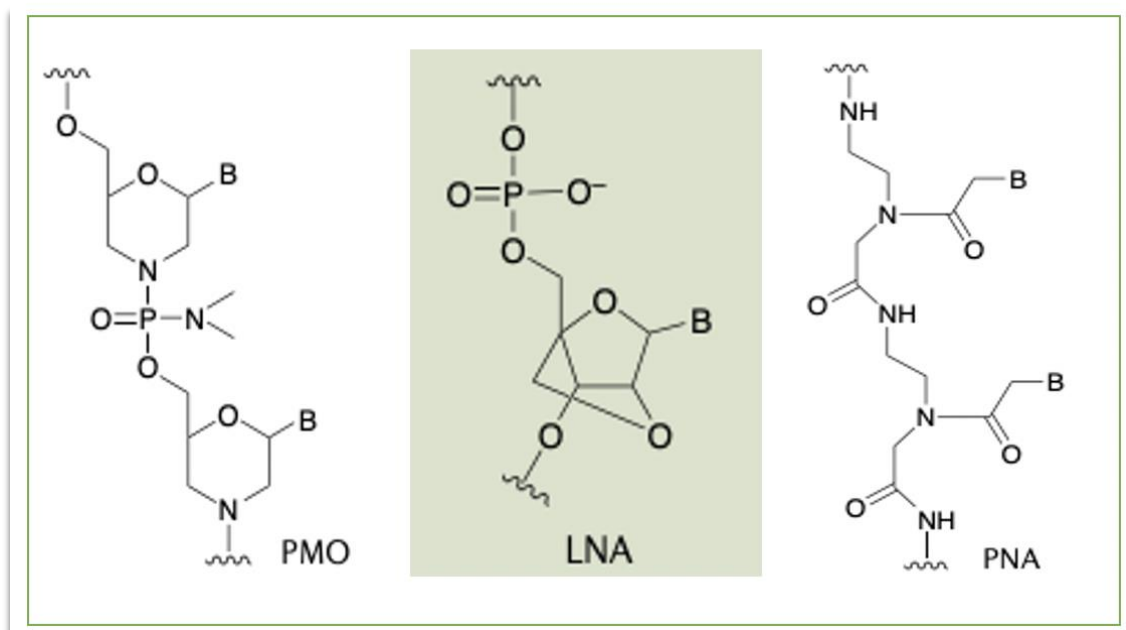


Fig. 2 | The Chemical modifications of ASOs backbone. These include PMO, phosphorodiamidate morpholino oligonucleotide; LNA, locked nucleic acid; PNA, peptide nucleic acid; *Adapted from (Kandasamy et al,2022)*

2.2-Stereochemistry

The phosphodiester linkage is achiral. However, the introduction of a sulfur atom in a PS linkage result in the generation of a chiral center at each modified phosphorous atom: the PS linkage is chiral with right-handed (Rp) and left-handed (Sp) isomers (figure 3). Consequently, a solution of PS-ASO of 20 nucleotides is a racemic mixture of the 219 possible permutations (that is, more than half a million different molecules). It has been shown that the physicochemical properties of each stereocenter are distinct in terms of hydrophobicity/ionic character, nuclease resistance, target affinity and RNase H activity. The racemic mixtures of oligonucleotide drugs contain many stereoisomers that are inefficient or even toxic. Identification of the most active stereoisomers would allow for lower doses with more efficacious compounds. The Wave Life Sciences company (Cambridge, Massachusetts) identified that a 3'-SpSpRp-5' 'stereochemical code' contained within the 'gap' region of gapmer ASOs (see 3 Mode of action, 3-1 Degradation of a target mRNA) renders the ASOs particularly potent with improved stability and specificity as compared to stereoisomer mixtures (Iwamoto et al., 2017).

The company has developed a scalable method of synthesizing oligonucleotides with defined stereochemistry at each PS linkage, and is advancing oligonucleotide drugs with defined stereochemistry for various indications (Roberts et al., 2020),(Iwamoto et al., 2017).

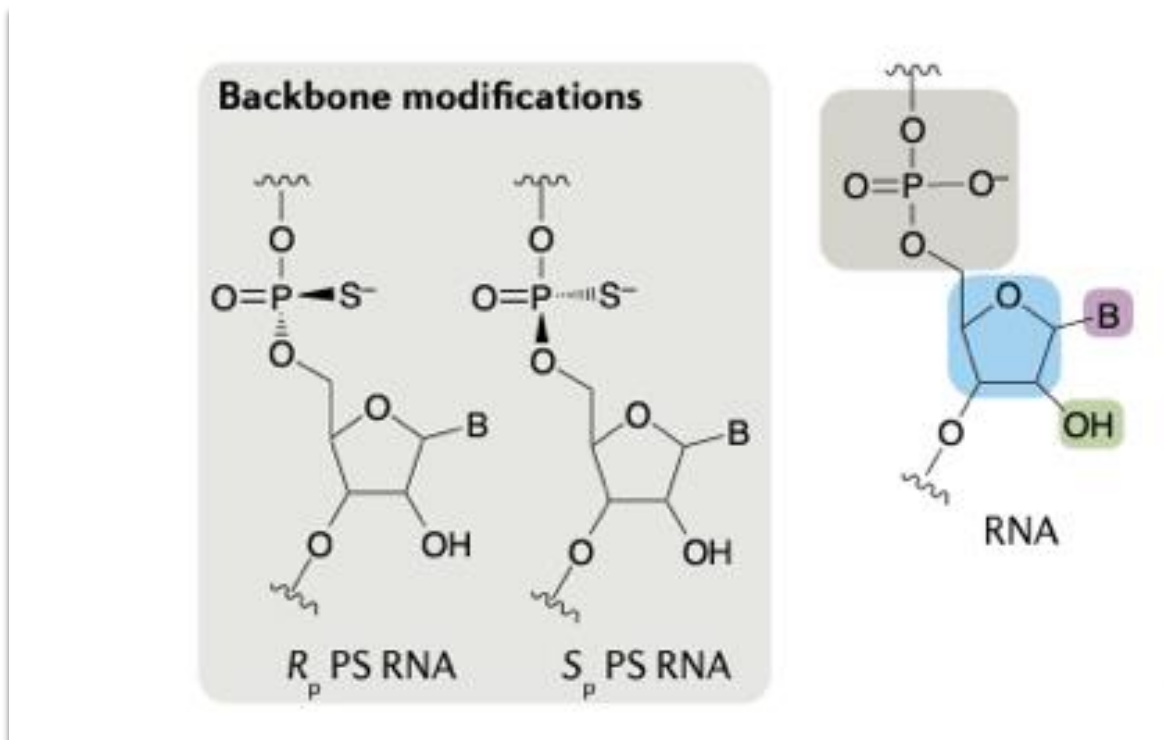


Fig. 3 | The Representation of PS stereoisomeric forms. The Introduction of an additional sulfur atom in a PS linkage results in the generation of a chiral center at each modified phosphorous atom, with the two possible stereoisomeric forms by designated S_p and R_p . Adapted from (Roberts et al,2020),

2.3-2' Ribose substitution

In addition to the phosphate inter-nucleotide linkage, the 2' position in the sugar is used by most nucleases to degrade nucleic acids. Replacement of the nucleophilic 2'-hydroxyl group of unmodified RNA by the 2'-O-methyl (2'-OMe) group or the O-methoxyethyl (2'-MOE) group, increases nucleases resistance, resulting in longer tissue elimination half-lives. These modifications increase the binding affinity for RNA and improves antisense oligonucleotide drug performance. Another modification, the 2'-constrained ethyl (2'-cEt) in which the 2' and 4' positions in the ribose are linked, increases similarly the ASOs performances (Crooke et al., 2021a), (Roberts et al., 2020) (Figure 4).

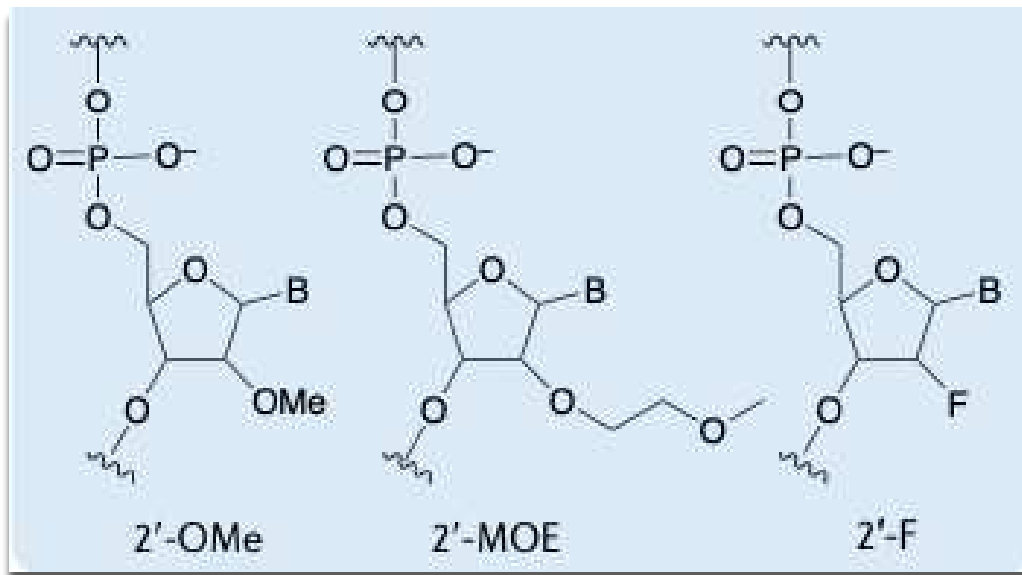


Fig. 4 | The Chemical modifications used in ASO. 2'-OMe, 2'-O-methyl; 2'-F, 2'-fluoro; 2'; 2'-MOE, 2'-O-methoxyethyl; Adapted from (Roberts et al,2020).

2.4-Other modifications

Other modifications are under investigation in order to enhance the delivery of ASOs to specific organs thereby increasing the drug performance while lowering the dose. For example, N-acetylgalactosamine (GalNAc) conjugation can be used to promote targeted delivery of oligonucleotides to the liver through binding to the asialoglycoprotein receptor expressed on hepatocytes (Crooke et al., 2021a)

Also, cell-penetrating peptides, sequences of 30 amino acids rich in arginine and lysine, can be covalently added to ASOs to increase their endocytosis in specific cell types. As an example, a glucagon-like peptide-1 receptor (GLP1R) agonist has been covalently bound to ASOs resulting in an increase of specific uptake of the ASOs in pancreatic insulin-secreting β -cells through internalization of GLP1R (Ämmälä et al., 2018).

3.Mode of action

ASOs bind to RNA through the Watson-Crick base pairing and modify splicing, translation or even induce the degradation of the RNA. Here, I will present here two mechanisms of action of ASOs associated with their use in therapy.

3.1-Degradation of a target RNA

Most of PS ASOs promote the degradation of their target RNA by the ubiquitously RNase H1 enzyme capable of hydrolyzing the RNA-DNA duplexes. RNase recognition of ASO is not aleatory, in fact a minimum of five consecutive deoxynucleotides, optimally eight to ten, are necessary to be an enzyme substrate. Flanking this unmodified deoxynucleotides core region or gapmer (Figure 5), several 2'-modified nucleotides such as 2'-MOE modified nucleotides increase the affinity of the ASO for its target RNA and also protect it from degradation by nucleases (Crooke et al., 2021a)

ASOs targeting mutant huntingtin and in particular RG6042 or Tominersen, act through this mechanism. This will be developed later (3-4-1).

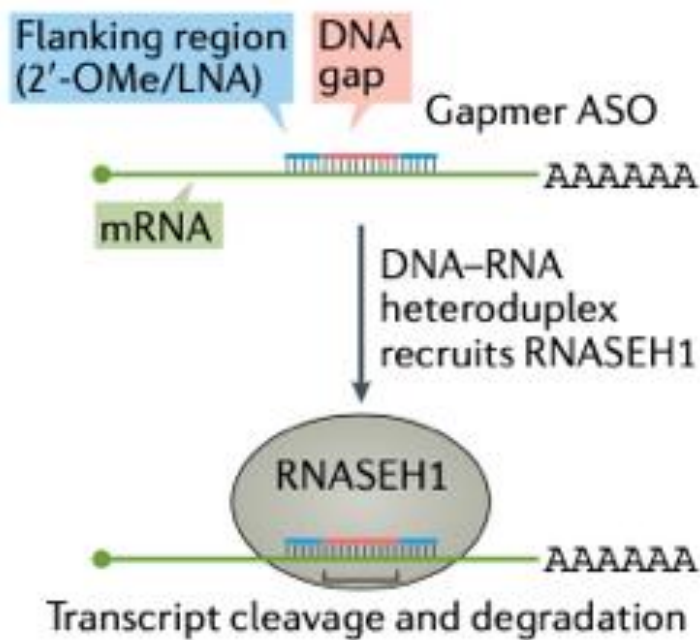


Fig. 5 | Degradation of a target RNA. Gapmer antisense oligonucleotides (ASOs) are composed of a central DNA segment with flanking regions that resemble RNA. These flanking regions typically contain modified bases like 2'-O-methyl (2'-OMe) or locked nucleic acid (LNA). These ASOs have a strong binding ability to specific RNA molecules. When the ASOs bind to their target transcripts, a hybrid structure is formed between RNA and DNA, which is then recognized by RNASEH1. As a result, the targeted RNA transcript is broken down and degrades. *Adapted from (Roberts et al,2020).*

3.2-Splice-switching ASOs

These ASOs allows the production of a desirable mRNA and the encoded protein by interfering with splicing sites in the pre-mRNA (Figure 6). I will here present the mechanism of

action of two FDA approved ASOs that bind to pre-mRNA i) to inhibit the splicing of exons (ex of nusinersen for the treatment of spinal muscular atrophy, and ii) to induce exon skipping (ex of eteplirsen for the treatment of Duchenne muscular dystrophy).

ASOs technology can upregulate the production of desirable mRNA and the encoded protein. Nusinersen, an ASO designed to restore the levels of the survival motor neuron (SMN) protein, is a successful example of such ASOs. It has been approved by FDA in 2016 for treating spinal muscular atrophy (SMA). SMA is a neuromuscular disorder characterized by progressive muscular atrophy and weakness. Infants with SMA type I (symptom onset ≤ 6 months) are unable to sit independently. Children with SMA type II (symptom onset 7–18 months) can sit unsupported, though some may lose this ability over time, and some may stand but are unable to walk independently. Children with SMA type III (symptom onset >18 months) can walk independently, but some may lose this ability over time. The disease is caused by loss-of-function of the SMN1 gene, which encodes a protein, SMN that has a key role in the formation and maintenance of neuromuscular junctions. The SMN2 gene does not compensate for the mutation as this locus generates 10% of the normal physiological levels of functional SMN protein and the majority of SMN produced from the SMN2 gene lacks exon 7, due to aberrant splicing. Patients suffer spinal cord and brainstem motor neuron degeneration. Nusinersen is a PS fully 2'-MOE-modified ASO that binds to SMN2 pre-mRNA to cause inclusion of exon 7 and generation of the full protein in motor neurons of the central nervous system (CNS). The ASO binds to intron 7 of the pre-mRNA by blocking intronic splicing site responsible for exon 7 exclusion. Clinical trials were successful and nusinersen (Spinraza) was approved by FDA in 2016. In infantile-onset SMA patients, nusinersen decreased the risk of death and permanent ventilation. Besides, some patients were able to sit independently and even to stand. Nusinersen is indicated for the treatment of children under 18 years with genetically confirmed spinal muscular atrophy (SMA) types I, II or III. Nusinersen (12mg, 5 ml) is injected intrathecally four times on days 0, 14, 28 and 63; followed by a maintenance dose of 12mg (5ml) once every 4 months thereafter (Darras et al., 2019), (Crooke et al., 2021a). Duchenne muscular dystrophy (DMD) is a rare, X-linked, fatal, degenerative neuromuscular disease that occurs in approximately 1 in every 3,500 to 5,000 males born worldwide. The disease is due to mutations in the DMD gene, which encodes dystrophin, a protein that anchors the cytoskeleton to the myofibre membrane. Partial or complete absence of dystrophin causes progressive muscle weakness and premature death. The most common mutation led to the loss of the DMD open-reading frame (ORF) resulting in a truncated form of the

protein. As the most crucial functional domains of dystrophin lie at the N and C terminal of the protein, ASOs were designed to allow the skipping of internal exons, which restores the expression of a dystrophin with its N and C terminal domains. PMOs showed higher levels of dystrophin protein restoration in the mdx mouse preclinical model as compared to 2'-OME oligonucleotides: they have higher serum stability and higher resistance to nuclease degradation in muscles. The PMO eteplirsen (Exondys 51) is the first drug approved to treat patients with DMD: eteplirsen triggers the excision of exon 51 during pre-mRNA splicing of the dystrophin RNA. Administered weekly by intravenous injection in young patient for a period of 4 years, the treatment seems to slow down the decline of ambulatory function as patients still walk as compared to untreated patients (Mendell et al., 2021). However, restoration of muscular dystrophin is moderate and clinical benefit is debated. This is probably due to a poor uptake of ASOs by muscle tissue. New ASOs are currently tested in mice: tricyclo-DNAs (tcDNA) in which an ethylene bridge is fused to a cyclopropane unit, have a high degree of dystrophin splicing correction in muscles (Relizani et al., 2017). A recent report shows the improved pharmacology and efficacy of stereopure PS-modified exon-skipping oligonucleotides containing phosphoryl guanidine (PN) backbones over PS-modified oligo nucleotides in the mdx mouse model of DMD (Kandasamy et al., 2022).

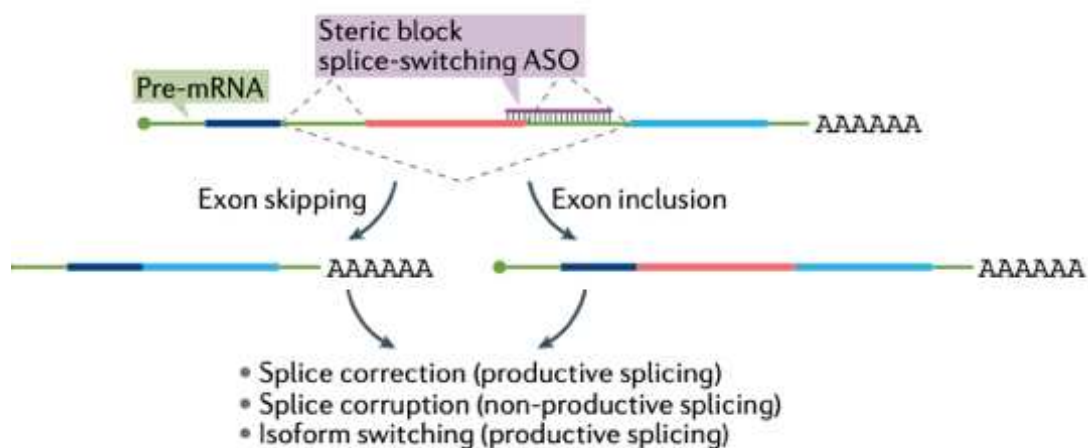


Fig. 6 | Splice switching ASO. Steric block oligonucleotides, which specifically target signals involved in pre-mRNA splicing, can manipulate alternative splicing by either encouraging the exclusion of certain gene segments or their inclusion (depending on the specific splicing signal being targeted). This manipulation leads to the generation of mature mRNA molecules that can undergo productive splicing, such as restoring the correct reading frame or switching to a different isoform. Alternatively, it can result in non-productive splicing, where an exon essential for protein function is removed and/or the translation reading frame is disrupted. Adapted from (Roberts et al, 2020).

3.3-Other mechanisms of action

Other mechanisms include A) inhibition of translation initiation (ASOs bind to regions close to AUG initiation codon and block the binding of the mRNA to the ribosomal machinery) (figure 7A). B) interference with upstream open reading frame that negatively regulate translation in order to activate protein expression (figure 7B), and C) binding to pre-mRNA sequences involved in cleavage and polyadenylation to modulate the use of polyadenylation sites, thereby altering the stability and levels of mRNA (figure 7C).

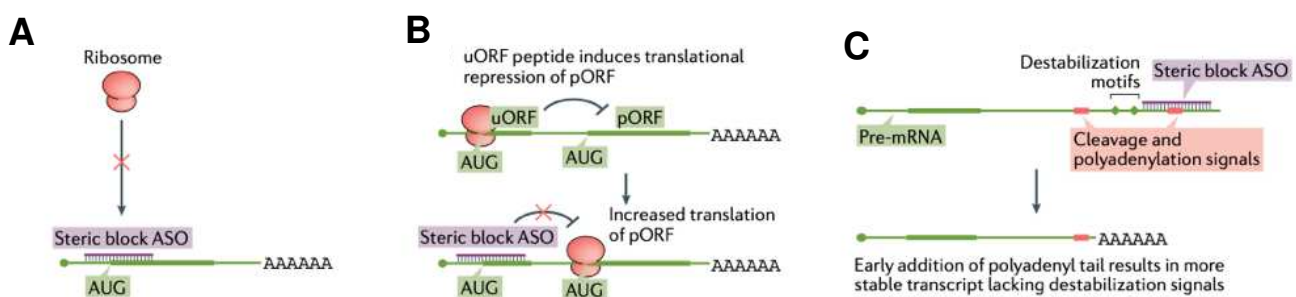


Fig. 7 | Other mechanism of ASO. (A) Steric block antisense oligonucleotides can interfere with translation initiation by specifically targeting the AUG start codon. **(B)** Additionally, they can disrupt the regulation of upstream open reading frames (uORFs) present in some transcripts, thereby activating the translation of the primary open reading frame (pORF). Another way steric block ASOs can exert their influence is by modulating transcript stability through the alteration of cleavage and polyadenylation signal usage. **(C)** For instance, targeting a distal polyadenylation signal with these ASOs leads to a preference for a weaker proximal polyadenylation signal. Consequently, the resulting shorter transcript lacks RNA destabilization signals, making it more stable, *adapted from (Roberts et al,2020)*.

4.Delivery

First generation ASOs were only administered intravenously due to large doses and pro-inflammatory effects. ASOs with 2'-MOE or 2-cET modifications have reduced pro-inflammatory effects and can be administered by subcutaneous or intramuscular injection. Oral formulations of ASOs are currently being developed. Some modifications of ASOs can promote the delivery to specific organs allowing per os administration. For instance, several GalNac modified ASOs (see 2-4 Other modifications) which target hepatocytes, are currently in clinical trials to treat nonalcoholic steatohepatitis, liver cancer and familial hypercholesterolaemia. As an example, ION449 (Ionis Pharmaceutical and AstraZeneca) is a GalNac-conjugated PS 2'-cEt ASO directed against the serine protease proprotein convertase subtilisin-kexin type 9 (PCSK9) which regulates

low-density lipoprotein (LDL) receptor levels. Elevated levels of LDL cholesterol (LDL-C) in the plasma are a risk factor in the development of cardiovascular diseases by increasing the formation of atherosclerotic plaques. PCSK9 is secreted by the liver and indirectly regulates plasma LDL levels by controlling the LDL receptor expression at the plasma membrane. In familiar forms of hypercholesterolaemia, gain-of-function mutations of PCSK9 leads to lower expression of LDL receptor at the cell surface which increases plasma levels of LDL cholesterol. The clinical phase 2b ETESIAN was concluded in April 2022: ION449 was able to lower liver-derived PCSK9 and to reduce blood cholesterol levels in patients injected subcutaneously monthly for 12 weeks.

Moreover, the feasibility of oral administration of ION449 was established in animal models and an oral formulation of ION449 is currently being evaluated in a Phase 1 study in healthy volunteers. Nevertheless, to date, the large doses required to reach clinical benefits hampers the commercially feasible oral administration.

Another difficulty related with dosage is the amount of tissue to be targeted by ASOs. This is particularly the case for skeletal muscles that represent approximately 40% of total body weight. For instance, restoration of muscular dystrophin following eteplirsen treatment is moderate despite repeated intravenous injections. Nevertheless, repeated injections of ASOs over a long period of time may prove efficient to promote a cumulative effect.

ASOs do not cross the blood brain barrier (BBB) hence systemic delivery is not an option. ASOs can be infused intrathecally, i.e., delivered into the subarachnoid space of the spinal cord. From here, the ASOs pass the pia mater to enter the parenchyma. Once in the brain, the ASOs diffuse broadly in the CNS and are readily taken up by neurons and glial. This route of delivery results in immediate high drug concentrations in the CSF and holds a promising application in neurodegenerative disease. For the treatment of SMA, nusinersen is administered intrathecally (3-2 Splice-switching ASOs). Amyotrophic lateral sclerosis (ALS) is a rare, fatal neurodegenerative disorder characterized by loss of motor neurons in the spinal cord and cortex, leading to loss of muscle function and death. Both sporadic and familial forms of the disease are observed with 2% caused by gain-of-function mutations in the super oxide dismutase 1 (SOD1) gene. The PS 2'-MOE ASO tofersen reduces levels of normal and mutant SOD1 mRNA via RNase H1 degradation. In 2021, results of the phase 3 clinical trial VALOR (Biogen Inc.) showed that intrathecal administration of tofersen (100 mg, three times the first month, then monthly) was able to slow down the progression of the disease (Ämmälä et al., 2018). ASOs developed for the treatment of HD are also injected intrathecally (Figure 8).

5. Cellular uptake

How ASO are taken into cells is not fully understood. Regarding PS-ASO, they are water soluble and bind to membrane bound protein and receptors. ASO are then internalized through endocytosis (Juliano, R., n.d.), (Sarah J Ross, n.d.). It has been described that PS-ASO interact with EGFR and are internalized with the receptor by clathrin-mediated endocytosis. PS-ASO traffic in early and late endosome together with EGFR (Wang et al., 2018). Therefore, it is easy to speculate that water soluble ASO may use the large repertory of tyrosine kinase receptors to enter the cells. Modifications of ASO have been performed to increase their cellular uptake. As an example, N-acetylgalactosamine (GalNAc) conjugation facilitates the uptake by hepatocytes that express the asialoglycoprotein receptor (Y. Kim et al., 2019).

Following endocytosis, ASOs contained in early endosomes are shuttled to late endosomes from where they are released into the cytosol. The process between the release from late endosome to hybridization to RNAs into the nucleus is unknown but may involve interaction with proteins (Crooke et al., 2021b). Release from late endosome is a rate-limiting step as ASO that stay trapped in the late endosome are degraded in lysosomes by endonucleases (Dowdy, 2023). Indeed, decreased ASO localization to lysosomes by depleting the lysosome transmembrane protein SID1 member 2 (SIDT2), increases the ASO activity in Hela and HEK293 suggesting that lysosome localized ASOs are inactive cells (Zhao et al., 2023). PS-ASOs are eliminated by glomerular filtration with a tissue elimination half-life of 2 to 4 weeks (Crooke et al., 2021b).

6. ASO in HD

As mutant HTT (mHTT) protein causes neurodegeneration, ASOs decreasing HTT protein production were developed in order to slow the progression of the disease.

6.1-Tominersen

6.1.1-Description

The first ASO developed and tested, targets both the HD mutant and the WT HTT mRNAs. Tominersen, also known as IONIS-HTTRx or RG6042, is a second-generation 2'-MOE PS ASO that was designed by IONIS Pharmaceutical to reduce concentrations of HTT mRNA. RG6042 is designed as a gapmer: its central region of 10 deoxyribose nucleosides is complementary to exon

36 of the HTT mRNA and is flanked by ribose nucleosides (5 per side) with 2' sugar modifications (replacement of the nucleophilic 2'-hydroxyl group by a O-methoxyethyl (2'-MOE) group to increase nucleases resistance) (Figure 8).

ct_oc_oa_ogTAACATTGACa_oc_oc_oac

Fig. 8 | Sequence of RG6042, aka tominersen. Lower-case letters indicate ribose nucleosides with 2' sugar modifications (substitution of 2'OH by 2'-O-methoxyethyl (2'-MOE)). Upper-case letters indicate deoxyribose nucleosides; o indicates phosphodiester (PO) linkage; non-labeled linkages indicate chiral phosphorothioate (PS) linkages (Wang et al., 2018)(Crooke et al., 2021b)(Sarah J Ross, n.d.).

6.1.2-Preclinical data

The ASO was tested in several HD mouse models (BACHD, YAC128, R6/2) as well as in the HD Hu97/18 mouse which expresses two copies of the full-length human HTT gene. Southwell and collaborators (Southwell et al., 2014) showed that a single injection of 300 µg of ASO in the right lateral ventricle of mice decreased HTT protein levels in the brain for 12 weeks with the exception of the cerebellum. The ASO-mediated therapy ameliorates behavior in HD mice models notably by reducing the anxiety and depressive-like phenotypes while preserving striatal neurons (Southwell et al., 2018).

6.1.3-Clinical Trials

In 2017, the completed phase 1/2a clinical trial of Tominersen (NTC02519036) in 46 patients with early manifest HD showed that 4 monthly doses of RG6042 administered intrathecally were able to lower the level of mHTT in the cerebrospinal fluid (CSF) by 40% at the highest dose tested (120 mg). The treatment was well tolerated (Tabrizi et al., 2019). The participants were invited to take part in the open-label extension study (NTC03342053) during which they received 120 mg tominersen every 4 or every 8 weeks during 15 months. At the end of the study, patients presented an increase of in the ventricular volume as well as an increase in neurofilament light (NfL) concentration in the CSF at day 141. Increase in NfL in the CSF is a biomarker of central nervous system neuro-axonal injury and reflects neurodegeneration in brain. However, the volumes of the caudate putamen and of the whole brain were not changed as compared to placebo.

Tominersen was further tested in a phase 3 clinical trial (NTC03761849). The highest dose (120 mg) was chosen to maximize target reduction in deep brain regions. The GENERATION HD1 trial enrolled 791 patients with manifest HD. Patients were distributed into three groups: the first group received tominersen every 8 weeks, the second group received tominersen every 16 weeks and placebo at alternate weeks, the last group was given placebo only every eight weeks. In March 2021, Roche has stopped the clinical trial for a lack of patient's treatment benefit through 17th months of treatment over placebo. The drug was not able to stop the natural course of the disease. Moreover, brain ventricles volume increased in every eight weeks regimen that may be indicative of accelerated neurodegeneration. The independent data monitoring committee, a group of outside experts tasked with ensuring the safety of trial participants and who have access to unblinded data, reported that patients treated with tominersen every 8 weeks performed worse on clinical rating scales and had higher frequencies of serious adverse events than the placebo.

Moreover, there was a significant increase in NfL concentration in the CSF. The second group of patients that received tominersen every 16 weeks, had functional ability, motor and cognitive function scores similar to placebo. Various hypothesis is proposed to explain the failure of tominersen. It is possible that peak drug concentrations are toxic and induce inflammation that damage neurons. High concentrations are required because tominersen must reach deep grey matter nuclei. It is also possible that lowering WT HTT levels may be deleterious for the survival of neurons despite studies reporting that partial lowering of WT HTT in the healthy brain is likely to be safe (Leavitt et al., 2020).

Nevertheless, lower doses of tominersen are now tested in a new open label phase 1 clinical trial termed GEN-PEAK (NCT04000594), which involves younger patients with lower disease burden. The purpose of this trial is to assess the pharmacokinetics and pharmacodynamics of tominersen.

6.1.4-Stereopure ASOs

The failure of tominersen creates a potential opportunity for other developers of Huntington's drugs. Wave Life Sciences and Takeda partnered on two antisense therapies that were tested in PRECISION-HD1 and 2 phase 1/2 trials. WVE-120101 and WVE-12012 are two stereopure gapmer ASOs with PN backbone directed against two single nucleotide polymorphism (SNP) (rs362307M SNP1 and rs362331 SNP2 respectively) SNPs unique to the mHTT mRNA. ASOs

were administered monthly via intrathecal injection up to 32mg to patients with early manifest HD. Both trials showed no statistically significant lowering of mHTT in the CSF (Kingwell, 2021). In September 2022, Wave Life Sciences announced positive update from phase 1b/2a SELECT-HD trial (NCT05032196) testing another stereopure ASO directed against SNP3. The ASO WVE-003 was administered to 18 participants at doses up to 90 mg. Participants enrolled at 30 mg, 60 mg and placebo had adequate follow-up to day 85 for biomarker analysis. At the time of analysis, none of the participants dosed with 90 mg had reached day 85 so this cohort was not included in the biomarker analysis. WVE-003 reduced mutant huntingtin (mHTT) protein levels by 22% in the CSF after one injection. Additionally, wild-type huntingtin (wtHTT) protein was preserved, which appears consistent with allele-selectivity. Additional single dose biomarker and safety data are expected in the first half of 2023.

7.ASO in cancer

There is no ASO-based anti-cancer therapy so far. However, ASOs are tested for the treatment of various solid and non-solid tumors and numerous clinical trials were attempted or are still running. For instance, LNA modified ASOs directed against metadherin have been tested experimentally. Metadherin promotes cancer progression by enhancing Wnt signaling in colorectal cancer and decreasing cytotoxic T cells infiltration while promoting immune checkpoint activation in lung cancer. These pro-cancer effects were abrogated upon treatment with the metadherin specific ASOs. The treatment was able to suppress tumor progression as well as liver and lung metastasis and increase the overall survival of mice the survival of mice (Shen et al., 2021). In an attempt to treat peritoneal metastasis of gastric cancer, Kanda and coll (Kanda et al., 2020) tested amido-bridged nucleic acid (AmNA)-modified ASOs to knockdown synaptotagmin XIII (SYT13). AmNA modified ASOs are analogs of locked nucleic acid (LNA) with modification of the amide bond bridged between the 2' and 4' carbons of the ribose. They show higher knockdown efficiency compared to LNA-modified ASOs. SYT13 activates focal adhesion kinase and downstream pathways that promote cell migration. Intraperitoneal administration of AmNA-modified anti-SYT13 reduced peritoneal nodules and increased life expectancy in a xenograft mouse model of metastatic gastric cancer. In estrogen receptor (ER)-positive subtype of breast cancer, targeting the circular RNA circPVT1 with an ASO, efficiently reduced tumor growth from MCF7 cells injected subcutaneously into nude mice (Yi et al., 2023).

Hyperactivation of tyrosine kinases receptors is a major cause of cancer as it activates the Ras-MAP kinase pathway, resulting in proliferation. Growth factor receptor-bound protein 2 (Grb2) is a cytosolic adaptor protein with a SH2 domain that binds the phosphorylated tyrosines of the activated tyrosine kinase receptors. Grb2 *recruits* SOS, a guanine nucleotide *exchange factor* that activates Ras. Suppression of Grb2 may prove to inhibit cancer progression. The BP1001 antisense oligonucleotide specific for Grb2, has been tested in a phase 1/1b clinical trial in patients with refractory or relapsed myeloid or lymphoblastic leukaemia, in monotherapy or in combination with low-dose cytarabine (ClinicalTrials.gov Identifier: NCT01159028) (Ohanian et al., 2018). A phase II study examines the effect of the ASO in association with venetoclax and decitabine on untreated acute myeloid leukemia (AML) patients (ClinicalTrials.gov Identifier: NCT02781883). Another phase 1/1b trial is examining the safety and tolerability of intravenous injected BP1001 in patients with advanced or recurrent solid tumors (ovarian and fallopian tubes cancer), as a single agent or in association with paclitaxel (ClinicalTrials.gov Identifier: NCT04196257). No data related to cancer progression/regression is available so far.

Regarding glioma, the ASO trabedersen (AP 12009) specific for the mRNA of the human transforming growth factor beta 2 (TGF-beta-2) was infused intratumorally using convection-enhanced delivery (CED) in adult patients with recurrent or refractory anaplastic astrocytoma or secondary glioblastoma. This trial was ended in 2014 and no conclusive data were published (ClinicalTrials.gov Identifier: NCT00761280). Earlier, a phase IIb study had shown an advantage in long-term survival for anaplastic astrocytoma patients treated with trabedersen when compared with standard chemotherapy (ClinicalTrials.gov Identifier: NCT00431561 (Bogdahn et al., 2011),(Uckun et al., 2019).

Mogilevsky and coll identified that the pre-mRNA of the enzyme Mnk2 is alternatively spliced to produce two isoforms Mnk2a and Mnk2b that acts as a tumor suppressor or a pro-oncogene respectively. Mnk2a levels are downregulated while Mnk2b levels are upregulated in glioblastoma. The authors designed an ASO that blocks the access of the splicing machinery to the Mnk2 pre-mRNA resulting in the conservation of the exon 14a and the production of the Mnk2a isoform at the expense of the pro-oncogenic isoform Mnk2b. This ASO decreased colony formation capacity and U87 cancer cell survival *in vitro* and sensitized tumor cells to TMZ (Mogilevsky et al., 2018). To our knowledge, there is no clinical trial testing this ASO.

An antisense oligonucleotide against IGF type 1 receptor (IMV-001) is currently tested in newly diagnosed glioblastoma. (ClinicalTrials.gov Identifier: NCT04485949). The results of the

Phase Ib Clinical Trial are published (Andrews et al., 2021)(ClinicalTrials.gov: NCT02507583). The treatment consists in treating resected glioma cells with IMV-001 and irradiation prior to encapsulation in biodiffusion chambers and grafting in the abdomen. The patients are then subjected to Stupp treatment. In patients with methylated MGMT promoter, the ASO was well tolerated and the progression free survival as well as the overall survival were increased as compared to patients treated with the Stupp protocol only.

Expression of the MGMT enzyme is a major hurdle in GBM therapy. To block MGMT mRNA translation, antisense morpholino oligonucleotides specific to MGMT were tested in human cells expressing MGMT, notably the glioma cell line T98G. The ASOs decreased MGMT levels and sensitized the cells to TMZ (Ambady et al., 2017). *In vivo*, irradiation increased the uptake by endocytosis of the ASO in a D283 medulloblastoma orthotopic xenograft model resulting in MGMT downregulation and increased efficacy of TMZ (Ambady et al., 2022).

More recently, an ASO was tested in a mouse model of the diffuse midline glioma with H3K27M mutation. This a pediatric form of glioma with a dramatic outcome. It is due to a mutation in the histone 3.3 gene *H3-3A*, replacing lysine 27 with methionine (K27M) which results in global reduction in di- and trimethylation of all histone H3 proteins. PS-MOE-ASOs of 20 nucleotides were designed to directly target the mutant *H3-3A* mRNA and tested *in vitro* and *in vivo* in a mouse model of the disease. The intracerebroventricular administration of the ASO increased H3K27me3 abundance, reduced tumor volume and induced neuronal and glial differentiation of tumor cells, increasing the overall survival of the animals (Zhang et al., 2023).

4- THESIS OBJECTIVES

Despite the current treatments for glioblastoma, the prognosis remains grim. The alkylating agent TMZ remains the most effective agent *against malignant glioma*. However, tumor cells and in particular GSCs develop resistance to the treatment, which account, at least in part, for the relapse and eventually the incurability of the disease. There is a pressing need to find a solution to improve the response to therapy and overcome TMZ resistance.

My thesis project aims at testing a potential new therapy for glioblastoma. This therapy relies on the downregulation of the protein huntingtin (HTT) in tumor cells in order to sensitize them to

TMZ. HTT exerts prosurvival effects in neurons and has been shown to participate to the DNA damage response. Past work at the lab showed that HTT regulates breast cancer metastasis suggesting that HTT could also modulate tumorigenesis. As TMZ induces cancer cell death by damaging the DNA, I hypothesized that downregulating HTT may exacerbate tumor cells apoptosis by exacerbating DNA damage. I used the RG6042 antisense oligonucleotide (ASO) developed by Ionis Pharmaceutical to downregulate HTT, both the mutant and the wt forms. *In vitro* tests were performed on glioma/glioblastoma cell lines to answer the following questions:

- I. Are glioma/glioblastoma cells lines more sensitive to TMZ when depleted of HTT?**
- II. How does downregulation of HTT induce cell death?**
- III. Is the MGMT status relevant to sensitization by HTT depletion?**

I then tested the strategy on proneural (PN) glioma stem cells obtained from a patient. The positive results obtained were an incentive to examine the strategy *in vivo* on nude mice bearing with human PN tumors.

Altogether, the results of my thesis showed that ASO specific to HTT holds promises to enhance the response of glioblastoma cells to TMZ.

RESULTS

PART I

Overcoming Temozolomide Resistance in Glioblastoma by targeting huntingtin with antisense oligonucleotides.

Rayane Kassem¹, Leslie Ratié¹, Camille Lafage¹, Eric Denarier¹, Emanuelle Huillard², Frédéric Saudou¹ and Sandrine Humbert^{1,2, *} and Fabienne Agasse^{1, *}

¹Univ. Grenoble Alpes, Inserm, U1216, CHU Grenoble Alpes, Grenoble Institut Neurosciences, 38000 Grenoble, France

²Institut du Cerveau-Paris Brain Institute, Sorbonne Université, Inserm, CNRS, Hôpital Pitié-Salpêtrière, Paris, France

*Correspondance :

Email: fabienne.agasse@univ-grenobles-alpes.fr; sandrine.humbert@icm-institute.org

ABSTRACT

Glioblastoma multiforme (GBM) is a deadly brain tumor with limited treatment options. The alkylating agent temozolomide (TMZ) significantly increases the median survival of patients. However, tumor cells develop resistance to TMZ. In this study, we explored a novel therapeutic approach to sensitize cells to TMZ. Huntingtin (HTT), which mutated form causes Huntington disease, is a prosurvival protein widely expressed by neurons. HTT is also expressed in glioblastoma. We downregulated the huntingtin (HTT) protein using an antisense oligonucleotide (ASO) that directs the HTT mRNA for RNase degradation. We treated ASO-transduced glioma cell lines with TMZ and found that HTT-depletion exacerbates TMZ-induced DNA double-strand breaks, poly(ADP-ribose) polymerase 1 (PARP1) cleavage, cell cycle arrest in G2 and eventually cell death by apoptosis. ASO-mediated HTT downregulation also sensitized patient-derived glioma stem cells (GSCs) that express the DNA repair enzyme O6-methylguanine-DNA methyltransferase (MGMT). Moreover, HTT-downregulation decreases stem cell properties namely expression of the proneural stem cell marker DLL3 and self-renewal. *In vivo*, in immunocompromised mice injected subcortically with MGMT expressing GSCs, a single intracerebroventricular administration of ASO followed by oral TMZ treatment delayed significantly proliferation, expression of DLL3 and tumor growth as compared to mice receiving a scramble oligonucleotide. The ASO-mediated HTT downregulation strategy to sensitize GSCs to TMZ holds promise for the treatment of glioblastoma.

Keywords: glioma stem cells, temozolomide, glioblastoma, huntingtin, antisense oligonucleotide, MGMT.

Highlights

- ASO directed against huntingtin (HTT) mRNA decreased HTT levels in glioma cells. ASO-mediated depletion of HTT increases TMZ-induced DNA damage and cell death in glioma cells.
- ASO-mediated depletion of HTT decreases self-renewal of glioblastoma stem cells.
- *In vivo*, ASO-mediated depletion of HTT associated to TMZ treatment delays tumor growth.
- ASO-mediated HTT depletion holds promise for the treatment of TMZ resistant glioblastoma.

INTRODUCTION

Glioblastoma are malignant primary brain tumors derived from glial cells. Based on histological appearance, the World Health Organization (WHO) classifies the different types of gliomas into prognostic grades ranging from I to IV. The most malignant astrocytic glioma, glioblastoma multiform (GBM) (WHO grade IV), represents more than 50 % of all gliomas and is the most common malignant primary brain tumor. Even though GBM is quite rare with a global incidence rate of 3.17 per 100,000, it remains significant due to the short median survival time of 3 years from the time of diagnosis. GBM affects mainly adults with a median age at diagnosis of 64 years. Males are more commonly affected with an incidence rate almost 1.6 times higher than in females.

The main reasons for the poor prognosis are the late stage of diagnosis combined with the poor efficiency of the treatments. Moreover, GBM lesions are large at the time of diagnosis. The tumor mass presents a high degree of regional heterogeneity in terms of cells and genetic mutations, and tumor cells rapidly invade the surrounding brain tissue. The majority of GBM harbors mutations in the retinoblastoma (Rb), p53 and receptor tyrosine kinase (RTK) pathways, promoting cell survival and proliferation (Chen et al., 2012). These mutations seem to be a core requirement for GBM pathogenesis. Standard therapy for GBM consists of surgery followed by radiotherapy and/or chemotherapy (Stupp et al., 2009). Tumor resection is never achieved due to its highly infiltrative nature. The main chemotherapeutic agent used for treatment of GBM is the alkylating agent temozolomide (TMZ). Taken orally, TMZ causes cytotoxicity by forming methyl-adducts, such as N3-methyladenine (N3-meA), N7-methyl-guanine (N7-meG), and O6-methyl-guanine (O6-meG), resulting in DNA strand breaks and subsequent cell death. However, some tumor cells escape TMZ cytotoxicity by expressing the protein O6-methylguanine-DNA methyltransferase (MGMT) which removes the TMZ-induced methylation of O6-methylated guanine bases. Other components of the DNA repair pathway can contribute to TMZ resistance such as deficiency in the Mismatch Repair (MMR) pathway, overexpression of Base Excision Repair (BER) proteins and Poly ADP-ribose polymerase (PARP) activation. Altogether, deregulation of these DNA repair mechanisms contributes to chemoresistance to TMZ.

There is a crucial need in identifying molecular targets to overcome TMZ resistance of GBM. Targeting the protein huntingtin (HTT) may prove to be a valid strategy. HTT is a scaffold protein of 348 kDa, widely expressed in adult tissues including the brain. HTT is mutated in the neurodegenerative disorder Huntington's disease (HD) (Saudou and

Humbert, 2016a). HTT exerts many functions not only in neurons but also in cancer cells (Moreira Sousa et al., 2013). In HD female patients, breast cancer prevalence is lower however its prognosis is poorer compare to non-HD breast cancer patients (Thion et al., 2015). Breast cancer cells expressing HD mutant HTT are more metastatic than non-HD breast cancer cells. It was shown that mutated HTT impairs the endocytosis of the epidermal growth factor receptor family member HER2. The resulting over activation of the receptor at the cytoplasmic membrane stimulates the PI3K/Akt pathway and increases proliferation and survival of breast cancer cells (Moreira Sousa et al., 2013). In healthy breast tissue, HTT is important in the establishment of E-cadherin adherens junctions between mammary epithelial cells (Elias et al., 2015) and HTT expression is downregulated in microinvasive human breast cancer (Thion et al., 2015). Moreover, high-grade gliomas express HTT that localizes in the cytoplasm where it interacts with p53, whereas in low-grade gliomas, HTT is found in the nucleus (Simeone et al., 2014). In neurons, nuclear phosphorylation of HTT by CDK5 is an early response to DNA damage and is associated with DNA damage response; unphosphorylatable HTT is toxic and triggers p53-mediated cell death (Anne et al., 2007). Altogether, these observations point out to a central role of HTT in the biology of cell cancer.

Here, we hypothesized that HTT plays a role in glioblastoma chemoresistance to TMZ. Our working hypothesis is that reducing HTT levels may impair the DNA repair mechanisms and sensitize GBM to DNA damaging agents such as TMZ. We decreased HTT levels in human glioma cell lines using previously described antisense oligonucleotides (ASOs) (Kordasiewicz et al., 2012; Southwell et al., 2014). We show that downregulation of HTT sensitizes glioma cells to TMZ, delays tumor growth in vivo and increases survival of tumor-bearing mice.

MATERIAL AND METHODS

Database analysis

Expression of HTT in tumors and overall survival according to HTT mRNA levels were investigated using The Cancer Genome Atlas (TCGA) and the Rembrandt (REpository for Molecular BRAin Neoplasia *DaTa*) datasets through the website Gliovis <http://gliovis.bioinfo.cnio.es/>.

Glioblastoma cells culture

U251, T98G and U87 human glioblastoma cell lines were cultured in complete culture medium containing Dulbecco's modified eagle medium (DMEM, #31966047, ThermoFisher) supplemented with 10% of fetal bovine serum (FBS, #CVFSVF0001, Eurobio) and 1% of penicillin/streptomycin (PS, #15140148, ThermoFisher). Cells were grown in a 95% air-5% CO₂ humidified incubator at 37°C. N13-1520 proneural (PN) glioma stem cells (GSCs) were obtained from a human glioblastoma resection (MTA with Gliotex, Institut du Cerveau, Paris). Cells were grown in DMEM-F12 (#31331093, ThermoFisher), 1% B27 (#17504044, ThermoFisher), 1% PS supplemented with 20 ng/ml epidermal growth factor (EGF, #53003018) and 20 ng/ml basic fibroblast growth factor (FGF2, #13256029, ThermoFisher).

Cell transfection with ASOs

Adherent glioblastoma cells were seeded at the desired density (30-70% confluency) the day before the transfection. N13-1520 glioblastoma stem cells (GSCs), obtained after dissociation of the neurospheres with Accutase (#A1110501, ThermoFisher), were adhered on poly-D-Lysine (20µg/ml, #7886, Merck) and laminin (20µg/ml, #L2020, Merck) for 24h prior transfection. Cells were transfected for 24h with antisense oligonucleotides (ASOs) at a final concentration of 200 nM using lipofectamine and following manufacturer's instructions (#11668019, ThermoFisher). Antisense oligonucleotides used are specific to *huntingtin* mRNA: RG6042

(<C*TCAG*>t*a*a*1*a*t*t*g*a*1*<ACCA*C>), PH1

(<T*CTCT*>a*t*t*g*c*a*c*a*t*t*<CCAA*G>), PH2

(<C*TCGA*>c*t*a*a*a*g*c*a*g*g*<ATTT*C>), PH3
(<C*CTGC*>a*t*c*a*g*c*t*t*t*a*<TTTG*T>). An ASO of a scramble sequence is used as control: SCR (<A*CATG*>a*c*c*g*c*a*c*t*c*a*<CTAT*A>) (all purchased from Eurogentec) (Southwell et al., 2014). Capitalised nucleotides are RNA nucleotide with 2'-O-(2-methoxy)ethyl modifications. Lowercase letters represent DNA bases. Phosphorothioate internucleotide linkage are represented by a *. 1 represents 5-methyl deoxycytosine. The transfection medium containing the ASOs was removed from the cells and replaced by fresh medium. The cells were used 48h after transfection and detached from the culture with trypsin 0.05% (#25300062, ThermoFisher).

TMZ and Lomustine treatment

Temozolomide (TMZ, #PHR1437, Sigma-Aldrich) was prepared as 50 mM stock solution in 33.3 mM citrate monohydrate (#C7129, Merck) (Nygren and Eksborg, 2012). TMZ solution was sonicated. Lomustine (CCNU, #L5918, Merck) was prepared as 50 mg/ml stock solution in absolute ethanol. Both TMZ and lomustine solutions were filtrated and frozen at -20°C until further use.

MTT Cell viability assay

Glioblastoma cells were seeded in 96-well plates and treated with increasing concentrations of TMZ and lomustine for 48h and 20h respectively. Each dilution was tested in triplicate. The medium was then replaced by fresh medium. N13-1520 cells were incubated for 48h with TMZ. Fresh medium was added to dilute twice the TMZ. MTT assay was performed 72h following the treatment by adding the MTT probe at 0.5 mg/ml (#M6494, ThermoFisher). Optical density (OD) was read on a microplate reader (Pherastar FS, BMG Labtech) at 490nm. The inhibitory concentration 50 (IC50) designates the concentration of TMZ and lomustine for which cell viability is decreased by 50% as compared to the control condition. Cells were thereafter treated for 48h at the IC50 defined for each cell lines when transfected with RG6042 to assess sensitization and dissect the mechanisms involved.

Protein extraction and Western blot

Cultured cells were washed with PBS and lysed with RIPA buffer (150 mM NaCl, 20 mM Tris-HCl pH 7.5, 1 mM EDTA, 2.5 mM sodium pyrophosphate, 1 mM EGTA, 1 % sodium deoxycholate and 1 % NP-40) supplemented with protease inhibitors (1/100, #P8340, Merck) and phosphatase inhibitors (1/100, #P5726, Merck). The soluble protein fraction was collected after centrifugation (21,000 g, 10 min at 4°C) and was kept at -80°C until further use. Protein concentration was measured by the BCA assay (#23228, ThermoFisher). Proteins (20 µg total) were diluted in SDS-PAGE sample buffer [6X concentrated: 350 mM Tris, 10% (w/v) SDS, 30% (v/v) glycerol, 0.6 M DTT, 0.06% (w/v) bromophenol blue] then boiled 5 min at 95°C and loaded on a 7% and 15% acrylamide/bisacrylamide gel. Proteins were transferred into PVDF membranes (polyvinylidene difluoride, #IPVH00010, Merck) during 2h30 min with constant current of 320 mA. PVDF membranes were blocked in Tris buffer containing 5% bovine serum albumin (BSA) in 0.1% Tween (TBS-T) for 1h at room temperature (RT) and probed overnight at 4°C with the following antibodies: rabbit monoclonal anti-HTT antibody (1/1000, D7F7, #5656S, Cell Signaling Technology), mouse monoclonal anti-vinculin antibody (1/10000, #V9131, Merck), rabbit polyclonal anti-MGMT antibody (1/1000, #2739S, Cell Signaling Technology), rabbit monoclonal anti-PARP-1 antibody (1/1000, #9532, Cell Signaling Technology), rabbit anti-phospho-histone H2A.X (Ser139) (γH2Ax, 1/1000, #2577, Cell Signaling Technology), rabbit anti-DLL3 (1/1000, #ab229902, Abcam), rabbit anti-phosphoChk2 (Thr68) (1/1000, #2197, Cell Signaling Technology), mouse anti-β-actin (1/10000, #A5441, Merck), rabbit anti-Cdc25C (1/1000, #4688S, Ozyme), mouse anti-Cdc25A (1/1000, #CC085-E, Enzo Life Science) membranes were washed 3x10 min with TBS-T and incubated for 40 min at RT with horseradish peroxidase (HRP)-conjugated secondary antibodies: goat anti-rabbit IgG (H+L) (1/2000, #511380, Jackson ImmunoResearch) and goat anti-mouse IgG1 (1/2000, #1070-05, Southern Biotech). Proteins of interest were detected using a chemiluminescent substrate (ECL SuperSignal™ West Pico PLUS Chemiluminescent Substrate, #34580X4, Merck) and the membranes were imaged on a Chemidoc imaging system (Biorad).

Caspase 3/7 activity

Apoptosis was evaluated in transfected cells plated in 96 well-plates treated cells and treated for 48h with TMZ at IC50 then washed with a fresh medium for 72h.

Luminescence detection of caspases activity was measured using the Caspase-Glo® 3/7 Reagent assay kit (#G8091, Promega) and following the manufacturer's instructions. Luminescence (relative light units) was read on a microplate reader (Pherastar FS, BMG Labtech) at 485nm and 520nm. Each condition was tested in triplicate.

Flow cytometry for Annexin V and propidium iodide (PI)

Apoptosis was determined using the Annexin V and propidium iodide (PI) staining-based FITC Annexin V Apoptosis Detection Kit (#556547, BD Biosciences). SCR and RG6042 cells treated in the absence or the presence of TMZ at IC50 for 48h were incubated with fluorescein isothiocyanate (FITC)-conjugated Annexin V and propidium iodide for 30 min and analyzed by flow cytometry (BD Accuri C6; Beckman Coulter Inc., Fullerton, CA). The assays were performed in triplicate with 20 000 events analyzed in each replicate. Data were analyzed using the FCS Express 7 software (<https://denovosoftware.com/>)

Cell cycle analysis

SCR and RG6042 cells treated for 48h with TMZ at IC50 then washed with a fresh medium for 72H, were fixed in 70% ice-cold ethanol and stored at 4°C until analysis. Cells (10^6) were stained in PBS supplemented with 2% FBS, RNase (100 µg/ml, #R6513, Merck), Triton X-100 (0.01%) and propidium iodide (PI, 10 µg/ml, #P4170, Merck) for 30 min at 37°C. Stained nuclei (15 000 events) were analyzed on a *BD Accuri C6*. FCS Express 7 software was used to assess cell cycle distribution. The assays were performed in triplicate.

Sphere assay

N13-1520 cells transfected with either SCR or RG6042, were seeded at a density of 6 cells/µl in serum-free medium supplemented with 5 µM of EGF and FGF2 and treated in

the absence or the presence of TMZ at IC50 (25 μ M). Cells were allowed to form neurospheres for 6 days. Cells were dissociated with Accutase and plated (cells/ μ l) in complete serum-free medium for 6 supplemental days. Secondary neurospheres were counted at the end of the culture session. Within each experiment, conditions were tested in triplicate.

RNA extraction and quantitative real-time PCR (qPCR)

Total RNA was extracted using the NucleoSpin RNA extraction kit (#740955, Macherey-Nagel). Total RNA was quantified by spectrophotometer on a NanoDrop One (ThermoFisher, #AZY1707341). RNA samples (1 μ g) were retrotranscribed using the iScript Ready-to-Use cDNA supermix (#1708840, Biorad). cDNAs were diluted 1:10 and submitted to qPCR with SsoAdvanced SYBR Green supermix (#1725272, Biorad). Primers used are hypoxanthine phosphoribosyltransferase 1 (HRPT1) (Cat# QT00059066, Qiagen), TATA box binding protein (TBP) (#QT00000721, Qiagen), 60S ribosomal protein L13 (RPL13) ((Cat# QT00067963, Qiagen), HTT (# QT00090937, Qiagen) and MGMT (# QT01004416, Qiagen). The PCR program consisted of a 95°C for 2 min for the first step; 40 cycles of 95°C for 10 sec, 55°C for 15 sec and 72°C for 10 sec for the second step; 95°C for 1 min, 60°C for 30 sec and 95°C for 30 sec for the last step. The foldchange quantification of target genes was calculated with the $2^{-\Delta\Delta C_t}$ method. Geometric averaging of TBP, HRPT1 and RPL13 was used as internal control. Each sample is analyzed in triplicate within an experiment. Data were analyzed from at least 6 independent experiments and presented as the mean \pm SEM.

In vivo experiments

The xenotransplantation was performed at the Optimal platform (Institute for Advanced Biosciences, IAB, Grenoble) by trained engineers. All animal experiments were performed in accordance with the institutional guidelines of the European Community (EU Directive 2010/63/EU) for the use of experimental animals and were approved by an ethic committee (Cometh38 Grenoble, France) and the French Ministry of Higher Education and Research under the reference: APAFIS#33138-2021090715215532 v6.

NMRI nude female mice (20, from Janvier labs) of 1.5 months of age were injected stereotactically with 140 000 cells resuspended in 2 μ l of PBS. Cells were injected into the

putamen at the injection coordinates previously described by Pollard and collaborators (Pollard et al., 2009). Briefly, mice were anesthetized by inhalation of 4% isoflurane (#792632, ISO-VET, Piramal Critical Care) and placed on the stereotaxic apparatus. Anesthesia was maintained during the surgery by inhalation of 2% isoflurane. The incision was made with a scalpel after disinfection of the skin with povidone-iodine (#B40600, PDI). Once the coordinates determined (1mm rostral and 2mm lateral to Bregma), the skull and the meninges were pierced using a 26G needle. The 26G needle placed on top of a Hamilton microsyringe (10ul) was lowered 3mm deep in the brain. The cells were infused at a steady velocity of 5µl per min thanks to a syringe driver. The needle was kept in place for 10 minutes to ensure minimal reflux along the needle tract upon removal. The hole on the skull was sealed with Horsley's bone wax (# 1029754, B. Braun Medical, France) and the skin incision was closed using surgical glue (Vetbond, #2629277). The total procedure time was ~20 mins per mouse. During all the procedure, eye gel (Ocry-gel, TVM Lab) was applied to avoid desiccation and the mice temperature was kept by placing the animals on a warm pad. Mice Behavior and body weight were then monitored 2 times a week.

Tumor growth was evaluated once a week using noninvasive bioluminescence imaging. Five minutes before imaging, vigil mice received an intraperitoneal injection of 150 µg/g of D-luciferin (Promega, France# P1041), were then anesthetized (isoflurane 4 % for induction and 2 % thereafter) and placed in the imaging system (IVIS Lumina, PerkinElmer, USA). The body temperature of the mice was maintained on a heating mat at 37°C. The mice wake up spontaneously a few seconds after the gas was stopped. Quantification and analysis were carried out using Living Image software (PerkinElmer, USA) by drawing regions of interest on the brain area. 81 days after implantation, mice were distributed into two experimental groups (n=10 mice/group) so that the mean and standard deviations of the bioluminescence signals from the brain were the same in the two groups. Mice were injected with ASOs. The procedure used was similar to the one described for the xenograft except that the ASOs were injected in the lateral ventricle contralaterally to the hemisphere where the tumor cells were injected (-0.3mm caudal and 1mm lateral to Bregma, 1.8mm deep). ASOs (300 µg) were resuspended in 10µl of PBS and injected at the speed of 5µl per minute. TMZ was prepared in McIlvaine buffer pH3 and administered by gavage to mice in a bolus of 200 µl. The mice were treated with two cycles of TMZ: for 26 days (from day 87 to day 112) at the dose of 10 mg/kg and for 12 days (from day 129 to day 140) at the dose of 30 mg/kg. Non-treated mice received a

bolus of McIlvaine buffer. All mice were sacrificed 3 weeks after the last gavage. Mice were euthanized by intraperitoneal injection of Exagon (400 mg/ml, 1 ml/kg, Richter Pharma) and intracardiacally perfused with PBS followed by cold paraformaldehyde (PFA) 4%. Brains were harvested, post-fixed for 2h in PFA 4%, cryopreserved in 30% sucrose and embedded in OCT Compound (VWR International).

Histology and immunolabeling

Brains were cryosectioned (35 μ m) and slices were kept in free-floating at -20°C in anti-freeze solution (18.75% (w/v) sucrose, 37.5% (v/v) ethylene glycol, 0.05% (w/v) sodium azide in PBS). Brain slices were mounted onto Superfrost plus adhesion glass slides (J1800AMNZ, EpreDia), let to dry and adhere overnight, and then rehydrated for 5 min in PBS. Slices were rinsed and blocked in 3% normal donkey serum in PBS containing 0.3% Triton X-100 and 1% BSA for 1h at room temperature then incubated overnight at room temperature in 1:500 of rabbit anti-Ki67 (# ab16667, Abcam), 1:750 of mouse anti-human nuclear antigen (anti-HuNu, MAB1281, Merck), and rabbit anti-human DLL3 (1/200, #71804S, Cell signalling Technology). Slices were rinsed, incubated in 1:250 of Cy2 Donkey Anti-Rabbit IgG (H+L) (#711-225-152), Cy5 Donkey IgG anti-Mouse IgG (H+L) (#715-175-150), or Cy3 Donkey Anti-Rabbit IgG (H+L) (#711-165-152) (all from Jackson ImmunoResearch) for 1h. After 3 rinses in PBS, slices were incubated with Hoechst 33342 (2 μ g/ml, #H3570, ThermoFisher) in PBS mounted, rinsed again 3 times in PBS and mounted in Dako mounting medium (#S3023, Dako). Images were acquired on the Axio Scan.Z1 slide scanner (Colibri.7; 20X objective; Zeiss).

Quantification and statistical analysis

For western blots, densitometry analyses of Pico signals were performed using NIH Image J software. Data are represented as mean \pm SEM of at least 4 independent experiments. Protein levels were displayed as percentage standardized to Vinculin and β actin. Statistical significance was assessed using the one-way ANOVA followed by Dunn's multiple comparisons test or the two-way ANOVA followed either by Tukey's multiple comparisons test or Sidak's multiple comparisons test. For caspase 3/7 activity and flow cytometry experiments, data are represented as mean \pm SEM of at least 4 independent experiments. Statistical significance was assessed using the two-way

ANOVA followed by Tukey's multiple comparisons test. For the MTT cell viability assay, measurements of optical densities without TMZ treatment (0 μ M) were normalized at 100%. Nonlinear regression (log(inhibitor) vs. normalized response) was applied to compare the fits between TMZ-treated and non-treated curves. Data are represented as mean \pm SEM of at least 3 independent experiments. For qPCR, fold change (log₂) mean \pm SEM of at least 6 independent experiments are presented. Statistical significance was assessed using the Kruskal-Wallis test followed by Dunn's multiple comparisons test. For the sphere assay, data are represented as mean \pm SEM of triplicates in 4 independent experiments. Statistical significance was assessed using the two-way ANOVA followed by Tukey's multiple comparisons test. In histology experiments, for each brain analyzed, 4 slices encompassing the tumor were treated in immunohistochemistry. For analysis of Ki67/HuNu and DLL3/HuNu cells were analysed using an in-house automated program on the NIH ImageJ software (National Institute of Health and the Laboratory for Optical and Computational Instrumentation, United States (Schneider et al., 2012)). Only cells positive for both Ki67 or DLL3 and HuNu were considered as positive for Ki67 or DLL3 respectively, as HuNu is a specific stain for human nuclei so only stains the human tumor cells. Three regions of interest (ROI) measuring 50 μ m \times 50 μ m each, were sampled on the tumor and another separate ROI on the contralateral striatum. Using NIH Image J software, double-positive stained cells were counted with the minimum and maximum size for nuclei was set at 20 μ m and 150 μ m respectively. The average positive cells were then calculated and used for analysis. Data bars are represented as mean \pm SEM of at least 5 animals in each condition. Statistical significance was assessed using non-parametric Mann-Whitney U test.

For all experiments, statistical significance was set to $p < 0.05$. All analyses were conducted using GraphPad Prism 9.0. Complete statistical analyses related to Figures 2, 3, 4, 5, 6 and to supplemental Figure S2 are listed in the Supplemental Excel Table S1.

RESULTS

Huntingtin is expressed in glioma.

HTT is an ubiquitous protein found in neurons as well as in glial cells in the normal brain tissue (Saudou and Humbert, 2016a). Using bioinformatics analysis of public brain tumor datasets, we found that the *huntingtin* gene was significantly less expressed in glioblastoma as compared to the normal tissue (*Tukey's HSD*, *** $p < 0.001$) (Figure 1A). There was a differential expression of HTT regarding the molecular subtypes of glioblastoma: HTT was more expressed in the proneural subtype as compared to the classical subtype (*Tukey's HSD*, *** $p < 0.001$) (Figure 1B). The glioma cytosine-phosphate-guanine (CpG) island methylator phenotype (G-CIMP), which comprises IDH1 mutant tumors, expressed higher levels of HTT mRNA as compared to non-G-CIMP GBMs consistent with the fact that most of the proneural (PN) tumors are G-CIMP (*Tukey's HSD*, * $p < 0.05$) (Figure 1C). We also observed that expression of high levels of HTT mRNA was an unfavorable prognostic factor in term of overall survival in male GBM patients (Wilcoxon ** $p = 0.005$) (Figure 1D) while there was no difference when considering both genders together (data not show). Altogether, these data show that HTT is expressed in GBM.

Downregulation of HTT sensitizes glioma cell lines to TMZ.

We investigated the role of HTT in chemoresistance in the glioma cell lines U87, U251 and T98G. All three cell lines are derived from human GBM and show specific characteristic according to their morphology (epithelial-like for U87; pleomorphic/astrocytoid-like for U251, fibroblastic-like for T98G), MGMT status (all negative except T98G), tumorigenicity after engraftment in immunodeficient mice (all tumorigenic except T98G), p53 status (all mutated except U87) and gene mutations in canonical cancer pathways. All three cell lines express HTT.

We used the antisense oligonucleotide ASO RG 6042 to downregulate HTT in glioma cell lines. This ASO is a short DNA sequence that binds to the HTT mRNA and directs its catalytic degradation through the action of endogenous RNAase H.

Cells were transfected with the ASO RG6042, or a scramble sequence of nucleotides (SCR), or treated only with the transfection reagent lipofectamine (CT for control). HTT

levels were quantified 48h after lipofection by western blot (Figure 2A). RG6042 downregulated by 70 % HTT protein levels in all the three cancer cell lines, attesting of the efficacy of the ASO in silencing HTT (one-way ANOVA, *** $p < 0.001$, RG6042-treated cells as compared to CT). Next, we evaluated the half maximal inhibitory concentration (IC_{50}) to TMZ in HTT-depleted GBM cells lines. SCR and RG6042 transfected cells were treated with increasing concentrations of TMZ for 48h followed by 72h in fresh complete medium. Cell survival was assessed by MTT at the end of the culture session (Figure 2B). The IC_{50} to TMZ was decreased by at least 50% in each cell lines following downregulation of HTT as compared to SCR transfected cells (Nonlinear fit, log(inhibitor) vs. normalized response) comparison of fits, **** $p < 0.0001$). These results show that HTT mediates chemoresistance to TMZ and that targeting HTT with ASO may improve TMZ efficacy in eradicating cancer cells.

We performed similar experiments with Lomustine, another alkylating agent. IC_{50} to Lomustine decreased in the three cell lines by at least 50% in HTT-depleted cells (Nonlinear fit, log(inhibitor) vs. normalized response, comparison of fits, **** $p < 0.0001$) (Figure 2C) suggesting a general sensitization effect of RG6042 to alkylating agents.

RG6042 exacerbates TMZ-induced G2 arrest.

TMZ treatment induces G2/M cell cycle arrest (Hirose et al., 2001). We asked whether HTT depletion would alter TMZ-induced G2/M cell cycle arrest. Cancer cells, either transfected with SCR or RG6042, were treated for 48h with TMZ at IC_{50} established previously by MTT (Figure 2B) in RG6042 treated cells namely 40 μ M for U87 and U251 and 800 μ M for T98G. The treatment was changed for fresh medium 72h before propidium iodide DNA staining and quantification by flow cytometry. TMZ increased G2M cell cycle arrest in SCR (two-way ANOVA, * $p < 0.05$ and ** $p < 0.01$ in U87 and U251 respectively as compared to SCR non-treated cells) and RG6042 transfected cell (two-way ANOVA, ## $p < 0.01$ and #### $p < 0.0001$ in U87 and U251 respectively as compared to RG6042 non-treated cells). In T98G SCR- cells, TMZ tend to stop the cell cycle in G2M without reaching the level of significance while in RG6042 treated cells, this effect was significant (two-way ANOVA, # $p < 0.01$ as compared to RG6042 non-treated cells). In all three cell lines, the TMZ-induced cell cycle arrest was further exacerbated in RG6042 cells as compared to SCR cells (two-way ANOVA, \$\$ $p < 0.01$ in U87 and U251 RG6042 cells treated with TMZ as compared to RG6042 non treated cells; \$ $p < 0.05$, in

T98G RG6042 cells treated with TMZ as compared to RG6042 non treated cells) (Figure 3A). Arrest in G2 occurred at the expense of S and G1 phases of the cell cycle. Statistical data are exhaustively presented in supplemental table 2.

As DNA damage induces cell cycle arrest by the activation of checkpoint kinases, we evaluated phosphorylation of checkpoint kinase 2 (pCHK2) at threonine 68 by ataxia telangiectasia mutated (ATM), a sensor of toxic DNA double strand breaks. SCR and RG6042 cells were treated with TMZ at IC₅₀ for 48h and then washed with fresh media for 72h. Concentrations of half of the IC₅₀ (later called ½ IC₅₀) were also tested to assess whether the mechanisms due to RG6042-mediated HTT depletion occurred at these lower concentrations. Western blotting was performed at the end of the culture session. TMZ-mediated increase of pCHK2 was more prominent in RG6042 cells as compared to SCR cells: at ½ IC₅₀ in U87 (two-way ANOVA, ***p<0.001) and at both ½ IC₅₀ and IC₅₀ in U251 (two-way ANOVA, **p<0.01, ***p<0.001) (Figure 3B). *For T98G, our preliminary results showed no effect on phosphorylation of CHK2. Further western blots will be conducted.*

These results show that RG6042 treatment exacerbates TMZ-induced cell cycle arrest by checkpoint kinase 2 phosphorylation.

RG6042 increases TMZ-induced apoptosis.

We next determined whether RG6042 increases apoptosis triggered by TMZ. Cancer cells from the three cell lines were either transfected with SCR or RG6042 and subsequently incubated for 48h with TMZ at IC₅₀. After 72h in fresh medium, apoptosis was determined by quantifying the activity of caspases 3 and 7. Apoptosis was significantly increased in RG6042 cells treated with TMZ by at least 40% as compared with SCR cells in the three cell lines (two-way ANOVA, *p<0.05, **p<0.001) (Figure 4A).

We further assessed apoptosis in flow cytometry by measuring propidium iodide (PI) uptake and Annexin V staining. The percentages of Annexin V positive cells (both propidium iodide negative and positive, representing cells in early and late apoptosis respectively) were increased in RG6042 cells treated with TMZ as compared to SCR cells in all three cell lines (two-way ANOVA, ***p<0.001) (Figure 4B) demonstrating that HTT depletion exacerbates TMZ-induced apoptosis.

Downregulation of HTT sensitizes cells to TMZ-induced DNA damage.

DNA methylation by TMZ induces DNA double-strand breaks over cell cycles, which are extremely cytotoxic. The increase of pCHK2 (Figure 3B) in RG6042 cells suggests that HTT downregulation increased the susceptibility of TMZ-cells to DNA double-strand breaks. Western blot detection of the DNA double-strand breaks marker γ H2Ax was performed in TMZ-treated cells (Figure 5A). Quantifications showed an increase in γ H2Ax in RG6042 cells treated with the IC₅₀ dose of TMZ as compared to SCR cells in all three cell lines (two-way ANOVA, ***p<0.001, ****p<0.0001). In T98G cells, DNA double-strand breaks were also induced with TMZ at a dose of 1/2 IC₅₀ (two-way ANOVA, **p<0.01).

Severe DNA damage eventually leads to cleavage of PARP-1 and cell death. We quantified PARP-1 cleavage in SCR and RG6042 cells treated with TMZ and found that PARP-1 is cleaved in the three cell lines previously depleted in HTT when treated with TMZ at IC₅₀ (two-way ANOVA, **p<0.01). In RG6042 T98G cells, 1/2 IC₅₀ of TMZ also induced PARP-1 cleavage as compared to SCR cells (two-way ANOVA, ***p<0.001) (Figure 5B).

Downregulation of HTT with RG6042 sensitizes proneural glioma stem cells to TMZ.

As proneural glioma stem cells expressed higher levels of HTT mRNA as compared to the molecular subtypes of GBM, we sought to determine whether RG6042 could also sensitize these cells to TMZ. We treated N13-1520 proneural GSCs with SCR and RG6042 ASOs and determined the levels of the HTT protein by immunoblotting. RG6042 decreased HTT (one-way ANOVA, *** p<0.001, RG6042-treated cells as compared to CT) (Figure 6A). Interestingly, the proneural GSCs marker DLL3 decreased in HTT-depleted cells (one-way ANOVA, *** p<0.001, RG6042-treated cells as compared to CT) indicating that the cells may lose their stem cells identity upon HTT removal (Figure 6A).

Next, we evaluated the IC₅₀ to TMZ in SCR and RG6042 cells by MTT assay (Figure 6B). The IC₅₀ was decreased by 50% in N13-1520 from 53.20 μ M to 26.82 μ M (Nonlinear fit, log(inhibitor) vs. normalized response) comparison of fits, ****p<0.0001). TMZ at IC₅₀ exacerbated caspases 3 and 7 activation in N13-1520 suggesting an increase in apoptosis (two-way ANOVA, ***p<0.001) (Figure 6C). As for the glioma cell lines, increase in TMZ-induced double strand breaks was found in HTT-depleted PN cells at 1/2

IC₅₀ and IC₅₀ (two-way ANOVA, **p<0.01, ***p<0.001) (Figure 6D). Altogether, RG6042 increased sensitization of proneural GSCs to TMZ by increasing DNA damage and apoptosis.

Proneural N13-1520 cells propagate *in vitro* as clonal aggregates of cells, called neurospheres. We exposed single cell suspensions of SCR and RG6042 N13-1520 cells with TMZ at IC₅₀ and let them develop as primary neurospheres. Cells dissociated from neurospheres were then allowed to grow as secondary neurospheres for 6 to 8 supplemental days. We counted the number of secondary neurospheres. RG6042 altered self-renewal capacity of proneural GSCs as less secondary spheres were obtained in RG6042 cells as compared to SCR cells (two-way ANOVA, ****p<0.0001). Treatment with TMZ at IC₅₀ decreased the formation of secondary spheres both in SCR and RG6042 cells however this decrease was more prominent in RG6042 as compared to SCR proneural cells (two-way ANOVA, ***p<0.001) (Figure 6E). Depletion of HTT further altered TMZ-induced self-renewal capacity of proneural GSCs.

RG6042 delays tumor growth in TMZ treated mice.

To determine whether RG6042 could sensitize GBM tumors to TMZ *in vivo* (Figure 7A), we injected the striatum of nude mice with firefly luciferase expressing N13-1520 cells (Day 0). Tumor growth was monitored weekly by bioluminescence and SCR and RG6042 ASOs were injected into the ventricle when steady increase in tumor growth was monitored (Day 82). Mice were treated with two cycles of TMZ administered by gavage (see supplemental figure 1 for weight monitoring along the treatment). Tumor sizes were estimated from bioluminescence signal (Figure 7B) and were expressed as mean percentages of signals measured before ASO injection (day 81) (Figure 7C). In Figure 7B, representative mice from the SCR and RG6042 treated groups are shown. The bioluminescence signal indicated that tumor growth is delayed in RG6042 mice. This is particularly obvious after the first cycle of TMZ. The delay in tumor growth was accentuated by the second cycle of TMZ gavage with a higher dose of TMZ.

Quantification of the bioluminescence signals showed smaller tumors in RG6042 as compared to SCR treated mice (Figure 7C) after the first cycle of TMZ and more noticeably after the second cycle of TMZ treatment. In both SCR and RG6042 treated mice, TMZ at 10 mg/kg reduced tumor growth but tumor growth of the RG6042 group was further slowed down as compared to the SCR group (two-way ANOVA, ** p=0.004).

At day 129, tumors of the RG6042 treated mice increased by 516% while tumors of the SCR treated mice increased by 912% and this difference was highly significant (two-way ANOVA, *** $p=0.0003$). After the end of the second cycle of TMZ at 30 mg/kg, tumor growth of the RG6042 group was further slowed down compared to the SCR group (two-way ANOVA, ** $p=0.0017$). At day 163, tumors of the RG6042 treated mice increased up to 1184% while tumors of the SCR treated mice increased up to 2092%. This difference was highly significant (two-way ANOVA, *** $p=0.0004$).

Together, these results show that RG6042 potentiates the cytotoxic effect of TMZ *in vivo*.

RG6042 decreases GSC proliferation and proportion of DLL3 GSCs in TMZ-treated mice.

Mice were sacrificed 3 weeks after the last gavage and brain slices were stained for the proliferation marker Ki67 and the human nuclear antigen (HuNu) to detect tumor cells. N13-1520 cells were found widely spread across the entire brain. We evaluated the proportion of Ki67 positive tumor cells within the ipsilateral striatum (referred to as the tumor in the following) where the tumor cells were implanted and in the contralateral striatum. Ki67 is expressed in cycling cells, which allows quantification of proliferation. As shown in Figure 7D, there was a significant decrease in the amount of Ki67⁺ cells (expressed as a percentage of HuNu⁺ cells) in the tumor as well as in the contralateral striatum (Mann-Whitney U test, ** $p=0.0043$ for both) in RG6042 treated mice as compared to SCR.

Considering that RG6042 decreases DLL3 expression in N13-1520 cells (Figure 6A) and that proliferation is diminished in RG6042 mice treated with TMZ, one can hypothesize that RG6042 reduces GSCs in TMZ-treated tumors. Indeed, there was a significant decrease in the percentage of DLL3⁺ GSCs (expressed as a percentage of HuNu⁺ cells) in tumor as well as in the contralateral striatum (Mann-Whitney U test, ** $p=0.0043$ for both) of RG6042 mice treated with TMZ as compared to SCR (Figure 7E). These results show that the RG6042 treatment decreased proliferating CSGs as well as the proportion of GSCs, which may account for the delay in tumor growth. Whether RG6042 induces tumor cells differentiation remains to be determined.

FIGURES

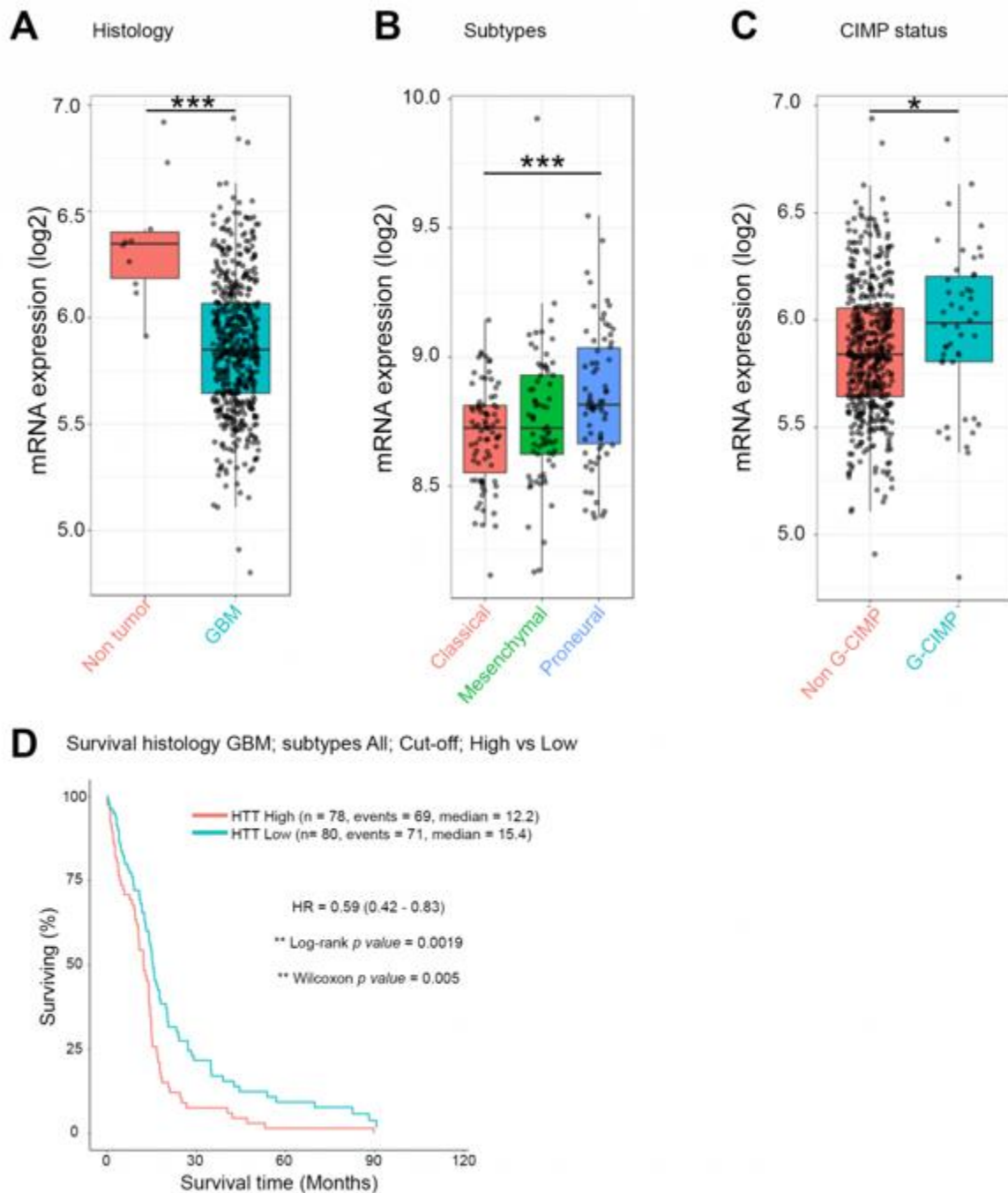


Figure 1. *HTT* gene expression in GBM. *HTT* mRNA expression in GBM (A) as compared to non-tumor brain tissue (TCGA GBM dataset), (B) regarding the molecular subtype of GBM (Rembrandt dataset), and (C) according to the methylation status G-CIMP versus non-G-CIMP (TCGA GBM dataset). (D) Kaplan-Meier survival curves of GBM male patients according to *HTT* mRNA expression (TCGA GBM dataset). * $p < 0.05$, *** $p < 0.001$.

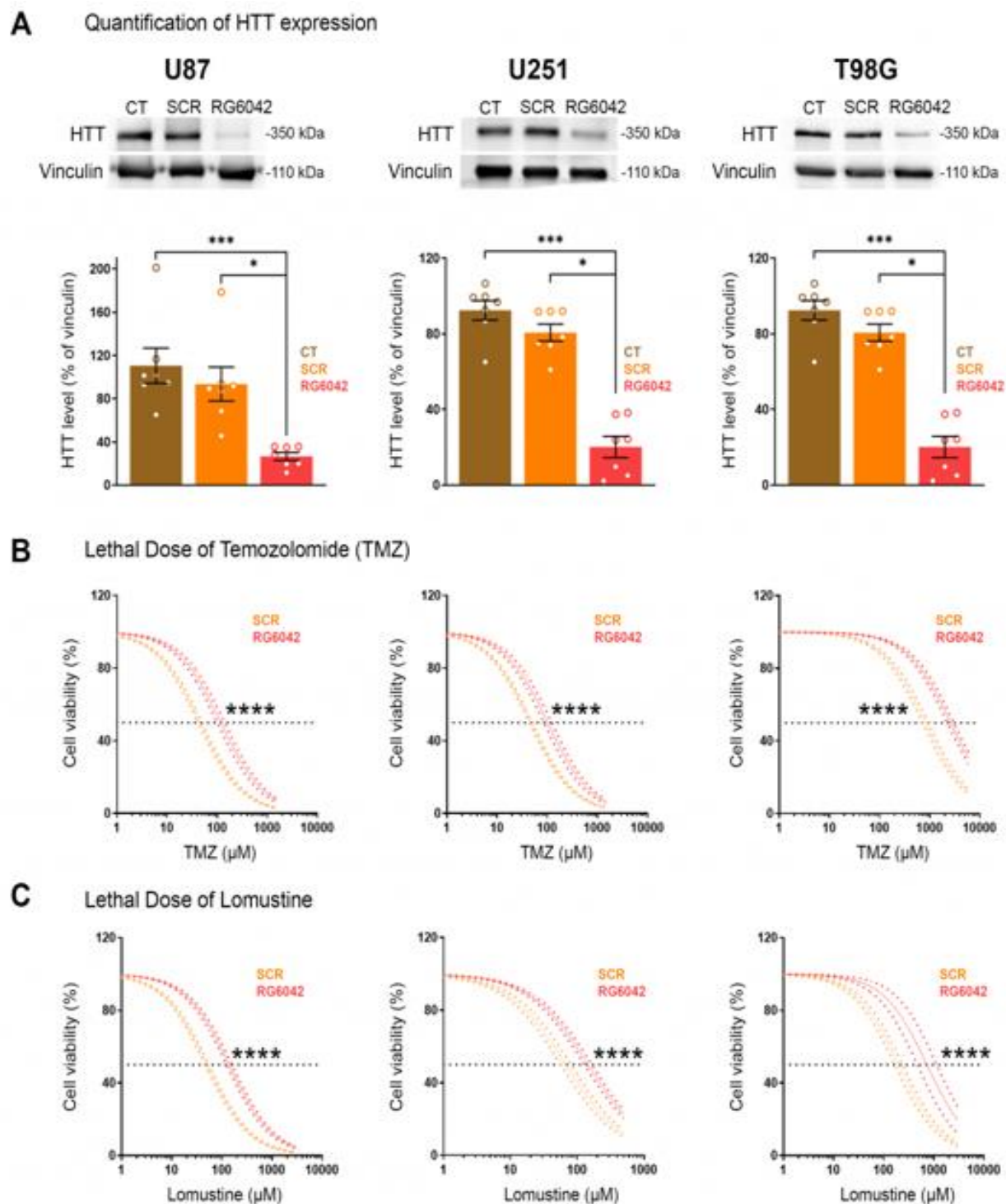


Figure 2. Downregulation of HTT with RG6042 sensitizes glioblastoma cells to TMZ. HTT expression was determined in lipofectamine treated cells (Control) and cells transfected with 200nM of either RG6042, an antisense oligonucleotide directed against the HTT mRNA, or with a scramble oligonucleotide (SCR). (A) Representative western blots for each cell line (U87, U251 and T98G) and respective quantifications. Vinculin serves as loading control. Mean \pm SEM, * p <0.05, ** p <0.01, *** p <0.001. (B) MTT cytotoxicity assay with TMZ in SCR and RG6042 transfected cells from the three different cell lines. (C) MTT cytotoxicity assay with lomustine in SCR and RG6042 transfected from the three cell lines. The data are expressed as the percent of cell survival. Mean \pm SEM, **** p <0.0001.

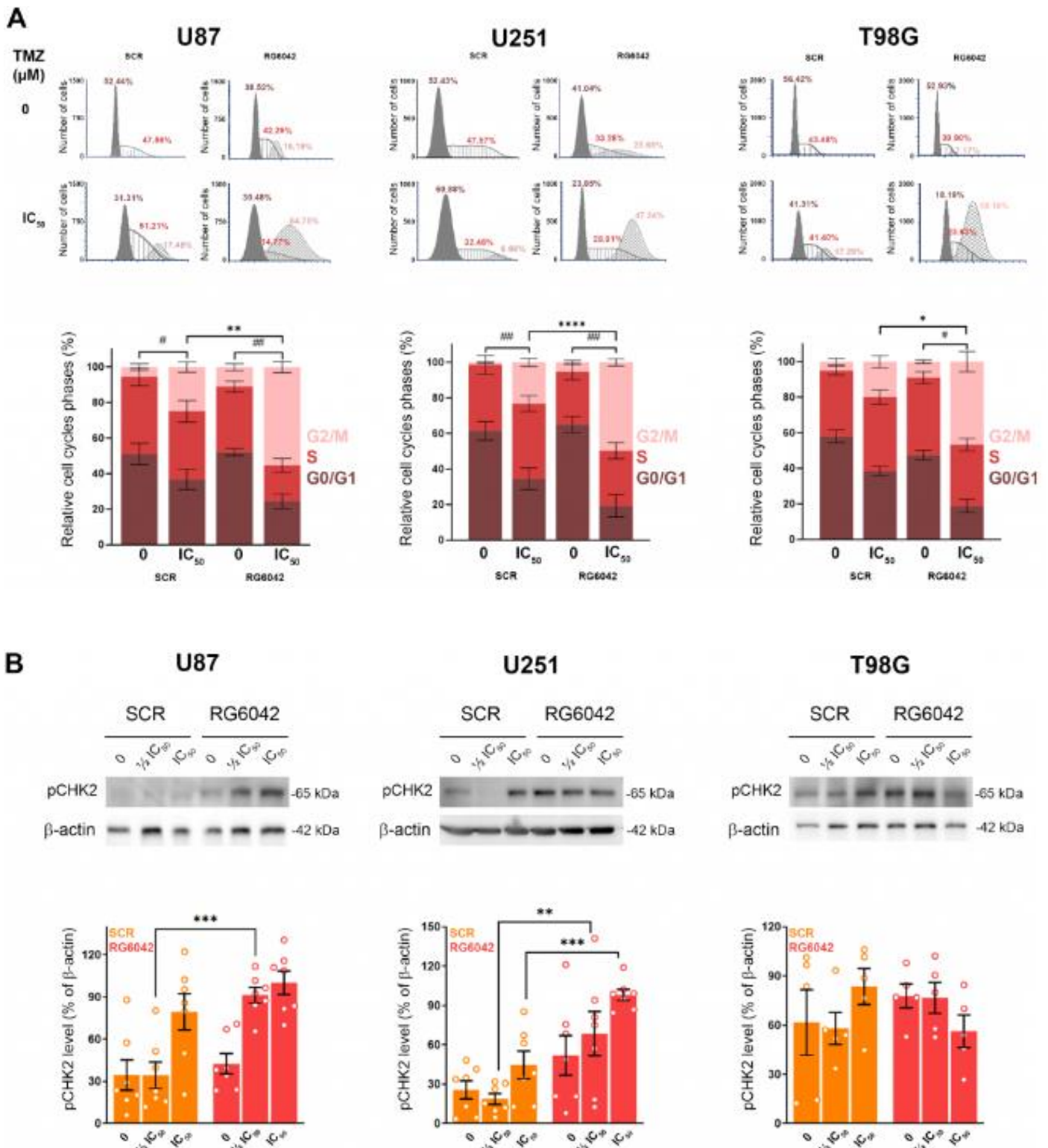
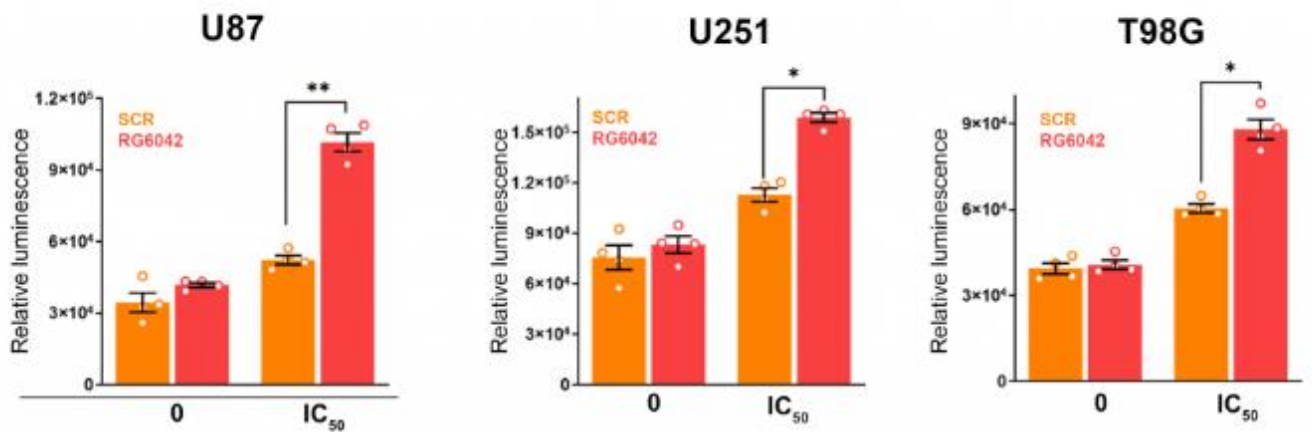


Figure 3. RG6042 exacerbates TMZ-induced G2 arrest. (A) Propidium iodide mediated evaluations of DNA content in SCR and RG6042 treated cells, incubated without (0) or with TMZ (IC₅₀). Percent of cells in the different phases of the cell cycle. Data are presented as mean ± SEM, ****p<0.00001; ##p<0.01. Only statistics regarding the G2 phase are presented here. Complete statistical analysis is provided in supplemental table 2. (B) Representative western blots for pCHK2 and respective quantifications of cells treated with TMZ at ½ IC₅₀ and IC₅₀. β-actin serves as loading control. Mean ± SEM, **p<0.01, ***p<0.001.

A Caspase 3/7 activity



B Apoptotic cells

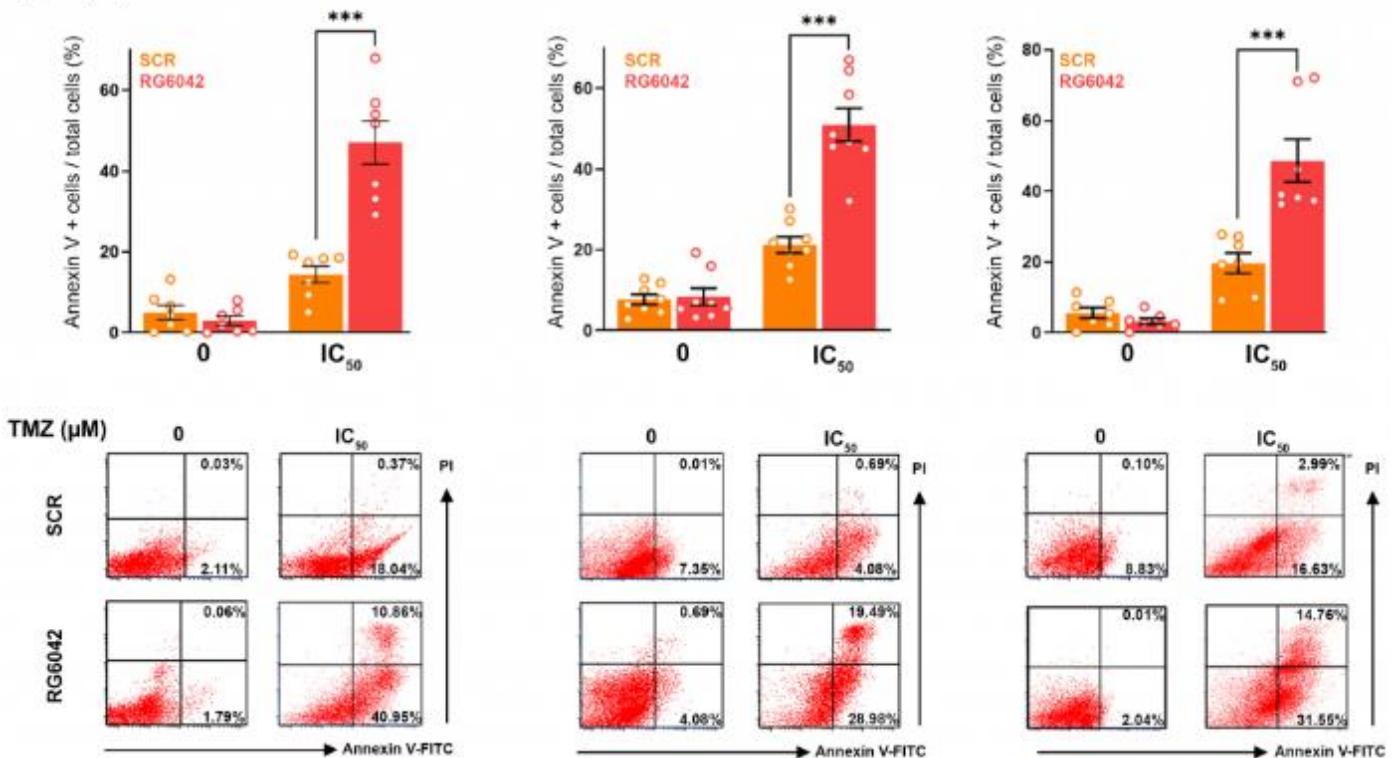


Figure 4. RG6042 increases TMZ-induced apoptosis. (A) Caspase 3 and 7 activities were measured by luminescence in SCR and RG6042 transfected U87, U251 and T98G cells treated without (0) or with TMZ (IC₅₀). Data are represented as mean ± SEM. *** p<0.001, ****p<0.0001. (B) Apoptosis was evaluated by flow cytometry analysis using Annexin V and propidium iodide (PI) staining. Apoptotic cell death (number of Annexin V positive cells) was quantified and presented as percent of total cells as mean ± SEM, *p<0.05, ***p<0.001, ****p<0.0001.

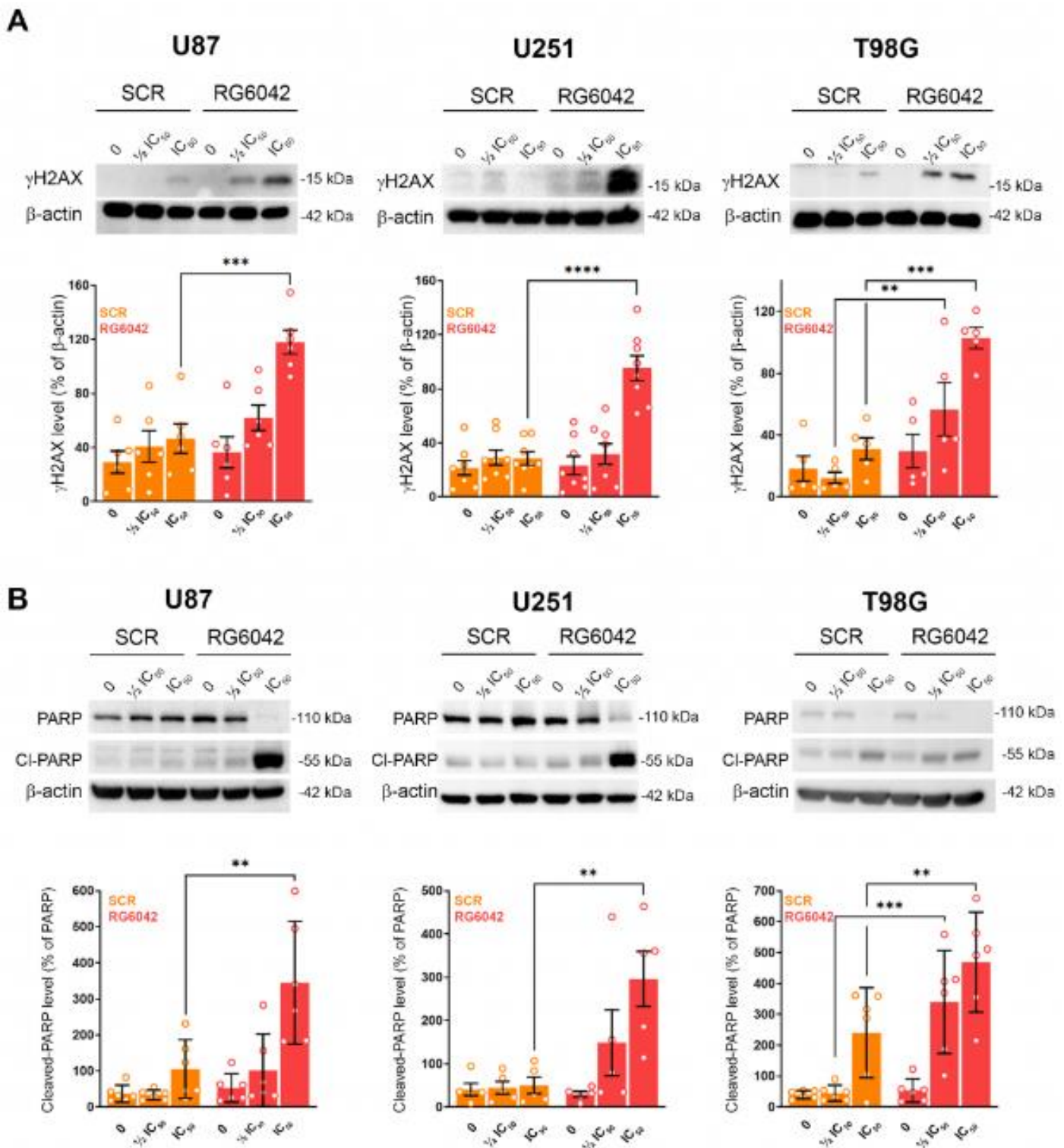


Figure 5. RG6042 exacerbates TMZ-induced DNA damage. (A) γ H2AX expression was determined in cells transfected with 200nM of either SCR or RG6042 ASO. Representative western blots for each cell line (U87, U251 and T98G). β -actin serves as loading control and quantifications are presented under the respective western blots. (B) PARP and cleaved PARP (CI-PARP) expressions were determined in cells transfected as described previously. β -actin serves as loading control and quantifications are presented under the respective western blots as mean \pm SEM, ** $p < 0.01$, *** $p < 0.001$, **** $p < 0.0001$.

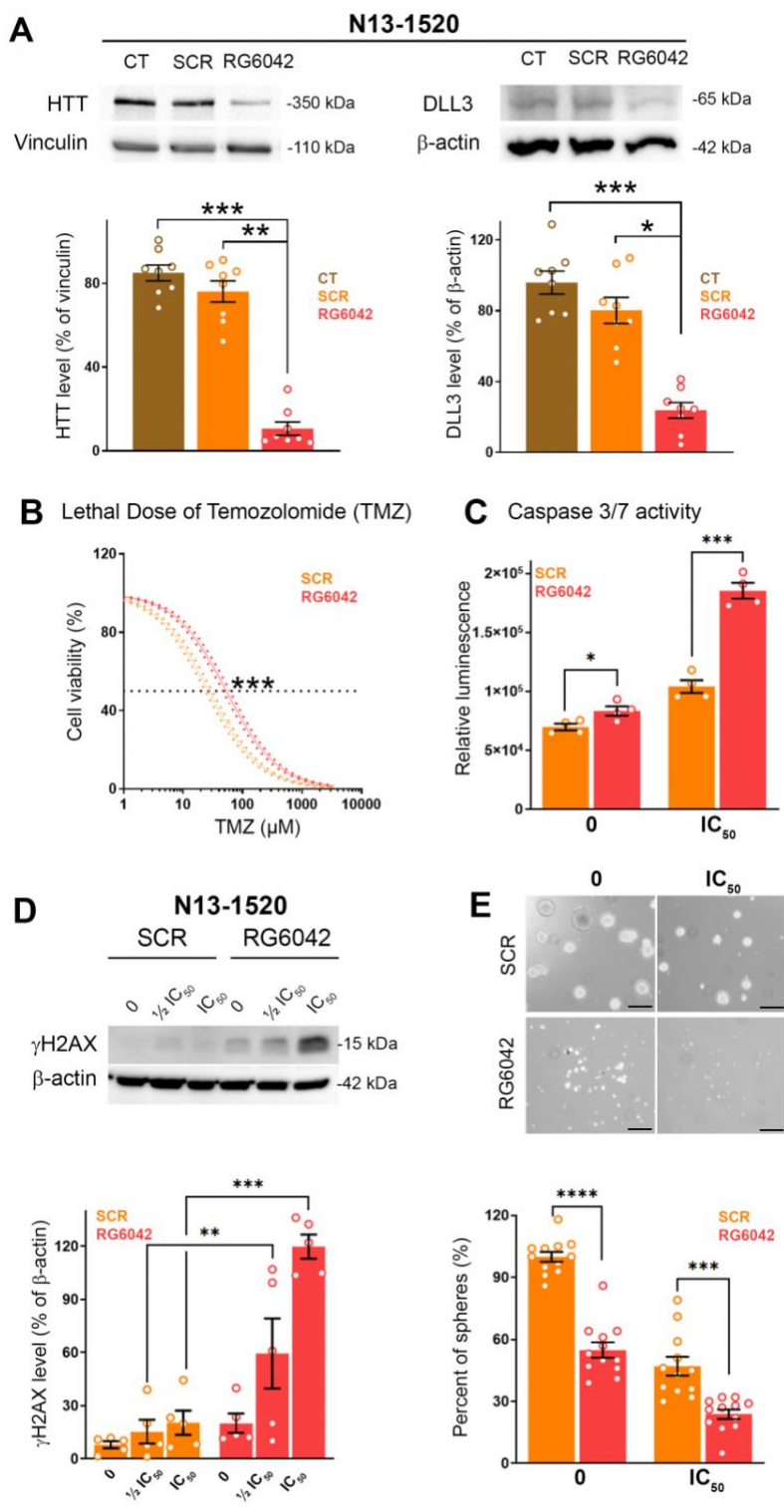


Figure 6. RG6042 sensitizes proneural glioblastoma stem cells to TMZ.

(A) HTT and DLL3 protein levels were determined in lipofectamine treated N13-1520 cells (CT) and in N13-1520 cells transfected either with 200 nM of SCR or RG6042 ASO for 48h. Representative western blots are presented with the respective quantification below, mean \pm SEM, * $p < 0.05$, ** $p < 0.01$, *** $p < 0.001$. (B) MTT cytotoxicity assay with TMZ in SCR and RG6042 transfected N13-1520 cells, mean \pm SEM, *** $p < 0.001$. (C) Caspase 3 and 7 activities were measured by luminescence in SCR and RG6042 transfected N13-1520 cells without (0) or with TMZ at IC₅₀. Data are represented as mean \pm SEM. * $p < 0.05$, *** $p < 0.001$. (D) γ H2AX expression in SCR and RG6042 transfected N13-1520 cells in the absence (0) or the presence of TMZ at IC₅₀. A representative western blot with β -actin as loading control and quantification are presented. Data are represented as mean \pm SEM, ** $p < 0.01$, *** $p < 0.001$. (E) Sphere assay with SCR and RG6042 cells. Single cells were allowed to grow as primary spheres for 6 to 8 days in the absence (0) or the presence of TMZ (IC₅₀). Single cells dissociated from primary spheres grow as secondary spheres without treatment. Representative photos of secondary spheres and quantification are presented as mean \pm SEM, *** $p < 0.001$, **** $p < 0.0001$.

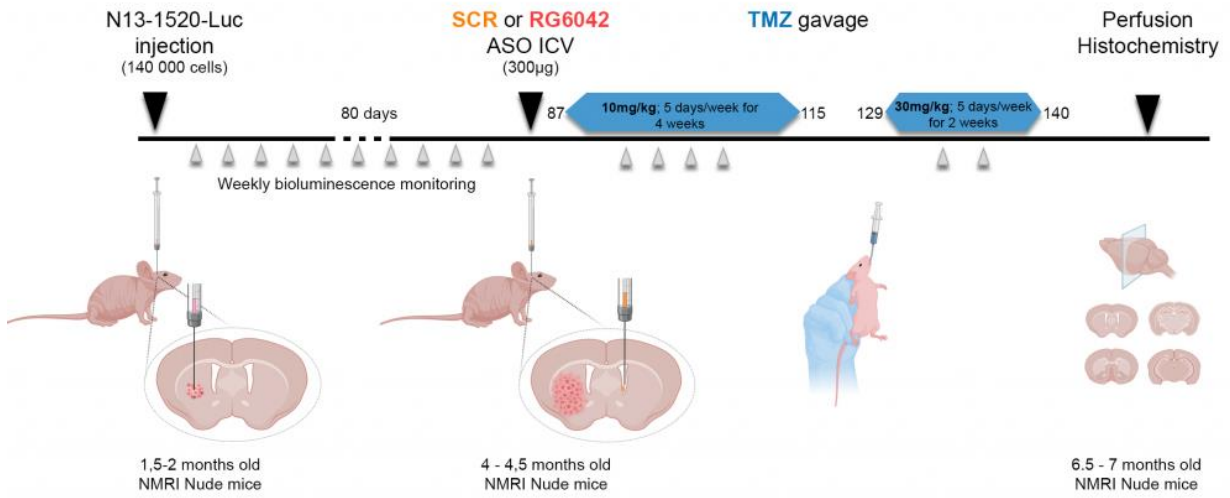
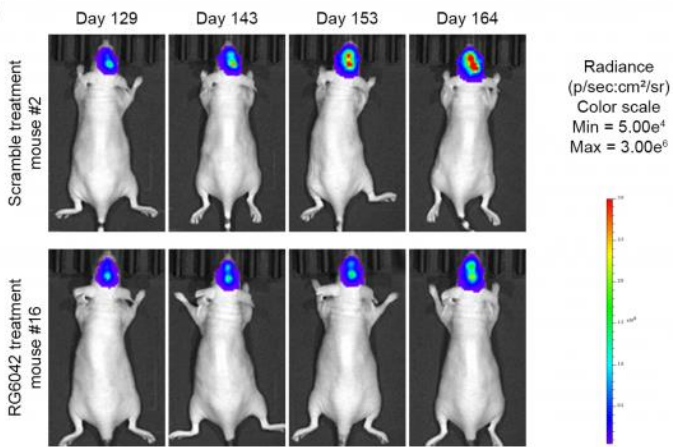
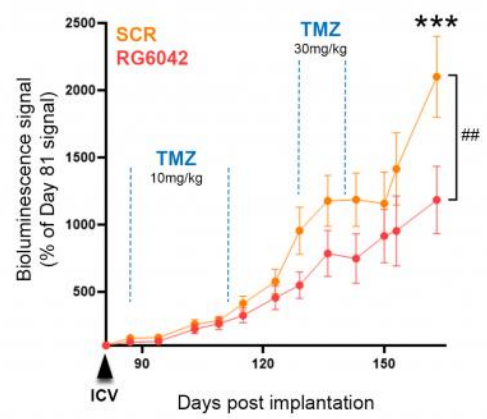
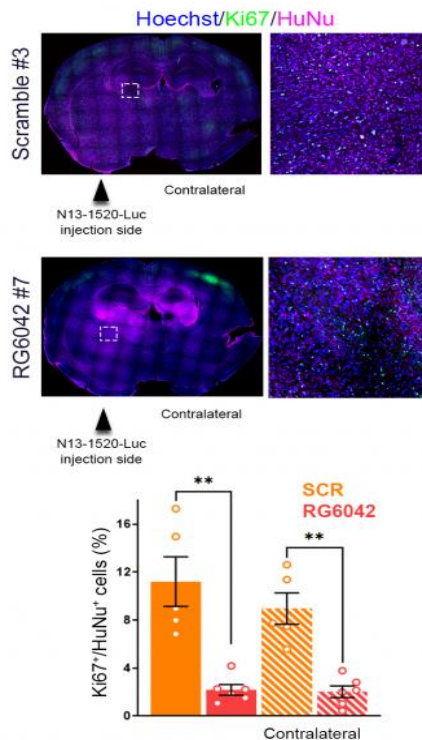
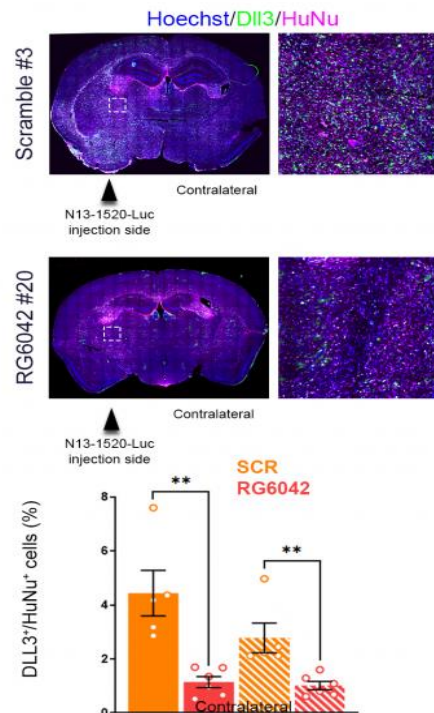
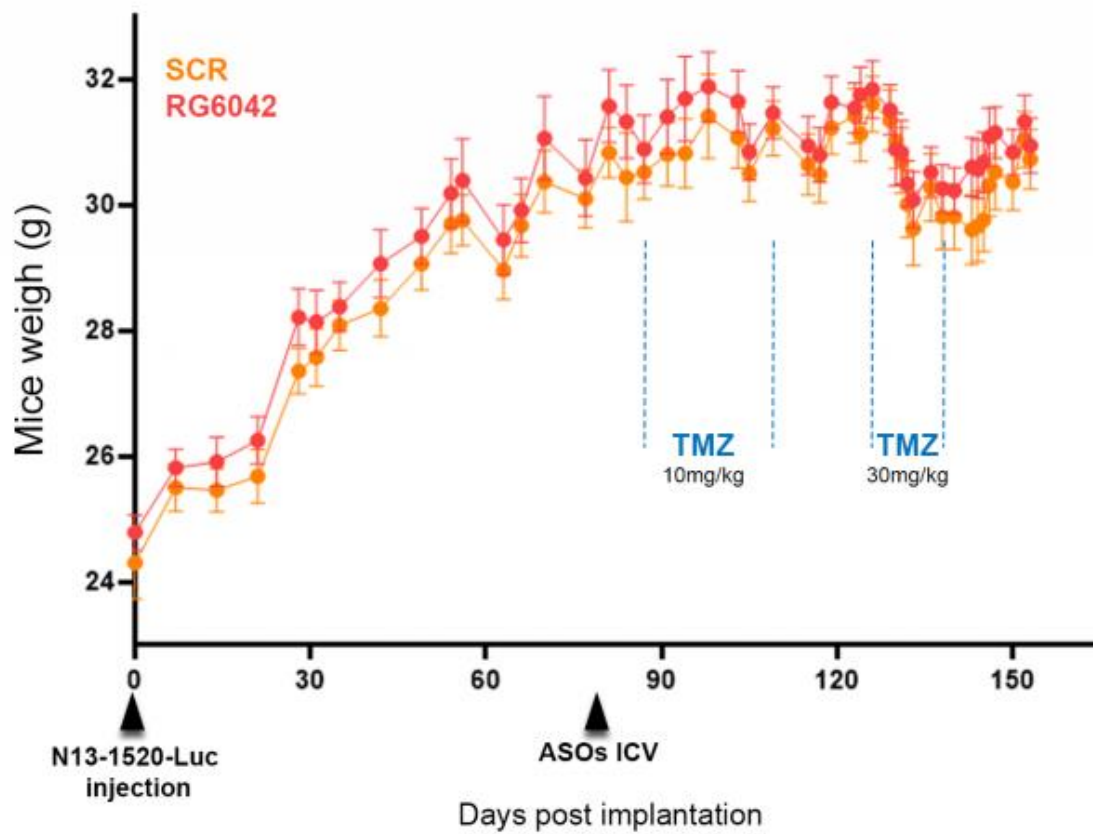
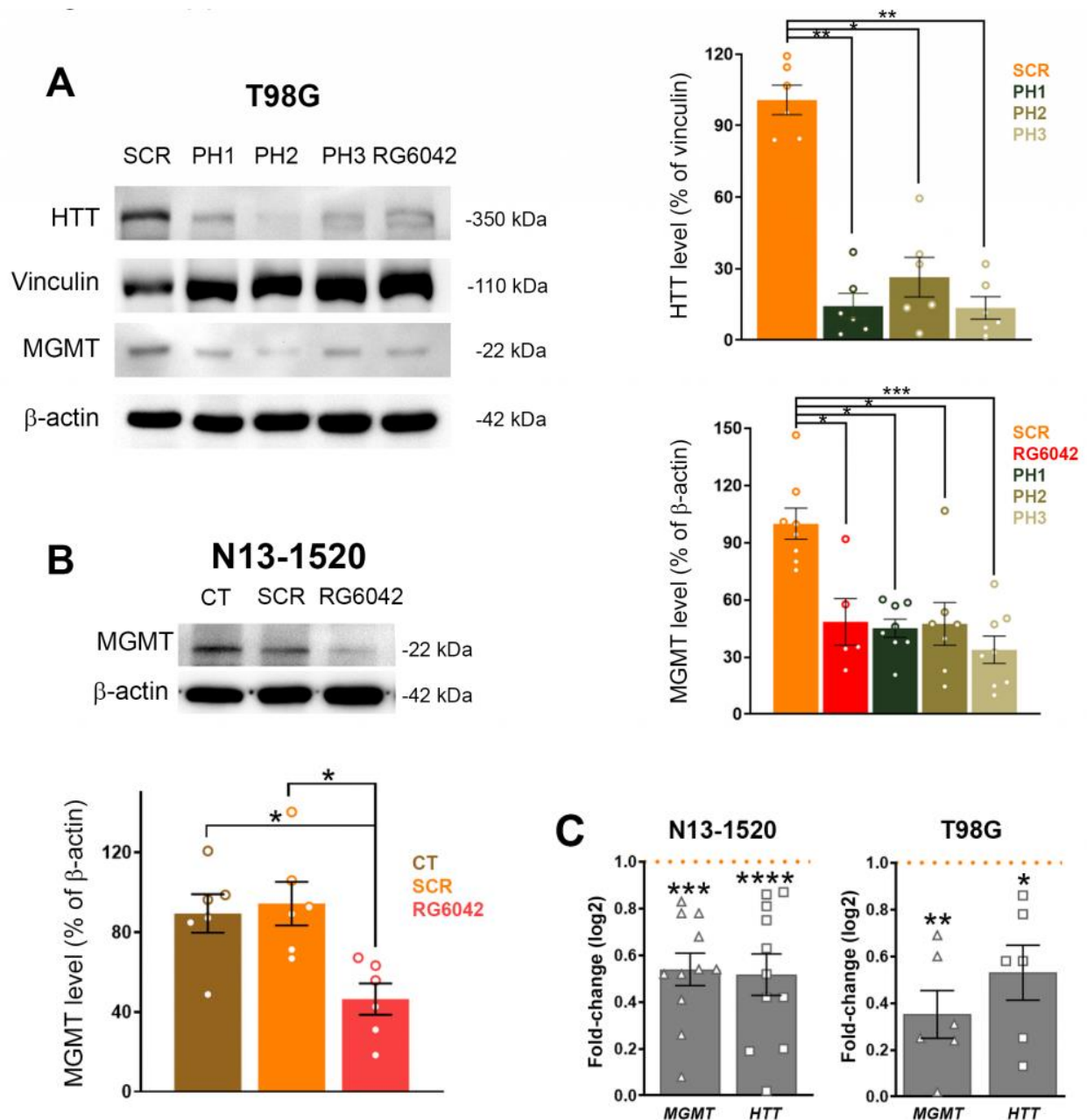
A**B****C****D****E**

Figure 7. RG6042 improves the TMZ treatment in a mouse model of glioblastoma. (A) Timeline of the *in vivo* experiment. NMRI Nude mice were grafted with N13-1520-Luc cells at day 0. Tumor growth was monitored weekly by measuring the bioluminescence emitted by luciferase expressing N13-1520 cells. Mice were injected with the ASOs in the contralateral ventricle at day 82 when three consequent weeks of significant tumor growth was monitored. From day 87, TMZ is administered by gavage at 10 mg/kg, 5 days/week for 4 weeks and then from day 129 at 30 mg/kg, 5 days/week for 2 weeks. Non-treated mice received a bolus of McIlvaine buffer. Mice were perfused at day 165 for histochemistry analyses. (B) Optical bioluminescence imaging was used to visualize tumor development at days 129, 143, 153 and 164 for mice #2 and #16 treated respectively with SCR and RG6042 ASOs. (C) Quantification of bioluminescence signals as percent of day 81 signals for SCR and RG6042 groups of mice (mean \pm SEM; ## p = 0.0017, two-way repeated measure ANOVA test). (** p =0.0004 using Sidak's multiple comparisons test). (D) Coronal sections through SCR or RG6042 brains are immunostained for Ki67 (green) and HuNu (magenta). Nuclei (blue) are counterstained with Hoechst 33342. Black arrowhead indicates the side of the N13-1520-Luc injection. High magnification of the striatal area within the tumor is depicted next to the entire section. Quantification of double-stained HuNu⁺/Ki67⁺ cells is presented below. (E) Coronal sections through SCR and RG6042 brains are immunostained for DLL3 (green) and HuNu (magenta). Nuclei (blue) are counterstained with Hoechst. High magnification of the striatal area within the tumor is depicted next to the entire section. Quantification of double-stained HuNu⁺/DLL3⁺ cells is presented below. Scale bars: 100 μ m. Data are presented mean \pm SEM, ** p <0.01.



Supplemental figure 1. Mice weights. All mice were *weighted* at least once a week from the day of implantation. No deleterious effects were observed following the first treatment session with TMZ at 10 mg/kg. However, the body weight underwent an immediate decrease (-5% in 5 days) at the beginning of the second treatment session with TMZ at 30 mg/kg before stabilizing and increasing back after the end of the treatment.



Supplemental figure 2. MGMT mRNA and protein levels are downregulated in RG6042 treated cells. (A) HTT and MGMT protein levels were determined in T98G cells transfected for 48h with 200 nM of SCR, RG6042, and 3 ASOs specific to HTT mRNA (PH1, PH2 and PH3). Vinculin and β -actin serve as loading controls. Quantifications of HTT and MGMT protein levels are presented as means \pm SEM, * p <0.05, ** p <0.01, *** p <0.001. (B) Representative western blot depicting MGMT protein levels in N13-1520 cells transfected with SCR and RG6042 or treated with lipofectamine as control (CT). β -actin serves as loading control. Quantifications are presented as means \pm SEM, * p <0.05. (C) Quantitative real-time PCR analysis of *HTT* and *MGMT* gene expressions in RG6042 treated T98G and N13-1520 cells as compared to mRNA levels in SCR treated cells set to 1 (orange dotted line). Data are presented as mean \pm SEM, * p <0.05, ** p <0.01, *** p =0.0001, **** p <0.0001.

DISCUSSION AND PERSPECTIVES

DISCUSSION AND PERSPECTIVES

In this work, we identified HTT as a molecular target to counteract TMZ-chemoresistance in GBM. HTT is found ubiquitously in healthy human organism with a greater expression in brain and testis (Saudou and Humbert, 2016a). In the brain, both neuronal and non-neuronal cells express HTT, within the cytoplasm and the nucleus. In brain tumors, analyses of expression datasets show that HTT mRNA is expressed both in low and high-grade gliomas although to a significant lesser extent in GBM (see figure 1 of the results part I). Surprisingly, higher levels of the HTT protein were reported in GBM as compared to low-grade gliomas as assessed by western blot and immunohistochemistry (Simeone et al., 2014) which may suggest that stabilization mechanisms of the protein are taking place.

Correlatively, the ubiquitin E3 ligase HUWE1 known to target HTT (Humbert and Saudou, unpublished data) for proteasome degradation is less expressed in GBM (cf Gliovis dataset analysis) (Figure 1)

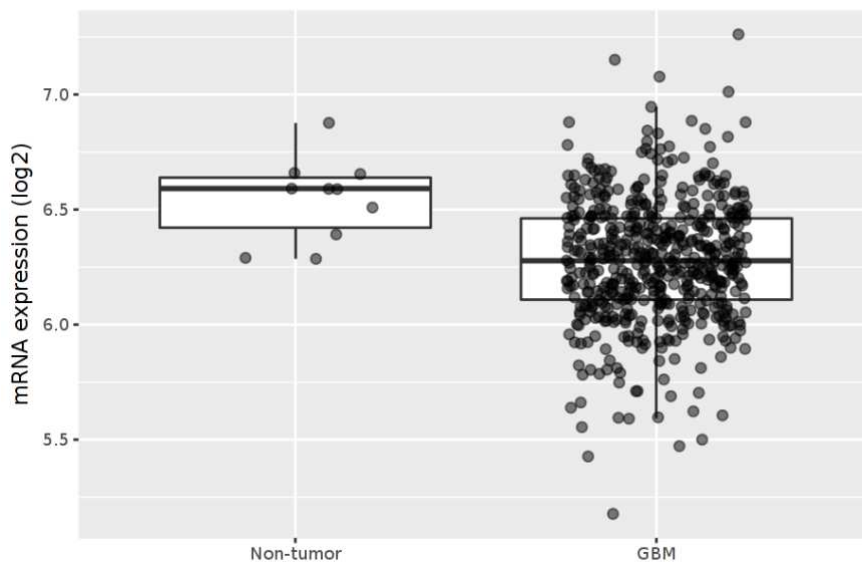


Figure.1I HUWE1 is less expressed in GBM compared to non-tumor cells.

Simeone and collaborators (Simeone et al., 2014) identified HTT as one of four key transcription factors potentially regulating the expression of proteins found to be differentially expressed in human GBM. Moreover, male patients with higher expression of HTT have shorter survival time as

compared to patients with lower HTT expression (see figure 1 of results part). Altogether, HTT seem to participate to the biology of glioblastoma. **We postulated that HTT plays a role in GBM chemoresistance and glioma stem cell dynamics.**

I-Significance of RG6042 in Downregulating HTT and Sensitizing GBM Cells to TMZ.

To investigate the impact of HTT on chemoresistance to TMZ, we reduced HTT levels in GBM cell lines. We utilized the **ASO RG6042**, also known as ISIS HuASO, HH1, IONIS-HTTRx or Tominersen, as previously described in the literature (Kordasiewicz et al., 2012), (Southwell et al., 2014)). RG6042 features phosphorothioate internucleotide linkage (PS), 2'-O-methoxyethyl (MOE), and deoxynucleotide sugar modifications rendering it water-soluble and resistant to exonucleases. RG6042 is designed as a gapmer, with its central region of 10 deoxyribose nucleosides being complementary to exon 36 of the HTT mRNA. Upon binding, RNase H degrades the mRNA. RG6042 targets both (WT) and (HD) HTT, aiming to downregulate HD HTT mRNA. In various HD mouse models, a single intracerebroventricular injection of the ASO successfully downregulated HD HTT and improved anxiety behavior associated with HD (Southwell et al., 2018). RG6042 has undergone clinical trials, with significantly decreased HTT levels observed in the cerebrospinal fluid of HD patients who received four intrathecal injections of the ASO (Tabrizi et al., 2019)). Our findings indicate that downregulating HTT levels with the ASO RG6042 sensitizes glioblastoma cells to TMZ, the standard of care for glioblastoma.

The cytotoxic effects of TMZ are amplified when cells are exposed to RG6042. *TMZ methylates DNA bases, particularly at the O6 position of guanine. O6-methylguanine adducts induce cytotoxicity as they mispair with thymine during DNA replication. This triggers futile cycles of DNA repair aimed at to reinserting cytosine, ultimately resulting in DNA double-strand breaks (DSBs), G2 cell cycle arrest and apoptosis (Hirose et al., 2001), (Zannini et al., 2014).* We have discovered that downregulating HTT increases TMZ-induced DSBs. In Huntington's disease (HD) patients, where HTT is mutated but present, DNA damage is heightened. Elevated phosphorylation of histone H2Ax at serine 139 (γ H2Ax) is detected in fibroblasts from HD patients and brain samples from the prefrontal cortex and the caudate ((Giuliano et al., 2003),(Lu et al., 2014) γ H2Ax levels are also elevated in the peripheral blood mononuclear cells of premanifest HD patients, suggesting it could serve as a disease biomarker(Lu et al., 2014;

[Maiuri et al., 2013](#)) Increased DNA damage in HD implies that the loss of native HTT *function or the toxic gain of function by mutant HD HTT* contribute to DNA damage induction. We did not observe an increase in γ H2Ax in non-treated RG6042 cells. Instead, DNA damage is exacerbated when TMZ is introduced to the cells, implying that HTT plays a role in the DNA damage response. Consistently, HD cells exhibit exacerbated DNA damage under oxidative stress ([Lu et al., 2014](#))([Maiuri et al., 2013](#)). Indeed, DNA damage, as assessed by comet assay, worsen in hTERT-immortalized fibroblasts from an HD patient as compared to healthy-immortalized fibroblast after a 30 minutes exposure to an oxidative stress inducer ([Maiuri et al., 2013](#)). Using a more sensitive method to detect DSBs (dSTRIDE), [Maiuri and collaborators](#) found that in basal condition, levels of DSBs are increased in untreated hTERT-immortalized HD human fibroblasts as compared to control ([Maiuri et al., 2022](#))([Anne et al., 2007](#)). Our study primarily focused on cancer cells with downregulated HTT, not HD neuronal cells. Nonetheless, it is conceivable that DNA damage is increased in RG6042 cancer cells as compared to SCR cancer cells at a level not detectable by Western blot analysis of γ H2Ax. Since cancer cells are highly proliferative and susceptible to base damage, DNA mutations, and breaks, The absence of HTT within the DNA damage response pathway may promote the accumulation of DNA damage and subsequent cell death.

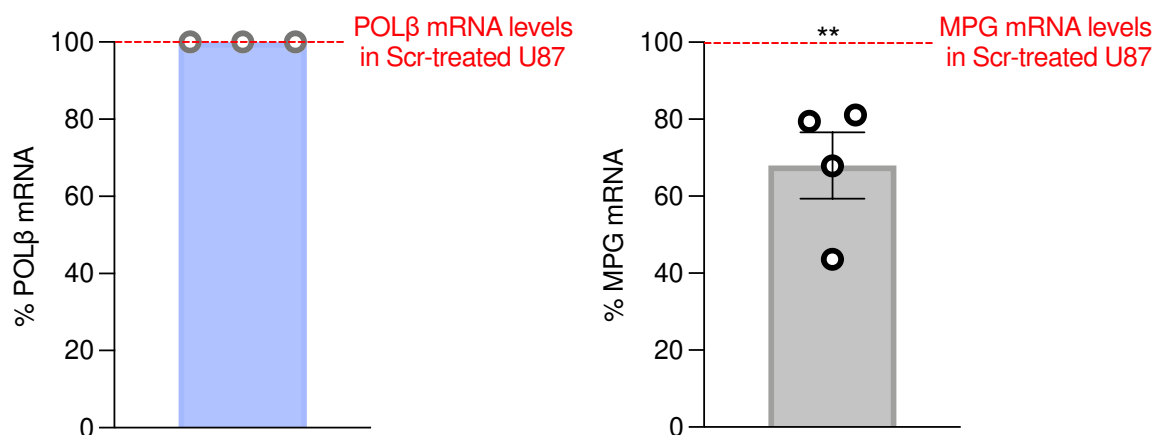
Consistently we observed an increase in apoptosis in RG6042 N13-1520 GSCs compared to SCR under basal conditions (without TMZ treatment) (Figure 6C). In line with the concept that HTT plays a key role in the DNA damage response, the alteration of wild-type HTT has been shown to increase neuronal cell death. Specifically, when HTT becomes unphosphorylatable due to the genetic substitution of serines 1181 and 1201 with alanines, by the kinase CDK5, striatal neurons enter cell death *via* the p53 pathway ([Anne et al., 2007](#)). Oxidative stress and genotoxic compounds induce DNA damage and cell death. In the context of HD or the alteration of wild-type HTT, DNA damage is exacerbated. Indeed, in striatal cells where HTT is rendered unphosphorylatable by CDK5, oxidative and genotoxic stress lead to a significant increase in γ H2Ax ([Anne et al., 2007](#)). In WT cells, phosphorylation of HTT by CDK5 is an early response to DNA damage when no cell death is observed. However, in cells where HTT is unphosphorylatable, DNA damage and cell death are intensified ([Anne et al., 2007](#)). Phosphorylation of HD HTT by CDK5 acts as a protective mechanism against HD HTT-induced p53-mediated cell death ([Anne et al., 2007](#)).

When DNA damages accumulate, CDK5 activity and levels decrease, resulting in reduced HTT phosphorylation and the initiation of p53-dependent cell death (Anne et al., 2007).

Apart from its role in regulating cell death in response to DNA damage, HTT has been demonstrated to act as a scaffold for DNA repair proteins within the nuclei of immortalized retinal pigment epithelial cells of human origin, both at irradiation sites and following oxidative stress induced by potassium bromate treatment (Maiuri et al., 2017). HTT co-localizes with DNA repair proteins involved in base excision repair (BER) at sites of single strand breaks, including the scaffolding protein XRCC1, the endonuclease APE1, the phosphorylated form of ataxia telangiectasia mutated (ATM), the high-mobility group box-1 (HMGB1) protein and the single-strand break marker poly (ADP-ribose) (PAR). Co-immunoprecipitation assays conducted in cells treated with H₂O₂ confirm that HTT is part of a complex involving the aforementioned BER proteins (Maiuri et al., 2017).

Considering that incomplete BER can convert single-strand breaks to DSBs during DNA replication, we hypothesized that BER might be affected by HTT depletion in RG6042 cells. We quantified mRNA levels of DNA *polymerase beta* (*pol β*), the primary *polymerase* in the BER pathway, and N-methylpurine-DNA glycosylase (MPG, aka alkyl-adenine DNA glycosylase, AAG), which initiates BER by removing methylated bases.

Our results showed a decrease in MPG and Polβ mRNA in RG6042 GBM cells suggesting that RG6042 impairs BER. Further studies are warranted to decipher how HTT depletion hampers BER (Fig 2).



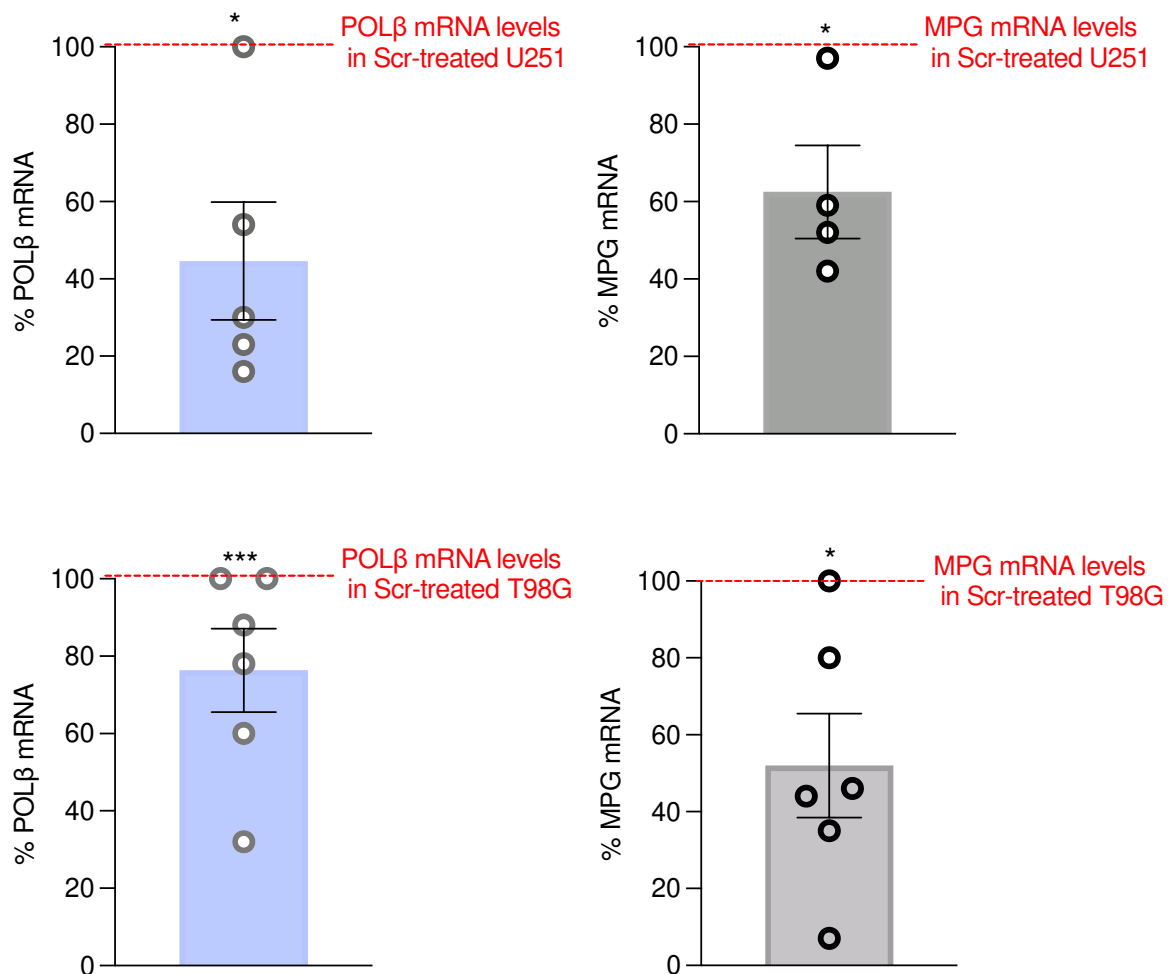


Figure.2I Pol β and MPG are downregulated in GBM HTT-depleted cells.

GBM cells were transfected for 48h with either 200nM of SCR or RG6042. RT-PCR assay was performed to measure mRNA levels of Pol β and MPG. The data are expressed as the percent of mRNA in SCR condition. Each condition is reproduced in triplicates, n=3 experiments. Mean ± SEM, * p<0.1, ** p<0.01, ***p<0.001.

Cell death is increased in HTT-depleted cells treated with TMZ, as evidenced by an increase of PI/annexinV staining, caspases 3/7 activity, and PARP-1 cleavage. PARP1 accumulates at DNA break sites and generates PAR chains on itself and other proteins. These PAR chains serve as a platform for the recruiting downstream repair factors. Excessive PAR polymerization, often due to extensive DNA damage, leads to NAD⁺ depletion, PARP-1 cleavage, and ultimately, cell death. A recent study demonstrated that HTT binds to PARylated proteins and PAR chains. HD patients exhibit a deficient PAR response to oxidative stress and elevated DNA damaged. Reducing mutant HD HTT using huntingtin-lowering splice modulator drug Branaplam increased PAR levels and

rescued DNA repair (Maiuri et al., 2022). WT HTT may, therefore, regulate PARylation upon damage to facilitate DNA repair, a process hindered in GSCs treated with RG6042.

Depleting HTT from cancer cells can potentially induce DNA damage and cell death through the increased production of reactive oxygen species (ROS). In HD, oxidative stress is increased due to mitochondrial dysfunction. In striatal immortalized neurons expressing the mutant (STHdhQ111) versus the WT HTT (STHdhQ7), there is an increase in superoxide production (Siddiqui et al., 2012) Mutant HTT leads to calcium leakage from mitochondria and increased DNA damage. Additionally, there is a decreased expression of antioxidant enzymes superoxide dismutase 1 and 2, all of which contribute to HD pathogenesis (F et al., 2023). We measured ROS levels in N13-1520 cells transfected with either SCR or RG6042 and found that ROS are increased in the absence of HTT (Figure 3). This increase in ROS could contribute to exacerbating the toxic effects of TMZ. Further experiments are needed to decipher how and to what extent the depletion of HTT with RG6042 enhances ROS production and potentiates the toxic effects of TMZ.

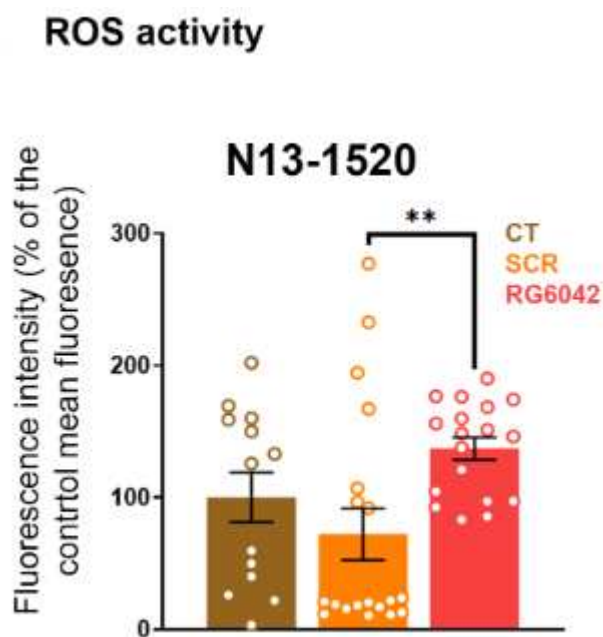


Figure.3I HTT depletion in N13-1520 PN GBM triggers an increase in ROS production.

N13-1520 were transfected for 48h with either 200nM of SCR or RG6042. DCFDA assay was performed to measure ROS levels. The data are expressed as the percent of ROS in control condition. Each condition is reproduced in triplicates, n=3 experiments. Mean \pm SEM, **p<0.01.

TMZ induces excessive DNA damage, triggering the activation of checkpoint kinases and halting the cell cycle arrest in G2/M for repair (). Our findings indicate that when HTT is downregulated, TMZ-induced cell cycle arrest is intensified. DSBs activate ATM, a serine/threonine

kinase belonging to the phosphoinositide 3-kinase (PI3K)-related kinase family. ATM phosphorylates various proteins and enzymes to coordinate cellular responses to DNA damage. Among the substrates of ATM, checkpoint protein 2 (CHK2), undergoes phosphorylation at threonine 68, leading to G2/M cell cycle arrest. In line with an increase in cells arrested in G2/M, we observed heightened phosphorylation of CHK2 at threonine 68 in RG6042-treated cells. The absence of HTT may reduce the recruitment of the repair machinery to the DNA, resulting in DNA damage accumulation and subsequent ATM and CHK2 activation.

In addition to apoptosis, TMZ also induces senescence allowing cancer cells to survive without proliferation ([Knizhnik et al., 2013](#))([Hirose et al., 2001](#))([Aasland et al., 2019](#)). Senescent cancer cells may later escape senescence and resume proliferation ([Beauséjour et al., 2003](#)). TMZ-induced senescence is activated during the G2/M phase, involving p53 phosphorylation at Ser15 and induction of p21. However, in p53 mutated U251 and T98G cell lines, TMZ-induced senescence involves other pathways. For example, in U251, survivin, an apoptosis-inhibiting protein, is required for entry into senescence following TMZ treatment. Knocking down surviving expression decreased the proportion of senescent cells in response to TMZ ([Song et al., 2017](#)). TMZ-induced cellular senescence is viewed as a survival strategy for tumor cells, allowing them to evade apoptosis. While we observed increased cell death in glioma cells treated with RG6042 and TMZ, we did not investigate whether HTT depletion affects the proportion of senescent glioma cells. This is a crucial aspect to explore considering the pro-tumoral potential of senescent glioma cells. Future research will assess whether RG6042 reduced TMZ-induced senescence, potentially redirecting cells towards apoptosis and reducing the pool of cells escaping TMZ toxicity.

Temozolomide-induced DSBs are repaired by homologous recombination (HR)([Gil Del Alcazar et al., 2016](#)). Increased HR efficiency is observed in TMZ-resistant glioma cells and inhibiting key HR proteins like Rad51 enhances sensitivity to alkylating agents ([Berte et al., 2016](#)). HR involves proteins that utilize the sister chromatid as a template for error-free DSB repair. Among them, BRCA1 serves as a scaffold for other HR proteins at the repair site, and HTT has been shown to interact with BRCA1-associated RING domain protein (BARD1), an interactor of BRCA1 (Little is known about the implication of HTT in HR. A study revealed an association between the age at onset of breast cancer in *BRCA1* mutated patients and the longer of the CAG repeats on the exon 1 of the HTT gene. Patients with *HTT* CAG repeats inferior to 27 develop breast cancer about

2.5 years earlier than patients with *HTT* CAG lengths under 27 ([Goehler et al., 2004](#)). This lack of data may be attributed to *HTT* function primarily being investigated in postmitotic neurons, where non-homologous end joining (NHEJ) repair prevails over HR. Further studies are warranted in order to disclose whether *HTT* is involved in HR. Of note, the presence of the ([Faber et al., 1998](#)), at DSBs is required for ATM activation and the recruitment of Rad51 and SETD2-depleted cells show reduced HR repair of DSBs ([Carvalho et al., 2014](#)).

II-*HTT* Downregulation Reduces *MGMT* Protein and mRNA Levels.

The primary cause of TMZ-induced toxicity is the formation of O6-methylguanine adducts. Tumor cells escape TMZ cytotoxicity by expressing the enzyme O-6-methylguanine-DNA methyltransferase (*MGMT*), which removes the O6 methylation. Both T98G and N13-1520 cells express *MGMT* and RG6042 sensitizes them to chemotherapy. We investigated whether downregulating *HTT* might affect *MGMT* levels through western blot analysis. Remarkably, we observed decreased *MGMT* protein levels in RG6042 treated T98G cells (supplemental figure 2A of results part). To assess whether reduced *MGMT* levels are a general consequence of *HTT* downregulation, we used ASOs targeting different regions of the *HTT* mRNA sequence (([Southwell et al., 2014](#))). In T98G cells transfected with *HTT*-specific ASOs PH1, PH2 and PH3, *MGMT* protein was downregulated (supplemental Figure 2A of results part). In addition, RG6042 decreased *MGMT* levels in N13-1520 (supplemental Figure 2B of results part). These results indicate that *HTT* downregulation simultaneously decreases *MGMT* protein levels. This downregulation occurs at the gene expression level, as *MGMT* mRNA is decreased in both RG6042 treated cell lines (supplemental Figure 2C of results part). The mechanism by which downregulation of *HTT* silences *MGMT* gene expression remains to be determined.

MGMT expression is regulated through the methylation of two gene regions rich in CpG dinucleotides: the differentially methylated region 1 and 2 (DMR1 and 2). We wondered whether RG6042 transfection affects *MGMT* gene methylation. Dr Florence Puch (CHU, Grenoble Alpes) performed methylation-specific PCR in T98G cells transfected with either SCR or RG6042 using the *MGMT*-Epimelt kit (#MD-*MGMT*-EPIMELT, Amplitech). Her findings revealed no difference in methylation levels. These results would suggest that RG6042 does not alter *MGMT* gene methylation. However, it is important to note that the CpGs analyzed by the kit are all part of the DMR2 region, and thus, the methylation status of the DMR1 region was not evaluated in this

preliminary study. Moreover, while the methylation status of DMR1 and 2 regions has been linked to transcription, in some cases, methylation in these regions does not correlate with gene silencing. For instance, hypermethylation of gene body cytosines has been shown to increase gene expression despite promoter methylation. In addition, decreased gene expression and mRNA levels have been reported in cells with an unmethylated promoter and a hypomethylated gene body ([Butler et al., 2020](#)). Consequently, it cannot be ruled out that RG6042 silences *MGMT* gene expression by methylation of other regions of the gene body and promoter. A comprehensive examination of the methylation status of both the promoter and the gene body would answer this question.

Different DNA methylation patterns have been reported in cell models of HD and these patterns correlate with transcriptional dysregulation. Specifically, the promoter of the gene encoding the prosurvival neurotrophin brain-derived neurotrophic factor (BDNF) is hypermethylated in embryonic mouse HD cortical and striatal neurons transfected with lentiviruses bearing the sequence for HD HTT ([Pan et al., 2016](#)). Pharmacological inhibition of DNA methyltransferases (DNMTs) with decitabine, as well as knocking down DNMT3A or DNMT1, counteracted the toxic effects of HD HTT, notably by restoring the expression of BDNF. However, the mechanisms by which HD HTT promotes DNA methylation at specific gene promoters remain open questions. Variations in the expression of DNMTs may be involved, as decrease in DNMT1 was found in HD striatal neurons (STHdhQ111). However, DNMT1 and 3A mRNA levels do not vary in another cellular model of HD (embryonic cortical neurons transfected with HTT exon1 with 72Q) ([Pan et al., 2016](#)). Given the observed alterations in DNA methylation in HD, it is reasonable to consider that absence of HTT may also impact DNA methylation. To tackle how HTT depletion might affect *MGMT* expression, Dr Florence Puch will re-examine the methylation status of the *MGMT* promoter in N13-1520 cells treated with or without RG6042 and perform qPCR to evaluate the levels of DNMT1 and 3A/B.

In addition to its role in DNA methylation, HTT has been shown to interact with transcription repressors that recruit chromatin modifiers. Among them, REST (Repressor Element 1-Silencing Transcription factor) binds to NRSE (or RE1 for neuron-restrictive silencing factor/repressor element 1 silencing transcription factor) motifs of neuronal genes, inhibiting their expression during both embryogenesis and adult neurogenesis ([Ballas et al., 2005](#)). REST limits the exhaustion of the hippocampal stem cells pool in adult mice by recruiting the co-repressors CoREST, mSin3A

and histone deacetylase 1 (HDAC1) at the RE1/NRSE site of the neural genes *ASCL1* and *NeuroD1*. REST maintains the pluripotency and self-renewal of mouse embryonic stem cells (Singh et al., 2004). In glioma, highly proliferative and infiltrative GSCs express high levels of REST (Kamal et al., 2012). REST mRNA is increased in GBM compared to normal brain tissue, and high expression levels correlates with poor survival. REST is found in the nucleus of glioma stem cells and downregulation of REST decreases tumorigenicity (Conti et al., 2012). HTT interacts and sequesters REST in the cytoplasm of neural cells. In HD, mutant HTT no longer interacts with REST, which accumulates in the nucleus. REST binding to DNA contributes to transcriptional dysregulation in HD. Notably, REST binding to RE-1 sequence of the BDNF gene decreases transcription (Zuccato et al., 2003). Results from Conti et al 2012 and Kamal et al 2012 suggest that REST silences genes involved in differentiation, maintaining glioma cells in a proliferative state. While it may be challenging to envision how decreasing HTT levels with RG6042 could affect REST-mediated silencing of differentiating genes. HTT depletion could act upstream of REST silencing by modifying methylation of bases at RE-1. Indeed, REST binding to DNA is enhanced by methylation at RE-1 sequences. For instance, in the developing mouse heart, the expression of the pacemaker hyperpolarization-activated cyclic nucleotide- modulated potassium channel protein 2 (*Hcn2*) is inhibited by REST binding the RE-1 and this binding is strongly enhanced when DNMT3B methylates non-CpGs in the RE-1 sequence. The level of DNA methylation at the non-CpGs reduces with progression of heart development (Zhang et al., 2017). Therefore, if DNA methylation decreases with HTT depletion, REST binding to RE-1 may be less efficient potentially leading to the re-expression of differentiative genes.

HTT directly interacts with MeCP2 (methyl-CpG-binding protein 2), a DNA methylation-dependent transcriptional repressor. MeCP2 binds methylated DNA and recruits transcriptional co-repressors to silence transcription by modifying the chromatin structure such as HDAC and histone methyltransferase. In HD, the interaction of mutant HTT with MeCP2 is enhanced at the BDNF promoter decreasing the expression of the gene (McFarland et al., 2014). In glioma cells, MeCp2 is associated with the *MGMT* promoter in *MGMT* silenced cell lines. MeCp2 binds to methylated CpG and recruits HDAC, repressing *MGMT* transcription. When CpGs are demethylated, MeCp2 no longer binds to the DMR1 region of *MGMT* and acetylation of H3 and 4 increases, inducing gene expression. The mechanism governing the direct interaction of WT HTT and MeCp2 in the regulation of MeCp2-mediated silencing of *MGMT* remain to be determined.

Additionally, as with REST, if HTT depletion decreases DNA methylation, MeCp2 binding to MDR1 may be compromised, leading to the de-repression of gene transcription.

HTT plays a crucial role in promoting the activity of the multi-subunit polycomb repressive complex 2 (PRC2), which methylates histone H3 on lysine 27, leading to the repression of gene transcription. This activity is heightened in HD. Moreover, there is a global loss of histone H3K27me3 at transcription starting sites in a mouse ES cell line depleted of HTT. In glioma, EZH2 (enhancer of zeste homolog 2), a subunit of PRC2, is highly expressed and is predictive of a poor survival ([Zhang et al., 2015](#)). Inhibition of EZH2 in glioma stem cells reduces stem cells properties, increasing the expression of neuronal differentiation genes and decreases proliferation and survival ([Kader et al., 2021](#)). The impact of HTT absence on gene silencing through EZH2 and whether MGMT downregulation is a consequence of HTT-EZH2 interaction disruption remain to be elucidated.

SETD2 is a histone methyltransferase specific for lysine-36 of histone H3. Traditionally considered a tumor suppressor, SETD2 mutations are found in pediatric high-grade gliomas ([Fontebasso et al., 2013](#)). SETD2 interacts with HTT, inhibiting the autoinhibitory capacity of SETD2. Beyond its role as a chromatin modifier, SETD2 methylates non-histone substrates, such as STAT1, promoting the IFN α -induced antiviral immune response in hepatocytes ([Chen et al., 2017](#)) and actin, positively regulating actin polymerization ([Seervai et al., 2020](#)). Recently, SETD2 was reported to methylate EZH2 at lysine 735 facilitating its recognition by E3 ligase and its degradation. Reduction of EZH2 limits prostate cancer metastasis ([Yuan et al., 2020](#)). As a direct interactor of both enzymes, SETD2 and EZH2, HTT may participate to the regulation of EZH2 by SETD2.

III-HTT Depletion's Impact on Glioma Stem Cells and Proliferation.

Depletion of HTT using RG6042 sensitizes GSCs, such as N13-1520, which belong to the proneural stem cell subtype. Among the molecular classes of GBM, PN cells expressed the highest levels of HTT mRNA (see figure 1 of results part). We found that HTT depletion decreases the stemness capacities of these cells, as demonstrated by a decrease in self-renewal observed in the neurosphere assay (see figure 6 of results part). These results suggest that RG6042 may exert an

inhibitory effect on the proliferation, as indicated by reduced BrdU incorporation in N13-1520 cells transfected with RG6042 compared to SCR and untreated cells (Figure 4).

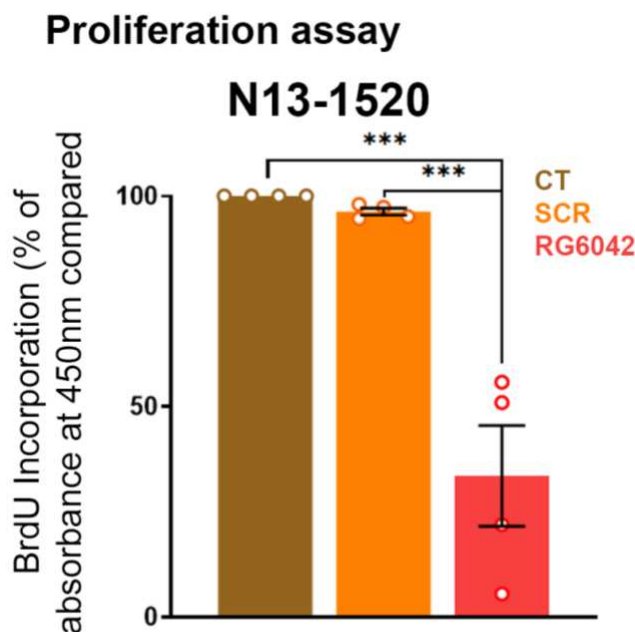


Figure.4I: RG6042 decreases proliferation in N13-1520 cells.

Cells were transfected for 48h with either SCR or RG6042. BrdU (10 nM) was added 2h before fixation. BrdU was revealed by ELISA. The data are expressed as the percent of BrdU incorporated in control condition. Each condition is reproduced in triplicates, n=3 experiments. Mean \pm SEM, ***p<0.001.

IV-The Role of HTT in Stem Cell Proliferation and Implications in Glioma

HTT actively participates in cell proliferation, notably in progenitor and stem cells. It controls mitosis of the neuroepithelial stem cells during early corticogenesis, being a crucial component of the molecular machinery responsible for proper spindle pole assembly and ensuring symmetric divisions that expand the stem cell pool. RNAi-mediated silencing of HTT in nestin-expressing stem cells disrupts spindle orientation, leading to the rapid exhaustion of the stem cell pool in the stem cells the ventricular zone of mouse embryos by promoting differentiation divisions towards the neuronal fate (Godin et al., 2010). Analysis of mitosis in HTT-depleted basal stem/progenitor cells reveals mitotic spindle misorientation resulting in the exhaustion of the stem cell pool and mammary gland hypoplasia. Depletion in HTT also affects neural stem cells

derived from mouse embryonic stem cells causing them to predominantly differentiate into glial cells at the expense of neurons (Conforti et al., 2013). The role of HTT in maintaining the stem cell pool is underscored by the reduction in neurogenesis observed in both human HD patients and rodent models of the disease (Ernst et al., 2014). Stem/progenitor cells derived from the subventricular zone cell cultures from rodent models of HD have a decreased capacity to generate neurons (Silva et al., 2018), emphasizing the importance of WT HTT in preserving stem cell properties. Therefore, reducing WT HTT in GSCs may diminish their stem cell capabilities, potentially triggering premature differentiation and cell-cycle exit. Thus, the expression of the PN stem cell marker DLL3 decreases upon transfection with RG6042 (see figure 6 of results part). GSCs typically do not terminally differentiate and therefore can reenter the cell cycle, as observed in GSCs treated on the long term with the astrocyte differentiation factor BMP4 (Carén et al., 2015). This failure in inducing complete differentiation and cell-cycle arrest is due to inappropriate chromatin remodeling and an incomplete DNA methylation associated with downregulation of oncogene pathway silencing (Carén et al., 2015). Whether absence of HTT can trigger terminal cell-cycle exit of GSCs remains to be determined.

GBM stem cells play a critical role in fueling tumor growth, making it imperative to limit the number of stem cells with tumorigenic capacities. We found that intracerebroventricular injection of RG6042 delays tumor growth in Nude mice harboring human PN stem cells treated with TMZ. This delay is associated reduced proliferation and a decrease in the number of PN stem cells. Ongoing research is focused on determining whether co-treatment with RG6042 and TMZ can lead to increased overall survival in mice.

V-Promising Potential of RG6042 and TMZ Co-Treatment for GBM

During my PhD I investigated whether downregulating HTT in brain tumor using RG6042 could sensitize the cancer cells to TMZ. RG6042, aka Tominersen, was initially designed to downregulate both wt and HD HTT in the brain of HD patients. The GENERATION HD1 clinical trial was halted due to a lack of effects on the natural course of the disease and safety concerns. Lower doses of the ASO are currently being tested in younger HD patients with lower disease burden (GEN-PEAK (NCT04000594)). Nevertheless, the downregulation of both forms of the protein was achieved in the CSF of HD patients administered with RG6042 *via* intrathecal injections. Therefore,

the downregulation of wt HTT in a brain harboring a tumor is feasible. In addition, partial lowering of WT HTT in the healthy brain is likely to be safe [\(Leavitt et al., 2020\)](#) [Leavitt et al., 2020](#) .

The results I obtained during my PhD indicate that the therapeutic strategy holds potential for the treatment of glioma. Given the limited efficacy of current treatments, the co-treatment of GBM with RG6042 and TMZ could be a game-changer for the treatment of GBM in humans.

PART II

In this part of the results, I investigated the Role of Huntingtin protein (HTT) in the lineage progression of subventricularzone (SVZ) stem cells.

Whereas multiple evidences suggest the presence of neurogenesis in the hippocampus, fewer reveal the process of neurogenesis in the SVZ. However, in the adult rodent brain, NSCs and progenitors' cells house in the SVZ, generating neurons for the olfactory bulb. NSCs in the adult rodent brain are characterized as self-renewing cells with multipotent properties, which could form clonal neurospheres when cultured in a serum-free medium with growth factors, giving rise to astrocytes, oligodendrocytes, and neurons upon adhesion and removal of growth factors.

Reduced neurogenesis has been observed in both the DG and SVZ in rodent models of HD, where NeuroD1 expression, proliferation, differentiation, and survival of hippocampal neurons are diminished. Similarly, OB neurogenesis is reduced in mouse and rat models of HD, with SVZ NSCs proliferating less. In the YAC128 mouse model, SVZ-derived neurospheres fail to differentiate into mature neurons.

In the human brain, the presence of adult-born neurons in the striatum diminishes in advanced stages of HD, and neurodevelopmental perturbations have been observed in HD human brain fetuses. These findings suggest that NSC properties are compromised in the diseased HD brain, and HTT is critical for neurogenesis, as demonstrated by the premature neuronal differentiation seen when HTT is ablated in neuroepithelial stem cells during cortical development.

We hypothesized that huntingtin (HTT) plays a crucial role in the progression of SVZ NSCs through their lineage.

Role of Huntingtin protein (HTT) in the lineage progression of subventricular zone (SVZ) stem cells.

Key-words: Huntingtin, sub-ventricular zone, stem cells, progenitor cells, Huntington's disease, stemness, differentiation.

INTRODUCTION

The subventricular zone (SVZ) harbors the largest source of neural stem cells (NSCs) and progenitors in the adult rodent brain that continuously generates neurons for the olfactory bulb, a process so-called neurogenesis. In the late 1960's, Joseph Altman was the first to show that new neurons are generated in the adult mammalian brain.

Using radioactive thymidine, Altman demonstrated that the new cells were added into two regions of the adult rat brain: the olfactory bulb (OB) and the dentate gyrus (DG) in the hippocampus ((Altman and Das, 1965b). NSCs in the adult rodent brain were characterized by Reynolds and Weiss in 1992 ((Reynolds and Weiss, 1992)) *in vitro* as proliferating self-renewing cells with multipotent properties. NSCs grow as clonal neurospheres when cultured in free-floating conditions in a serum-free medium and in the presence of growth factors, and spontaneously give rise to astrocytes, oligodendrocytes and neurons once adhered and deprived of growth factor. *In vivo*, three cell types composed the SVZ: The A, B and C cells ((Doetsch et al., 1999)). NSCs correspond to a subset of astrocytes referred to as B1 cells that retain an apical contact with the ventricle.

NSCs proliferate in the presence of stimulus and give rise to intermediate progenitors (type C cells), which in turn differentiate in neuroblasts (type A cells). From the SVZ, neuroblasts migrate tangentially through the rostral migratory stream (RMS) to the olfactory bulb, where they differentiate into local circuit interneurons.

Neurogenesis is a multistep process involving stem cells maintenance in the SVZ niche in a quiescent state, activation of stem cells to a proliferative state, transition to the progenitor stage from which the cell is committed to differentiate into neurons or glial cells, and differentiation/maturation of these cells. Each of these steps is regulated by environmental cues both diffusible and contact-dependent, which have been extensively studied along the past 20 years. Intrinsic regulators of these steps are more elusive and remain to be deciphered. We hypothesize that the protein huntingtin (HTT) is important for the progress through the SVZ NSCs lineage.

HTT is a scaffold protein of 348 kDa, widely expressed in adult tissues including the brain. Its mutated form causes the neurodegenerative disorder Huntington's disease (HD). The mutation responsible for HD is an abnormal expansion of a CAG repeat, exceeding 35, in the HTT gene coding for a polyglutamine (polyQ) stretch. Mutant HTT (mHTT) leads to dysfunction and ultimately death of cortical and striatal neurons which account for the symptoms of the disease ((Saudou and Humbert, 2016b)). The onset of the disease occurs around 40 years old and is characterized by a triad of motor, cognitive, and psychiatric symptoms.

Decrease of neurogenesis in both the DG and SVZ in HD brains is reported in numerous rodent models of HD. In the R6/2 mouse model of Huntington's disease (HD), *NeuroD1* expression, proliferation, differentiation, and survival of hippocampal neurons are decreased in the DG ((Fedele et al., 2011)). Similarly, the OB neurogenesis is reduced in mouse and rat model of HD where SVZ NSCs proliferate less ((Kandasamy et al., 2022; Kohl et al., 2010)). In the YAC128 mouse model, a hemizygous model expressing the human full-length mHTT with 128 CAG repeats, SVZ-derived neurospheres fail to differentiate in mature neurons ((Silva et al., 2018)).

Regarding the human brain, Ernst and coworkers reported the presence of adult-born neurons in the striatum and the absence of these in the advanced stage of HD ((Ernst et al., 2014)). More recently, Barnat and colleagues showed that neurodevelopment is perturbed in HD human brain fetuses ((Barnat et al., 2017)). These observations suggest that NSCs properties are impaired in the diseased HD brain. In fact, HTT is critical for neurogenesis as ablation of HTT in neuroepithelial stem cells during cortical development favors precocious neuronal differentiation at the expense of their maintenance ((Godin et al., 2010)). Altogether, these data suggest that HTT is involved in the biology of neural stem cells and neurogenesis.

We hypothesized that variations of HTT protein levels direct the transition from stem cells to progenitor cells as we observed in a set of preliminary experiments that HTT is downregulated in progenitor cells. We propose to describe variations of HTT levels along the SVZ lineage and to decipher how HTT protein variations regulate the transition from stem to progenitor cells during neurogenesis. As neurogenesis is impaired in HD, we will address the same questions in SVZ stem cells from the Q111 mouse, a rodent model of the disease. We also plan to determine the molecular mechanisms underlying the variations of HTT levels in order to identify molecular target(s) that could help us to restore proper stem cell dynamics in HD brains.

MATERIALS AND METHODS

Mice

CD1 WT mice were purchased from *Janvier* (JANVIER LABS, France). Homozygous HdhQ111/HdhQ111 CD1 (Q111) mice were obtained from heterozygous crossing of HdhQ111/+ CD1 mice that express the human HTT exon 1 sequence with 109 repeats of CAG (Wheeler et al., 1999). Animals were maintained with access to food and water ad libitum and kept at a constant temperature (19°C–22°C) and humidity (40%–50%) on a 12:12-hr light/dark cycle. All experimental procedures were performed in an authorized establishment (Grenoble Institut des Neurosciences, INSERM U1216, license B3851610008) in strict accordance with the recommendations of the European Community (86/609/EEC) and the French National Committee (2010/63) for care and use of laboratory animals, under the supervision of authorized investigators (permission 91-448 to S. Humbert). Wild-type (WT) off springs were obtained by mating WT CD1 male mice with CD1 female mice. Homozygous off springs for Q111 (Q111) were obtained by mating homozygous Q111 male mice with homozygous Q111 female mice.

SVZ cell culture and drug treatment

Subventricular zone (SVZ) were dissected from early postnatal day 0 to 5 (P0- P5) wild-type (WT) and Q111 homozygous mice (Q111). SVZ cells were cultured in DMEM/F12 (#31331) completed with 1% of penicillin and streptomycin (PS, #15140148) and 1 % of B27 (#17504044) (all from ThermoFisher) and supplemented with 20 ng/ml of epidermal growth factor (EGF, #E9644, Sigma-Aldrich) and 20 ng/ml of basic fibroblast growth factor (FGF-2, #13256029, ThermoFisher). Cells were grown either in suspension to generate free-floating neurospheres, or in adherence on poly-D-lysine (PDL) (20 µg/ml, #P7886, Sigma-Aldrich) and laminin (20 µg/ml, #L2020, Sigma-Aldrich) to grow as stem/progenitor cell monolayers. Both cell culture types were grown for 5-6 days in a 95% air-5% CO₂ humidified incubator at 37°C.

Five to six-day-old neurospheres were collected, centrifuged (500 *g*, 5 min) and resuspended for 15 min at 37°C in accutase (#A1110501, ThermoFisher) to generate single cell suspensions. Single cells were seeded onto PDL-coated petri dishes (100 µg/ml) in DMEM/F12 supplemented with 1% B27 and 1% PS but devoid of growth factors. These

conditions trigger differentiation of SVZ cells. Cells were harvested by trypsinization 24h and 48h after plating and are referred as to progenitor cells. For longer period of differentiation, 2% fetal bovine serum (FBS) was added to the medium (#CVFSVF0001, Eurobio) to promote differentiation. Cells were harvested by trypsinization 3, 5 and 10 days after plating (DIV for days in vitro). To block proteasome activity progenitor cells were treated with 4nM of MG132(#474790, Merck) dissolved in 0.01% of DMSO, for 10h then harvested by trypsinization.

Protein extraction and Western blot

Stem/progenitor cell monolayers and differentiated cells were trypsinized and harvested by centrifugation. Free-floating neurospheres were harvested by centrifugation. Cells were resuspended in RIPA lysis buffer (150 mM NaCl, 20 mM Tris-HCl pH 7.5, 1 mM EDTA, 2.5 mM sodium pyrophosphate, 1 mM EGTA, 1 % sodium deoxycholate and 1 % NP-40) supplemented with protease (1/100, #P8340, Sigma-Aldrich) and phosphatase inhibitors (1/100, #P5726, Sigma-Aldrich). The soluble protein fraction was collected after centrifugation (21,000g, 10 min at 4°C). Protein concentration was measured by the BCA method (#23228, ThermoFisher). Proteins (30 µg total) were diluted in SDS-PAGE sample buffer [6X concentrated: 350 mM Tris, 10% (w/v) SDS, 30% (v/v) glycerol, 0.6 M DTT, 0.06% (w/v) bromophenol blue] then boiled 5 min at 95°C and loaded on both acrylamide/bisacrylamide gels: 5% (for HUWE1, vinculin and Huntingtin proteins), 7% (for Huntingtin, vinculin and EGFR proteins) and 15% (for Sox2, β actin and βIII tubulin proteins). Proteins were transferred to PVDF membranes (polyvinylidene difluoride, #IPVH00010, Merck Millipore) during 2h40 min with constant current of 320 mA. PVDF membranes were blocked in Tris buffer containing 5% bovine serum albumin (BSA) in 0.1% Tween (TBS-T) for 1h at room temperature (RT) and probed overnight at 4°C with primary antibodies (Table 1). Membranes were washed with TBS-T and incubated for 40 min at RT with horseradish peroxidase (HRP)- conjugated secondary antibodies: goat anti- rabbit IgG (H+L) (1/2000, #511380), rabbit anti-goat IgG (H+L) (1/2000, #305-035- 003) (both from Jackson Immunoresearch), and goat anti-mouse IgG1 (1/2000, #1070-05, Southern Biotech). Proteins of interest were detected using a chemiluminescent substrate (ECL, #RPN2236, Merk) and the membranes were imaged on a Chemidoc imaging system (Biorad).

Immunoprecipitation

Stem/progenitor cell monolayers and progenitor cells were trypsinized and harvested by centrifugation. Cells were resuspended in lysis buffer (50mM TRIS-HCl (pH 7.4), 1% NP-40 and 5mM EDTA) supplemented with protease (1/100, #P8340, Sigma-Aldrich) and phosphatase inhibitors (1/100, #P5726, Sigma-Aldrich). Total lysate was diluted in SDS-PAGE sample buffer [6X concentrated: 350 mM Tris, 10% (w/v) SDS, 30% (v/v) glycerol, 0.6 M DTT, 0.06% (w/v) bromophenol blue] then boiled 5 min at 95°C. Approximately 10⁴ (50uL) of mouse IgG beads (#00951543, Invitrogen) were washed 3 times in lysis buffer supplemented with protease and phosphatase inhibitors then incubated either with 1mg of protein (250uL) and 5uL of monoclonal HTT 4C8 antibody or incubated with 250uL of proteins with 5uL of IgG isotype and left to immunoprecipitate HTT overnight at 4°C with rotation to prevent beads settling out of suspension. After, beads were washed 5 times with lysis buffer supplemented with protease and phosphatase inhibitors, supernatant was eluted and beads were diluted in SDS-PAGE sample buffer [6X concentrated: 350 mM Tris, 10% (w/v) SDS, 30% (v/v) glycerol, 0.6 M DTT, 0.06% (w/v) bromophenol blue] then boiled 5 min at 95°C. Western blot was performed as described before.

Immunocytochemistry

SVZ cells were cultured 5 DIV after plating on poly-D-lysine-coated coverslips following the same protocol as depicted in figure 4 and fixed in 4% paraformaldehyde (PFA) for 15 min at room temperature (RT). Cells were permeabilized and nonspecific binding sites blocked using a mixture of 1% Triton X-100 and 3% normal donkey serum (NDS) in PBS for 30 min at RT. Cells were subsequently incubated overnight at 4°C with the primary antibodies as listed in Table 1 diluted in PBS containing 0.1% Triton X-100 and 0.3% NDS. Coverslips were rinsed in PBS and incubated for 2 hours at RT with secondary antibodies Alexa fluor 594 anti-mouse IgG (H+L) and Alexa fluor 488 anti-rabbit IgG (H+L) both produced in donkey (from ThermoFischer Scientific) diluted 1:500 in PBS. Cell nuclei were stained with Hoechst 33342 (2µg/mL in PBS). Coverslips were mounted in Dako fluorescent medium (Dako). Fluorescent images were recorded using fluorescent slide scanner (Axio Scan.Z1, Zeiss).

RNA extraction, quantitative real-time PCR (qPCR) and TaqMan PCR

Total RNA was extracted from stem/progenitor cell monolayers and 48h progenitor cells from both genotypes using the NucleoSpin RNA extraction kit (#740955, Macherey-Nagel). Total RNA was quantified by spectrophotometer on a Nanodrop (Thermofisher). RNA samples (1 µg) were retrotranscribed using the iScript Ready-to-Use cDNA supermix (#1708840, Biorad). cDNAs were diluted 1:10 and submitted to qPCR with SsoAdvanced SYBR Green supermix (#1725272, Biorad) or submitted to TaqMan PCR with iTaq™ Universal Probes Supermix (#1725131, Biorad). Primers used are listed in table 1. The RT-PCR program consisted of a 95°C for 2 min for the first step; 40 cycles of 95°C for 10 sec, 55°C for 15 sec and 72°C for 10 sec for the second step; 95°C for 1 min, 60°C for 30 sec and 95°C for 30 sec for the last step. Meanwhile the TaqMan program consisted of a 50°C for 2 mins, 95°C for 10 mins then 40 cycles of 95°C for 15 secs, 60°C for 1 min Data were analyzed from three independent experiments and presented as the mean ± SEM. The fold-change quantification of target genes was calculated with the $2^{-\Delta\Delta C_t}$ method.

Geometric averaging of mouse TATA box-binding protein (mTBP), phosphoglycerate kinase 1 (PGK1) and cyclophilin G (CYCLO G) was used as internal control for RT-PCR and Glyceraldehyde -3-phosphate dehydrogenase (GAPDH) and phosphoglycerate kinase 1 (PGK1) for TaqMan PCR.

Gene name	Sequence
CYCLO G	F: 5'-AAAGCCGATGACAAGGAG-3'
	R: 5'-AAGAATCGTCGCTGGTATG-3'
mTBP	F: 5'-ACATCTCAGCAACCCACACA-3'
	R: 5'-GGGGTCATAGGAGTCATTGG-3'
PGK	F: 5'-TAGTGGCTGAGATGTGGCACAG-3'
	R: 5'-GCTCACTTCCTTCTCAGGCAG-3'
HTT	(Cat# QT00146902, Qiagen)
HES 5	(Cat#12001950, Biorad)
MASH1	(Cat#12001950, Biorad)
DLX2	(Cat#12001950, Biorad)
GAPDH	(Cat#10031231, Biorad)

Table 1: Primer sequences

Quantification and statistical analysis

Densitometry analyses of Western blot bands were performed using Image Lab or Image J software and protein levels are expressed as ratio of its expression relative to Vinculin. Data are represented as mean \pm SEM of 4 cultures per condition.

Immunoreactive cells were obtained from cells counted in 4 independent microscopy fields (approximately 100 cells per field) in a single culture and cell counts are expressed as mean \pm SEM values. The percentages of GFAP, GalC and β III tubulin positive cells in WT and Q111 SVZ cell cultures were calculated from cell counts in four independent microscopic fields (approximately 100 cells per field) per culture. Data are represented as mean \pm SEM of 4 cultures per condition. Statistics were performed using Kruskal-wallis test followed by Dunn's multiple comparisons test and was set to $p < 0.05$. All analyses were conducted using Graph pad Prism 8.

RESULTS

Establishment of a differentiation protocol

Neural stem cells from the SVZ of early postnatal mice (P0 to P5) were cultured in suspension to generate free-floating neurospheres either, or in adherence on poly-D-lysine (PDL) and laminin to grow as “quiescent” stem cells in a medium devoid of serum and supplemented with EGF and FGF-2. In suspension, cells proliferate in a clonally manner to form aggregates or neurospheres (Figure 1). Five-day-old neurospheres are then dissociated into single cells and plated on poly-D-lysine to initiate adherence and differentiation. Growth factors are withdrawn from the medium to induce cell cycle exit. Forty-eight hours after plating, most of the cells present a bipolar shape, characteristic of progenitors. To stimulate differentiation, 2% FBS is added after 48 hours and onwards (Belenguer *et al.*, 2016)¹. Multipolarized cells are observed at DIV 3, 5, 7 and 10 consistent with ongoing differentiation.

Expression of stem cells and progenitors' markers along the lineage

In order to validate the culture model, the expression of stem cells and progenitors' markers along the lineage was determined by western blot and qPCR. Sox2 is a transcription factor that is expressed in multipotent, self-renewing and proliferating stem cells. Consistently, Sox2 is found in neurospheres ((Doetsch *et al.*, 2002)) and, to a lesser extent, in stem cells cultured in monolayers. Sox2 is no more express upon growth factors removal (Figure 2A and B).

EGFR, the receptor for EGF, is expressed in proliferating stem/progenitor cells but not in progenitors upon EGF and FGF2 removal as observed in western blots (Figure 2A and B).

According to these results, stem cells cultured in adherence in the presence of growth factors will be referred from now on as to quiescent stem cells, stem/progenitor cells in neurospheres will be referred as to activated stem cells, dissociated SVZ cells plated in the absence of growth factors for 24h to 48h will be referred as to progenitors. mRNA levels of DLX2, a marker of C cells in the SVZ lineage, which are progenitors, was determined by qPCR. I found that DLX2 is highly expressed in progenitors as compared to quiescent and activated stem cells (Figure 2C).

Expression of HTT varies along WT and Q111 SVZ lineage

The expression of HTT along the SVZ lineage was evaluated by western blot (Figure 3A). HTT is highly expressed in quiescent and activated stem cells. At the progenitors' stage, expression of HTT drops significantly by 60% (Figure 3A and 3C). Serum is added at DIV 3 and onwards to promote differentiation as shown by the expression of β III tubulin at DIV 5 (Figure 3A). HTT is re-expressed when cells differentiate (Figure 3A). At the mRNA level, HTT is highly expressed in activated stem cells while expression drops significantly in progenitors as assessed by TaqMan qPCR (Figure 3C). HTT mRNA drops by 40% at the progenitor stage as compared to the quiescent stage (Figure 3C). These results show that the decrease of HTT at the progenitor stage is due, at least in part, to a decrease expression of the HTT gene.

Levels of HTT were also evaluated in SVZ cells cultured from Q111 homozygous mice to determine whether the pattern observed in WT cells is altered in HD. Unlike in WT cells, HTT remains expressed at the progenitor stage (Figure 7A and 7B). HTT protein is not detected in early differentiating cells (3 DIV and 5 DIV).

HTT protein is degraded at the progenitor stage.

As the decrease of HTT levels at the progenitor stage is drastic, and considering that the half-life of HTT is of at least 24h (14) it is conceivable that HTT may be degraded by the ubiquitin pathway. To test this hypothesis, cells were dissociated from neurospheres and plated to differentiate for 24h. MG132, a proteasome and autophagy inhibitor that blocks the degradation of ubiquitinated proteins, was added for 10h. Cells were then harvested for protein extraction. Analysis by western blot shows that HTT is present in MG132 treated progenitors as compared to non-treated progenitors (Figure 4A and 4B). This result suggests that ubiquitinated HTT is accumulated in progenitors treated with MG132.

Co-immunoprecipitations were performed with anti-HTT and anti-polyubiquitin antibodies. The resulting immunoprecipitated proteins were run on SDS page gel and immunoblotted for the detection of polyubiquitinated HTT. HTT and polyubiquitin expressions and interactions were upregulated at progenitor stage when treated with 4nM of MG132 compared to non-treated progenitor cells and quiescent cells (Figure 5A and B).

More experiments are still required to conclude.

HUWE1 is expressed in SVZ WT progenitor cells.

The E3 ubiquitin protein ligase HUWE1 has been shown to interact with HTT in a yeast two-hybrid assay performed previously in the lab (data not shown). HUWE1 may therefore tag HTT for degradation in progenitors. Firstly, the expression of HUWE1 was evaluated along the SVZ WT lineage. Preliminary western blot showed that HUWE1 is expressed at the progenitor stage (Figure 6). Further experiments are required to draw out a conclusion about the regulation of HTT degradation by HUWE1 in SVZ WT lineage.

mHTT reduces neuronal differentiation

Immunostaining was performed in order to test whether mHTT alters neuronal and glial differentiation of SVZ stem cells. SVZ cells were plated on poly-D-lysine-coated coverslips. The same protocol as described in Fig 4A was used to differentiate the cells. At DIV 5, cells were fixed and immunostained to reveal GFAP positive astrocytes and β III tubulin positive neurons. Cells were counted. The number of astrocytes is significantly increased in Q111 as compared to WT cultures. However, the number of neurons is decreased in Q111 as compared to WT cultures (Figure 8). These observations suggest the mHTT alters neuronal differentiation while favoring glial differentiation.

DISCUSSION

In this study, we have explored the intricate dynamics of HTT expression during the differentiation of neural stem cells, specifically within the subventricular zone (SVZ) lineage. Our findings reveal a biphasic expression pattern of HTT in the wild-type (WT) lineage, characterized by high expression in quiescent and activated stem cells, followed by a sharp decrease at the progenitor stage. Notably, this regulatory pattern differs in the Q111 lineage, where HTT persists at the progenitor stage. Additionally, we have identified HUWE1, an E3 ubiquitin protein ligase, as an integral player in this process. HUWE1's expression at the

progenitor stage suggests its role in HTT regulation. Furthermore, we have examined various markers, including Sox2 and EGFR, as indicators of stem cells and progenitors, and DLX2, a marker of C cells in the SVZ lineage, which are progenitors. These markers help characterize different stages along the neural stem cell lineage and contribute to our understanding of the observed HTT dynamics.

HUWE1, as a ubiquitin ligase, plays a crucial role in tagging proteins for ubiquitination and subsequent degradation by the proteasome. This mechanism is central to cellular homeostasis and quality control, ensuring that damaged or surplus proteins are efficiently removed. The expression of HUWE1 at the progenitor stage suggests its involvement in the regulation of HTT levels. One plausible hypothesis is that HUWE1 interacts with HTT and mediates its ubiquitination, marking it for proteasomal degradation. This hypothesis aligns with the observed decrease in HTT levels at the progenitor stage. Given that the half-life of HTT is relatively long, the rapid reduction in its levels suggests active degradation mechanisms are at play. The addition of MG132, a proteasome and autophagy inhibitor, results in the accumulation of ubiquitinated HTT in progenitors. This observation strongly supports the notion that the ubiquitin-proteasome pathway is involved in HTT degradation during neural stem cell differentiation. Furthermore, co-immunoprecipitation experiments demonstrate an interaction between HTT and polyubiquitin when progenitor cells are treated with MG132. This interaction suggests that HTT becomes ubiquitinated, marking it for proteasomal degradation.

While these findings provide preliminary evidence for HUWE1's involvement in HTT degradation, more experiments will establish a conclusive link between HUWE1 and HTT regulation in the SVZ WT lineage. Further investigations should aim to elucidate the specific mechanisms through which HUWE1 targets HTT for ubiquitination and degradation, contributing to our understanding of neural stem cell biology and potential implications for Huntington's disease.

The biphasic expression of HTT in the WT lineage holds critical significance in the context of neural stem cell differentiation. In the WT lineage, HTT is initially highly expressed in quiescent and activated stem cells, but its levels drop significantly at the progenitor stage. This dynamic pattern of HTT expression suggests a finely tuned regulatory mechanism during differentiation. The initial high expression of HTT in quiescent and activated stem cells may serve various functions. HTT is known to be involved in various cellular processes, including

transcriptional regulation, intracellular transport, and synaptic function. In the context of neural stem cells, its initial high expression may support the maintenance of stemness and self-renewal capacity. However, the sharp decrease in HTT levels at the progenitor stage likely serves a distinct purpose. As neural stem cells transition into progenitors, they need to undergo significant cellular changes to commit to a specific lineage and initiate differentiation. The reduction in HTT levels could be a critical step in this process, allowing for the derepression of genes or pathways necessary for progenitor identity and differentiation.

Now, when we observe the Q111 lineage, a distinct pattern emerges. HTT remains expressed at the progenitor stage in Q111 cells, in contrast to its downregulation in WT cells. This disparity raises intriguing questions about the underlying mechanisms and the implications for Huntington's disease (HD). One possibility is that the expanded polyglutamine repeat in the Q111 HTT protein alters its regulation and stability. This could lead to its persistence in Q111 progenitors, potentially disrupting normal cellular processes. The exact mechanisms driving this difference need further investigation but could involve altered interactions with regulatory proteins or differences in post-translational modifications.

Additionally, mtt HTT disrupts neurogenesis, skewing differentiation towards glial cells. The decrease in neurons in Q111 SVZ cultures may result from the selective loss of immature neurons. Additionally, further investigations should assess whether this reduction in neurons is compensated for in later differentiation stages. Thus, mtt HTT hinders neuronal differentiation, promoting glial differentiation in SVZ cultures. These experiments, in line with previous research ((Godin et al., 2010)), revealed that the absence of HTT promotes neuronal differentiation while depleting the pool of neuroepithelial cells. Additionally, mutant HTT interferes with neurogenesis during embryonic development (Molina-Calavita et al., 2014)). These findings are consistent with previous research indicating that the absence of HTT directs glial differentiation over neuronal differentiation in mouse embryonic stem cells ((Conforti et al., 2013)).

Collectively, our results suggest that HTT regulation plays a pivotal role in determining the fate of SVZ cells. HTT plays a crucial role in facilitating the transition from the stem cell state to the differentiating state. This implies a significant regulatory function for HTT in governing the transition between these distinct cellular states within the developmental lineage.

Understanding why HTT is expressed in Q111 progenitors while downregulated in WT progenitors could provide crucial insights into the molecular pathways disrupted in HD. It may also shed light on potential therapeutic targets to mitigate the effects of expanded HTT in HD. Further research into the specific molecular interactions and pathways involved in HTT regulation in both WT and Q111 neural stem cells is warranted to unravel the intricacies of this phenomenon.

The findings in this project are consistent with the results obtained in the first project, where HTT downregulation in PN-GBM stem cells contributed to the downregulation of DLL3, a marker of pro-neural stem cells.

FIGURES

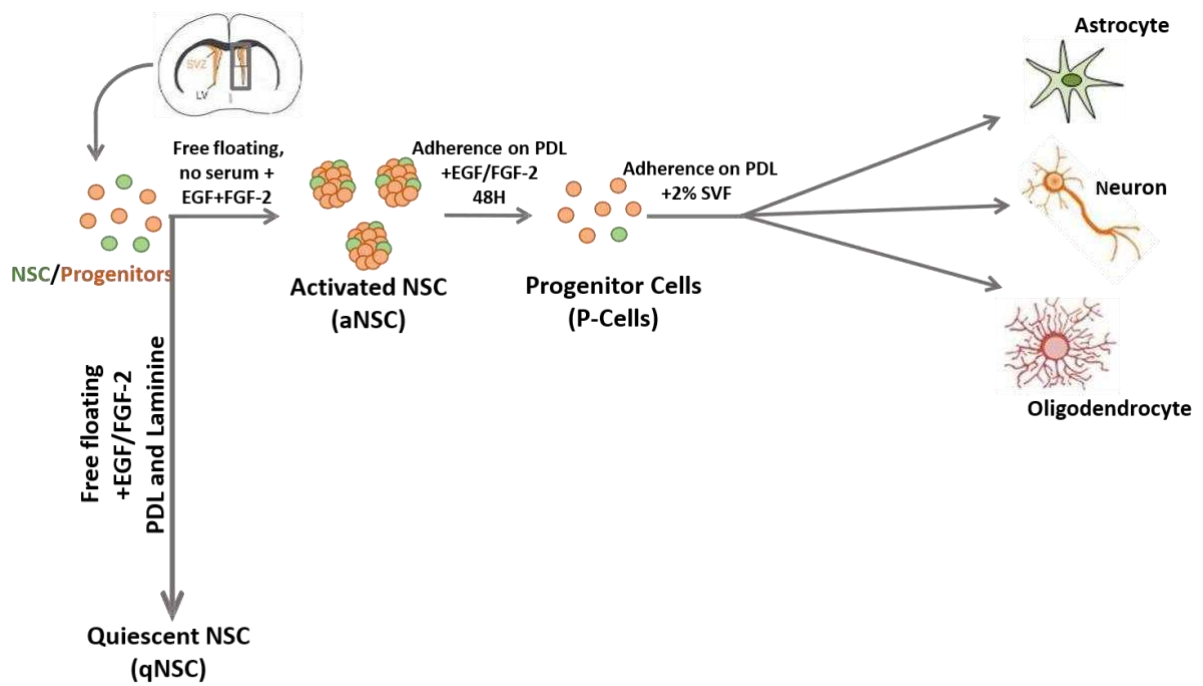


Figure.11 In vitro differentiation protocol of SVZ-NSCs.

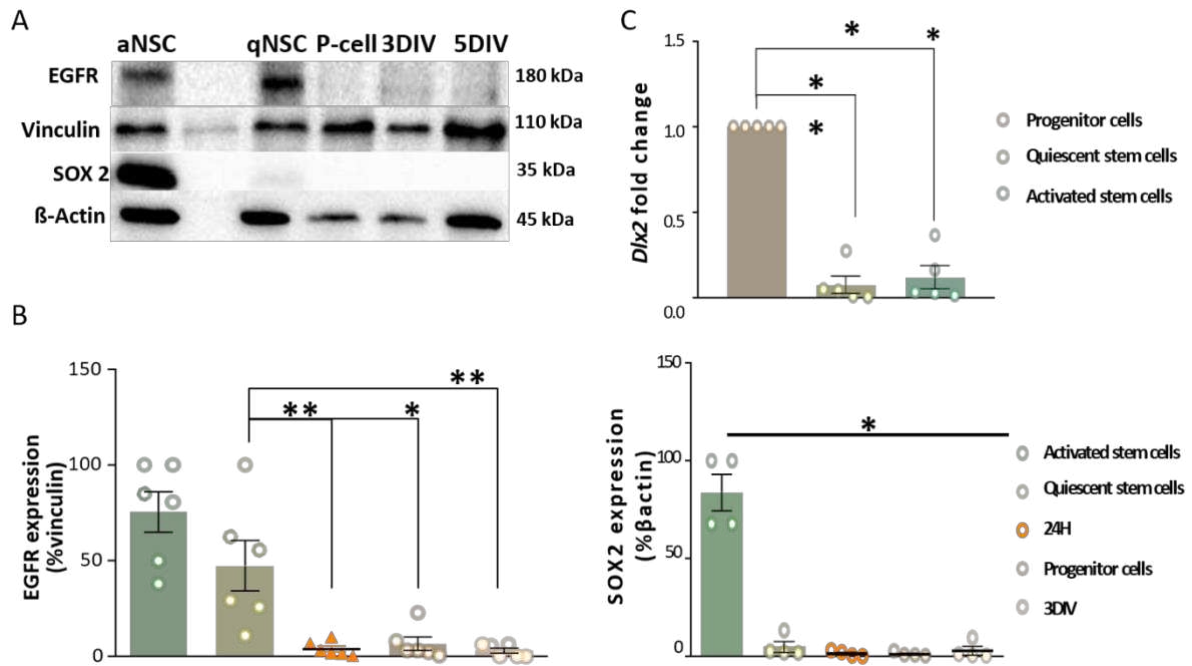


Figure.2I Expression of SVZ lineage markers. A) Representative western blots for EGFR and SOX 2 at different stages of the lineage. β -Actin and vinculin serve as loading controls for total proteins. B) Quantifications of the western blots. At least 4 experiments were done. Kruskal-wallis test followed by Dunn's multiple comparisons test, errors bars: SEM, * $p < 0.05$, ** $p < 0.001$. C) Quantification of DLX2 mRNA in SVZ WT lineage normalized on the expression found in progenitors. 5 experiments were carried out, Kruskal-wallis test followed by Dunn's multiple comparisons test, errors bars: SEM, * $p < 0.05$, ** $p < 0.01$.

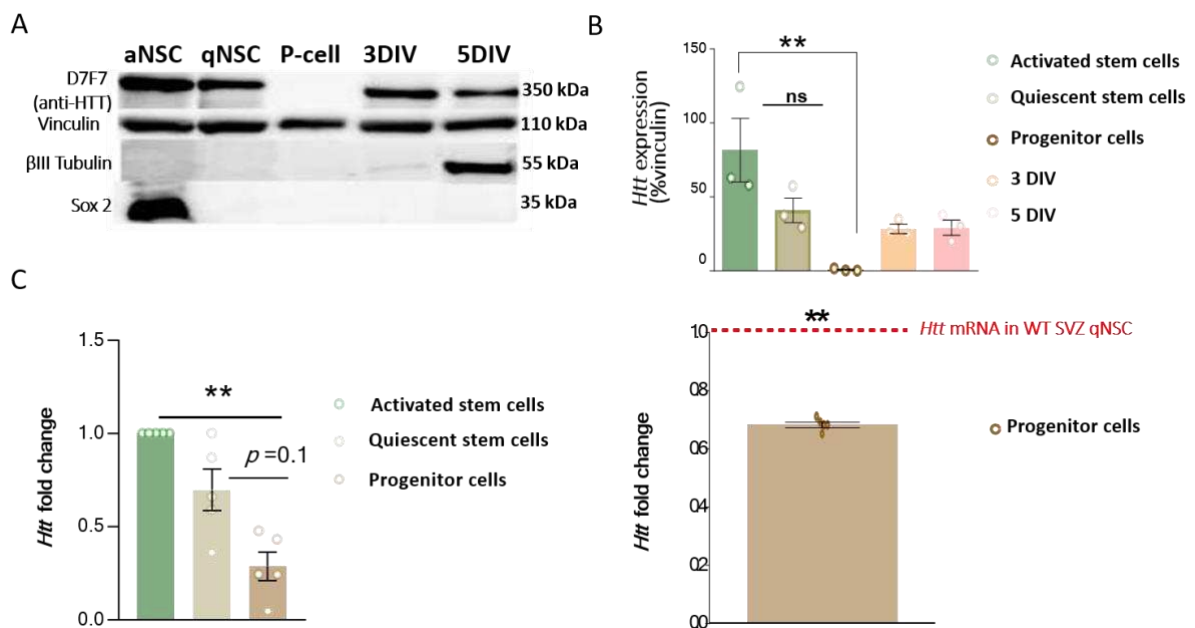


Figure.3I Expression of Huntingtin protein in SVZ WT. A) Representative western blot depicting the variation of HTT protein levels in aNSC, qNSC, progenitors' cells and after induction of differentiation at 3 and 5 DIV in SVZ WT. Sox 2 immunostaining detects highly proliferative and self-renewing cells in neurosphere stem cells. β III Tubulin immunostaining detects differentiated neurons . Vinculin serves as loading control for total proteins. B) Quantification of HTT protein levels in WT cell culture. 3 experiments were done. C) Quantifications of RT-PCR and TaqMan PCR. Kruskal-wallis test followed by Dunn's multiple comparisons test and Mann whitney, errors bars: SEM, * $p < 0.05$, ** $p < 0.001$.

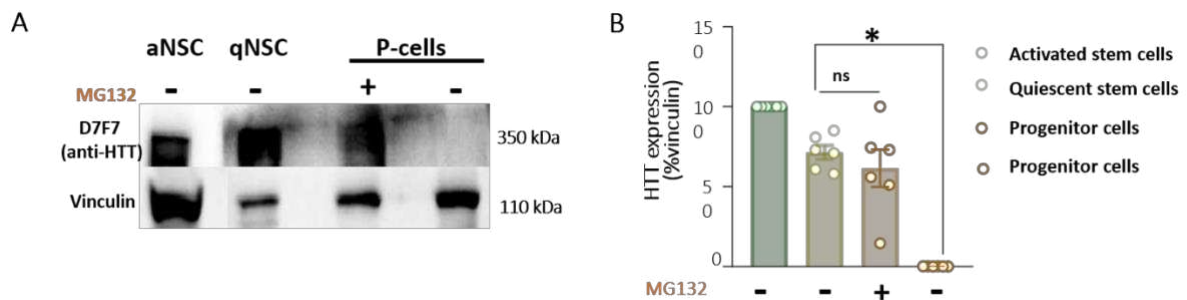


Figure.4I HTT protein is degraded at the progenitor stage. A) Representative western blot of HTT expression in SVZ WT progenitors in the absence or the presence of 4nM of MG132. Levels of HTT in aNSC and qNSC are shown as positive controls. Vinculin serves as a loading control for total proteins. B) Quantifications of the western blots. 6 experiments were done. Kruskal-wallis test followed by Dunn's multiple comparisons test, errors bars: SEM, * $p < 0.05$.

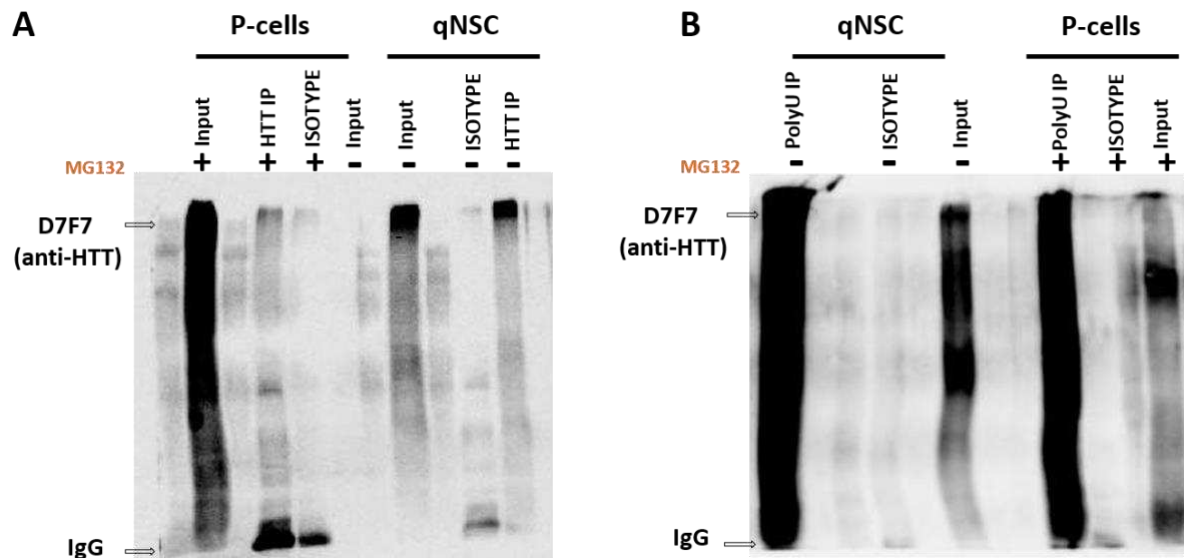


Figure.5I Co-immunoprecipitation of HTT and PolyU in SVZ WT progenitor cells treated with MG132. A) Representative western blot of HTT expression strains in SVZ WT progenitors treated with 4nM of MG132 and aNSC, using an anti-HTT mAB coupled to magnetic beads, B) Representative western blot of PolyU expression strains in SVZ WT progenitors treated with 4nM of MG132 and qNSC, using an anti-PolyU mAB coupled to

magnetic beads, as described in the material and methods. Equivalent quantities of input and isotype bounded beads were loaded and detected with anti HTT mAB.

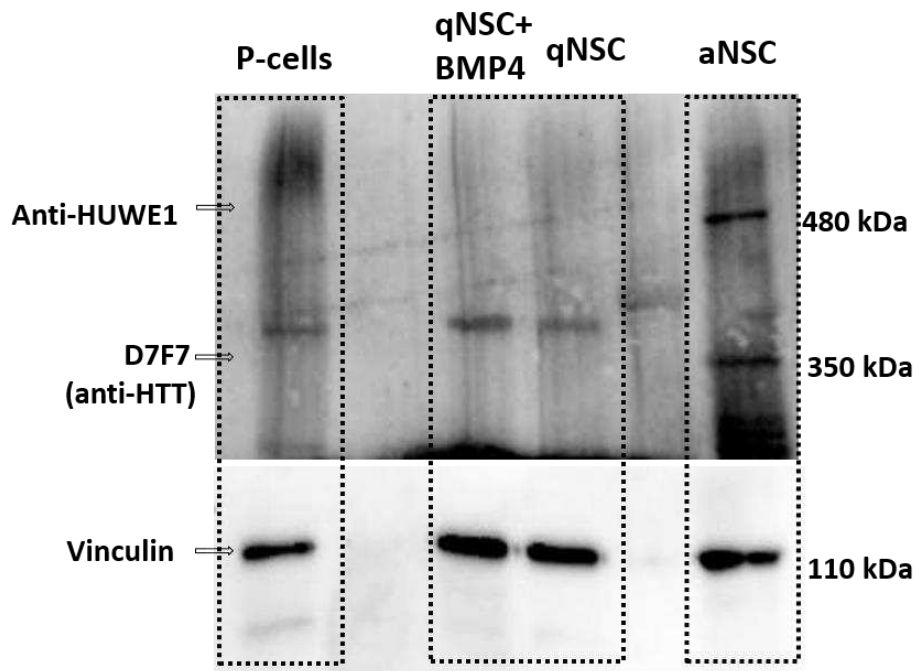


Figure.6I Expression of HUWE1 protein in SVZ WT lineage. Representative western blot for HUWE1 at different time-points of SVZ lineage. Vinculin serves as a loading control for total proteins.

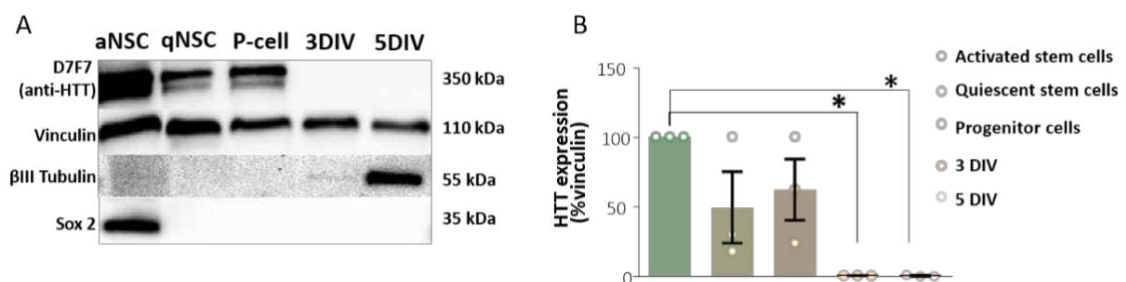


Figure.7I Expression of Huntingtin protein in SVZ Q111. A) Representative western blot depicting the variation of HTT protein levels in neurosphere stem cells, quiescent cells cultured in monolayer, progenitors' cells and SVZ cells after induction of differentiation at 3 and 5 DIV in SVZ Q111. Sox 2 immunostaining detects highly proliferative and self-renewing cells in neurosphere stem cells. βIII Tubulin immunostaining detects differentiated neurons. Vinculin serves as loading control for total proteins. B) Quantification of HTT protein levels in Q111 cell culture, 3 experiments were done, Kruskal-wallis test followed by Dunn's multiple comparisons, errors bars: SEM, *p<0.05.

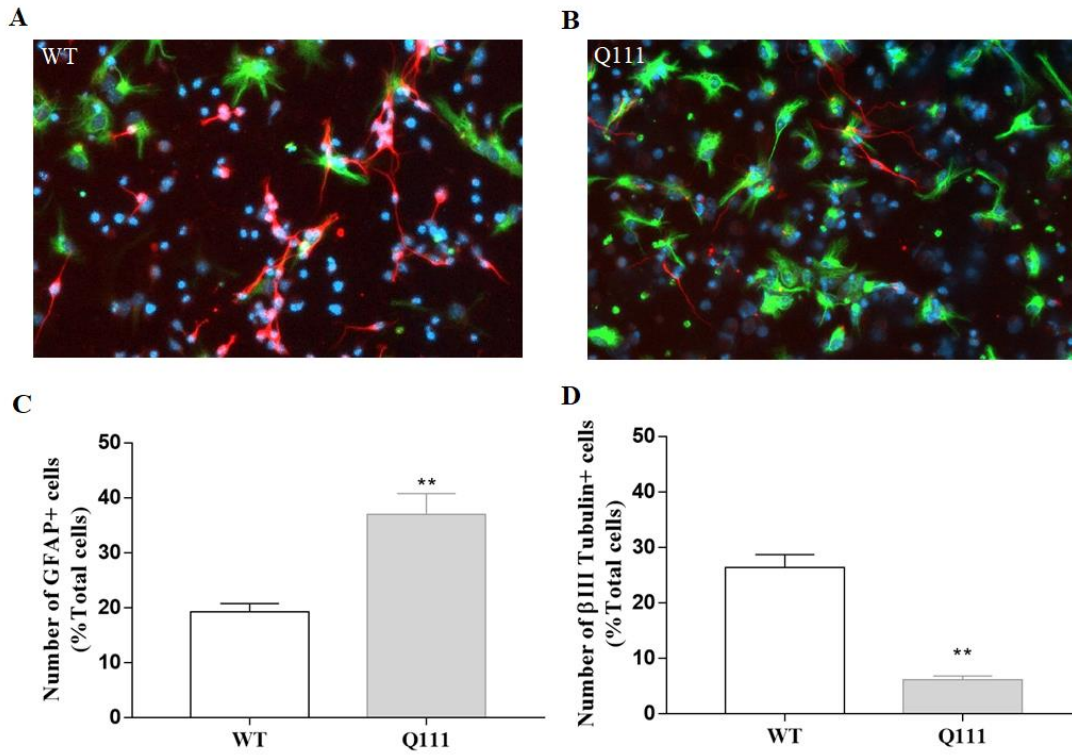


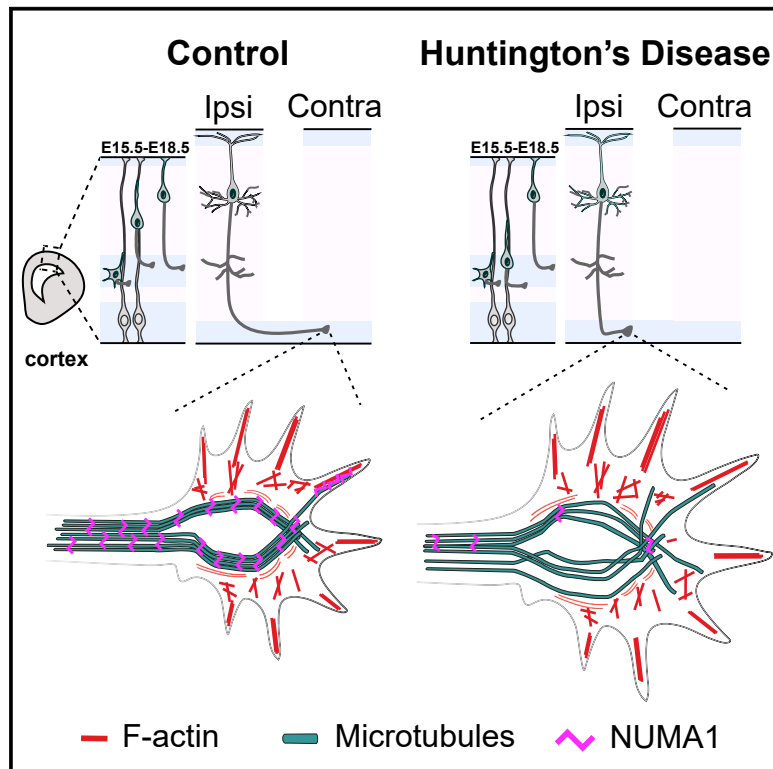
Figure 8I: Defect in neuronal differentiation in Q111. Immunocytochemistry was performed on DIV 5 WT (A) and Q111 (B) SVZ cultures. Astrocytes were immunolabelled for GFAP (green) and neurons for βIII tubulin (red). Nuclei were counterstained with Hoechst (blue). Quantification of GFAP+ astrocytes (C) and βIII tubulin+ neurons (D). Data are represented as mean ± SEM. Mann Whitney U-test, ** p-value < 0.01.



PART III

Developmental defects in Huntington's disease show that axonal growth and microtubule reorganization require NUMA1

Graphical abstract



Authors

Mariacristina Capizzi, Rémi Carpentier, Eric Denarier, ..., Marina Mapelli, Yohann Couté, Sandrine Humbert

Correspondence

sandrine.humbert@univ-grenoble-alpes.fr

In brief

Capizzi et al. show that Huntington's disease (HD) limits axonal growth during development. The microtubules in the axonal growth cones are disorganized in HD because of NUMA1 downregulation. Restoring NUMA1 levels rescues axonal growth in HD mice.

Highlights

- Huntington's disease (HD) causes axonal growth defects during development
- NUMA1 downregulation in HD leads to microtubule disorganization in the growth cone
- NUMA1 downregulation phenocopies HD-induced axonal growth defects
- Restoring NUMA1 expression rescues axonal growth *in vivo*

Article

Developmental defects in Huntington's disease show that axonal growth and microtubule reorganization require NUMA1

Mariacristina Capizzi,¹ Rémi Carpentier,¹ Eric Denarier,¹ Annie Adrait,² Rayane Kassem,¹ Marina Mapelli,³ Yann Couté,² and Sandrine Humbert^{1,4,*}

¹Univ. Grenoble Alpes, Inserm, U1216, CEA, Grenoble Institute Neurosciences, 38000 Grenoble, France

²Univ. Grenoble Alpes, Inserm UMR BioSanté, U1292, CNRS, CEA, FR2048, 38000 Grenoble, France

³IEO, European Institute of Oncology IRCCS, Via Adamello 16, 20139 Milan, Italy

⁴Lead contact

*Correspondence: sandrine.humbert@univ-grenoble-alpes.fr

<https://doi.org/10.1016/j.neuron.2021.10.033>

SUMMARY

Although the classic symptoms of Huntington's disease (HD) manifest in adulthood, neural progenitor cell behavior is already abnormal by 13 weeks' gestation. To determine how these developmental defects evolve, we turned to cell and mouse models. We found that layer II/III neurons that normally connect the hemispheres are limited in their growth in HD by microtubule bundling defects within the axonal growth cone, so that fewer axons cross the corpus callosum. Proteomic analyses of the growth cones revealed that NUMA1 (nuclear/mitotic apparatus protein 1) is downregulated in HD by miR-124. Suppressing NUMA1 in wild-type cells recapitulates the microtubule and axonal growth defects of HD, whereas raising NUMA1 levels with antagomiR-124 or stabilizing microtubules with epothilone B restores microtubule organization and rescues axonal growth. NUMA1 therefore regulates the microtubule network in the growth cone, and HD, which is traditionally conceived as a disease of intracellular trafficking, also disturbs the cytoskeletal network.

INTRODUCTION

Huntington's disease (HD) is caused by an abnormal CAG expansion in the coding region of the *huntingtin* gene, which leads to the production of huntingtin protein (HTT) that bears an abnormally long polyglutamine tract. The classic motor and cognitive symptoms of HD do not typically appear until adulthood, but neuroimaging studies have revealed clear abnormalities in brain structure and function in presymptomatic mutation carriers (Nopoulos et al., 2011; Scahill et al., 2020; Tang et al., 2013; Tereshchenko et al., 2020). Although such changes may be a mix of compensatory, degenerative, and developmental processes, one recent study in HD subjects showed that their lack of asymmetry between the right and left Sylvian fissure (which should be formed around the 14th gestational week) must arise during embryogenesis (Mangin et al., 2020). This was the most suggestive evidence for very early developmental derangement in humans until we were able to study fetal HD mutation carrier tissue and demonstrate molecular abnormalities in neural progenitor cells (Barnat et al., 2020). Because there are so few human samples available, however, and we were limited to studying tissue from 13-week-old fetuses, we were unable to follow the evolution of these molecular defects.

The literature provides a number of hints as to where we should look. HD is most prominently associated with degenera-

tion of the corticostriatal circuit, which may have as much to do with insufficient wild-type HTT function as with dysfunction of the mutant HTT (mHTT). During cortical development, projection neurons produced in the ventricular zone undergo a multipolar-bipolar transition and migrate along the glial fibers to reach their designated layer in the cortical plate, where they integrate and mature. The HTT protein normally maintains the pool of cycling neural progenitors and ensures the multipolar-bipolar transition of newborn neurons and their proper migration (Barnat et al., 2017; Godin et al., 2010). In HD mice, mHTT causes mitotic spindle misorientation of dividing progenitors and decreases cortical thickness at embryonic day (E) 14.5 and E16.5 (Molina-Calavita et al., 2014). mHTT also interferes with the migration and maturation of post-mitotic neurons (Barnat et al., 2017; Cepeda et al., 2003; McKinstry et al., 2014; Molero et al., 2016). Our study of human HD mutation carrier fetuses (Barnat et al., 2020) showed that, as in HD mouse models, the number of proliferating cells is diminished, and more neural progenitors enter lineage specification prematurely. To this subtle defect in neurogenesis we can add defects in neural migration, as some layer-specific neocortical neurons mislocalize in the mouse (Barnat et al., 2017). It is not known whether the neurons are able to integrate properly into the circuit once they reach their destination. We therefore asked whether HD affects axonal growth.

Axonal growth takes place through the growth cone, a highly motile structure located at the tip of the growing axon (reviewed in Lewis et al., 2013; McCormick and Gupton, 2020; Pasterkamp and Burk, 2021; Pinto-Costa and Sousa, 2021). The growth cone receives guidance cues from the extracellular environment and remodels the cytoskeleton accordingly to enable axonal outgrowth. This cytoskeletal reorganization inside the growth cone generates two opposing forces: a “push” from the axonal shaft, driven by microtubule polymerization, and a “pull” from the retrograde flow of ACTIN at the front of the growth cone. Studies in cell models examining how neuritic outgrowth might be affected in HD have yielded somewhat inconsistent results: one study reported longer neurites in neural cultures derived from HD patient-derived induced pluripotent stem cells (iPSCs) (HD iPSC Consortium, 2017), but other studies show shorter neurites in neural cultures derived from HD iPSCs (Mehta et al., 2018), in primary cultures of hippocampal neurons expressing the first exon of mHTT (Ilieva et al., 2019), and in HD neuroblastoma cell lines (Reis et al., 2011). Multiple neuroimaging studies, however, clearly show that the corpus callosum, which integrates function across the hemispheres, is thinner in HD gene carriers (reviewed in Casella et al., 2020; Estevez-Fraga et al., 2021). In HD mice, as in humans, diffusion imaging reveals thinning of the white matter (WM) tracts of the corpus callosum (reviewed in Casella et al., 2020). This thinning has been attributed to the degeneration of callosal axons and myelination deficiencies, but given the early developmental defects in HD, we hypothesized that it actually reflects abnormal axonal growth.

RESULTS

Axonal growth of callosal projection neurons is attenuated in HD from P0

To analyze the axonal growth of callosal neurons in HD, we studied an HD knockin mouse model in which the first exon of the HTT gene is replaced by a human exon 1 carrying 111 CAG repeats (Hdh^{Q7/Q111}) (Wheeler et al., 2002). Hdh^{Q7/Q111} heterozygous mice express mHTT at the endogenous level, recapitulate the genetics of human HD, and provide a reliable model of neurodevelopmental processes that take place in HD human embryos (Barnat et al., 2020).

Callosal projection neurons originating from pyramidal neurons of the superficial cortical layers II/III connect homotopically to the contralateral cortex (Fame et al., 2011). We performed *in utero* electroporation (IUE) of the membrane-targeted red fluorescent protein (mem-RFP) in the somatosensory cortex of mouse embryos at E15.5, when the neurons that form layers II and III are born (Figure 1A) (Hand et al., 2015). We then measured axonal length at postnatal day (P) 0, when fibers begin to cross the corpus callosum (Figure 1B, upper panels). Axons were shorter in Hdh^{Q7/Q111} embryos than in their Hdh^{Q7/Q7} controls and remained so even at P4 (Figure 1B, lower panels). Another HD mouse model, zQ175, showed the same axonal growth defect (Figure S1A) (Menalled et al., 2012).

We next analyzed neuronal development at P21, when the axons have reached their final destination and are connected to the contralateral side. As before, we electroporated mem-

RFP in the somatosensory cortex of E15.5 mouse embryos and selected four regions of interest (Figure 1C). Previous studies reported that layer II/III neurons form branches both ipsi- and contralaterally in layers I/II/III and V but not in layer IV (see, e.g., Hand et al., 2015; Lewis et al., 2013). We made the same observation in P21 axons of Hdh^{Q7/Q7} mice (Figures S1B and S1C). To assess ipsilateral arborization (region 1, somatosensory cortex), we calculated the signal intensity in layer V (Figure S1B); this signal was similar in Hdh^{Q7/Q7} and Hdh^{Q7/Q111} animals. For the contralateral region, we chose region 2, within the area corresponding to the somatosensory cortex, where branching reached its maximum density for both genotypes (Figures 1C and S1C). Signal intensities were lower in Hdh^{Q7/Q111} layers II/III and V than in Hdh^{Q7/Q7} animals (Figure S1C).

To determine whether the sparser arborization in the contralateral region was due to fewer axons arising from the ipsilateral side, we measured the signal intensity in the WM region of region 2 and found it to be lower in the Hdh^{Q7/Q111} animals (i.e., they had fewer axons than controls) (Figure S1C). We next traced the axons along the corpus callosum (Figure 1C, region 3) and measured signal intensity along the line with a fixed width of 200 pixels. Axonal density in the Hdh^{Q7/Q111} corpus callosum was lower than in Hdh^{Q7/Q7} controls (Figure 1D). To measure the contralateral arborization relative to the number of axons that actually reached the contralateral side, we evaluated the signal intensity in layers V and II/III relative to the WM (Figure S1C, bottom graphs). Here the HD mice showed greater arborization, which likely reflects compensation for the lower number of axons.

Last, we analyzed the pattern of branching along the cortex from the corpus callosum to the contralateral region (Figure 1E). We drew a line coronally, focusing on layer II/III, where the axons end (Figure 1C, region 4). In control sections, there were several branching points in the parietal (Figure 1E, areas a and b) and somatosensory regions (Figure 1E, areas c and d). In HD, the major branching area was in the somatosensory cortex. In agreement with our previous quantification (Figure S1C), branching was less dense in HD than in control brains.

Thus, the limitation in axonal growth seen in newborn HD mice continues to affect branching in the contralateral cortex even at P21.

Microtubule disorganization leads to HD cortical neuron growth cone defects

To investigate the morphology of callosal axons at a single-cell resolution, we established a cellular model of layer II/III neurons. We developed primary cultures of wild-type (Hdh^{Q7/Q7}) cortical neurons from E16.5 embryonic mouse brains electroporated at E15.5 with a plasmid encoding myristoylated-Venus (mVenus), a variant of the yellow fluorescent protein (Figure 2A). At 4 days *in vitro* (DIV4), we identified mVenus-positive cells by staining against the cortical layer markers Satb2 and Ctip2, which are expressed in callosal projection and layer V neurons, respectively (Alcamo et al., 2008). Most of the mVenus-positive neurons were SATB2-positive and CTIP2-negative. We developed cultured cells from Hdh^{Q7/Q7} and Hdh^{Q7/Q111} embryos using the same cell culture conditions and measured the axonal length of mVenus-positive cells. Axons were shorter in HD than in

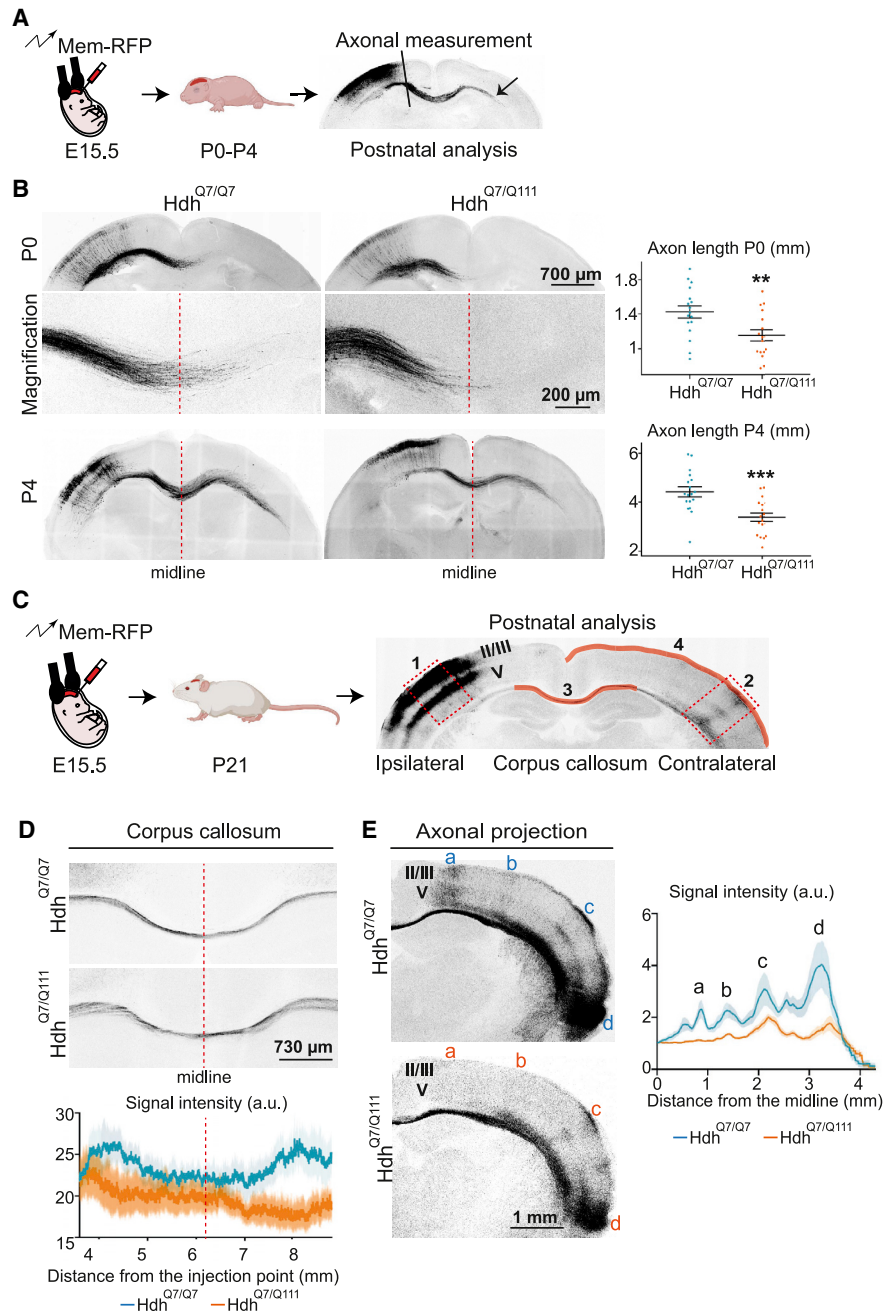


Figure 1. Axonal growth and branching are impaired in HD mice from birth through P21

(A) Selective labeling of layer II/III neurons with membrane-RFP (Mem-RFP) by electroporation at E15.5 and postnatal axonal length measurement. The arrow indicates the end of the axon tract.

(B) Representative coronal sections of P0 and P4 Hdh^{Q7/Q7} and Hdh^{Q7/Q111} cortices with magnification of the corpus callosum for P0. Histograms compare axonal length. P0, unpaired t test, **p = 0.0076 (Hdh^{Q7/Q7}, 1,625 ± 70.7; Hdh^{Q7/Q111}, 1,353 ± 64.22; n = 17 brains for each condition). P4, unpaired t test, ***p = 0.0004 (Hdh^{Q7/Q7}, 4,423 ± 202.2; Hdh^{Q7/Q111}, 3,384 ± 170.8; n = 18 brains for each condition). Error bars denote SEM.

(C) Using the same electroporation scheme, we analyzed four regions of interest (numbered 1–4) at P21 in (D) and (E) and in Figures S1B and S1C.

(D) Representative images of coronal sections of P21 Hdh^{Q7/Q7} and Hdh^{Q7/Q111} cortices showing the corpus callosum. Line scan analysis shows signal intensity (in arbitrary units [a.u.]) along the corpus callosum (region 3). The shaded regions represent SEM.

(E) Representative images of coronal sections of the contralateral side in P21 Hdh^{Q7/Q7} and Hdh^{Q7/Q111} cortices. The line scan analysis shows signal intensity along layer II/III from the parietal to the auditory cortex (region 4). The shaded region represents SEM.

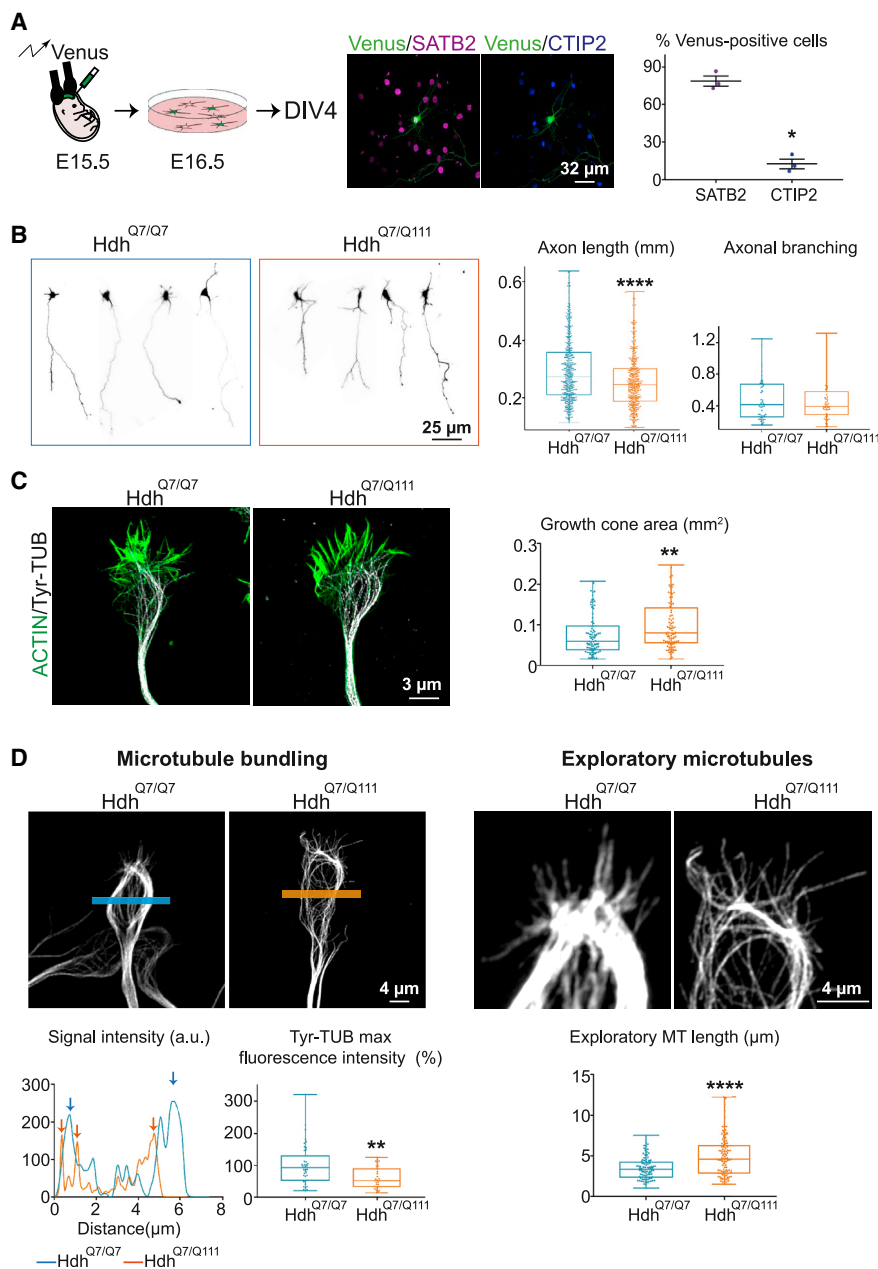


Figure 2. Growth cone morphology and microtubule organization are modified in HD cultured neurons

(A) Schematic of E16.5 primary cell culture of layer II/III neurons that are labeled with mVenus (green) by *in utero* electroporation at E15.5; at DIV4, mVenus-positive neurons are immunostained for SATB2 and CTIP2. The graph quantifies double-positive mVenus-SATB2 and mVenus-CTIP2 cells. Paired t test, * $p = 0.035$ (SATB2, 79.03% \pm 7.08%; CTIP2, 12.41% \pm 6.90%; $n = 3$ independent experiments for each condition).

(B) Representative Hdh^{Q7/Q7} and Hdh^{Q7/Q111} neurons. Axon lengths compared at right using Mann-Whitney test, **** $p < 0.0001$ (Hdh^{Q7/Q7}, median 273.5; Hdh^{Q7/Q111}, median 244.9; $n \geq 425$ axons from five independent experiments for each condition). Primary branches for 100 μm of axon in each genotype were compared using unpaired t test, $p = 0.798$ (Hdh^{Q7/Q7}, median 0.4132; Hdh^{Q7/Q111}, 0.3905; $n \geq 45$ axons from four independent experiments for each condition).

(C) Representative confocal Airyscan images of growth cones immunolabeled with phalloidin (ACTIN, green) and anti-tyrosinated TUBULIN antibody (tyr-TUB, gray). Growth cone areas by genotype compared using Mann-Whitney test, ** $p = 0.002$ (Hdh^{Q7/Q7}, median 59.17; Hdh^{Q7/Q111}, median 79.43; $n \geq 91$ growth cones from four independent experiments for each condition).

(D) Representative confocal Airyscan images of growth cones immunolabeled with anti-tyr-TUB antibody. Representative line scan analysis (relative fluorescence intensity) and quantification of tyr-TUB maximum fluorescence intensity in the two genotypes using Mann-Whitney test, ** $p = 0.002$ (Hdh^{Q7/Q7}, median 92.03; Hdh^{Q7/Q111}, median 51.058; $n \geq 30$ growth cones from three independent experiments for each condition). Lengths of exploratory microtubules in the two genotypes compared using Mann-Whitney test, **** $p < 0.0001$ (Hdh^{Q7/Q7}, median 3.34; Hdh^{Q7/Q111}, median 4.59; $n \geq 98$ exploratory microtubules from four independent experiments for each condition). Error bars denote SEM.

wild-type cultured neurons (Figure 2B), mimicking the *in vivo* condition (Figure 1). Axonal branching, however, was similar in control and HD neurons at this developmental stage *in vitro* (Figure 2B).

As a decrease in neuritic growth correlates with an increase in growth cone size (Ren and Suter, 2016), we labeled the F-ACTIN network with phalloidin to delineate the growth cone periphery and to compare the growth cone area in control and HD neurons. As expected from the inhibited axonal growth in HD, the growth cone area in cortical Hdh^{Q7/Q111} neurons was significantly larger than in Hdh^{Q7/Q7} neurons (Figure 2C). The growth cone owes much of its morphology and directional motility to the dynamic reorganization of microtubules. In the shaft of the axon, microtubules are bundled together, but upon entering the growth cone

they splay out into individual “exploratory microtubules” that extend into the distal, motile domain and invade the ACTIN cytoskeleton (Dent et al., 2011). To examine the microtubules, we used an anti-tyrosinated TUBULIN antibody that reveals both the main microtubule bundle and the exploratory microtubules (Figure 2D). This tyrosinated TUBULIN signal was significantly lower in HD growth cones, indicating fewer microtubules in the bundle (Figure 2D). This was confirmed by the lower mean maximum fluorescence intensities in HD compared with control neurons (Figure 2D, blue and orange arrows on line scan correspond to the bundles in control and HD growth cones, respectively). The exploratory microtubules in the peripheral domain were also longer in Hdh^{Q7/Q111} than in Hdh^{Q7/Q7} neurons. We

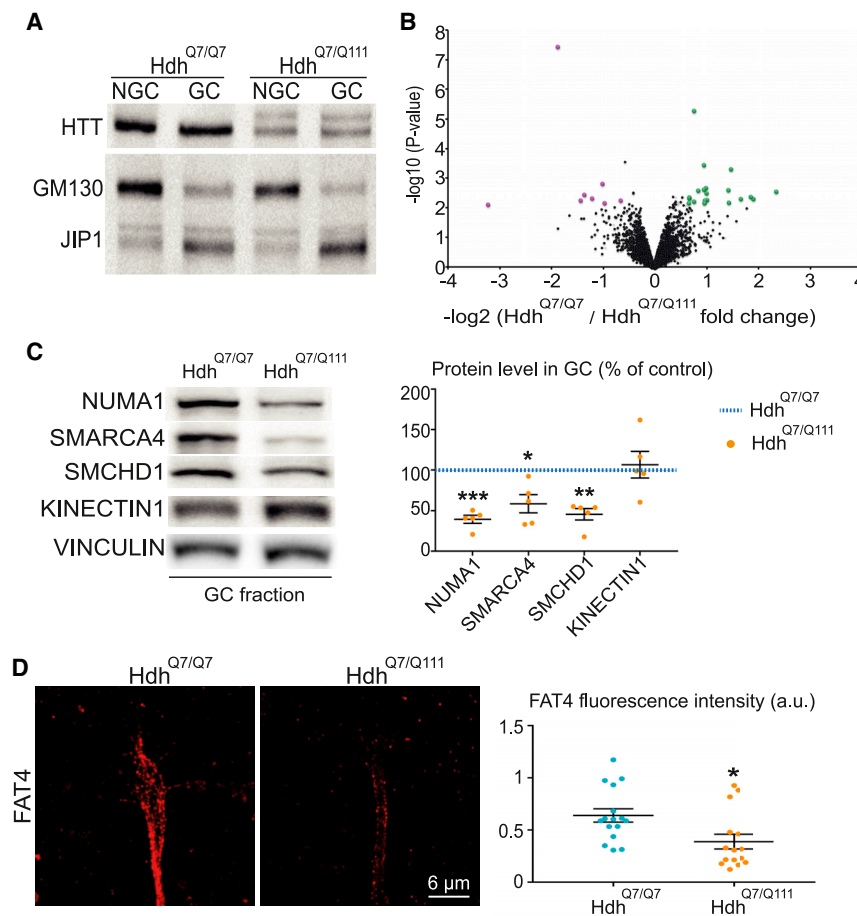


Figure 3. Proteomic analysis highlights alterations in growth cone proteins in HD

(A) HTT, GM130, and JIP1 immunoblotting analyses of non-growth cone (NGC) and growth cone (GC) fractions of Hdh^{Q7/Q7} and Hdh^{Q7/Q111} cortices. (B) Volcano plot displaying the differential abundance of proteins in Hdh^{Q7/Q7} and Hdh^{Q7/Q111} growth cone preparations analyzed by MS-based quantitative proteomics. The volcano plot represents the $-\log_{10}$ (limma p value) on the y axis plotted against the \log_2 (fold change Hdh^{Q7/Q7}/Hdh^{Q7/Q111} growth cones) on the x axis. Green and purple dots represent proteins more abundant in Hdh^{Q7/Q7} or Hdh^{Q7/Q111} mice, respectively (five biological replicates, \log_2 fold change ≥ 0.67 or ≤ -0.67 , $p \leq 0.01$; Benjamini-Hochberg false discovery rate [FDR] $< 5\%$).

(C) Immunoblotting analyses of growth cone (GC) fractions for NUMA1, SMARCA4, SMCHD1, KINECTIN1, and VINCULIN, quantified on the right as amount in Hdh^{Q7/Q111} cortices expressed as percentage of Hdh^{Q7/Q7} in $n = 5$ paired experiments. Paired t test, *** $p = 0.0003$ (NUMA1, mean of difference -60 ± 5.021); * $p = 0.021$ (SMARCA4, mean of difference 41.39 ± 11.27); ** $p = 0.0015$ (SMCHD1, mean of difference 54.41 ± 7.08); $p = 0.71$ (KINECTIN1, mean of difference 6.65 ± 16.51). (D) Representative confocal images of growth cones immunostained for FAT4 (red). Histogram to the right shows FAT4 fluorescence intensity. Unpaired t test, * $p = 0.01$ (Hdh^{Q7/Q7}, 639.2 ± 63.98 ; Hdh^{Q7/Q111}, 388.7 ± 70.32 ; $n \geq 5$ growth cones from three independent experiments for each condition). Error bars denote SEM.

conclude that HD defective axonal growth is associated with microtubule disorganization in the growth cones.

HD alters the protein composition of growth cones

To decipher the molecular basis of HD-induced defects in axonal growth in an unbiased manner, we performed mass spectrometry (MS)-based quantitative proteomic analysis on control and HD growth cones prepared from cortices of newborn Hdh^{Q7/Q7} and Hdh^{Q7/Q111} mice using sucrose density-gradient ultracentrifugation (Leshchyns'ka and Sytnyk, 2013). We chose P0 because the axons are undergoing intense growth at this stage (Lewis et al., 2013). We controlled our enrichment protocol by analyzing the *cis*-Golgi matrix protein (GM130) and the growth cone JNK-interacting protein 1 (JIP1) (Figure 3A). As expected (Dajas-Bailador et al., 2008), GM130 was mostly in the non-growth cone fraction, while JIP1 was enriched in the growth cone fraction.

This analysis yielded 2,873 different proteins identified with at least two peptides (Table S1). We compared this list of proteins with a reference growth cone proteome (Igarashi, 2014) and found that 97% of the major growth cone markers were present in our growth cone proteome from Hdh^{Q7/Q7} and Hdh^{Q7/Q111} mice (Table S2), but none differed in abundance between the two genotypes. Among the 2,873 proteins, 20 were less abundant and 8 more abundant in Hdh^{Q7/Q111} growth cone prepara-

tions (Figure 3B; Table S1). These proteins belonged to six main functional categories (Table S3). The two major classes were DNA- and RNA-binding proteins, among which chromatin modifiers and transcription factors were the most abundant class that was downregulated in HD. Several other studies have highlighted the presence of transcription factors in the axon growth cone (Ji and Jaffrey, 2014; Suzuki et al., 2020), though a relationship between transcription and axonal growth has yet to be established. We found several microtubule-, lipid-, and ubiquitin-binding proteins and proteins involved in transport (e.g., KINECTIN1 [KTN1]). Several cell adhesion proteins, such as FAT atypical cadherin 4 (FAT4), were also differentially regulated in HD. We validated candidate proteins in each of these categories by immunoblotting growth cone-enriched fractions from P0 cortices of Hdh^{Q7/Q7} and Hdh^{Q7/Q111} mice (Figure 3C). We focused on the downregulated hits because MS analysis detected only a small number of peptides for the upregulated ones (Table S1, column E). We then focused on proteins for which antibodies were available. We confirmed the downregulation of the transcription activator SMARCA4 and the structural maintenance of chromosomes flexible hinge domain-containing protein 1 (SMCHD1) but could not confirm KTN1 downregulation in the HD growth cone (Figure 3C). Immunocytochemistry confirmed the strong downregulation of FAT4 in the HD growth cone (Figure 3D).

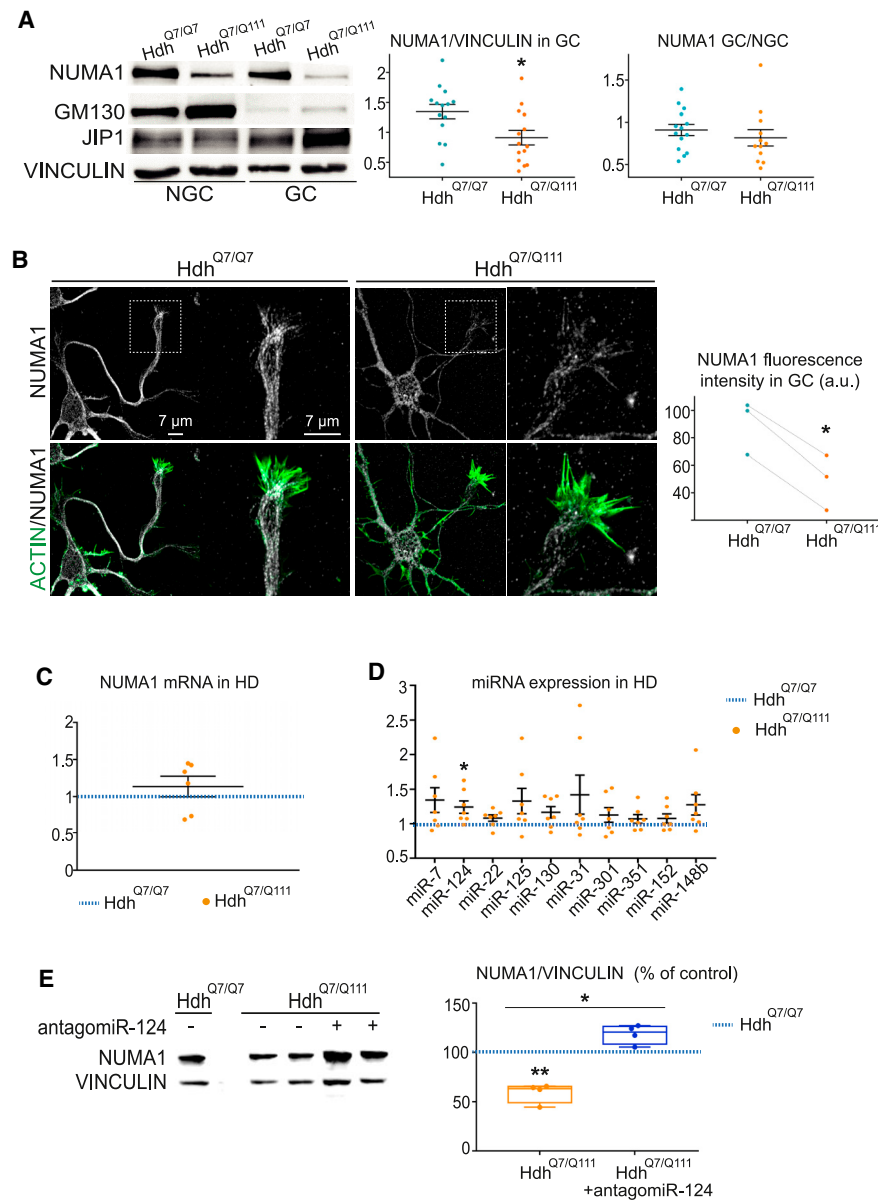


Figure 4. NUMA1 expression is decreased in HD by miR-124

(A) Immunoblotting for NUMA1, VINCULIN, GM130, and JIP1 in non-growth cone (NGC) and growth cone (GC) fractions. Histogram to the right quantifies NUMA1 in the GC fraction and, at the far right, in the GC fraction relative to the NGC fraction of both genotypes, in at least five independent experiments for each condition. Unpaired t test, * $p = 0.017$ (Hdh^{Q7/Q7}, 1.35 ± 0.12 ; Hdh^{Q7/Q111}, 0.912 ± 0.122); ns ($p = 0.43$; Hdh^{Q7/Q7}, 0.91 ± 0.07 ; Hdh^{Q7/Q111}, 0.817 ± 0.096).

(B) Representative confocal images of cortical neurons at DIV4 and magnification of Hdh^{Q7/Q7} and Hdh^{Q7/Q111} growth cones immunolabeled with anti-NUMA1 antibody (gray) and phalloidin (green, to show ACTIN). The graph shows NUMA1 fluorescence intensity in both genotypes across three paired experiments. Paired t test, * $p = 0.04$ (mean of difference between Hdh^{Q7/Q7} and Hdh^{Q7/Q111}, 41.7 ± 3.335).

(C) The graph shows NUMA1 mRNA expression analyzed using qRT-PCR in P0 cortices. Relative quantification was measured by means of the comparative cycle threshold ($\Delta\Delta Ct$) method. Paired t test, $p = 0.37$ (Hdh^{Q7/Q111}, mean of difference 0.14 ± 0.14 ; $n = 6$ independent experiments).

(D) The graph shows miRNA expression analyzed using qRT-PCR in P0 cortices, using the comparative cycle threshold ($\Delta\Delta Ct$) method. Paired t test, $p = 0.1$ (miR-7, mean of difference 0.68 ± 0.36); * $p = 0.037$ (miR-124, mean of difference 0.48 ± 0.18), $p = 0.1$ (miR-22, mean of difference 0.16 ± 0.09), $p = 0.1$ (miR-125, mean of difference 0.65 ± 0.37), $p = 0.1$ (miR-130, mean of difference 0.33 ± 0.17), $p = 0.2$ (miR-31, mean of difference 0.84 ± 0.56), $p = 0.3$ (miR-301, mean of difference 0.25 ± 0.21), $p = 0.3$ (miR-351, mean of difference 0.14 ± 0.13), $p = 0.3$ (miR-152, mean of difference 0.15 ± 0.13), $p = 0.1$ (miR-148b, mean of difference 0.55 ± 0.30).

(E) NUMA1 and VINCULIN immunoblotting in DIV4 Hdh^{Q7/Q7} and Hdh^{Q7/Q111} cortical neurons treated as indicated. NUMA1 was assessed 72 h after transfection. Graph to the right shows NUMA1 protein levels in Hdh^{Q7/Q111} neurons as percentage of its level in control neurons. One-way ANOVA, Tukey's

(legend continued on next page)

Among these candidates, we were particularly interested in the microtubule-binding nuclear/mitotic apparatus protein 1 (NUMA1) (Figure 3B) because it promised insight into the bundling defect that we observed in the HD growth cone: the C-terminal domain of NUMA1 has a stretch of 100 amino acids that directly bind and bundle microtubules (Haren and Merdes, 2002). NUMA1 protein levels were also 3.6-fold lower in HD mice than in controls; this result seems highly reliable, as the protein was identified and quantified with 18 different peptides (Table S1). Although NUMA1 has been shown to bundle microtubules during cell division (Forth et al., 2014; Gallini et al., 2016; Merdes et al., 1996), we postulated that it might be important for bundling during axonal growth. We verified NUMA1 expression by immunoblotting (Figure 3C) and found that NUMA1 protein levels were downregulated in the HD growth cone fraction, in agreement with our MS-based quantitative characterization.

miR-124 and protein degradation pathways lead to NUMA1 downregulation in HD

NUMA1 downregulation in P0 HD cortical growth cone fractions was proportional to its decrease in non-growth cone fractions that include cell bodies, axons, and dendrites (Figure 4A). NUMA1 protein was also markedly decreased in both the nuclear and the cytosolic extracts of HD brains compared with control (Figure S2A). We then stained cortical neurons at DIV4 for the presence of NUMA1: NUMA1 staining was visible in the cell body, along neurites, and in the growth cone in controls (Figure 4B). NUMA1 levels were overall lower in all cellular compartments of Hdh^{Q7/Q111} than in Hdh^{Q7/Q7} neurons (Figures 4A and 4B). These data suggest that the lower level of NUMA1 in the HD growth cone reflects a genuine decrease in abundance rather than a defect in the distribution of the protein.

To determine whether NUMA1 mRNA levels were deregulated in HD at the transcriptional or post-transcriptional level (Figure 4C), we performed quantitative reverse transcriptase PCR (qRT-PCR). NUMA1 mRNA levels were similar in P0 control and HD cortices, indicating that NUMA1 downregulation in HD occurs mostly at the post-transcriptional level. We decided to look for microRNAs (miRNAs), which have been closely linked to the post-translational regulation of almost all fundamental biological pathways, including axonal growth during cortical development (Wilson and Cáceres, 2020). We performed an *in silico* analysis of mouse NUMA1 3' UTR using the biotool TargetScan and found ten miRNAs with putative binding sites in the 3' UTR of NUMA1. Among them, only miR-124 was significantly upregulated in HD compared with control cortices (Figure 4D). To see whether NUMA1 is a target of miR-124, we electroporated primary cultures of Hdh^{Q7/Q111} neurons with antagomiR-124 (Figure 4E). Inhibiting miR-124 markedly increased NUMA1 in HD cells.

We also investigated the two main mechanisms of protein degradation, autophagy and the ubiquitin-proteasome system (UPS) (Figures S2B and S2C). We treated HD cortical neurons with bafilomycin or MG132 (lysosome and proteasome inhibitors,

respectively). As expected, bafilomycin increased the levels of the autophagy adaptor protein p62, and treatment with MG132 increased ubiquitination overall. Both treatments augmented NUMA1 protein levels in HD compared with the non-treated conditions. There are probably several mechanisms at work to regulate NUMA1 protein levels in HD, with miR-124 acting upstream to suppress NUMA1 even before lysosomal or proteasomal degradation.

NUMA1 localizes to microtubules in the growth cones of cortical neurons

Because NUMA1 has never been reported to play a role in axonal development, we first investigated this possibility in control conditions. We immunoblotted extracts from primary cultures of cortical neurons at different DIV corresponding to different stages of maturation (Lewis et al., 2013). NUMA1 expression remained constant during the first week of maturation (dendrite and axonal outgrowth) and decreased after DIV6, when neurons start to establish interneuronal connections (Figure 5A). This expression pattern was consistent with previous studies (Ferhat et al., 1998; Torii et al., 2020) and suggests that NUMA1 plays a role in neuronal maturation.

We also stained cortical neurons in culture for the presence of NUMA1. In DIV3 neurons, NUMA1 was found in the cell body, along neurites, and in the growth cone (Figure 5B, upper panels). We looked specifically at NUMA1 localization in axonal growth cones by immunostaining for the presence of TAU and F-ACTIN, which label axons and the growth cone periphery, respectively (Figure 5B, lower panels). NUMA1 staining was strong in the axonal shaft and in the growth cone but did not show obvious colocalization with F-ACTIN. We then analyzed NUMA1 distribution with regard to the microtubule cytoskeleton (Figure 5C). NUMA1 was particularly enriched in the main microtubule bundle. It also decorated the exploratory microtubules in the peripheral domain that contact the growth cone cortex. To confirm the association between NUMA1 and microtubules, we used a detergent extraction assay on cortical neurons to wash out proteins that are not associated with the cytoskeleton (Figure 5D). As expected, detergent treatment eliminated cytosolic GFP, whereas the endogenous NUMA1 signal remained in the growth cone, where it strongly localized with the major microtubule bundle in the central domain. Confirming these observations, NUMA1 was enriched with polymerized microtubules in a microtubule co-sedimentation assay from protein extract of P0 cortical tissue (Figure S3).

Downregulation of NUMA1 recapitulates the HD defect in axonal outgrowth

We next investigated NUMA1's contribution to axonal outgrowth of callosal fibers in the P4 brain. Because NUMA1 is important for mitosis, cell polarization, and migration (di Pietro et al., 2016; Jin et al., 2017; Torii et al., 2020), anything that interfered with these functions would likely affect postnatal axonal growth. We therefore

multiple-comparisons test, ** $p = 0.0077$ (mean of difference between Hdh^{Q7/Q7} and Hdh^{Q7/Q111} 0.4), $p = 0.06$ (mean of difference between Hdh^{Q7/Q7} and Hdh^{Q7/Q111}+AntagomiR-124 -0.18), * $p = 0.01$ (mean of difference between Hdh^{Q7/Q111} and Hdh^{Q7/Q111}+AntagomiR-124 -0.59; $n = 4$ independent experiments for each condition).

Error bars denote SEM.

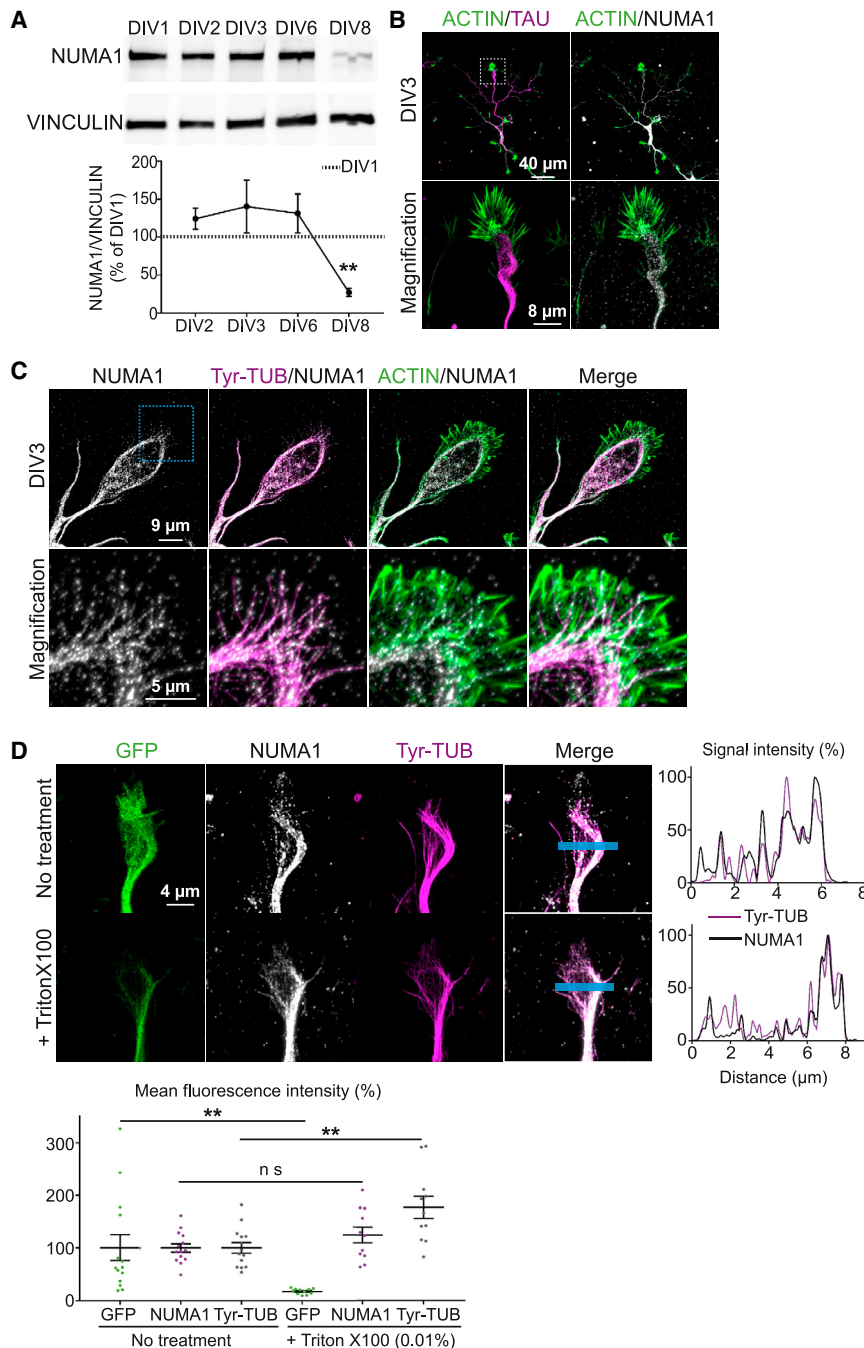


Figure 5. NUMA1 is enriched on microtubules in growth cones

(A) NUMA1 and VINCULIN immunoblotting analysis at indicated DIV. The graph corresponds to the quantitative evaluation of NUMA1 protein in *Hdh*^{Q7/Q7} cortical neurons express in percentage of DIV1. One-way ANOVA with multiple comparisons followed by Dunnett's post hoc test, ***p* = 0.002 (DIV8, -72.85 ± 5.35).

(B) Representative neurons immunostained for F-ACTIN (green), TAU-1 (magenta), and NUMA1 (gray). All confocal images taken with Airyscan. (C) Representative growth cones immunostained for NUMA1 (gray), tyr-TUB (magenta), and F-ACTIN (green).

(D) Representative growth cones immunostained for GFP (green), NUMA1 (gray), and tyr-TUB (magenta). Before immunostaining, neurons were treated (+Triton X-100) or not with detergent to extract soluble proteins. Line scan analyses show fluorescence intensities of NUMA1 and tyr-TUB staining; graphs represent at least five growth cones for three independent experiments for each condition. Unpaired t test, ***p* = 0.003 (GFP no treatment, 100 ± 14.77 ; +Triton X-100, 17.18 ± 1.545), ***p* = 0.002 (tyr-TUB no treatment, 100 ± 10.12 ; +Triton X-100, 177 ± 20.83), *p* = 0.136 (NUMA1 no treatment, 100 ± 8.00 ; +Triton X-100, 124 ± 14.83).

Error bars denote SEM.

ifen-dependent ERT2-CRE construct so that CRE expression can be induced in P0 pups by tamoxifen injection (Figures 6A and 6C). Both conditions (NUMA1 decreased from embryonic or postnatal stages only) recapitulated the HD phenotype to the same extent, with callosal projections crossing the midline but being shorter than controls (Figures 6B and 6C). Thus, NUMA1 depletion during the postnatal period, independent of neuronal migration, is sufficient to affect axonal outgrowth of callosal fibers *in vivo*.

To decipher the mechanisms involved in NUMA1-induced deregulation of axonal outgrowth, we cultured E16.5 wild-type cortical neurons that were previously electroporated with mVenus at E15.5 (Figure S4A). As NUMA1 contributes to

axonal polarization (Torii et al., 2020), we decreased the expression of NUMA1 by infecting cells with lentivirus expressing short hairpin RNA (shRNA) against the NUMA1 mRNA at late DIV1, when the cells are polarized and the axon specified in our primary cortical cultures. Immunoblotting revealed that NUMA1 was efficiently downregulated at DIV4 (Figure S4B). As *in vivo*, NUMA1-depleted callosal neurons *in vitro* had shorter axons (Figure S4C) and larger growth cones (Figure 6D) than control neurons. The main microtubule bundle in the central domain of the growth cone was markedly disorganized, and the exploratory

used IUE to decrease NUMA1 in post-mitotic cells once they exit the cell cycle or once their migration is completed (Figure 6A). We first decreased NUMA1 in newborn neurons by electroporating lox-GFPshNUMA1 or lox-GFP only in E15.5 embryos with a plasmid expressing CRE under the control regulatory sequence of the NeuroD promoter (ND:CRE) (Figures 6A and 6B). In this way, NeuroD is expressed in newborn neurons but not in cycling progenitors or TBR2-positive intermediate progenitors. Second, to target cells that have ended their migration, we electroporated E15.5 embryos with lox-GFPshNUMA1 or lox-GFP with a tamox-

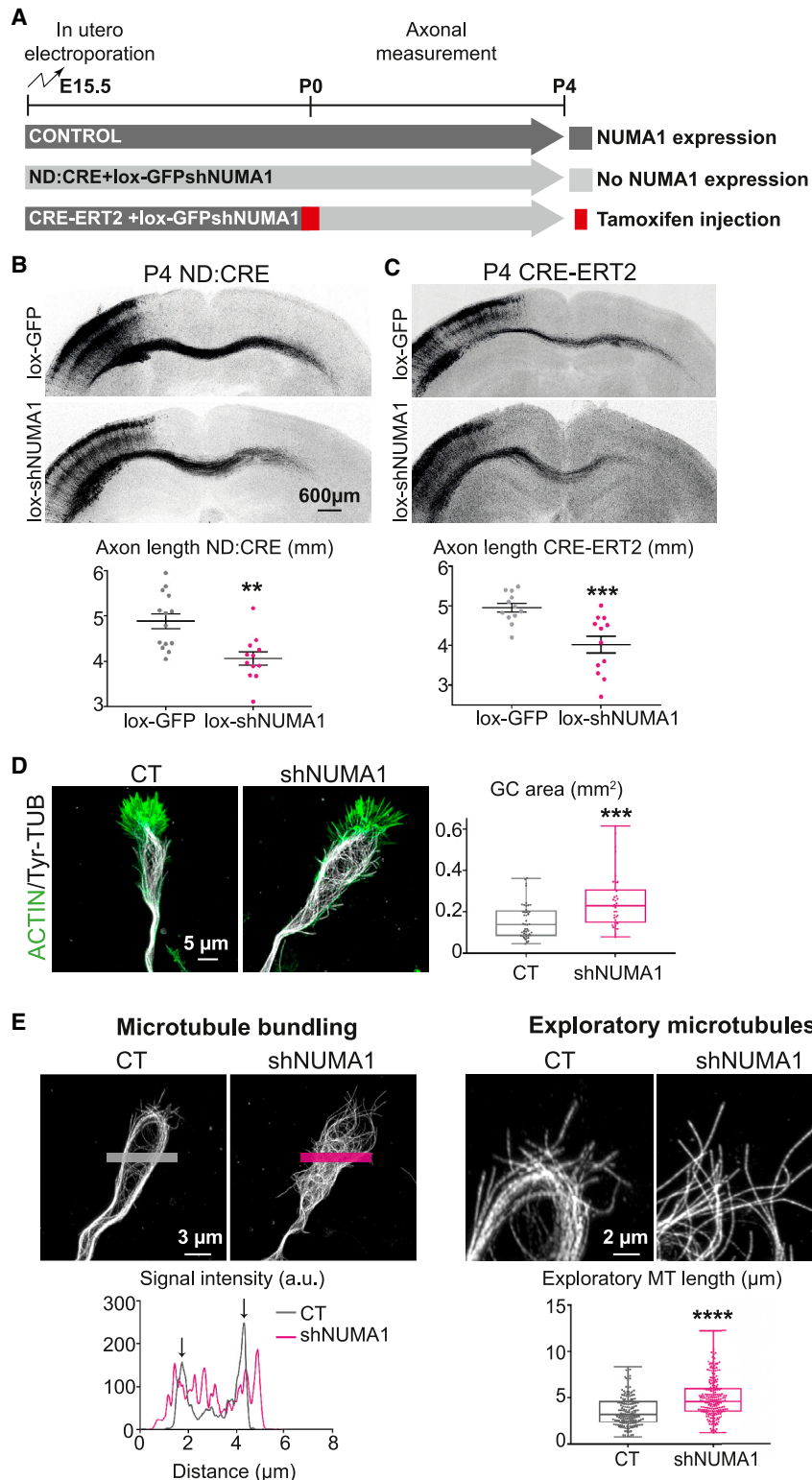


Figure 6. NUMA1 depletion impairs axonal growth in mice

(A) Procedure to delete NUMA1 in layer II/III neurons from embryonic neuronal differentiation to P4 or from the end of neuronal migration (P0) to P4. The control was wild-type mice electroporated with ND-CRE +lox-GFP or CRE-ERT2 +lox-GFP.

(B) Representative coronal sections of P4 ND:CRE + lox-GFP and ND:CRE + lox-GFPshNUMA1 cortices. Histograms quantify axonal length. Unpaired t test, **p = 0.001 (ND:CRE + Lox-GFP, 4,886 ± 163.7, n = 14; ND:CRE + lox-GFPshNUMA1, 4,060 ± 145.2; n = 12 brains for each condition).

(C) Representative coronal sections of P4 CRE-ERT2 + lox-GFP and CRE-ERT2 + lox-GFPshNUMA1 cortices. Histograms quantify axonal length. Unpaired t test, ***p = 0.0008 (CRE-ERT2 + Lox-GFP, 4,953 ± 110.6; CRE-ERT2 + lox-GFPshNUMA1, 4,017 ± 214; n = 12 brains for each condition).

(D) Representative confocal images of growth cones immunolabeled with phalloidin (ACTIN, green) and anti-tyrosinated TUBULIN antibody (tyr-TUB, gray). The graph compares growth cone areas in control (CT) and NUMA1-depleted (shNUMA1) conditions. Unpaired t test, ***p = 0.0001 (control, median 139.1; shNUMA1, median 228.3; n ≥ 10 growth cones from four independent experiments for each condition).

(E) Representative confocal Airyscan images of growth cones immunolabeled with anti-tyr-TUB antibody show effects of NUMA1 suppression. Left histogram: representative line scan analysis (relative fluorescence intensity). Right histogram: lengths of exploratory microtubules. Mann-Whitney test, ****p < 0.0001 (control, median 3.17; shNUMA1, median 4.58; n ≥ 172 exploratory microtubules from four independent experiments for each condition).

Error bars denote SEM.

Expression of NUMA1 restores microtubule bundling and rescues axonal length in HD mice

To determine whether HD-induced defects in axonal development are caused by the downregulation of NUMA1, we prepared primary cultures of cortical neurons from E16.5 Hdh^{Q7/Q7} and Hdh^{Q7/Q111} brains electroporated at E15.5 with a plasmid encoding cytosolic NUMA1 (i.e., NUMA1 without its nuclear localization signal) tagged with GFP (GFP-NUMA1) (Figure 7A). We next assessed whether NUMA1 promotes axonal growth in HD through

microtubules in the peripheral domain grew longer (Figure 6E). Loss of NUMA1 thus recapitulates HD-induced defects in axonal growth and microtubule organization in the growth cone.

its ability to bind and organize the microtubule arrays. For that purpose, we expressed a plasmid encoding a version of the NUMA1 protein in which the microtubule-binding domain

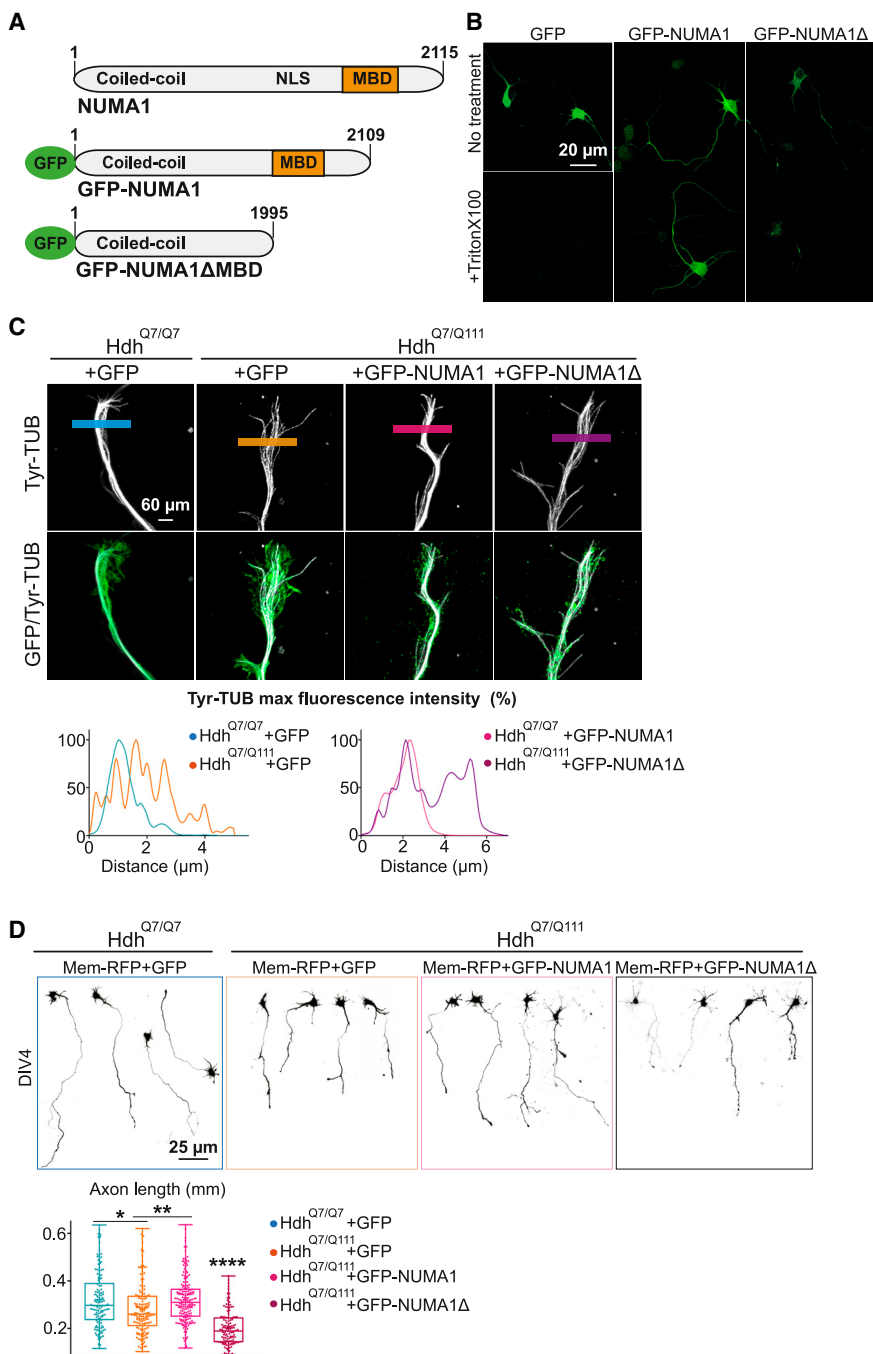


Figure 7. NUMA1 expression rescues the axonal defect of HD cortical neurons in culture

(A) Schematic of NUMA1 constructs. NLS, nuclear localization signal; MBD, microtubule-binding domain.

(B) Representative confocal images of GFP-stained cortical neurons expressing the indicated constructs. Before immunostaining, neurons were treated (+Triton X-100) or not to extract soluble proteins. In this panel, GFP-NUMA1ΔMBD is abbreviated as GFP-NUMA1Δ.

(C) Representative confocal Airyscan images of growth cones immunostained with anti-GFP (green) and anti-tyrosinated TUBULIN (tyr-TUB, gray) antibodies. Below: representative line scan analyses of relative fluorescence intensity.

(D) Representative Hdh^{Q7/Q7} and Hdh^{Q7/Q111} neurons expressing the indicated constructs. Histograms show axonal lengths. One-way ANOVA with multiple comparisons followed by Tukey's post hoc test, **p = 0.0051 (mean of difference between Hdh^{Q7/Q7} and Hdh^{Q7/Q111} 39.57), p = 0.999 (mean of difference between Hdh^{Q7/Q7} and Hdh^{Q7/Q111} + NUMA1 1.46), ****p < 0.0001 (mean of difference between Hdh^{Q7/Q7} and Hdh^{Q7/Q111} + NUMA1ΔMBD 119), **p = 0.0035 (mean of difference between Hdh^{Q7/Q111} and Hdh^{Q7/Q111} + NUMA1 -38.11), ****p < 0.0001 (mean of difference between Hdh^{Q7/Q111} and Hdh^{Q7/Q111} + NUMA1ΔMBD 76.46), ****p < 0.0001 (mean of difference between Hdh^{Q7/Q111} + NUMA1 and Hdh^{Q7/Q111} + NUMA1ΔMBD 117.6). n ≥ 132 axons from four independent experiments for each condition. Error bars denote SEM.

(Figure 7C), but GFP-NUMA1 expression was sufficient to rescue microtubule bundling and restore axonal growth (Figure 7D). In contrast, GFP-NUMA1ΔMBD exacerbated the axonal defect (Figure 7D). Thus, the microtubule-binding domain of NUMA1 is required to regulate axonal growth.

AntagomiR-124 expression and epothilone B treatment restore axonal growth in HD mice

Finally, to see if we could prevent the HD-induced defects *in vivo*, we restored NUMA1 protein levels by electroporating

GFP-NUMA1 in E15.5 Hdh^{Q7/Q111} embryos and measuring the axons at P0 (Figure 8A). (NUMA1's size, 250 kDa, prevented us from expressing it by postnatal viral injections.) Callosal fibers in HD neurons expressing GFP-NUMA1 grew as long as those in controls.

We also restored NUMA1 expression postnatally by using antagomiR-124 (Figure 8B). We injected antagomiR-124 in the facial vein of P0 Hdh^{Q7/Q111} animals and analyzed the axonal growth of callosal fibers at P4. HD callosal fibers treated with

was deleted (GFP-NUMA1-ΔMBD) (Figure 7A) (Gallini et al., 2016).

As expected, using a detergent extraction assay as before (Figure 5D), GFP-NUMA1 remained associated with the microtubule cytoskeleton, while GFP-NUMA1-ΔMBD did not (Figure 7B). We used the status of the central microtubule bundle in growing axons as a readout of the HD phenotype, as the integrity of this structure is required for proper axonal growth. HD neurons again showed defective bundling of the central microtubule domain

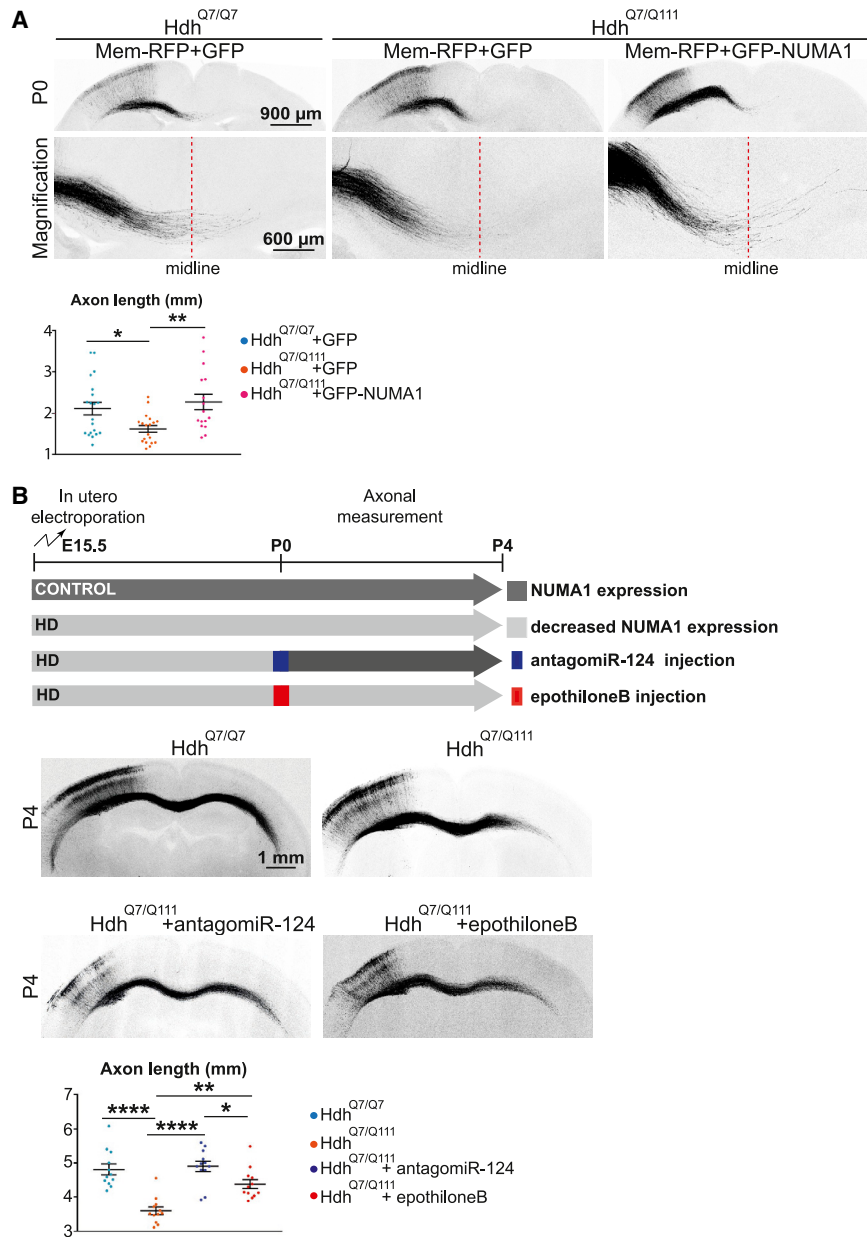


Figure 8. NUMA1 expression and microtubule stabilization rescue axonal length of HD cortical neurons *in vivo*

(A) Representative coronal sections of P0 Hdh^{Q7/Q7} and Hdh^{Q7/Q111} cortices expressing GFP or GFP-NUMA1. Histogram quantifies axon length in the three conditions. One-way ANOVA with multiple comparisons followed by Tukey's post hoc test, * $p = 0.041$ (mean of difference between Hdh^{Q7/Q7} and Hdh^{Q7/Q111} 493.9), ** $p = 0.008$ (mean of difference between Hdh^{Q7/Q111} and Hdh^{Q7/Q111} + NUMA1 653.8), $p = 0.721$ (mean of difference between control and Hdh^{Q7/Q111} + NUMA1 160). $n \geq 132$ axons from four independent experiments for each condition.

(B) Schematic of experimental procedure to recover Hdh^{Q7/Q111} axonal growth of layer II/III neurons from P0 to P4. For each condition, the embryos were electroporated with Mem-RFP at E15.5. The P0 Mem-RFP positive pups were injected with PBS for Hdh^{Q7/Q7} and Hdh^{Q7/Q111}, with PBS + antagomiR-124 for Hdh^{Q7/Q111} or PBS + epothilone B for Hdh^{Q7/Q111}. Representative coronal sections of P4 Hdh^{Q7/Q7} and Hdh^{Q7/Q111} cortices expressing Mem-RFP and treated with antagomiR-124 or epothilone B. Histograms below show axon lengths in each condition. One-way ANOVA, Tukey's multiple-comparisons test, **** $p < 0.0001$ (mean of difference between Hdh^{Q7/Q7} and Hdh^{Q7/Q111} 1,192 μm), $p > 0.99$ (mean of difference between Hdh^{Q7/Q7} and Hdh^{Q7/Q111} + antagomiR-124 -28.83 μm), $p = 0.26$ (mean of difference between Hdh^{Q7/Q7} and Hdh^{Q7/Q111} + epothilone B 434.4 μm), **** $p < 0.0001$ (mean of difference between Hdh^{Q7/Q111} and Hdh^{Q7/Q111} + antagomiR-124 -1,221 μm), ** $p = 0.0057$ (mean of difference between Hdh^{Q7/Q111} and Hdh^{Q7/Q111} + epothilone B -757.5 μm), $p = 0.22$ (mean of difference between Hdh^{Q7/Q111}+antagomiR-124 and Hdh^{Q7/Q111} + epothilone B -463 μm). $n = 12$ brains from four independent experiments for each condition. Error bars denote SEM.

antagomiR-124 grew as long as the controls (Figure 8A). Electroporating antagomiR-124 in E15.5 HD embryos produced a similar rescue (Figure S5A). Together with our results on NUMA1 downregulation in E15.5 Hdh^{Q7/Q7} and NUMA1 expression in E15.5 Hdh^{Q7/Q111} (Figures 6A–6C and 8A), this strongly supports the idea that the mechanisms by which antagomiR-124, NUMA1, and mHTT regulate axonal growth are independent of neuronal migration.

Finally, we targeted the microtubule defect in HD using epothilone B, a microtubule-stabilizing drug. Epothilone B crosses the blood-brain barrier and has been used to promote axonal regeneration in mouse (Kugler et al., 2020; Ruschel et al., 2015). In HD cortical neurons in culture, epothilone B treatment restored the

organization of the main microtubule bundle in the central domain of the growth cone (Figure S5B). We also injected epothilone B subcutaneously in P0 Hdh^{Q7/Q111} animals and analyzed callosal fibers at P4 (Figure 8B). Epothilone B-treated HD animals grew callosal fibers as long as controls.

Therefore, the limited axonal growth in early HD can be rescued by NUMA1 expression, which restores the organization of the microtubule array in the growth cone.

DISCUSSION

A thin callosum and attenuated connectivity between the two cortical hemispheres can be observed decades before the first clinical symptoms of HD in mutation carriers (reviewed in Estevez-Fraga et al., 2021). We show that these early defects arise from impaired axonal growth during development, rather than

through a degenerative process. The growth of callosal axons is compromised in HD mice from P0; at P4, callosal fibers are able to cross the corpus callosum but still show delayed outgrowth compared with the control condition. This axonal growth deficiency has two major consequences for the maturation of cortical connections. First, a proportion of HD axons fails to reach the contralateral side to establish connections at all. Second, the fibers that reach their final destination augment their branching within layers II/III and V, but this is insufficient to compensate for the diminished cortical ramifications. The branching defect in HD could also result from the fibers arriving on the contralateral side too late to receive the proper signals.

Deepening our understanding of trafficking defects in HD

HD is rightfully considered a disease of impaired trafficking, but the present study shows that HD affects the cytoskeletal infrastructure itself. HTT has been known for some time to rely on microtubules for not just axonal transport of vesicles but also other functions in ciliogenesis and mitotic spindle orientation, all of which are altered in HD (Saudou and Humbert, 2016). Whether HD interferes with microtubule organization and dynamics has been largely unknown. We previously showed that the dynamic instability of microtubules was diminished in HD mouse embryonic fibroblasts and that they persisted abnormally after membrane contact (Molina-Calavita et al., 2014). It is now clear that in HD, the microtubule array in the growth cone is itself disorganized, with impaired microtubule bundling in the central domain and longer exploratory microtubules in the peripheral domain, resulting in an overall increased growth cone area. As the growth cone advances, the peripheral domain becomes the new central domain while the previous central domain, in turn, gives rise to the axonal shaft by constricting the growth cone and bundling microtubules, resulting in a net elongation of the axon (Pinto-Costa and Sousa, 2021). Thus, the disorganization of microtubules observed in the growth cone of HD callosal neurons contributes to their poor elongation, which can be rescued *in vivo* by the microtubule-stabilizing agent epothilone B. Determining whether microtubule disorganization also contributes to the impairment of microtubule-based functions of HTT will require further study.

Unexpected functions for NUMA1 in microtubule organization and axonal growth

Most studies on NUMA1 have focused on its role in spindle formation and orientation (di Pietro et al., 2016). During spindle assembly, the interaction of NUMA1 with dynein/dynactin promotes microtubule tethering to the poles; in metaphase, NUMA1 binds to dynein/dynactin and to the leucine-glycine-asparagine (LGN) protein to recruit dynein to the cortex, where it exerts attractive forces on astral microtubules for cell division. NUMA1 also binds directly to microtubules and leads to the formation of stable bundles during division (Forth et al., 2014; Gallini et al., 2016; Haren and Merdes, 2002; Merdes et al., 1996). Here, we show that NUMA1, by directly binding to microtubules, also organizes the central microtubule bundles in the growth cone.

Only a few studies have investigated the role of NUMA1 in differentiating and mature neurons. Ferhat et al. (1998) observed

NUMA1 in the cell body of developing sympathetic and hippocampal neurons. They found that NUMA1 protein levels increased during the first days *in vitro* before decreasing at later stages (as we also found) and suggested that NUMA1 could be a component of the somatodendritic microtubule arrays of the neurons (Ferhat et al., 1998). More recent studies highlight the role of NUMA1 in the development of cortical neurons. NUMA1 cooperates with the non-catalytic regulatory p80 subunit of katanin, whose mutation causes microlissencephaly (Jin et al., 2017), to regulate not only cortical neurogenesis but also the radial migration of newly generated neurons. NUMA1 is also required at a later stage of neuronal development during the assembly of the axonal initial segment (Torii et al., 2020). NUMA1 inhibits Neurofascin endocytosis, leading to its accumulation on the plasma membrane and promoting the enrichment of other proteins of the axonal initial segment and its stabilization (Torii et al., 2020). Once the axon initial segment is stabilized, NUMA1 is no longer required for its maintenance. We now show that NUMA1 is essential for growth cone integrity and axonal growth independent of its role in neurogenesis, migration, and polarization.

During neuronal maturation in HD, NUMA1 protein levels are severely downregulated by miR-124; the remaining levels of NUMA1 in HD can be increased by treatment with ubiquitin and autophagy inhibitors. Interestingly, Eshraghi et al. (2021) recently reported that mHTT stalls ribosomes, globally repressing protein synthesis, including that of NUMA1. Along similar lines, or at least to similar effect, the cellular stress that occurs in HD also downregulates NUMA (Jayaraman et al., 2017). In these studies, the authors proposed that the mechanisms involve the interaction of mHTT and NUMA1 with ribosomal proteins. Whether such mechanisms could also contribute to the downregulation of NUMA1 in HD neuronal maturation remains to be tested.

An integrated model of early development in HD

Because the striatum is the first region to show neuronal loss in HD (Rüb et al., 2016), the contribution of the cerebral cortex to HD has been relatively neglected. Accumulating evidence supports the notion that the striatal degeneration is, in fact, caused by defective cortical signaling to the striatum (Tereshchenko et al., 2020; Virlogeux et al., 2018; Wang et al., 2014; Zhao et al., 2016). Neurons projecting to the striatum (layer V neurons) are particularly susceptible in HD patients (Hedreen et al., 1991), and cortical layer II/III neurons that project through the corpus callosum to the contralateral hemisphere also degenerate in HD patients (Hedreen et al., 1991). Thus, similar to what has been proposed for the cortico-striatal connection, the reduced cortico-cortical connectivity shown here could explain the thin corpus callosum observed in presymptomatic gene carriers.

We show that the growth of callosal axons is compromised in HD mice. Whether the number of upper layer neurons and their migration is also affected in HD is not clear (Barnat et al., 2017; Molina-Calavita et al., 2014). It could well be the case, given that wild-type HTT regulates the maintenance of their pool and their migration (Barnat et al., 2017; Tong et al., 2011); this would precede the axonal growth defect and could influence it,

although part of the impairment in axonal growth involves a cell-autonomous mechanism, as indicated by axonal growth defects of HD callosal neurons in cell cultures. It is worth noting that HD callosal neurons showed branching defects *in vivo* but not when they were isolated in cell cultures. This suggests that the defective branching on the contralateral side is not due to an autonomous mechanism but rather that these HD axons are not exposed to the proper extracellular signaling. As noted above, this may be a matter of timing. It is also possible, however, that there are abnormalities in extracellular signaling in HD that also contribute to the impaired branching.

It is now clear that HD interferes with the fundamental processes of cortical development: neurogenesis (Barnat et al., 2020), neuronal migration (Barnat et al., 2017), and (from the present study) axonal growth and maturation into the proper circuit. A young mature HD brain has fewer neurons than a control one; not all neurons will reach their final destination, and for those that do, their connectivity is altered. These subtle deficits form the substrate for subsequent compensatory events, prodromal clinical signs and degeneration.

Precisely how each defective stage interferes with the subsequent one, with additive or compensatory effects, remains to be established. It is of the utmost importance to consider HD longitudinally and to differentiate between pathogenic and compensatory changes so that therapies can be directed against the former while promoting, or at least not undermining, the latter (Al-Ramahi et al., 2018). The exact contribution of abnormal development to adult pathology also needs to be well mapped, so that we can integrate neurodevelopment in our therapeutic strategies. Our data here create at least a theoretical possibility that therapies delivered very early in life could delay the onset of classic HD symptoms.

STAR★METHODS

Detailed methods are provided in the online version of this paper and include the following:

- **KEY RESOURCES TABLE**
- **RESOURCE AVAILABILITY**
 - Lead contact
 - Materials availability
 - Data and code availability
- **EXPERIMENTAL MODEL AND SUBJECT DETAILS**
- **METHOD DETAILS**
 - *In utero* electroporation, brain fixation and cell culture
 - Neonatal mouse treatment
 - Cell treatment
 - Immunocytochemistry
 - Permeabilization assay
 - Growth cone fractionation
 - Mass spectrometry-based quantitative proteomics
 - Microtubule co-sedimentation assay
 - Nuclear and cytoplasmic proteins extraction
 - Western blot
 - Quantitative real-time PCR
 - Plasmid constructs
 - Image acquisition

● QUANTIFICATION AND STATISTICAL ANALYSIS

- Data analysis
- Statistical analyses

SUPPLEMENTAL INFORMATION

Supplemental information can be found online at <https://doi.org/10.1016/j.neuron.2021.10.033>.

ACKNOWLEDGMENTS

We kindly thank Béatrice Blot and staff of animal facilities (Grenoble Institute Neurosciences [GIN]) for technical support, Monia Barnat for discussions, Julien Le Fric for sharing samples, Sophie Lenoir for help with animal experimentation, the GIN imaging facility platform (PIC-GIN) for help with image acquisitions, and Vicky Brandt and Frédéric Saudou for helpful comments on the manuscript. This work was supported by grants from Agence Nationale pour la Recherche (ANR; ANR-15-IDEX-02 NeuroCoG in the framework of the “Investissements d’avenir” program to S.H.; AXION: ANR-18-CE16-0009-01 to S.H.), Fondation pour la Recherche Médicale (FRM; équipe labellisée DEQ20170336752 to S.H.; PhD fellowship FDT202001010865 to R.C.), and the AGEMED program of Inserm (S.H.). Proteomic experiments were partly supported by ANR under projects ProFI (Proteomics French Infrastructure, ANR-10-INBS-08) and GRAL, a program from the Chemistry Biology Health (CBH) Graduate School of University Grenoble Alpes (ANR-17-EURE-0003).

AUTHOR CONTRIBUTIONS

M.C. and S.H. designed the study and wrote the manuscript, which was commented on by all authors. M.C. performed most of the experiments and data analyses. R.C. performed co-sedimentation assay and permeabilization assay and participated in MS sample preparation. R.K. performed qRT-PCR experiments and analyses. E.D. generated tools for image analyses and performed analyses. A.A. and Y.C. performed quantitative proteomic analyses. M.M. provided expertise and reagents.

DECLARATION OF INTERESTS

The authors declare no competing interests.

Received: April 14, 2021
Revised: September 14, 2021
Accepted: October 21, 2021
Published: November 17, 2021

REFERENCES

- Al-Ramahi, I., Lu, B., Di Paola, S., Pang, K., de Haro, M., Peluso, I., Gallego-Flores, T., Malik, N.T., Erikson, K., Bleiberg, B.A., et al. (2018). High-throughput functional analysis distinguishes pathogenic, nonpathogenic, and compensatory transcriptional changes in neurodegeneration. *Cell Syst.* 7, 28–40.e4.
- Alcamo, E.A., Chirivella, L., Dautzenberg, M., Dobreva, G., Fariñas, I., Grosschedl, R., and McConnell, S.K. (2008). *Satb2* regulates callosal projection neuron identity in the developing cerebral cortex. *Neuron* 57, 364–377.
- Barnat, M., Le Fric, J., Benstaali, C., and Humbert, S. (2017). Huntington-mediated multipolar-bipolar transition of newborn cortical neurons is critical for their postnatal neuronal morphology. *Neuron* 93, 99–114.
- Barnat, M., Capizzi, M., Aparicio, E., Boluda, S., Wennagel, D., Kacher, R., Kassem, R., Lenoir, S., Agasse, F., Braz, B.Y., et al. (2020). Huntington's disease alters human neurodevelopment. *Science* 369, 787–793.
- Bouyssié, D., Hesse, A.M., Mouton-Barbosa, E., Rompais, M., Macron, C., Carapito, C., Gonzalez de Peredo, A., Couté, Y., Dupieris, V., Burel, A., et al. (2020). Proline: an efficient and user-friendly software suite for large-scale proteomics. *Bioinformatics* 36, 3148–3155.

- Casabona, M.G., Vandenbrouck, Y., Attree, I., and Couté, Y. (2013). Proteomic characterization of *Pseudomonas aeruginosa* PAO1 inner membrane. *Proteomics* *13*, 2419–2423.
- Casella, C., Lipp, I., Rosser, A., Jones, D.K., and Metzler-Baddeley, C. (2020). A critical review of white matter changes in Huntington's disease. *Mov. Disord.* *35*, 1302–1311.
- Cepeda, C., Hurst, R.S., Calvert, C.R., Hernández-Echeagaray, E., Nguyen, O.K., Jocoy, E., Christian, L.J., Ariano, M.A., and Levine, M.S. (2003). Transient and progressive electrophysiological alterations in the corticostriatal pathway in a mouse model of Huntington's disease. *J. Neurosci.* *23*, 961–969.
- Dajas-Bailador, F., Jones, E.V., and Whitmarsh, A.J. (2008). The JIP1 scaffold protein regulates axonal development in cortical neurons. *Curr. Biol.* *18*, 221–226.
- Dent, E.W., Gupton, S.L., and Gertler, F.B. (2011). The growth cone cytoskeleton in axon outgrowth and guidance. *Cold Spring Harb. Perspect. Biol.* *3*, a001800.
- di Pietro, F., Echard, A., and Morin, X. (2016). Regulation of mitotic spindle orientation: an integrated view. *EMBO Rep.* *17*, 1106–1130.
- Eshraghi, M., Karunadharma, P.P., Blin, J., Shahani, N., Ricci, E.P., Michel, A., Urban, N.T., Galli, N., Sharma, M., Ramírez-Jarquín, U.N., et al. (2021). Mutant Huntingtin stalls ribosomes and represses protein synthesis in a cellular model of Huntington disease. *Nat. Commun.* *12*, 1461.
- Estevez-Fraga, C., Scahill, R., Rees, G., Tabrizi, S.J., and Gregory, S. (2021). Diffusion imaging in Huntington's disease: comprehensive review. *J. Neurol. Neurosurg. Psychiatry* *92*, 62–69.
- Fame, R.M., MacDonald, J.L., and Macklis, J.D. (2011). Development, specification, and diversity of callosal projection neurons. *Trends Neurosci.* *34*, 41–50.
- Ferhat, L., Cook, C., Kuriyama, R., and Baas, P.W. (1998). The nuclear/mitotic apparatus protein NuMA is a component of the somatodendritic microtubule arrays of the neuron. *J. Neurocytol.* *27*, 887–899.
- Forth, S., Hsia, K.C., Shimamoto, Y., and Kapoor, T.M. (2014). Asymmetric friction of nonmotor MAPs can lead to their directional motion in active microtubule networks. *Cell* *157*, 420–432.
- Gallini, S., Carminati, M., De Mattia, F., Pirovano, L., Martini, E., Oldani, A., Asteriti, I.A., Guarguaglini, G., and Mapelli, M. (2016). NuMA phosphorylation by aurora-A orchestrates spindle orientation. *Curr. Biol.* *26*, 458–469.
- Godin, J.D., Colombo, K., Molina-Calavita, M., Keryer, G., Zala, D., Charrin, B.C., Dietrich, P., Volvert, M.L., Guillemot, F., Dragatsis, I., et al. (2010). Huntingtin is required for mitotic spindle orientation and mammalian neurogenesis. *Neuron* *67*, 392–406.
- Gombash Lampe, S.E., Kaspar, B.K., and Foust, K.D. (2014). Intravenous injections in neonatal mice. *J. Vis. Exp.* *93*, e52037.
- Hand, R.A., Khalid, S., Tam, E., and Kolodkin, A.L. (2015). Axon dynamics during neocortical laminar innervation. *Cell Rep.* *12*, 172–182.
- Haren, L., and Merdes, A. (2002). Direct binding of NuMA to tubulin is mediated by a novel sequence motif in the tail domain that bundles and stabilizes microtubules. *J. Cell Sci.* *115*, 1815–1824.
- HD iPSC Consortium (2017). Developmental alterations in Huntington's disease neural cells and pharmacological rescue in cells and mice. *Nat. Neurosci.* *20*, 648–660.
- Hedreen, J.C., Peyser, C.E., Folstein, S.E., and Ross, C.A. (1991). Neuronal loss in layers V and VI of cerebral cortex in Huntington's disease. *Neurosci. Lett.* *133*, 257–261.
- Igarashi, M. (2014). Proteomic identification of the molecular basis of mammalian CNS growth cones. *Neurosci. Res.* *88*, 1–15.
- Ilieva, M., Nielsen, T.T., Michel, T., and Pankratova, S. (2019). FGF2 and dual agonist of NCAM and FGF receptor 1, Enreptin, rescue neurite outgrowth loss in hippocampal neurons expressing mutated huntingtin proteins. *J. Neural Transm. (Vienna)* *126*, 1493–1500.
- Jayaraman, S., Chittiboyina, S., Bai, Y., Abad, P.C., Vidi, P.A., Stauffacher, C.V., and Lelièvre, S.A. (2017). The nuclear mitotic apparatus protein NuMA controls rDNA transcription and mediates the nucleolar stress response in a p53-independent manner. *Nucleic Acids Res.* *45*, 11725–11742.
- Ji, S.J., and Jaffrey, S.R. (2014). Axonal transcription factors: novel regulators of growth cone-to-nucleus signaling. *Dev. Neurobiol.* *74*, 245–258.
- Jin, M., Pomp, O., Shinoda, T., Toba, S., Torisawa, T., Furuta, K., Oiwa, K., Yasunaga, T., Kitagawa, D., Matsumura, S., et al. (2017). Katanin p80, NuMA and cytoplasmic dynein cooperate to control microtubule dynamics. *Sci. Rep.* *7*, 39902.
- Kugler, C., Thielscher, C., Tambe, B.A., Schwarz, M.K., Halle, A., Bradke, F., and Petzold, G.C. (2020). Epothilones improve axonal growth and motor outcomes after stroke in the adult mammalian CNS. *Cell Rep Med* *1*, 100159.
- Leshchyns'ka, I., and Sytnyk, V. (2013). Isolation of growth cones from mouse brain. *Bio-protocol* *3*, e853.
- Lewis, T.L., Jr., Courchet, J., and Polleux, F. (2013). Cell biology in neuroscience: Cellular and molecular mechanisms underlying axon formation, growth, and branching. *J. Cell Biol.* *202*, 837–848.
- Mangin, J.F., Rivière, D., Duchesnay, E., Cointepas, Y., Gaura, V., Verny, C., Damier, P., Krystkowiak, P., Bachoud-Lévi, A.C., Hantraye, P., et al. (2020). Neocortical morphometry in Huntington's disease: Indication of the coexistence of abnormal neurodevelopmental and neurodegenerative processes. *Neuroimage Clin.* *26*, 102211.
- McCormick, L.E., and Gupton, S.L. (2020). Mechanistic advances in axon pathfinding. *Curr. Opin. Cell Biol.* *63*, 11–19.
- McKinstry, S.U., Karadeniz, Y.B., Worthington, A.K., Hayrapetyan, V.Y., Ozlu, M.I., Serafin-Molina, K., Risher, W.C., Ustunkaya, T., Dragatsis, I., Zeitlin, S., et al. (2014). Huntingtin is required for normal excitatory synapse development in cortical and striatal circuits. *J. Neurosci.* *34*, 9455–9472.
- Mehta, S.R., Tom, C.M., Wang, Y., Bresee, C., Rushton, D., Mathkar, P.P., Tang, J., and Mattis, V.B. (2018). Human Huntington's disease iPSC-derived cortical neurons display altered transcriptomics, morphology, and maturation. *Cell Rep.* *25*, 1081–1096.e6.
- Menalled, L.B., Kudwa, A.E., Miller, S., Fitzpatrick, J., Watson-Johnson, J., Keating, N., Ruiz, M., Mushlin, R., Alosio, W., McConnell, K., et al. (2012). Comprehensive behavioral and molecular characterization of a new knock-in mouse model of Huntington's disease: zQ175. *PLoS ONE* *7*, e49838.
- Merdes, A., Ramyar, K., Vecchio, J.D., and Cleveland, D.W. (1996). A complex of NuMA and cytoplasmic dynein is essential for mitotic spindle assembly. *Cell* *87*, 447–458.
- Molero, A.E., Arteaga-Bracho, E.E., Chen, C.H., Gulino, M., Winchester, M.L., Pichamoorthy, N., Gokhan, S., Khodakhah, K., and Mehler, M.F. (2016). Selective expression of mutant huntingtin during development recapitulates characteristic features of Huntington's disease. *Proc. Natl. Acad. Sci. U S A* *113*, 5736–5741.
- Molina-Calavita, M., Barnat, M., Elias, S., Aparicio, E., Piel, M., and Humbert, S. (2014). Mutant huntingtin affects cortical progenitor cell division and development of the mouse neocortex. *J. Neurosci.* *34*, 10034–10040.
- Nopoulos, P.C., Aylward, E.H., Ross, C.A., Mills, J.A., Langbehn, D.R., Johnson, H.J., Magnotta, V.A., Pierson, R.K., Beglinger, L.J., Nance, M.A., et al.; PREDICT-HD Investigators and Coordinators of the Huntington Study Group (2011). Smaller intracranial volume in prodromal Huntington's disease: evidence for abnormal neurodevelopment. *Brain* *134*, 137–142.
- Pasterkamp, R.J., and Burk, K. (2021). Axon guidance receptors: Endocytosis, trafficking and downstream signaling from endosomes. *Prog. Neurobiol.* *198*, 101916.
- Perez-Riverol, Y., Csordas, A., Bai, J., Bernal-Llinares, M., Hewapathirana, S., Kundu, D.J., Inuganti, A., Griss, J., Mayer, G., Eisenacher, M., et al. (2019). The PRIDE database and related tools and resources in 2019: improving support for quantification data. *Nucleic Acids Res.* *47* (D1), D442–D450.
- Pinto-Costa, R., and Sousa, M.M. (2021). Microtubules, actin and cytolinkers: how to connect cytoskeletons in the neuronal growth cone. *Neurosci. Lett.* *747*, 135693.
- Reis, S.A., Thompson, M.N., Lee, J.M., Fossale, E., Kim, H.H., Liao, J.K., Moskowitz, M.A., Shaw, S.Y., Dong, L., Haggarty, S.J., et al. (2011). Striatal

neurons expressing full-length mutant huntingtin exhibit decreased N-cadherin and altered neurogenesis. *Hum. Mol. Genet.* **20**, 2344–2355.

Ren, Y., and Suter, D.M. (2016). Increase in growth cone size correlates with decrease in neurite growth rate. *Neural Plast.* **2016**, 3497901.

Rüb, U., Seidel, K., Heinsen, H., Vonsattel, J.P., den Dunnen, W.F., and Korf, H.W. (2016). Huntington's disease (HD): the neuropathology of a multisystem neurodegenerative disorder of the human brain. *Brain Pathol.* **26**, 726–740.

Ruschel, J., Hellal, F., Flynn, K.C., Dupraz, S., Elliott, D.A., Tedeschi, A., Bates, M., Sliwinski, C., Brook, G., Dobrindt, K., et al. (2015). Axonal regeneration. Systemic administration of epothilone B promotes axon regeneration after spinal cord injury. *Science* **348**, 347–352.

Saudou, F., and Humbert, S. (2016). The biology of huntingtin. *Neuron* **89**, 910–926.

Scahill, R.I., Zeun, P., Osborne-Crowley, K., Johnson, E.B., Gregory, S., Parker, C., Lowe, J., Nair, A., O'Callaghan, C., Langley, C., et al. (2020). Biological and clinical characteristics of gene carriers far from predicted onset in the Huntington's Disease Young Adult Study (HD-YAS): a cross-sectional analysis. *Lancet Neurol.* **19**, 502–512.

Suzuki, N., Akiyama, T., Warita, H., and Aoki, M. (2020). Omics approach to axonal dysfunction of motor neurons in amyotrophic lateral sclerosis (ALS). *Front. Neurosci.* **14**, 194.

Tang, C.C., Feigin, A., Ma, Y., Habeck, C., Paulsen, J.S., Leenders, K.L., Teune, L.K., van Oostrom, J.C., Guttman, M., Dhawan, V., and Eidelberg, D. (2013). Metabolic network as a progression biomarker of premanifest Huntington's disease. *J. Clin. Invest.* **123**, 4076–4088.

Tereshchenko, A.V., Schultz, J.L., Bruss, J.E., Magnotta, V.A., Epping, E.A., and Nopoulos, P.C. (2020). Abnormal development of cerebellar-striatal circuitry in Huntington disease. *Neurology* **94**, e1908–e1915.

Tong, Y., Ha, T.J., Liu, L., Nishimoto, A., Reiner, A., and Goldowitz, D. (2011). Spatial and temporal requirements for huntingtin (Htt) in neuronal migration and survival during brain development. *J. Neurosci.* **31**, 14794–14799.

Torii, T., Ogawa, Y., Liu, C.H., Ho, T.S., Hamdan, H., Wang, C.C., Oses-Prieto, J.A., Burlingame, A.L., and Rasband, M.N. (2020). NuMA1 promotes axon initial segment assembly through inhibition of endocytosis. *J. Cell Biol.* **219**, e201907048.

Virlogeux, A., Moutaux, E., Christaller, W., Genoux, A., Bruyère, J., Fino, E., Charlot, B., Cazorla, M., and Saudou, F. (2018). Reconstituting corticostriatal network on-a-chip reveals the contribution of the presynaptic compartment to Huntington's disease. *Cell Rep.* **22**, 110–122.

Wang, N., Gray, M., Lu, X.H., Cantle, J.P., Holley, S.M., Greiner, E., Gu, X., Shirasaki, D., Cepeda, C., Li, Y., et al. (2014). Neuronal targets for reducing mutant huntingtin expression to ameliorate disease in a mouse model of Huntington's disease. *Nat. Med.* **20**, 536–541.

Wheeler, V.C., Gutekunst, C.A., Vrbanc, V., Lebel, L.A., Schilling, G., Hersch, S., Friedlander, R.M., Gusella, J.F., Vonsattel, J.P., Borchelt, D.R., and MacDonald, M.E. (2002). Early phenotypes that presage late-onset neurodegenerative disease allow testing of modifiers in Hdh CAG knock-in mice. *Hum. Mol. Genet.* **11**, 633–640.

Wieczorek, S., Combes, F., Lazar, C., Giai Gianetto, Q., Gatto, L., Dorffer, A., Hesse, A.M., Couté, Y., Ferro, M., Bruley, C., and Burger, T. (2017). DAPAR & ProStaR: software to perform statistical analyses in quantitative discovery proteomics. *Bioinformatics* **33**, 135–136.

Wilson, C., and Cáceres, A. (2020). New insights on epigenetic mechanisms supporting axonal development: histone marks and miRNAs. *FEBS J.*

Zhao, X., Chen, X.Q., Han, E., Hu, Y., Paik, P., Ding, Z., Overman, J., Lau, A.L., Shahmoradian, S.H., Chiu, W., et al. (2016). TRiC subunits enhance BDNF axonal transport and rescue striatal atrophy in Huntington's disease. *Proc. Natl. Acad. Sci. U S A* **113**, E5655–E5664.

STAR★METHODS

KEY RESOURCES TABLE

REAGENT or RESOURCE	SOURCE	IDENTIFIER
Antibodies		
anti-Tyrosinated TUBULIN (YL1/2, Tyr-TUB)	Provided by M.-J. Moutin, Grenoble Institute Neuroscience	N/A
anti-NUMA1	Abcam	Cat#ab109262, RRID:AB_10863599
anti-atto-488-phalloidin	Sigma-Aldrich	Cat#49409
anti-SATB2	Abcam	Cat#ab51502, RRID:AB_882455
anti-CTIP2	Abcam	Cat#ab18465, RRID:AB_2064130
anti-VINCULIN	Sigma	Cat#V9131, RRID:AB_477629
anti-JIP1(B-7)	Santa Cruz Biotechnology	Cat#sc-25267, RRID:AB_627838
anti-GM130	BD Transduction Laboratories	Cat#610822, RRID:AB_398141
anti-KINECTIN1	Genetex	Cat#GTX66105
anti-FAT4	Thermo Fisher	Cat#PA5-72970, RRID:AB_2718824
anti-SMCHD1	Novus Biologicals	Cat#NBP1-82978, RRID:AB_11020741
anti-SMARCA4	Abcam	Cat#ab110641, RRID:AB_10861578
anti-LAMINB1	Abcam	Cat#ab133741, RRID:AB_2616597
anti-poly Ubiquitin	LifeSpanBio	Cat#LS-C107107-25, RRID:AB_10627218
anti-p62	Sigma	Cat#P0067, RRID:AB_1841064
anti-TAU	Abcam	Cat#ab75714, RRID:AB_1310734
anti- α -TUBULIN	Sigma	Cat#T9026, RRID:AB_477593
anti-GFP	Abcam	Cat#ab13970, RRID:AB_300798
donkey anti-mouse IgG (H+L) - Cy2 conjugate	Jackson ImmunoResearch	Cat#715-225-151, RRID:AB_2340827
donkey anti-mouse IgG (H+L) - Cy3 conjugate	Jackson ImmunoResearch	Cat#715-225-150, RRID:AB_2340826
donkey anti-rat IgG (H+L) - Cy5 conjugate	Jackson ImmunoResearch	Cat#715-175-151, RRID:AB_2340820
goat anti-rabbit IgY (H+L) - Alexa Fluor® 555 conjugate	ThermoFisher scientific	Cat#A21428, RRID:AB_2535849
goat anti-mouse IgG1 - HRP conjugate	SouthernBiotech	Cat#1070-05, RRID:AB_2650509
donkey anti-mouse IgG H&L (HRP)	Abcam	Cat#ab6820, RRID:AB_955438
Bacterial and virus strains		
LV.pLKO1-shNUMA1mm-GFP	(Gallini et al., 2016)	N/A
LV.pLKO1-gfp	(Gallini et al., 2016)	N/A
Chemicals, peptides, and recombinant proteins		
Hoechst 33342	ThermoFisher	Cat#H3570
Dako Fluorescent mounting medium	Agilent	Cat#S302380-2
Proteases Inhibitor	Sigma-Aldrich	Cat#P8340
Phosphatases Inhibitor	Sigma-Aldrich	Cat#P5726
Triton X-100	Sigma-Aldrich	Cat#X100-500ML
pCALNL-GFP-U6-shNUMA1	This paper	N/A
pCALNL-GFP	Addgene	Cat#13770
pCAG-ERT2creERT2	Addgene	Cat#13777
pNeuroD-IRES-CRE-GFP (ND: CRE)	Provided by L. Nguyen, University of Liège, Belgium.	N/A
pCAGGS-NLS-GFP	Provided by L. Nguyen, University of Liège, Belgium.	N/A
AntagomiR-124	QIAGEN	Cat#339132
EpothiloneB	Div Bio Science	Cat#S1364
Bafilomycin	Sigma	Cat#B1793

(Continued on next page)

Continued

REAGENT or RESOURCE	SOURCE	IDENTIFIER
MG132	Sigma	Cat#474790
Tamoxifen	Sigma	Cat#T5648
PFA formaldehyde 32%	Euromedex	Cat#15714-S
Taxol/Paclitaxel	Sigma-Aldrich	Cat#T7191
glutaraldehyde solution 25%	Sigma-Aldrich	Cat#G5882-50ML
Sodium borohydride	Sigma-Aldrich	Cat#452874
Porcine tubulin	TEBU BIO	Cat#T240-A
Recombinant DNA		
pCAG_GFP	(Barnat et al., 2017)	N/A
pCAG_GFP-NUMA1ΔNLS	This paper	N/A
pCAG_GFP-NUMA1ΔNLSΔMBD	This paper	N/A
pCAG-mVENUS (pSCV2)	Provided by J. Courchet, Neuromyogène, Lyon, France	N/A
pCAG-TdTomato-1C-HS1BGFP-SV40pA	Addgene	Cat#26771
Experimental models: Organisms/strains		
SWISS-CD1	Janvier Lab	N/A
<i>Hdh</i> ^{Q7/Q111}	Provided by M.-F. Chesselet, UCLA, US.	N/A
<i>Hdh</i> ^{Q7/Q175}	The Jackson Lab	B6J.129S1-Htttm1Mfc/190ChdJ
Software and algorithms		
ImageJ/Fiji	NIH	https://imagej.nih.gov/ij/download.html
Adobe Illustrator		N/A
Graph pad Prism 7.0		N/A
Deposited data		
Mass spectrometry data	ProteomeXchange repository	http://www.proteomexchange.org/ , dataset identifier PXD023885

RESOURCE AVAILABILITY

Lead contact

Further information and requests for resources and reagents should be directed to and will be fulfilled by the Lead Contact, Sandrine Humbert (sandrine.humbert@univ-grenoble-alpes.fr).

Materials availability

All unique/stable reagents generated in this study are available from the Lead Contact without restriction.

Data and code availability

The data that support the findings of this study are either provided as supplementary material or are available from the corresponding author [S.H.] upon reasonable request.

EXPERIMENTAL MODEL AND SUBJECT DETAILS

Hdh^{Q111/Q111} mice are in a CD1 background and *Hdh*^{Q7/Q175} in a C57BL/6J background. All mice are derived from heterozygous crosses. All experimental procedures were performed in authorized establishments (Grenoble Institute of Neurosciences, INSERM U1216, license #B3851610008) in strict accordance with the local animal welfare committee (Comité Local Grenoble Institute Neurosciences, C1EA-04), EU guidelines (directive 2010/63/EU) and the French National Committee (2010/63) for care and use of laboratory animals.

METHOD DETAILS

***In utero* electroporation, brain fixation and cell culture**

E15.5 embryos were electroporated *in utero* with 2 μg/μl of the plasmids of interest as previously described (Barnat et al., 2017). mem-RFP or Venus-positive cortices were either fixed or dissociated for cell culture, respectively. For cell culture, Venus-positive cortices

were harvested at E16.5, dissected, and digested in Papain enzyme solution. Papain was inactivated using FBS (10%) and cells were washed with opti-MEM-glucose. Cells were cultured on poly-L-lysine matrices in Neurobasal supplemented with B27 (2%), glutamax (1%), and Penicillin/Streptomycin (1%). The cells were plated at a density of 800,000 cells/well in 6-well plates and fixed at DIV4.

Mem-RFP positive animals were intracardiacally perfused with PBS followed by cold paraformaldehyde (PFA) 4%. Brains were harvested, post-fixed overnight in PFA 4% and sectioned (300 μ m) through the entire somatosensory cortex. After 3 rinses in PBS, slices were mounted in Dako mounting medium.

Neonatal mouse treatment

All the treatments were performed in P0 mice. Tamoxifen (Sigma, 100 mg/kg) and epothilone B (Div Bio Science, 0.75 mg/kg) were injected subcutaneously. The antagomiR-124 (QIAGEN, 300nM) was administered with an intravenous injection as described in (Gombash Lampe et al., 2014).

Cell treatment

All drug treatments were done on cortical neurons at DIV4. Neurons were treated for 10h with 10 μ M MG132 (Sigma, 474790); for 6h with 100nM bafilomycin (Sigma, B1793). Cells were lysed and proteins analyzed by western blot. To evaluate the efficiency of epothilone B to bundle and stabilize microtubules *in vitro*, neurons were treated for with 10nM epothilone B. AntagomiR-124 (QIAGEN, 339132) was delivered via direct uptake (gymnosis) at a concentration of 100nM in the culture medium.

Immunocytochemistry

Cortical neurons were fixed at DIV4 with Glutaraldehyde (0.5%), Triton X-100 (0.1%) in cytoskeleton buffer (10mM MES, 138mM KCl, 3mM MgCl₂, 2mM EGTA, pH 6.1) supplemented with 10% sucrose at 37°C. Glutaraldehyde auto-fluorescence was quenched with 10 min incubation in Sodium Borohydride 1mg/mL. Blocking was performed with PBS-BSA (5%) for 1h at 20°C. Primary antibodies were incubated overnight at 4°C. Secondary fluorochrome-conjugated antibodies were applied 1h30 at 20°C and phalloidin 30min at 20°C. Washes were done in PBS. The following antibodies and reagents were used: rabbit monoclonal anti-NUMA1, diluted 1:200; rat monoclonal anti-tyrosinated TUBULIN antibody (YL1/2), diluted 1:4000; rabbit polyclonal anti-FAT4, diluted 1:100; phalloidin-ATTO488, diluted 1:1000; chicken polyclonal anti-TAU antibody, diluted 1:1000; chicken polyclonal anti-GFP antibody, diluted 1:2000. Secondary antibodies were coupled to Cy2, Cy3 or Cy5 (Jackson Immuno-Research Laboratories).

Permeabilization assay

Cortical neurons were electroporated at DIV0 with 1 μ g of GFP encoding plasmid and were mixed (1:2) with non-electroporated cells in order to have isolated GFP-positive neurons. At DIV4, cells were treated with BRB80 (80mM PIPES, 1mM EGTA, 1mM MgCl₂, pH 6.7) supplemented with Paclitaxel 10 μ M (Taxol) and Triton X-100 (0.05%), and warmed at 37°C for 3min before fixation. Growth cones were immunostained as described above and all images were acquired with the same parameters and displayed with the same threshold.

Growth cone fractionation

Growth cone and non-growth cone fractions were separated from P0 cortices as in (Leshchyns'ka and Sytnyk, 2013). Briefly, twelve cortices were homogenized by 10 strokes using glass potters, loaded onto a discontinuous 0.75/1.0/2.33M sucrose gradient and spin at 242,000 g for 1h at 4°C in a SW32Ti rotor. Growth cone fractions were collected at the interface load/0.75M sucrose and non-growth cone fractions collected between 0.75/1.0M sucrose and then analyzed by Western Blot.

Mass spectrometry-based quantitative proteomics

Proteins extracted from five biological replicates of growth cones purified from Hdh^{Q7/Q7} and Hdh^{Q7/Q111} mice were solubilized in Laemmli buffer and stacked in the top of a 4%–12% NuPAGE gel (Invitrogen). After staining with R-250 Coomassie Blue (Biorad), proteins were digested in-gel using trypsin (modified, sequencing purity, Promega), as previously described (Casabona et al., 2013).

The resulting peptides were analyzed by online nanoliquid chromatography coupled to MS/MS (Ultimate 3000 RSLCnano and Q-Exactive HF, Thermo Fisher Scientific) using a 185 min gradient. For this purpose, the peptides were sampled on a precolumn (300 μ m x 5 mm PepMap C18, Thermo Scientific) and separated in a 75 μ m x 250 mm C18 column (Reprosil-Pur 120 C18-AQ, 1.9 μ m, Dr. Maisch). The MS and MS/MS data were acquired by Xcalibur (Thermo Fisher Scientific).

Peptides and proteins were identified by Mascot (version 2.6.0, Matrix Science) through searches against the i) Uniprot database (*Mus musculus* taxonomy, February 2018 version, <https://www.uniprot.org/>); ii) a homemade database containing the sequences of classic proteins found in proteomic analyses (human keratins, trypsin, etc.), and iii) the corresponding reversed databases. Trypsin/P was chosen as the enzyme and two missed cleavages were allowed. Precursor and fragment mass error tolerances were set at 10 and 25 milli mass unit, respectively. Peptide modifications allowed during the search were: Carbamidomethyl (C, fixed), Acetyl (Protein N-term, variable) and Oxidation (M, variable). The Proline software (Bouyssié et al., 2020) was used for the compilation, grouping, and filtering of the results (conservation of rank 1 peptides, peptide length \geq 7 amino acids, peptide score \geq 25, allowing to reach a false discovery rate of peptide-spectrum-match identifications $<$ 1% as calculated on peptide-spectrum-match scores by employing the reverse database strategy). Proline was then used to perform a compilation, grouping and MS1 label-free

quantification of the identified protein groups. MS data have been deposited to the ProteomeXchange Consortium via the PRIDE partner repository (Perez-Riverol et al., 2019) with the dataset identifier PXD023885.

Statistical analysis was performed using the ProStar software (Wieczorek et al., 2017) on the basis of the quantitative data obtained with the five biological replicates analyzed per genotype. We removed proteins identified in the contaminant database, proteins identified with fewer than two peptides, proteins identified by MS/MS in fewer than three replicates of one condition, and proteins detected in fewer than four replicates of one condition. After log₂ transformation, abundance values were normalized by median centering, before missing value imputation (slsa algorithm for partially observed values in the condition, and DetQuantile algorithm for totally absent values in the condition). Statistical testing was conducted with *limma*, whereby differentially expressed proteins were sorted out using a log₂ (Fold Change) cut-off of 0.67 and a p value cut-off of 0.01, leading to a FDR inferior to 5% according to the Benjamini-Hochberg estimator.

Microtubule co-sedimentation assay

Polymerization of porcine TUBULIN (T240-A) was performed in BRB80 (80mM PIPES, 1mM EGTA, 1mM MgCl₂, pH 6.7) supplemented with GTP (1mM) and glycerol (2.5%) for 1h at 37°C. Paclitaxel 50 μM (Taxol) was added for 15min at the end of polymerization. P0-P1 cortices were lysed at 50 μg/μL in BRB80 supplemented with protease and phosphatase inhibitors, then subjected to vortex/ice cycles for 20min. The lysates were cleaned by 245,000 g ultracentrifugation for 40 min at 4°C to discard potential polymerized microtubules in the pellet. The supernatant was collected and incubated or not (control) with 2 μM of polymerized microtubules for 30min at RT. The TUBULIN detected by western blot in the control line is the endogenous TUBULIN. Total fraction (input) was collected before ultracentrifugation at 100,000 g for 30min at 23°C in a TLA100.3 rotors. Supernatant was discarded and pellet fractions were obtained by re-suspending pellet in a volume equal to the initial volume. 20μl of each fraction were loaded onto the gel for western blot analysis.

Nuclear and cytoplasmic proteins extraction

P0 cortices were harvested in cytoplasmic protein low-salt extraction buffer (10 mM HEPES pH 7.9, 10 mM KCl, 0.1 mM EDTA, 1 mM DTT, 0.5 mM PMSF, 0.6% Nonidet P-40 supplemented with 1/100 protease and phosphatases inhibitors, Sigma-Aldrich, P8340 and P5726). The cortices were homogenized by pipetting up and down approximately 10 times with a P1000 Gilson. After 15min on ice, the cytosolic fraction was collected after centrifugation at 10,000 rpm for 10min at 4°C. The pellet was washed 4 times with cold PBS. The nuclear proteins were extracted from resuspension of the pellet with RIPA buffer (150mM NaCl, 1% Nonidet P-40, 0.5% sodium deoxycholate, 0.1% SDS, 50mM Tris HCl pH8.0 supplemented with 1/100 protease and phosphatases inhibitors, Sigma-Aldrich P8340 and P5726). The suspension was briefly sonicated to homogenize the lysate. After 15 min on ice, the samples were centrifuged at 16,000 g for 15min at 4°C and the supernatant (nuclear fraction) was collected.

Western blot

Cortical neurons were harvested in protein extraction buffer (20mM Tris-HCl pH7.4, 137mM NaCl, 2mM EDTA, 1% Triton X-100 supplemented with 1/100 protease and phosphatases inhibitors, Sigma-Aldrich, P8340 and P5726) and frozen at 80°C until protein extraction. Protein extraction of neurons was performed by pipetting up and down approximately 10 times with a P1000 Gilson. The supernatants were collected after centrifugation at 10,000rpm for 10 min at 4°C. Protein concentration was measured by the BCA method. Proteins were treated with SDS-PAGE sample buffer [6X concentrated: 350mM Tris 10% (w/v), SDS 30% (v/v) in glycerol, 0.6M DTT, 0.06% (w/v) bromophenol blue], boiled 5min at 95°C, and loaded on 8%. Polyacrylamide gel.

Proteins were transferred onto PVDF (polyvinylidene difluoride) membranes, blocked with 5% bovine serum albumin and 0.5% Tween (Euromedex) in TBS (TBST) for 1h at room temperature, and probed overnight at 4°C with the following primary antibodies diluted in 5% bovine serum albumin TBST: 1:1000 rabbit anti-NUMA1 (ab109262, Abcam), 1:2000 rabbit anti-VINCULIN (V9131, Sigma), 1:250 mouse anti-GM130 (610822, BD transduction), 1:500 mouse anti-JIP1 (B-7, sc-25267 Santa Cruz Biotechnology), 1:5000 mouse anti-αTUBULIN (T9026, Sigma), 1:1000 rabbit anti-LAMIN B1 (ab133741, abcam), 1:1000 mouse anti-poly-UBIQUITIN antibody (Clinisciences, LS-C107107-25), 1:500 rabbit anti-p62 (Sigma, P0067). Washes were performed with TBS-Tween (0.1%). HRP-conjugated antibodies were incubated for 1h at room temperature and membranes were revealed by using ECL reagent (ThermoFisher Scientific) with a Chemidoc imaging device (Biorad).

Quantitative real-time PCR

For NUMA1 mRNA analysis, total RNA was extracted from P0 cortices using the NucleoSpin RNA extraction kit (Macherey-Nagel, 740955). RNA samples were retrotranscribed with the iScript Ready-to-Use cDNA supermix (Biorad, 1708840). One microgram of cDNA was submitted to qPCR using the SsoAdvanced SYBR Green supermix (Biorad, 1725272) with a specific pair of primers for NUMA1 (Gene Globe ID QT00109557, QIAGEN). CycloG (5'-AAGAATCGTCGCTGGTATG-3', 5'-AAAGCCGATGACAAGGAG-3'), MTBP (5'-GGGGTCATAGGAGTCATTGG-3', 5'-ACATCTCAGCAACCCACACA-3'), and PGK1 (5'-TAGTGGCTGAGATGTGGCA CAG-3', 5'-GCTCACTTCTTCTCAGGCAG-3') genes were used as internal controls. Fold changes were calculated using the 2-ΔΔCt method. Data were analyzed from six independent experiments and presented as the mean ± SEM.

For miRNA quantification, RNA was extracted from P0 cortices using the miRNeasy Tissue/Cells Advanced Mini Kit (QIAGEN, 217604). Of the extracted RNA, 10 ng was used for reverse transcription following the manufacturer's instructions using miRCURY LNA RT Kit (QIAGEN, 339340). qPCR reactions were performed following manufacturer's instructions for miRCURY LNA SYBR

Green PCR Kit (QIAGEN, 339345) with a specific pair of primers for mmu-miR-124-3p (QIAGEN, MIMAT0000134-YP00206026); mmu-miR-148b-3p (QIAGEN, MIMAT0000580-YP00204047); mmu-miR-130b-3p (QIAGEN, MIMAT0000387-YP00204317); mmu-miR-7a-1-3p (QIAGEN, MIMAT0004670-YP00205888); mmu-miR-31-5p (QIAGEN, MIMAT0000538-YP00205159); mmu-miR-22-3p (QIAGEN, MIMAT0000531-YP00204606); mmu-miR-152-3p (QIAGEN, MIMAT0000162-YP00204294); mmu-miR-125b-5p (QIAGEN, MIMAT0000423-YP00205713); mmu-miR-351-5p (QIAGEN, MIMAT0000609-YP00205011); mmu-miR-301a-3p (QIAGEN, MIMAT0000688-YP00205601) and U6 snRNA (hsa, mmu) (QIAGEN, YP00203907) was used as internal control. miRNAs changes were quantified with the $2^{-\Delta\Delta CT}$ method using RNU6-1 (RNA, U6 small nuclear 1) as control.

Plasmid constructs

To delete the NLS region in the pCDH-Ubc-NUMA1FL and pCDH-Ubc-NuMA1deltaMBD constructs (Gallini et al., 2016), we performed an inverse PCR with the following oligos: Delta NLS sense 5'-TCACCACCGTGTCCCTGGAACTCATCAGG-3';

Delta NLS anti-sense 5'-GGGACACGGTGGTGATACCGGTGCC-3'. Subsequently both constructs were sub cloned into a pCAG-GFP vector (addgene 11150) using Pro Ligation-Free Cloning Kit from (abm E086/E087). BsrGI was used as restriction site. For the lox-STOP-lox-GFPshNUMA1 constructs, we used a pCALNL-GFP-hU6 plasmid into which we cloned the shNUMA1. To build the pCALNL-GFP-hU6 the humanU6 promoter has been PCR amplified from the pLKO.1 (addgene 10878) and cloned into the pCALNL-GFP plasmid (addgene, 13770) into the XbaI unique restriction site using Pro Ligation-Free Cloning Kit (abm E086/E087). shNUMA1 was introduced in the AgeI unique restriction site of this resulting vector, annealing the 2 following oligos: sens (targeted sequence is in bold)

5'gatttaaattgaattccggc**cttagtctctggacctaga**actcagag**ttctaggtccagagactaagg**ttttggggatccccgggtcgcaccatg3'; anti-sense (targeted sequence is in bold) 5'catggtggcgaccggggatccccaaaa**cccttagtctctggacctaga**actcagag**ttctaggtccagagactaagg**ccggaa tcaatttaaatc-3'. All constructs were sequenced (GENEWIZ).

Image acquisition

For the *in vitro* axonal tracking, cortical neurons were imaged with Axio Scan.Z1 slide scanner (Colibri.7; 20X objective; Zeiss). The brain sections for *in vivo* axonal track were acquired using an inverted confocal microscopy (LSM710, Zeiss). High-resolution images on growth cones were acquired using an inverted confocal microscope (LSM710, Zeiss) with Airyscan detector and a 63 objective (1.4 NA, Zeiss).

QUANTIFICATION AND STATISTICAL ANALYSIS

Data analysis

All the data were analyzed using NIH ImageJ (<https://imagej.nih.gov/ij/>). For axonal tracking in cell culture, the axon was defined as the longest neurite measuring at least 100 μ m, using the ImageJ segmented line tool. Measurements were taken from the neck of the axon at the base of the soma to the growth cone. For axon branching in cell culture, we considered an extension of at least 15 μ m to constitute a branch. On brain sections, axon tracts were traced using the edge of the mem-RFP labeled region as the starting point.

In P21 mice, we analyzed 4 different regions of interest (1 to 4, Figure 1C). For region 1 in the ipsilateral cortex, we measured the mean in layer V after subtracting the mean intensity background from a cortical region presenting no specific staining. Region 2 was traced in the contralateral somatosensory cortex, where the branching was at its maximum for both genotypes; we measured the mean in layers V, II/III, and white matter (WM) V after subtracting the mean intensity background from a cortical region with no specific staining. Region 3 represents a line scan of 200-pixel width drawn across the middle region of corpus callosum. Finally, region 4 represents a line scan of 200-pixel width drawn in layer II/III all along the contralateral cortex from the parietal to the auditory region, where the last branching point was present in the control condition. Growth cone areas were measured from the axon shaft up to the tips of filopodia, defined by phalloidin staining. Exploratory microtubules were measured from their tips to the main microtubule bundle. To assess the microtubule bundling state, we plotted the maximum value obtained after measuring the mean fluorescence intensity of Tyr- TUBULIN staining along a line scan width of 60 pixels.

Statistical analyses

GraphPad Prism 6.0 software (San Diego, CA) was used for statistical analyses. Outliers were identified applying the Rout method. Sample sizes were chosen based on similar experiments in the references to ensure statistically significant results while minimizing the number of animals used. Significance was assessed using a two-tailed Student's t test or Mann-Whitney U test, depending on the normality test (Shapiro-Wilk normality test or Kolmogorov-Smirnov test). The samples following a Gaussian distribution were expressed as mean \pm SEM. Data without a normal distribution were displayed as box-whisker plots representing the 25th, 50th and 75th percentiles.

RESEARCH ARTICLE

NEURODEVELOPMENT

Huntington's disease alters human neurodevelopment

Monia Barnat¹, Mariacristina Capizzi^{1*}, Esther Aparicio^{1*}, Susana Boluda², Doris Wennagel¹, Radhia Kacher¹, Rayane Kassem¹, Sophie Lenoir¹, Fabienne Agasse¹, Barbara Y. Braz¹, Jeh-Ping Liu³, Julien Ighil⁴, Aude Tessier⁵, Scott O. Zeitlin³, Charles Duyckaerts², Marc Dommergues⁴, Alexandra Durr^{6,†}, Sandrine Humbert^{1,†}

Although Huntington's disease is a late-manifesting neurodegenerative disorder, both mouse studies and neuroimaging studies of presymptomatic mutation carriers suggest that Huntington's disease might affect neurodevelopment. To determine whether this is actually the case, we examined tissue from human fetuses (13 weeks gestation) that carried the Huntington's disease mutation. These tissues showed clear abnormalities in the developing cortex, including mislocalization of mutant huntingtin and junctional complex proteins, defects in neuroprogenitor cell polarity and differentiation, abnormal ciliogenesis, and changes in mitosis and cell cycle progression. We observed the same phenomena in Huntington's disease mouse embryos, where we linked these abnormalities to defects in interkinetic nuclear migration of progenitor cells. Huntington's disease thus has a neurodevelopmental component and is not solely a degenerative disease.

Huntington's disease (HD) is a neurodegenerative disease that is part of the larger family of "proteopathies," which includes the polyglutamine diseases, amyotrophic lateral sclerosis, and Alzheimer's and Parkinson's diseases. These diverse disorders share a delayed onset in mid-adulthood or later despite the expression, at least in hereditary cases, of the disease-driving protein from the first days of life. This raises the question of whether early events might set the stage for later disease. For example, huntingtin (HTT), the protein mutated in HD, is essential for development, at least in mice (1–3). The mutant HTT (mHTT) impairs neural progenitor cell division and neuronal migration and maturation (4–6), giving HD mice a thinner cortex (7). The fact that expression of either mHTT or hypomorphic HTT solely during early life is sufficient to produce HD features in adult mice strongly suggests that there is a developmental component to the disease (8, 9).

In support of this notion, human neuroimaging studies have revealed smaller intracranial volume in HD mutation carriers as young as 7 years of age (10, 11). Loss of cortical volume takes place long before any symptoms appear, and defects in the corticostriatal net-

work lead to striatal dysfunction and degeneration (12–15). Studies in neurons derived from HD human induced pluripotent stem cells (iPSCs) have identified changes in gene expression that support an altered developmental program (16, 17), and mHTT alters neuronal identity in cortical populations of HD brain organoids (18). But does mHTT affect early human development? And if so, how early? To answer these questions, we recruited HD mutation carriers who sought prenatal testing in order to determine whether the fetus carried an HD-causing mutation.

Mutant huntingtin mislocalizes in human and mouse embryos

We were able to procure rare intact cortical tissues from four HD mutation carrier fetuses and four healthy controls at gestation week 13 (GW13) (table S1). At this developmental stage, the cortical neurons that project to the striatum and later deteriorate in HD are arising from the division of progenitor cells at the ventricular zone. These apical progenitors extend processes toward both the apical and basal surfaces of the neuroepithelial wall, and their nuclei move back and forth between surfaces in concert with cell cycle progression in a process known as interkinetic nuclear migration. This process, common to all developing pseudostratified neuroepithelia (19, 20), maintains the balance between progenitor renewal and differentiation by controlling when apical progenitor nuclei are exposed to proliferative versus neurogenic signals, and in what proportions.

To examine the expression pattern of HTT at the ventricular zone of the GW13 cortex, we used an antibody that recognizes both HTT and mHTT (4C8; Fig. 1, A and B, and fig. S1A). In wild-type tissues, HTT staining demarcated

the apical surface of the ventricular zone and spread diffusely throughout the basal region. In cortical tissue of HD mutation carriers, however, HTT staining concentrated at the apical endfeet (the apical surface of the processes).

Given the preciousness of the human tissue, we turned to mice to further investigate these observations, using embryonic day 13.5 (E13.5) mouse embryos, which correspond to GW13 in human neurodevelopment. We studied an HD knock-in mouse model in which the first exon of the *HTT* gene is replaced by human exon 1 carrying 111 CAG repeats (Hdh^{Q111/Q111}) (21). Immunostaining coronal sections revealed a pattern of HTT expression that paralleled our observations in human fetuses (fig. S1B). To determine the distribution of mHTT specifically, we used another HD knock-in mouse model in which Flag tags are inserted in the N terminus of wild-type HTT (Hdh^{F7Q/+}) or mutant HTT carrying 140 CAG repeats (Hdh^{F140Q/+}) (22) (fig. S1C). The Flag labeling showed that mHTT localized to the apical surface and was decreased in the basal region.

Mutant huntingtin impairs endosome secretion and recycling

Apical progenitors maintain their polarity through endocytosis and the trafficking of proteins from the trans-Golgi network to the plasma membrane at the apical endfeet (19). In HD, both endocytosis and Golgi-membrane trafficking are dysregulated (23). Because one of HTT's main functions is to transport vesicles, we used markers of the endosomal pathway to map the subcellular localization of HTT in HD and to gauge whether transport is affected this early in HD.

We stained for calnexin (a marker of the endoplasmic reticulum), GRASP65 (Golgi assembly stacking protein of 65 kDa to mark the cis-Golgi network), TGN38 (trans-Golgi network integral membrane protein 38), EEA1 (early endosome antigen 1), and transferrin receptor (recycling endosomes). In control samples, HTT colocalized partially with these markers (figs. S2 and S3). In both human and mouse HD samples, however, HTT strongly colocalized with TGN38, EEA1, and transferrin receptor, and to a lesser extent with calnexin and GRASP65. These results suggest that mHTT hinders endosomal trafficking in apical progenitors, even at this very early stage of development.

Mutant huntingtin disrupts neuroepithelial junctional complexes

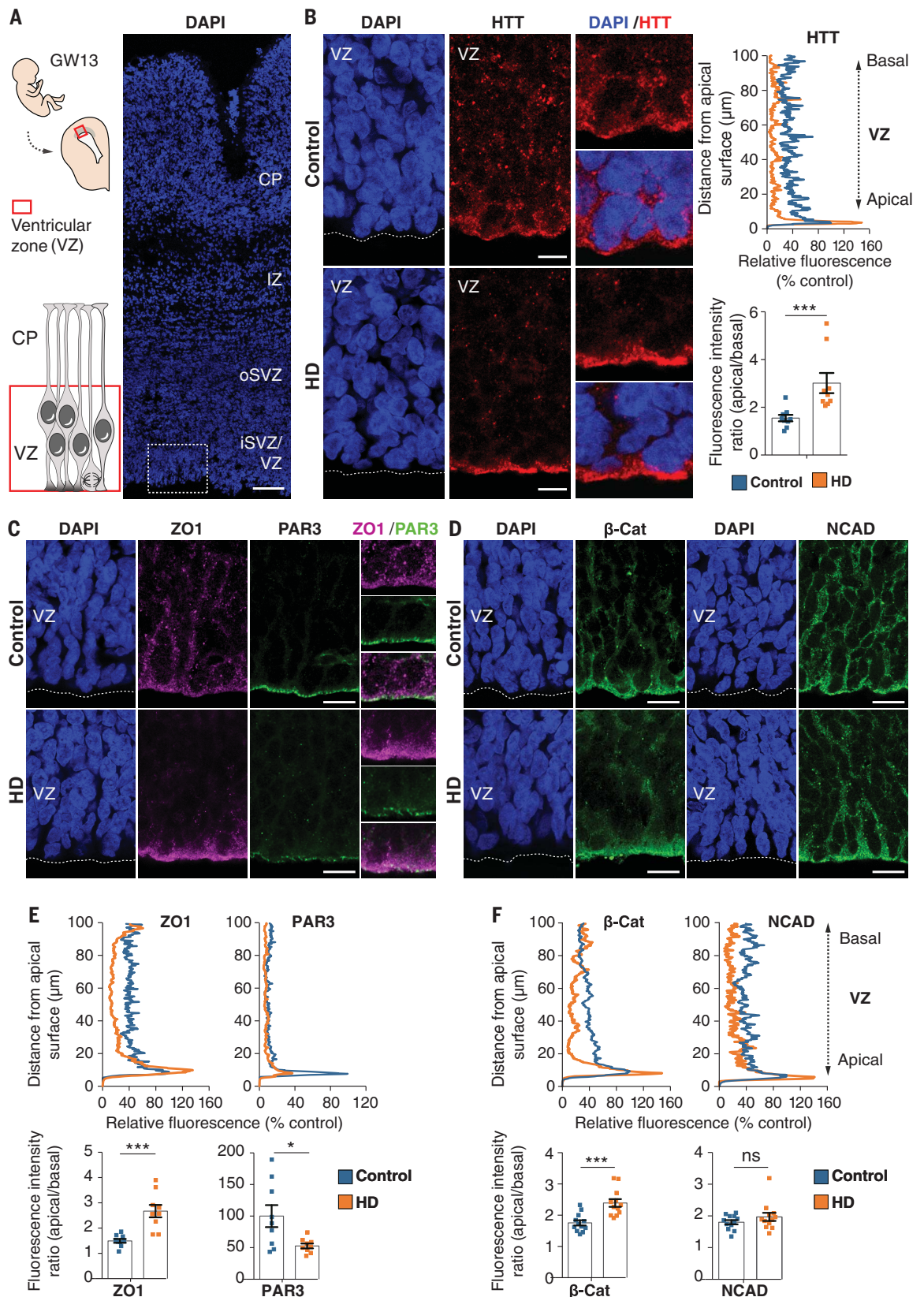
Apical endfeet contain junctional complexes (19, 24) composed of tight-junction and adherens-junction proteins, including ZO1, PAR3, NCAD, and β -catenin (25), that link neighboring progenitors to each other, thereby sealing the neuroepithelium. Because HTT regulates the trafficking of these proteins,

¹Univ. Grenoble Alpes, INSERM, U1216, Grenoble Institut Neurosciences, Grenoble, France. ²Department of Neuropathology Raymond Escourolle, AP-HP, Pitié-Salpêtrière University Hospital, Paris, France. ³Department of Neuroscience, University of Virginia School of Medicine, Charlottesville, VA 22908, USA. ⁴AP-HP, Sorbonne University, Service de Gynécologie Obstétrique, Pitié-Salpêtrière Hospital, Paris, France. ⁵AP-HP, Unité d'Embryofœtopathologie, Necker Hospital, Paris, France. ⁶Sorbonne University, Paris Brain Institute, APHP, INSERM U1127, CNRS UMR7225, Pitié-Salpêtrière Hospital, Paris, France

*These authors contributed equally to this work.

†Corresponding author. Email: alexandra.durr@upmc.fr (A.D.); sandrine.humbert@inserm.fr (S.H.)

Fig. 1. Huntingtin and junctional complex proteins mislocalize in the ventricular zone of human fetuses carrying HD-causing mutations. (A) Left: Diagram showing the position of the fetal ventricular zone relative to the cortical plate (CP). Right: Coronal brain sections of GW13 control human cortex were counterstained with 4',6-diamidino-2-phenylindole (DAPI). The dotted square shows the region imaged in (B). Scale bar, 100 μ m. (B) Left: Coronal GW13 brain sections from control fetus and fetus carrying HD-causing mutation were immunostained for HTT. Scale bars, 10 μ m. Right: Representative line-scan analysis (relative fluorescence intensity) of HTT immunostaining and quantification of apical/basal human HTT fluorescence intensity in the ventricular zone. For each condition, $n = 3$ fetuses from different mothers; $***P = 0.0044$ (unpaired t test). (C and D) Coronal GW13 fetal brain sections were immunostained for ZO1 and PAR3 (C) and β -catenin and NCAD (D). Scale bars, 15 μ m. (E and F) Representative line-scan analysis (relative fluorescence intensity) of indicated immunostainings (top) and quantification of indicated fluorescence intensities in the ventricular zone (bottom graphs). For each condition, $n = 3$ fetuses from different mothers. ZO1: $***P = 0.0003$ (unpaired t test); PAR3: $*P = 0.0177$ (unpaired t test); β -cat: $***P = 0.0003$ (unpaired t test); NCAD: $P = 0.4682$ (Mann-Whitney U test), ns (not significant). Results are means \pm SEM. VZ, ventricular zone; iSVZ, inner subventricular zone; oSVZ, outer subventricular zone; IZ, intermediate zone; CP, cortical plate. Nuclei were counterstained with DAPI.



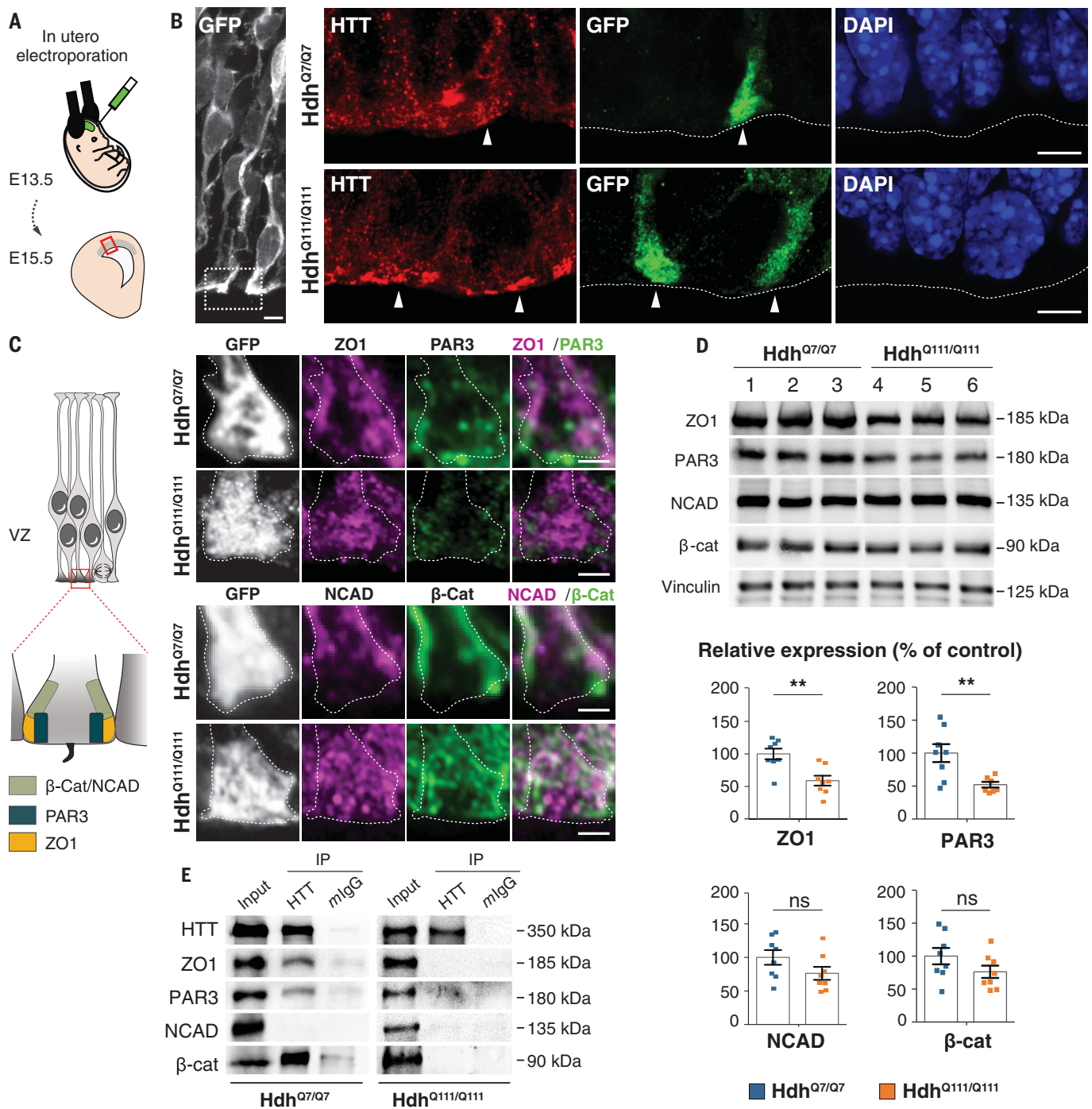


Fig. 2. Junctional protein complexes are disrupted in the apical endfeet of HD mouse embryos. (A) Schematic of the in utero electroporation experiment. (B and C) Mouse embryos were electroporated at E13.5 with a pCAG-GFP construct to delineate the apical endfoot in E15.5 cortices. (B) Hdh^{Q7/Q7} and Hdh^{Q111/Q111} cortical sections were immunostained for GFP (left) and for HTT and GFP (right). White arrowheads point to apical endfeet. Nuclei were counterstained with DAPI. (C) Left: Diagram indicating the position of junctional complexes at the apical endfeet. Right: Cortical sections were immunostained for GFP, ZO1, and PAR3 (upper panel) and GFP,

NCAD, and β-Cat (lower panel). Scale bars, 5 μm (B), 2 μm (C). (D) ZO1, PAR3, NCAD, β-catenin, and vinculin immunoblotting analyses of lysates from E15.5 Hdh^{Q7/Q7} and Hdh^{Q111/Q111} cortices. Bar graphs correspond to the quantitative evaluation of the indicated proteins. For each condition, $n =$ at least 7 embryos from different mothers. ZO1: $**P = 0.0026$; PAR3: $**P = 0.0075$; NCAD: $P = 0.1255$; β-cat: $P = 0.1476$ (unpaired t tests). Results are means \pm SEM. (E) HTT-associated complexes were immunoprecipitated with the 4C8 antibody from E15.5 Hdh^{Q7/Q7} and Hdh^{Q111/Q111} cortical extracts. Mouse IgG (mlgG) was used as a negative control.

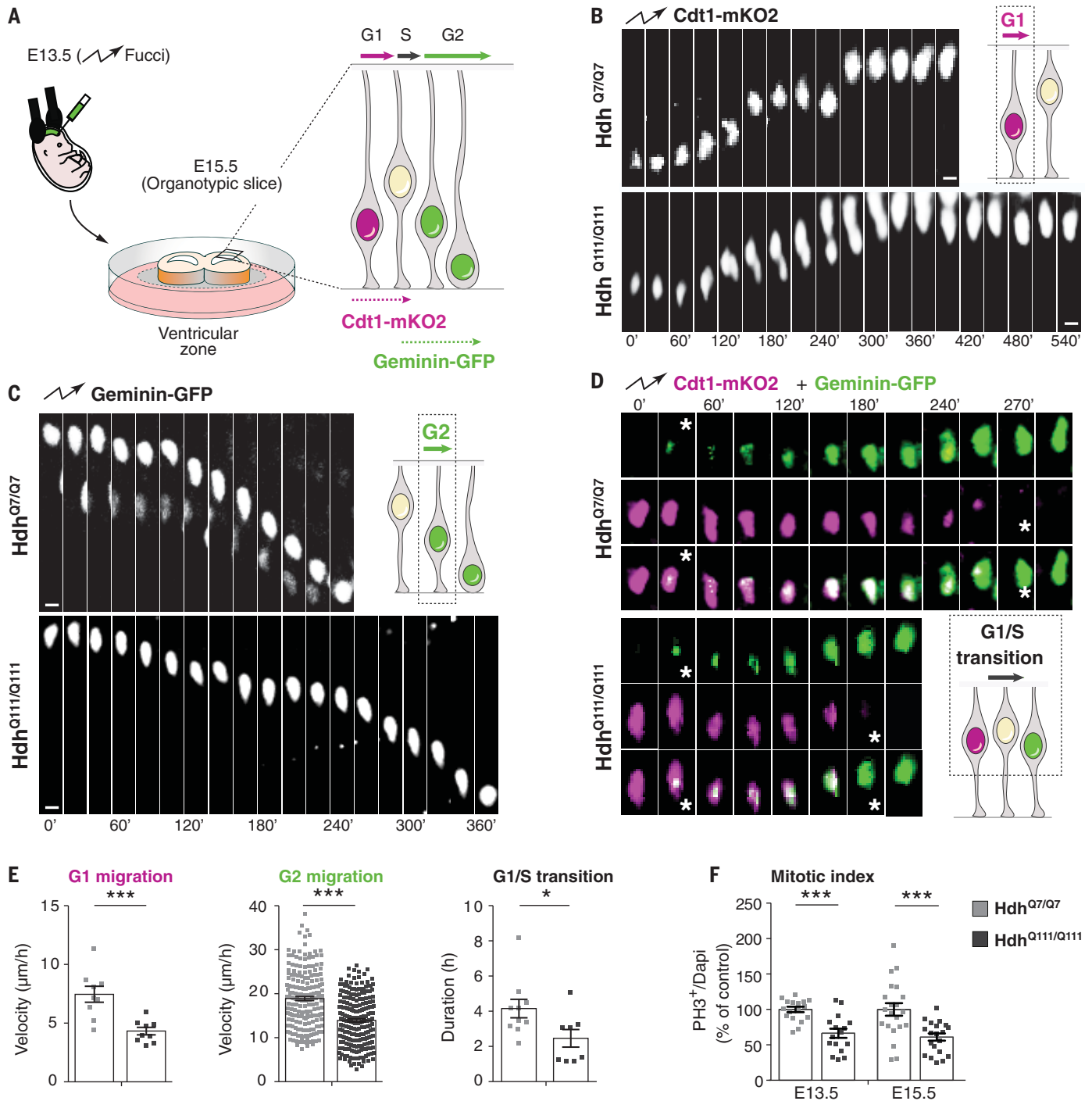


Fig. 3. Interkinetic nuclear migration and mitosis of cortical apical progenitors are impaired in HD mouse embryos. (A) Schematic of the experiment for analysis of interkinetic nuclear migration. E13.5 Hdh^{Q7/Q7} and Hdh^{Q111/Q111} embryos were electroporated with Cdt1-mKO2 and geminin-GFP constructs. After 48 hours, the movement of the GFP- and mKO2-labeled nuclei was followed by spinning disc microscopy, taking one image every 10 or 15 min for 10 hours. (B to D) Representative images showing the movement of nuclei in G₁, G₂, and G₁/S transition phases as indicated. (D) Stars indicate the beginning and ending of the G₁/S transition. Scale bars, 5 μm . (E) Quantitative differences in the velocity of G₁-phase nuclei [for each condition, $n = 9$ cells from three

embryos from different mothers; $***P = 0.0008$ (unpaired t test)], velocity of G₂-phase nuclei [for each condition, $n =$ at least 202 cells from four embryos from different mothers; $***P < 0.0001$ (Mann-Whitney U test)], and length of G₁/S transition [for each condition, $n =$ at least 8 cells from three embryos from different mothers; $*P = 0.0356$ (unpaired t test)]. (F) Bar graphs show the percentage of phospho-histone 3 (PH3) cells (mitotic index) of dividing progenitors [E13.5: for each condition, $n =$ at least 2151 cells from four embryos from different mothers, $***P < 0.0001$ (unpaired t test); E15.5: for each condition, $n =$ at least 1801 cells from three embryos from different mothers, $***P = 0.0005$ (unpaired t test)]. Results are means \pm SEM.

which are dysregulated in HD (6, 26–30), we hypothesized that mHTT hinders the correct positioning of these junctions, which would diminish the integrity of the neuroepithelium. As predicted, HTT partially codistributed with

ZO1, PAR3, β -catenin, and NCAD at the apical endfeet of human GW13 control and mouse E13.5 neuroepithelium (figs. S4 and S5A). The levels of ZO1, NCAD, and β -catenin were high at the apical surface of the human and

mouse control ventricular zone and even higher in HD tissues, with a concomitant reduction in these proteins in the basal region (Fig. 1, C to F, and fig. S5, B to E). PAR3 was also misregulated in HD but in a different pattern

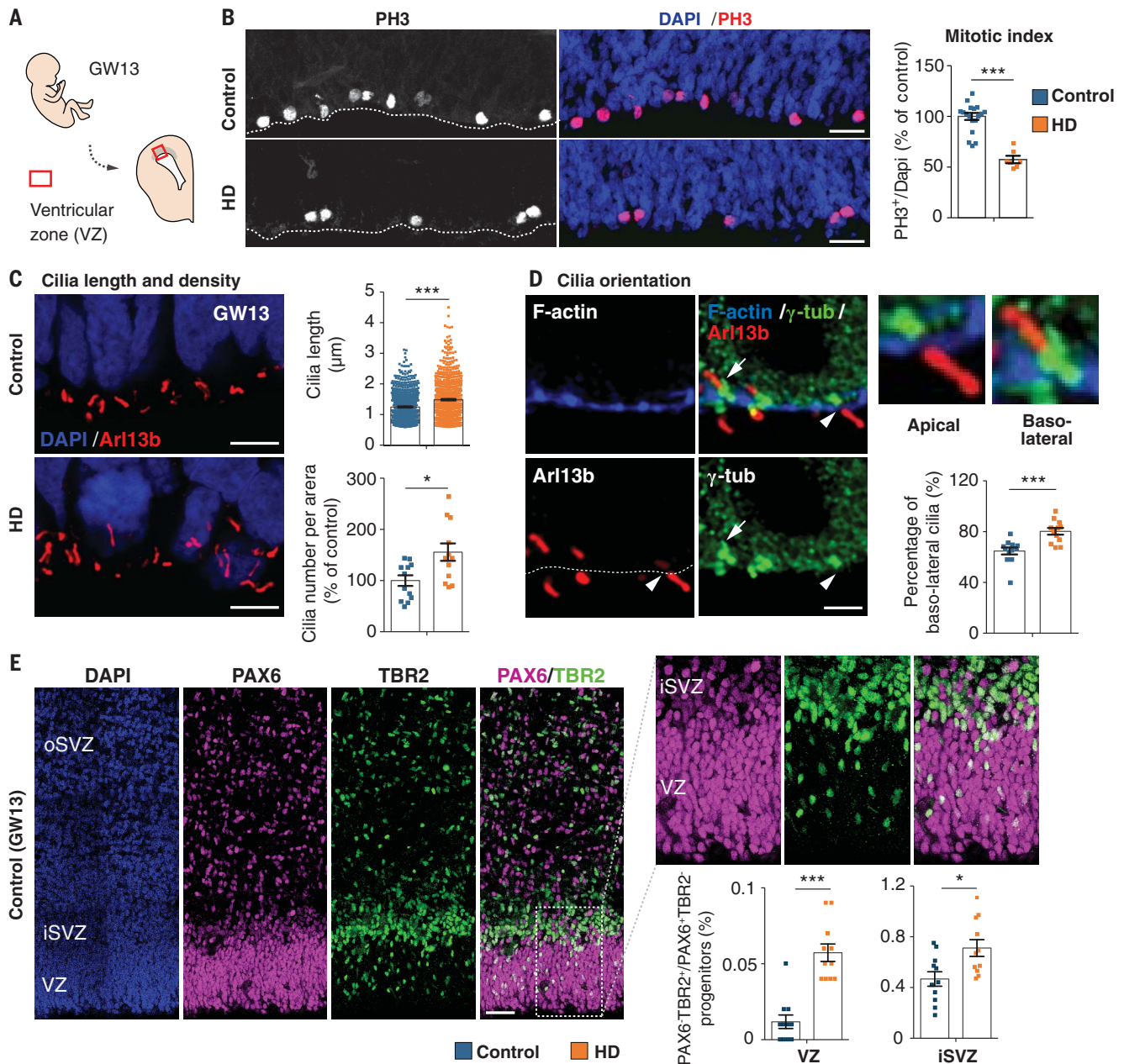


Fig. 4. Mutant huntingtin shifts neurogenesis toward neuronal lineage.

(A) Diagram showing the position of the fetal ventricular zone. (B) Cortical sections of GW13 fetuses were immunostained with antibody against phospho-histone 3 (PH3) and the mitotic index was quantified. For each condition, n = at least 1146 cells from three fetuses from different mothers; $***P < 0.0001$ (Mann-Whitney U test). Scale bars, 25 μ m. (C) Coronal GW13 brain sections from control fetus and fetus carrying HD-causing mutation (HD) were immunostained for the cilia marker Arl13b. Scale bars, 5 μ m. Bar graphs show cilia length [for each condition, n = at least 770 cilia from four fetuses from different mothers; $***P < 0.0001$ (Mann-Whitney U test)] and cilia density [for each condition, n = 4 fetuses from different mothers; $*P = 0.0104$ (unpaired t test)] at the apical surface. (D) Coronal brain sections of GW13

human cortex were immunostained for F-actin, γ -tubulin (γ -tub), and Arl13b. Scale bars, 2 μ m. White arrowheads and white arrows show apical and basolateral cilia, respectively. Bar graph shows the percentage of basolateral cilia at the apical surface. For each condition, n = at least 260 cilia from four fetuses from different mothers; $***P = 0.0003$ (Mann-Whitney U test). (E) Typical PAX6 and TBR2 staining of a GW13 human fetal sample analyzed. Scale bars, 50 μ m. Bar graphs show the percentage of PAX6/TBR2-positive cells (PAX6⁺/TBR2⁺) over PAX6-positive, TBR2-negative (PAX6⁺/TBR2⁻) progenitors [for each condition, three fetuses from different mothers were analyzed; VZ, n = at least 2447 cells, $***P < 0.0001$ (Mann-Whitney U test); iSVZ, n = at least 1580 cells, $*P = 0.011$ (unpaired t test)]. Results are means \pm SEM. Nuclei were counterstained with DAPI.

from these other proteins: Its expression levels were down-regulated, so its demarcation of the apical surface in control samples was diminished, rather than intensified, in HD.

To better understand how junctional complexes in individual apical endfeet are affected in HD, we electroporated E13.5 control and HD mouse embryos in utero with a pCAG-GFP (green fluorescent protein) construct and performed immunohistochemistry on E15.5 coronal sections (Fig. 2, A and B). At this stage in mice and at the corresponding stage GW16 in humans (table S1), the mislocalization of HTT and junction proteins in HD apical progenitors persisted (figs. S6 and S7). Indeed, GFP-expressing knock-in HD progenitors, but not controls, showed a bright line of HTT along the apical surface (Fig. 2B). In control embryos, ZO1, NCAD, and β -catenin immunostaining marked the sides of the apical endfeet; PAR3 staining was more apical (Fig. 2C). In Hdh^{Q111/Q111} embryos, ZO1, NCAD, and β -catenin spread throughout the apical endfeet and PAR3 staining was diminished. These observations were corroborated by immunoblotting protein extracts from Hdh^{Q7/Q7} and Hdh^{Q111/Q111} E15.5 cortices (Fig. 2D). The levels of NCAD and β -catenin were similar in control and HD conditions, but ZO1 and PAR3 protein levels were lower in the mutant mice. Coimmunoprecipitation showed that HTT associates with ZO1, PAR3, and β -catenin, but these interactions were disrupted in HD (Fig. 2E and fig. S8).

Mutant HTT alters progression through the cell cycle

The integrity of the apical junctional complexes is essential for progression through interkinetic nuclear migration, when the nuclei of progenitor cells born at the apical surface move toward the basal side during the G₁ phase of the cell cycle, enter and complete the S phase, then return to the apical surface, where they undergo division (19, 20, 31, 32). Given that the junctional complexes do not form properly with mHTT, we examined cell cycle progression in the apical progenitors.

To measure apical (G₁ phase) and basal (G₂ phase) movements in vivo, we used the fluorescent ubiquitination-based cell cycle indicator (FUCCI), which tracks the expression of markers of the different phases of the cell cycle (33). We electroporated wild-type E13.5 embryos with plasmids encoding CDT1 (chromatin licensing and DNA replication factor 1)-mKO2 and geminin-GFP, then carried out time-lapse imaging on acute cortical slices 2 days after in utero electroporation (Fig. 3A) so that we could distinguish cycling progenitors in G₁ from neurons exiting the cell cycle and migrating away from the ventricular zone (fig. S9A and movie S1). As expected, CDT1 levels peaked during G₁ and fell upon entry into S phase, whereas geminin levels were high during S phase and

G₂ (fig. S9B and movie S2). The velocities of nuclear movement in G₁ and G₂ in control cells were as previously reported (34) (Fig. 3, B, C, and E, and movies S3 to S6), but in Hdh^{Q111/Q111} embryos, migrating nuclei moved more slowly in both G₁ and G₂, causing these phases to lengthen while the G₁/S phase transition was shortened (Fig. 3, D and E, and movies S7 and S8). We next immunostained cortical sections of Hdh^{Q111/Q111} embryos and GW13 HD carrier fetuses with antibody against phospho-histone 3 (PH3), a marker of mitosis, and evaluated the mitotic index (Fig. 3F and Fig. 4, A and B). HD mice and human mutation carriers had roughly half the mitotic index of controls. In HD, therefore, the pool of proliferating cells is diminished.

Mutant HTT biases neurogenesis toward the neuronal lineage

The cell cycle correlates with the assembly (during G₀) and disassembly (at the onset of M phase) of the primary cilium at the apical progenitor endfeet (19, 32). Immunostaining with the cilia marker Arl13b, a member of the adenosine diphosphate ribosylation factor-like family, revealed that both the length and density of the cilia were greater at the apical area of the developing cortex in HD human and mouse samples than in controls (Fig. 4C and fig. S10A), which confirms that the cells were not progressing through the cell cycle properly (20). Because a longer G₁ phase and a shorter G₁/S transition characterize progenitors committed toward the neuronal lineage (32, 35), we asked whether mHTT favors the production of apical over basal progenitors.

We evaluated cilia orientation by labeling brain sections with F-actin (to delineate the apical surface) and Arl13b and γ -tubulin (to label the basal body) (Fig. 4D and fig. S10B). The proportion of basolateral cilia, which signal the generation of basal progenitors (36), was greater in HD human and mouse samples than in controls. To discriminate between apical progenitors and basal progenitors, which are more engaged in the neuronal lineage (37), we labeled for the transcription factors PAX6 and TBR2, respectively. HD human and mouse samples showed a greater proportion of basal progenitors at the ventricular zone, subventricular zone, and inner subventricular zone than did controls (Fig. 4E and fig. S10C).

Discussion

Our data show that mHTT mislocalizes at junctional complexes, disrupts the polarity of human and mouse neuroepithelium, and interferes with the cell cycle of apical progenitors, leading to fewer proliferating cells and more neural progenitors prematurely entering lineage specification. This is consistent with previous evidence that HTT regulates

cellular adhesion, polarity, and epithelial organization (27). In the presence of mHTT, the epithelial-mesenchymal transition is accelerated (28). It is possible that mHTT contributes to cellular disorganization through other means as well, such as by interfering with the orientation of the mitotic spindle (7). Given that HTT also establishes apical polarity in the mammary epithelium, where it forms a complex with PAR3, aPKC, and RAB11A and ensures the apical translocation of PAR3-aPKC through RAB11A (29), we speculate that HTT may act to maintain epithelial cell polarity throughout the body.

A recent neuroimaging study found that the posterior Sylvian fissure, normally asymmetrical between the right and left hemispheres, lacks asymmetry in the HD population studied (38). Because the Sylvian fissure appears early in utero, the authors concluded that this abnormal symmetry arises during fetal development. Our results show that mHTT does alter very early stages of brain development in human HD, even though the samples we analyzed were from mutation carriers with small pathological expansions (39, 40, and 42 repeats) that would typically cause later manifestations of HD. The defects we observed likely render the corticostriatal circuitry more vulnerable to the later dysfunctions characteristic of HD (23), as proposed for another polyglutamine disease, spinocerebellar ataxia type 1 (39). The path to degeneration is complex, however, and weaves together both pathogenic and compensatory mechanisms. For example, a recent study found that HD mutation carriers as young as 6 years of age show compensatory hyperconnectivity between the striatum and cerebellum; this initially enlarges the striatum but the metabolic load soon overwhelms it, the connections are rapidly lost, and the striatum atrophies well before the onset of motor symptoms (40).

It is now beyond doubt that neurodegenerative diseases can have a developmental component. For HD, this discovery opens the door for future studies to identify molecular treatments. For example, the HD iPSC Consortium characterized isoxazole-9 after finding that it reverts abnormal neuronal differentiation in HD-derived pluripotent stem cells (17). It may be that treatment should be given very early in life; it remains to be seen whether reducing mHTT levels in adulthood, even in the prodromal stage, would be sufficient to forestall symptom progression, because the brain circuitry is already altered.

REFERENCES AND NOTES

1. M. P. Duyao et al., *Science* **269**, 407–410 (1995).
2. S. Zeitlin, J. P. Liu, D. L. Chapman, V. E. Papaioannou, A. Efstratiadis, *Nat. Genet.* **11**, 155–163 (1995).
3. A. Reiner, I. Dragatsis, S. Zeitlin, D. Goldowitz, *Mol. Neurobiol.* **28**, 259–276 (2003).
4. J. D. Godin et al., *Neuron* **67**, 392–406 (2010).

5. S. U. McKinstry *et al.*, *J. Neurosci.* **34**, 9455–9472 (2014).
6. M. Barnat, J. Le Friec, C. Benstaali, S. Humbert, *Neuron* **93**, 99–114 (2017).
7. M. Molina-Calavita *et al.*, *J. Neurosci.* **34**, 10034–10040 (2014).
8. E. E. Arteaga-Bracho *et al.*, *Neurobiol. Dis.* **96**, 144–155 (2016).
9. A. E. Molero *et al.*, *Proc. Natl. Acad. Sci. U.S.A.* **113**, 5736–5741 (2016).
10. J. K. Lee *et al.*, *Neurology* **79**, 668–674 (2012).
11. P. C. Nopoulos *et al.*, *Brain* **134**, 137–142 (2011).
12. S. J. Tabrizi *et al.*, *Lancet Neurol.* **10**, 31–42 (2011).
13. C. C. Tang *et al.*, *J. Clin. Invest.* **123**, 4076–4088 (2013).
14. A. Virlogeux *et al.*, *Cell Rep.* **22**, 110–122 (2018).
15. X. Zhao *et al.*, *Proc. Natl. Acad. Sci. U.S.A.* **113**, E5655–E5664 (2016).
16. K. L. Ring *et al.*, *Stem Cell Rep.* **5**, 1023–1038 (2015).
17. HD iPSC Consortium, *Nat. Neurosci.* **20**, 648–660 (2017).
18. P. Conforti *et al.*, *Proc. Natl. Acad. Sci. U.S.A.* **115**, E762–E771 (2018).
19. Y. Arai, E. Taverna, *Front. Cell. Neurosci.* **11**, 384 (2017).
20. T. Miyata, M. Okamoto, T. Shinoda, A. Kawaguchi, *Front. Cell. Neurosci.* **8**, 473 (2015).
21. V. C. Wheeler *et al.*, *Hum. Mol. Genet.* **11**, 633–640 (2002).
22. S. Zheng, N. Ghitani, J. S. Blackburn, J. P. Liu, S. O. Zeitlin, *Mol. Brain* **5**, 28 (2012).
23. F. Saudou, S. Humbert, *Neuron* **89**, 910–926 (2016).
24. F. S. Chou, R. Li, P. S. Wang, *Cell. Mol. Life Sci.* **75**, 1027–1041 (2018).
25. R. S. Bultje *et al.*, *Neuron* **63**, 189–202 (2009).
26. J. D. Godin, G. Poizat, M. A. Hickey, F. Maschat, S. Humbert, *EMBO J.* **29**, 2433–2445 (2010).
27. V. Lo Sardo *et al.*, *Nat. Neurosci.* **15**, 713–721 (2012).
28. C. Moreira Sousa *et al.*, *EMBO Mol. Med.* **5**, 309–325 (2013).
29. S. Elias, J. R. McGuire, H. Yu, S. Humbert, *PLOS Biol.* **13**, e1002142 (2015).
30. M. S. Thion *et al.*, *J. Natl. Cancer Inst.* **107**, djv208 (2015).
31. E. Taverna, M. Götz, W. B. Huttner, *Annu. Rev. Cell Dev. Biol.* **30**, 465–502 (2014).
32. C. Norden, *J. Cell Sci.* **130**, 1859–1863 (2017).
33. A. Sakaue-Sawano *et al.*, *Cell* **132**, 487–498 (2008).
34. Y. Kosodo *et al.*, *EMBO J.* **30**, 1690–1704 (2011).
35. Y. Arai *et al.*, *Nat. Commun.* **2**, 154–165 (2011).
36. M. Wilsch-Bräuninger, J. Peters, J. T. Paridaen, W. B. Huttner, *Development* **139**, 95–105 (2012).
37. M. N. Manuel, D. Mi, J. O. Mason, D. J. Price, *Front. Cell. Neurosci.* **9**, 70 (2015).
38. J. F. Mangin *et al.*, *Neuroimage Clin.* **26**, 102211 (2020).
39. C. R. Edamakanti, J. Do, A. Didonna, M. Martina, P. Opal, *J. Clin. Invest.* **128**, 2252–2265 (2018).
40. A. V. Tereshchenko *et al.*, *Neurology* **94**, e1908–e1915 (2020).

ACKNOWLEDGMENTS

We are grateful to the patients and their families. We thank L. Benammar and M. Biet for their logistical help; midwife O. Philippon for her support; C. Benstaali and E. Martin for help with experiments; staff of the animal facility and of the Photonic Imaging Center (part of the ISdV core facility and certified by the IBiSA label) of GIN for technical help; F. Saudou, members of the Humbert laboratory, and V. L. Brandt for helpful discussions; and the Association Huntington France (AHF) for continuous support.

Funding: Supported by grants from Agence Nationale pour la

Recherche (ANR-15-IDEX-02 NeuroCoG, S.H.; Network of centers of excellence in neurodegeneration COEN, A.D. and S.H.); Fondation pour la Recherche Médicale (DEQ 20170336752, S.H.); Fondation pour la Recherche sur le Cerveau (S.H.); and the AGEMED program from INSERM (S.H.). M.B. and S.H. are INSERM investigators. E.A. was supported by a CIFRE (2012-0401) doctoral fellowship. M.C. is supported by a La ligue contre le cancer post-doctoral fellowship. J.-P.L. and S.O.Z. are supported by NIH NS077926. **Author contributions:** M.B., A.D., and S.H. designed the study; M.B. and S.H. wrote the manuscript, which was commented on by all authors; M.B. performed most of the experiments; M.C. performed biochemical experiments and immunohistochemistry; E.A. performed interkinetic nuclear migration experiments; D.W., R.Kac., R.Kas., and F.A. performed immunohistochemistry; S.L. and B.Y.B. provided mouse embryonic brains; J.L., A.T., A.D., and M.D. collected human data; S.B. and C.D. performed fetopathological examinations; and J.-P.L. and S.O.Z. provided embryonic brains from Flag-tagged Hdh mice. **Competing interests:** None declared. **Data and materials availability:** All data are available in the manuscript or the supplementary materials.

SUPPLEMENTARY MATERIALS

science.sciencemag.org/content//369/6505/787/suppl/DC1
Materials and Methods
Figs. S1 to S10
Table S1
Movies S1 to S8

15 March 2019; resubmitted 27 April 2020
Accepted 29 June 2020
Published online 16 July 2020
10.1126/science.aax3338

Huntington's disease alters human neurodevelopment

Monia Barnat, Mariacristina Capizzi, Esther Aparicio, Susana Boluda, Doris Wennagel, Radhia Kacher, Rayane Kassem, Sophie Lenoir, Fabienne Agasse, Barbara Y. Braz, Jeh-Ping Liu, Julien Ighil, Aude Tessier, Scott O. Zeitlin, Charles Duyckaerts, Marc Dommergues, Alexandra Durr and Sandrine Humbert

Science **369** (6505), 787-793.
DOI: 10.1126/science.aax3338 originally published online July 16, 2020

Neural progenitors disrupted

Symptoms of Huntington's disease (HD) manifest in adulthood despite the aberrant protein being present much earlier in persons carrying the disease-causing mutation. Barnat *et al.* studied the cellular effects of the HD mutation on human and mouse fetal brain development (see the Perspective by DiFiglia). The authors found that neural progenitor cells at the brain's ventricular zone reach out to both the apical and basal surfaces of the neuroepithelial wall, and their cellular nuclei shuttle back and forth as the cell cycle progresses. With the aberrant protein, these epithelial junctions are disrupted, epithelial polarity is disturbed, and the cell cycle favors premature neuronal differentiation.

Science, this issue p. 787; see also p. 771

ARTICLE TOOLS	http://science.sciencemag.org/content/369/6505/787
SUPPLEMENTARY MATERIALS	http://science.sciencemag.org/content/suppl/2020/07/15/science.aax3338.DC1
RELATED CONTENT	http://stm.sciencemag.org/content/scitransmed/10/461/eaar3959.full http://stm.sciencemag.org/content/scitransmed/10/458/eaat7108.full http://stm.sciencemag.org/content/scitransmed/11/514/eaaw8546.full http://stm.sciencemag.org/content/scitransmed/6/268/268ra178.full http://stm.sciencemag.org/content/scitransmed/8/364/364ps18.full http://science.sciencemag.org/content/sci/369/6505/771.full
REFERENCES	This article cites 40 articles, 11 of which you can access for free http://science.sciencemag.org/content/369/6505/787#BIBL
PERMISSIONS	http://www.sciencemag.org/help/reprints-and-permissions

Use of this article is subject to the [Terms of Service](#)

Science (print ISSN 0036-8075; online ISSN 1095-9203) is published by the American Association for the Advancement of Science, 1200 New York Avenue NW, Washington, DC 20005. The title *Science* is a registered trademark of AAAS.

Copyright © 2020 The Authors, some rights reserved; exclusive licensee American Association for the Advancement of Science. No claim to original U.S. Government Works

REFERENCES

- Aasland, D., Götzinger, L., Hauck, L., Berte, N., Meyer, J., Effenberger, M., Schneider, S., Reuber, E.E., Roos, W.P., Tomicic, M.T., Kaina, B., Christmann, M., 2019. Temozolomide Induces Senescence and Repression of DNA Repair Pathways in Glioblastoma Cells via Activation of ATR-CHK1, p21, and NF- κ B. *Cancer Res.* 79, 99–113. <https://doi.org/10.1158/0008-5472.CAN-18-1733>
- Abel, T.W., Clark, C., Bieri, B., Chytil, A., Aakre, M., Gorska, A., Moses, H.L., 2009. GFAP-Cre-mediated activation of oncogenic K-ras results in expansion of the subventricular zone and infiltrating glioma. *Mol. Cancer Res. MCR* 7, 645–653. <https://doi.org/10.1158/1541-7786.MCR-08-0477>
- Agarwala, S.S., Kirkwood, J.M., 2000. Temozolomide, a novel alkylating agent with activity in the central nervous system, may improve the treatment of advanced metastatic melanoma. *The Oncologist* 5, 144–151. <https://doi.org/10.1634/theoncologist.5-2-144>
- Alcantara Llaguno, S., Chen, J., Kwon, C.-H., Jackson, E.L., Li, Y., Burns, D.K., Alvarez-Buylla, A., Parada, L.F., 2009. Malignant astrocytomas originate from neural stem/progenitor cells in a somatic tumor suppressor mouse model. *Cancer Cell* 15, 45–56. <https://doi.org/10.1016/j.ccr.2008.12.006>
- Altman, J., Das, G.D., 1965a. Autoradiographic and histological evidence of postnatal hippocampal neurogenesis in rats. *J. Comp. Neurol.* 124, 319–335. <https://doi.org/10.1002/cne.901240303>
- Altman, J., Das, G.D., 1965b. Autoradiographic and histological evidence of postnatal hippocampal neurogenesis in rats. *J. Comp. Neurol.* 124, 319–335. <https://doi.org/10.1002/cne.901240303>
- Ambady, P., Wu, Y.J., Kersch, C.N., Walker, J.M., Holland, S., Muldoon, L.L., Neuwelt, E.A., 2022. Radiation enhances the delivery of antisense oligonucleotides and improves chemo-radiation efficacy in brain tumor xenografts. *Cancer Gene Ther.* 29, 533–542. <https://doi.org/10.1038/s41417-021-00324-6>
- Ambady, P., Wu, Y.J., Walker, J.M., Kersch, C., Pagel, M.A., Woltjer, R.L., Fu, R., Muldoon, L.L., Neuwelt, E.A., 2017. Enhancing the cytotoxicity of chemoradiation with radiation-guided delivery of anti-MGMT morpholino oligonucleotides in non-methylated solid tumors. *Cancer Gene Ther.* 24, 348–357. <https://doi.org/10.1038/cgt.2017.27>
- Ämmälä, C., Drury, W.J., Knerr, L., Ahlstedt, I., Stillemark-Billton, P., Wennberg-Huldt, C., Andersson, E.-M., Valeur, E., Jansson-Löfmark, R., Janzén, D., Sundström, L., Mueller, J., Claesson, J., Andersson, P., Johansson, C., Lee, R.G., Prakash, T.P., Seth, P.P., Monia, B.P., Andersson, S., 2018. Targeted delivery of antisense oligonucleotides to pancreatic β -cells. *Sci. Adv.* 4, eaat3386. <https://doi.org/10.1126/sciadv.aat3386>
- Andrade, M.A., Bork, P., 1995. HEAT repeats in the Huntington's disease protein. *Nat. Genet.* 11, 115–116. <https://doi.org/10.1038/ng1095-115>
- André, E.A., Braatz, E.M., Liu, J.-P., Zeitlin, S.O., 2017. Generation and Characterization of Knock-in Mouse Models Expressing Versions of Huntingtin with Either an N17 or a Combined PolyQ and Proline-Rich Region Deletion. *J. Huntingt. Dis.* 6, 47–62. <https://doi.org/10.3233/JHD-160231>

- Andrews, D.W., Judy, K.D., Scott, C.B., Garcia, S., Harshyne, L.A., Kenyon, L., Talekar, K., Flanders, A., Atsina, K.-B., Kim, L., Martinez, N., Shi, W., Werner-Wasik, M., Liu, H., Prosniak, M., Curtis, M., Kean, R., Ye, D.Y., Bongiorno, E., Sauma, S., Exley, M.A., Pigott, K., Hooper, D.C., 2021. Phase Ib Clinical Trial of IGV-001 for Patients with Newly Diagnosed Glioblastoma. *Clin. Cancer Res. Off. J. Am. Assoc. Cancer Res.* 27, 1912–1922. <https://doi.org/10.1158/1078-0432.CCR-20-3805>
- Anne, S.L., Saudou, F., Humbert, S., 2007. Phosphorylation of huntingtin by cyclin-dependent kinase 5 is induced by DNA damage and regulates wild-type and mutant huntingtin toxicity in neurons. *J. Neurosci. Off. J. Soc. Neurosci.* 27, 7318–7328. <https://doi.org/10.1523/JNEUROSCI.1831-07.2007>
- Atwal, R.S., Desmond, C.R., Caron, N., Maiuri, T., Xia, J., Sipione, S., Truant, R., 2011. Kinase inhibitors modulate huntingtin cell localization and toxicity. *Nat. Chem. Biol.* 7, 453–460. <https://doi.org/10.1038/nchembio.582>
- Atwal, R.S., Xia, J., Pinchev, D., Taylor, J., Epan, R.M., Truant, R., 2007. Huntingtin has a membrane association signal that can modulate huntingtin aggregation, nuclear entry and toxicity. *Hum. Mol. Genet.* 16, 2600–2615. <https://doi.org/10.1093/hmg/ddm217>
- Ballas, N., Grunseich, C., Lu, D.D., Speh, J.C., Mandel, G., 2005. REST and its corepressors mediate plasticity of neuronal gene chromatin throughout neurogenesis. *Cell* 121, 645–657. <https://doi.org/10.1016/j.cell.2005.03.013>
- Bao, S., Wu, Q., McLendon, R.E., Hao, Y., Shi, Q., Hjelmeland, A.B., Dewhirst, M.W., Bigner, D.D., Rich, J.N., 2006. Glioma stem cells promote radioresistance by preferential activation of the DNA damage response. *Nature* 444, 756–760. <https://doi.org/10.1038/nature05236>
- Barbarite, E., Sick, J.T., Berchmans, E., Bregy, A., Shah, A.H., Elsayyad, N., Komotar, R.J., 2017. The role of brachytherapy in the treatment of glioblastoma multiforme. *Neurosurg. Rev.* 40, 195–211. <https://doi.org/10.1007/s10143-016-0727-6>
- Barnat, M., Capizzi, M., Aparicio, E., Boluda, S., Wennagel, D., Kacher, R., Kassem, R., Lenoir, S., Agasse, F., Braz, B.Y., Liu, J.-P., Ighil, J., Tessier, A., Zeitlin, S.O., Duyckaerts, C., Dommergues, M., Durr, A., Humbert, S., 2020. Huntington's disease alters human neurodevelopment. *Science* 369, 787–793. <https://doi.org/10.1126/science.aax3338>
- Barnat, M., Le Friec, J., Benstaali, C., Humbert, S., 2017. Huntingtin-Mediated Multipolar-Bipolar Transition of Newborn Cortical Neurons Is Critical for Their Postnatal Neuronal Morphology. *Neuron* 93, 99–114. <https://doi.org/10.1016/j.neuron.2016.11.035>
- Bashir, T., Cloninger, C., Artinian, N., Anderson, L., Bernath, A., Holmes, B., Benavides-Serrato, A., Sabha, N., Nishimura, R.N., Guha, A., Gera, J., 2012. Conditional astroglial Rictor overexpression induces malignant glioma in mice. *PloS One* 7, e47741. <https://doi.org/10.1371/journal.pone.0047741>
- Bates, G.P., Dorsey, R., Gusella, J.F., Hayden, M.R., Kay, C., Leavitt, B.R., Nance, M., Ross, C.A., Scahill, R.I., Wetzell, R., Wild, E.J., Tabrizi, S.J., 2015. Huntington disease. *Nat. Rev. Dis. Primer* 1, 15005. <https://doi.org/10.1038/nrdp.2015.5>
- Beauséjour, C.M., Krtolica, A., Galimi, F., Narita, M., Lowe, S.W., Yaswen, P., Campisi, J., 2003. Reversal of human cellular senescence: roles of the p53 and p16 pathways. *EMBO J.* 22, 4212–4222. <https://doi.org/10.1093/emboj/cdg417>
- Beier, D., Hau, P., Proescholdt, M., Lohmeier, A., Wischhusen, J., Oefner, P.J., Aigner, L., Brawanski, A., Bogdahn, U., Beier, C.P., 2007. CD133(+) and CD133(-) glioblastoma-derived cancer stem cells show differential growth characteristics and molecular profiles. *Cancer Res.* 67, 4010–4015. <https://doi.org/10.1158/0008-5472.CAN-06-4180>

- Ben M'Barek, K., Pla, P., Orvoen, S., Benstaali, C., Godin, J.D., Gardier, A.M., Saudou, F., David, D.J., Humbert, S., 2013. Huntingtin mediates anxiety/depression-related behaviors and hippocampal neurogenesis. *J. Neurosci. Off. J. Soc. Neurosci.* 33, 8608–8620. <https://doi.org/10.1523/JNEUROSCI.5110-12.2013>
- Benn, C.L., Landles, C., Li, H., Strand, A.D., Woodman, B., Sathasivam, K., Li, S.-H., Ghazi-Noori, S., Hockly, E., Faruque, S.M.N.N., Cha, J.-H.J., Sharpe, P.T., Olson, J.M., Li, X.-J., Bates, G.P., 2005. Contribution of nuclear and extranuclear polyQ to neurological phenotypes in mouse models of Huntington's disease. *Hum. Mol. Genet.* 14, 3065–3078. <https://doi.org/10.1093/hmg/ddi340>
- Berg, T.J., Marques, C., Pantazopoulou, V., Johansson, E., von Stedingk, K., Lindgren, D., Jeannot, P., Pietras, E.J., Bergström, T., Swartling, F.J., Governa, V., Bengzon, J., Belting, M., Axelson, H., Squatrito, M., Pietras, A., 2021. The Irradiated Brain Microenvironment Supports Glioma Stemness and Survival via Astrocyte-Derived Transglutaminase 2. *Cancer Res.* 81, 2101–2115. <https://doi.org/10.1158/0008-5472.CAN-20-1785>
- Bernstock, J.D., Gary, S.E., Klinger, N., Valdes, P.A., Ibn Essayed, W., Olsen, H.E., Chagoya, G., Elsayed, G., Yamashita, D., Schuss, P., Gessler, F.A., Paolo Peruzzi, P., Bag, A.K., Friedman, G.K., 2022. Standard clinical approaches and emerging modalities for glioblastoma imaging. *Neuro-Oncol. Adv.* 4, vdac080. <https://doi.org/10.1093/noajnl/vdac080>
- Berte, N., Piée-Staffa, A., Piecha, N., Wang, M., Borgmann, K., Kaina, B., Nikolova, T., 2016. Targeting Homologous Recombination by Pharmacological Inhibitors Enhances the Killing Response of Glioblastoma Cells Treated with Alkylating Drugs. *Mol. Cancer Ther.* 15, 2665–2678. <https://doi.org/10.1158/1535-7163.MCT-16-0176>
- Bhide, P.G., Day, M., Sapp, E., Schwarz, C., Sheth, A., Kim, J., Young, A.B., Penney, J., Golden, J., Aronin, N., DiFiglia, M., 1996. Expression of normal and mutant huntingtin in the developing brain. *J. Neurosci. Off. J. Soc. Neurosci.* 16, 5523–5535. <https://doi.org/10.1523/JNEUROSCI.16-17-05523.1996>
- Bogdahn, U., Hau, P., Stockhammer, G., Venkataramana, N.K., Mahapatra, A.K., Suri, A., Balasubramaniam, A., Nair, S., Oliushine, V., Parfenov, V., Poverennova, I., Zaaroor, M., Jachimczak, P., Ludwig, S., Schmaus, S., Heinrichs, H., Schlingensiepen, K.-H., Trabedersen Glioma Study Group, 2011. Targeted therapy for high-grade glioma with the TGF- β 2 inhibitor trabedersen: results of a randomized and controlled phase IIb study. *Neuro-Oncol.* 13, 132–142. <https://doi.org/10.1093/neuonc/noq142>
- Bonnet, D., Dick, J.E., 1997. Human acute myeloid leukemia is organized as a hierarchy that originates from a primitive hematopoietic cell. *Nat. Med.* 3, 730–737. <https://doi.org/10.1038/nm0797-730>
- Brada, M., Judson, I., Beale, P., Moore, S., Reidenberg, P., Statkevich, P., Dugan, M., Batra, V., Cutler, D., 1999. Phase I dose-escalation and pharmacokinetic study of temozolomide (SCH 52365) for refractory or relapsing malignancies. *Br. J. Cancer* 81, 1022–1030. <https://doi.org/10.1038/sj.bjc.6690802>
- Bradley, S.V., Holland, E.C., Liu, G.Y., Thomas, D., Hyun, T.S., Ross, T.S., 2007. Huntingtin interacting protein 1 is a novel brain tumor marker that associates with epidermal growth factor receptor. *Cancer Res.* 67, 3609–3615. <https://doi.org/10.1158/0008-5472.CAN-06-4803>
- Bradley, S.V., Oravec-Wilson, K.I., Bougeard, G., Mizukami, I., Li, L., Munaco, A.J., Sreekumar, A., Corradetti, M.N., Chinnaiyan, A.M., Sanda, M.G., Ross, T.S., 2005. Serum antibodies to huntingtin interacting protein-1: a new blood test for prostate cancer. *Cancer Res.* 65, 4126–4133. <https://doi.org/10.1158/0008-5472.CAN-04-4658>

- Braganza, M.Z., Kitahara, C.M., Berrington de González, A., Inskip, P.D., Johnson, K.J., Rajaraman, P., 2012. Ionizing radiation and the risk of brain and central nervous system tumors: a systematic review. *Neuro-Oncol.* 14, 1316–1324. <https://doi.org/10.1093/neuonc/nos208>
- Braun, S.M.G., Jessberger, S., 2014. Adult neurogenesis: mechanisms and functional significance. *Dev. Camb. Engl.* 141, 1983–1986. <https://doi.org/10.1242/dev.104596>
- Braz, B.Y., Wennagel, D., Ratié, L., de Souza, D.A.R., Deloulme, J.C., Barbier, E.L., Buisson, A., Lanté, F., Humbert, S., 2022. Treating early postnatal circuit defect delays Huntington’s disease onset and pathology in mice. *Science* 377, eabq5011. <https://doi.org/10.1126/science.abq5011>
- Brennan, C.W., Verhaak, R.G.W., McKenna, A., Campos, B., Nounshmehr, H., Salama, S.R., Zheng, S., Chakravarty, D., Sanborn, J.Z., Berman, S.H., Beroukhim, R., Bernard, B., Wu, C.-J., Genovese, G., Shmulevich, I., Barnholtz-Sloan, J., Zou, L., Vegesna, R., Shukla, S.A., Ciriello, G., Yung, W.K., Zhang, W., Sougnez, C., Mikkelsen, T., Aldape, K., Bigner, D.D., Van Meir, E.G., Prados, M., Sloan, A., Black, K.L., Eschbacher, J., Finocchiaro, G., Friedman, W., Andrews, D.W., Guha, A., Iacocca, M., O’Neill, B.P., Foltz, G., Myers, J., Weisenberger, D.J., Penny, R., Kucherlapati, R., Perou, C.M., Hayes, D.N., Gibbs, R., Marra, M., Mills, G.B., Lander, E., Spellman, P., Wilson, R., Sander, C., Weinstein, J., Meyerson, M., Gabriel, S., Laird, P.W., Haussler, D., Getz, G., Chin, L., TCGA Research Network, 2013. The somatic genomic landscape of glioblastoma. *Cell* 155, 462–477. <https://doi.org/10.1016/j.cell.2013.09.034>
- Burri, S.H., Gondi, V., Brown, P.D., Mehta, M.P., 2018. The Evolving Role of Tumor Treating Fields in Managing Glioblastoma: Guide for Oncologists. *Am. J. Clin. Oncol.* 41, 191–196. <https://doi.org/10.1097/COC.0000000000000395>
- Butler, M., Pongor, L., Su, Y.-T., Xi, L., Raffeld, M., Quezado, M., Trepel, J., Aldape, K., Pommier, Y., Wu, J., 2020. MGMT Status as a Clinical Biomarker in Glioblastoma. *Trends Cancer* 6, 380–391. <https://doi.org/10.1016/j.trecan.2020.02.010>
- Cahill, D.P., Levine, K.K., Betensky, R.A., Codd, P.J., Romany, C.A., Reavie, L.B., Batchelor, T.T., Futreal, P.A., Stratton, M.R., Curry, W.T., Iafate, A.J., Louis, D.N., 2007. Loss of the mismatch repair protein MSH6 in human glioblastomas is associated with tumor progression during temozolomide treatment. *Clin. Cancer Res. Off. J. Am. Assoc. Cancer Res.* 13, 2038–2045. <https://doi.org/10.1158/1078-0432.CCR-06-2149>
- Calabrese, C., Poppleton, H., Kocak, M., Hogg, T.L., Fuller, C., Hamner, B., Oh, E.Y., Gaber, M.W., Finklestein, D., Allen, M., Frank, A., Bayazitov, I.T., Zakharenko, S.S., Gajjar, A., Davidoff, A., Gilbertson, R.J., 2007. A perivascular niche for brain tumor stem cells. *Cancer Cell* 11, 69–82. <https://doi.org/10.1016/j.ccr.2006.11.020>
- Cancer Genome Atlas Research Network, 2008. Comprehensive genomic characterization defines human glioblastoma genes and core pathways. *Nature* 455, 1061–1068. <https://doi.org/10.1038/nature07385>
- Cantidio, F.S., Gil, G.O.B., Queiroz, I.N., Regalin, M., 2022. Glioblastoma - treatment and obstacles. *Rep. Pract. Oncol. Radiother. J. Gt. Cancer Cent. Poznan Pol. Soc. Radiat. Oncol.* 27, 744–753. <https://doi.org/10.5603/RPOR.a2022.0076>
- Capela, A., Temple, S., 2002. LeX/ssea-1 is expressed by adult mouse CNS stem cells, identifying them as nonependymal. *Neuron* 35, 865–875. [https://doi.org/10.1016/s0896-6273\(02\)00835-8](https://doi.org/10.1016/s0896-6273(02)00835-8)
- Capizzi, M., Carpentier, R., Denarier, E., Adrait, A., Kassem, R., Mapelli, M., Couté, Y., Humbert, S., 2022. Developmental defects in Huntington’s disease show that axonal growth and microtubule reorganization require NUMA1. *Neuron* 110, 36-50.e5. <https://doi.org/10.1016/j.neuron.2021.10.033>

- Carén, H., Stricker, S.H., Bulstrode, H., Gargica, S., Johnstone, E., Bartlett, T.E., Feber, A., Wilson, G., Teschendorff, A.E., Bertone, P., Beck, S., Pollard, S.M., 2015. Glioblastoma Stem Cells Respond to Differentiation Cues but Fail to Undergo Commitment and Terminal Cell-Cycle Arrest. *Stem Cell Rep.* 5, 829–842. <https://doi.org/10.1016/j.stemcr.2015.09.014>
- Caron, N.S., Desmond, C.R., Xia, J., Truant, R., 2013. Polyglutamine domain flexibility mediates the proximity between flanking sequences in huntingtin. *Proc. Natl. Acad. Sci. U. S. A.* 110, 14610–14615. <https://doi.org/10.1073/pnas.1301342110>
- Carvalho, S., Vítor, A.C., Sridhara, S.C., Martins, F.B., Raposo, A.C., Desterro, J.M.P., Ferreira, J., de Almeida, S.F., 2014. SETD2 is required for DNA double-strand break repair and activation of the p53-mediated checkpoint. *eLife* 3, e02482. <https://doi.org/10.7554/eLife.02482>
- Caviston, J.P., Ross, J.L., Antony, S.M., Tokito, M., Holzbaur, E.L.F., 2007. Huntingtin facilitates dynein/dynactin-mediated vesicle transport. *Proc. Natl. Acad. Sci. U. S. A.* 104, 10045–10050. <https://doi.org/10.1073/pnas.0610628104>
- Chen, K., Liu, J., Liu, S., Xia, M., Zhang, X., Han, D., Jiang, Y., Wang, C., Cao, X., 2017. Methyltransferase SETD2-Mediated Methylation of STAT1 Is Critical for Interferon Antiviral Activity. *Cell* 170, 492–506.e14. <https://doi.org/10.1016/j.cell.2017.06.042>
- Chen, L.-Y., Redon, S., Lingner, J., 2012. The human CST complex is a terminator of telomerase activity. *Nature* 488, 540–544. <https://doi.org/10.1038/nature11269>
- Chinot, O.L., Wick, W., Mason, W., Henriksson, R., Saran, F., Nishikawa, R., Carpentier, A.F., Hoang-Xuan, K., Kavan, P., Cernea, D., Brandes, A.A., Hilton, M., Abrey, L., Cloughesy, T., 2014. Bevacizumab plus radiotherapy-temozolomide for newly diagnosed glioblastoma. *N. Engl. J. Med.* 370, 709–722. <https://doi.org/10.1056/NEJMoa1308345>
- Choi, S., Yu, Y., Grimmer, M.R., Wahl, M., Chang, S.M., Costello, J.F., 2018. Temozolomide-associated hypermutation in gliomas. *Neuro-Oncol.* 20, 1300–1309. <https://doi.org/10.1093/neuonc/nyo016>
- Codega, P., Silva-Vargas, V., Paul, A., Maldonado-Soto, A.R., Deleo, A.M., Pastrana, E., Doetsch, F., 2014. Prospective identification and purification of quiescent adult neural stem cells from their in vivo niche. *Neuron* 82, 545–559. <https://doi.org/10.1016/j.neuron.2014.02.039>
- Colin, E., Zala, D., Liot, G., Rangone, H., Borrell-Pagès, M., Li, X.-J., Saudou, F., Humbert, S., 2008. Huntingtin phosphorylation acts as a molecular switch for anterograde/retrograde transport in neurons. *EMBO J.* 27, 2124–2134. <https://doi.org/10.1038/emboj.2008.133>
- Colopi, A., Fuda, S., Santi, S., Onorato, A., Cesarini, V., Salvati, M., Balistreri, C.R., Dolci, S., Guida, E., 2023. Impact of age and gender on glioblastoma onset, progression, and management. *Mech. Ageing Dev.* 211, 111801. <https://doi.org/10.1016/j.mad.2023.111801>
- Conforti, P., Camnasio, S., Mutti, C., Valenza, M., Thompson, M., Fossale, E., Zeitlin, S., MacDonald, M.E., Zuccato, C., Cattaneo, E., 2013. Lack of huntingtin promotes neural stem cells differentiation into glial cells while neurons expressing huntingtin with expanded polyglutamine tracts undergo cell death. *Neurobiol. Dis.* 50, 160–170. <https://doi.org/10.1016/j.nbd.2012.10.015>
- Cong, X., Held, J.M., DeGiacomo, F., Bonner, A., Chen, J.M., Schilling, B., Czerwieńiec, G.A., Gibson, B.W., Ellerby, L.M., 2011. Mass spectrometric identification of novel lysine acetylation sites in huntingtin. *Mol. Cell. Proteomics MCP* 10, M111.009829. <https://doi.org/10.1074/mcp.M111.009829>

- Conti, L., Crisafulli, L., Caldera, V., Tortoreto, M., Brilli, E., Conforti, P., Zunino, F., Magrassi, L., Schiffer, D., Cattaneo, E., 2012. REST controls self-renewal and tumorigenic competence of human glioblastoma cells. *PLoS One* 7, e38486. <https://doi.org/10.1371/journal.pone.0038486>
- Crooke, S.T., Baker, B.F., Crooke, R.M., Liang, X.-H., 2021a. Antisense technology: an overview and prospectus. *Nat. Rev. Drug Discov.* 20, 427–453. <https://doi.org/10.1038/s41573-021-00162-z>
- Crooke, S.T., Liang, X.-H., Baker, B.F., Crooke, R.M., 2021b. Antisense technology: A review. *J. Biol. Chem.* 296, 100416. <https://doi.org/10.1016/j.jbc.2021.100416>
- Culver, B.P., Savas, J.N., Park, S.K., Choi, J.H., Zheng, S., Zeitlin, S.O., Yates, J.R., Tanese, N., 2012. Proteomic analysis of wild-type and mutant huntingtin-associated proteins in mouse brains identifies unique interactions and involvement in protein synthesis. *J. Biol. Chem.* 287, 21599–21614. <https://doi.org/10.1074/jbc.M112.359307>
- Darras, B.T., Chiriboga, C.A., Iannaccone, S.T., Swoboda, K.J., Montes, J., Mignon, L., Xia, S., Bennett, C.F., Bishop, K.M., Shefner, J.M., Green, A.M., Sun, P., Bhan, I., Gheuens, S., Schneider, E., Farwell, W., De Vivo, D.C., ISIS-396443-CS2/ISIS-396443-CS12 Study Groups, 2019. Nusinersen in later-onset spinal muscular atrophy: Long-term results from the phase 1/2 studies. *Neurology* 92, e2492–e2506. <https://doi.org/10.1212/WNL.00000000000007527>
- Defossez, G., Uhry, Z., Delafosse, P., Dantony, E., d’Almeida, T., Plouvier, S., Bossard, N., Bouvier, A.M., Molinié, F., Woronoff, A.S., Colonna, M., Grosclaude, P., Remontet, L., Monnereau, A., French Network of Cancer Registries (FRANCIM), 2021. Cancer incidence and mortality trends in France over 1990-2018 for solid tumors: the sex gap is narrowing. *BMC Cancer* 21, 726. <https://doi.org/10.1186/s12885-021-08261-1>
- Del Vecchio, C.A., Giacomini, C.P., Vogel, H., Jensen, K.C., Florio, T., Merlo, A., Pollack, J.R., Wong, A.J., 2013. EGFRvIII gene rearrangement is an early event in glioblastoma tumorigenesis and expression defines a hierarchy modulated by epigenetic mechanisms. *Oncogene* 32, 2670–2681. <https://doi.org/10.1038/onc.2012.280>
- DiFiglia, M., 2002. Huntingtin fragments that aggregate go their separate ways. *Mol. Cell* 10, 224–225. [https://doi.org/10.1016/s1097-2765\(02\)00609-3](https://doi.org/10.1016/s1097-2765(02)00609-3)
- Doetsch, F., Caillé, I., Lim, D.A., García-Verdugo, J.M., Alvarez-Buylla, A., 1999. Subventricular zone astrocytes are neural stem cells in the adult mammalian brain. *Cell* 97, 703–716. [https://doi.org/10.1016/s0092-8674\(00\)80783-7](https://doi.org/10.1016/s0092-8674(00)80783-7)
- Doetsch, F., García-Verdugo, J.M., Alvarez-Buylla, A., 1997. Cellular composition and three-dimensional organization of the subventricular germinal zone in the adult mammalian brain. *J. Neurosci. Off. J. Soc. Neurosci.* 17, 5046–5061. <https://doi.org/10.1523/JNEUROSCI.17-13-05046.1997>
- Doetsch, F., Petreanu, L., Caille, I., Garcia-Verdugo, J.M., Alvarez-Buylla, A., 2002. EGF converts transit-amplifying neurogenic precursors in the adult brain into multipotent stem cells. *Neuron* 36, 1021–1034. [https://doi.org/10.1016/s0896-6273\(02\)01133-9](https://doi.org/10.1016/s0896-6273(02)01133-9)
- Dowdy, S.F., 2023. Endosomal escape of RNA therapeutics: How do we solve this rate-limiting problem? *RNA N. Y. N* 29, 396–401. <https://doi.org/10.1261/rna.079507.122>
- Dragatsis, I., Efstratiadis, A., Zeitlin, S., 1998. Mouse mutant embryos lacking huntingtin are rescued from lethality by wild-type extraembryonic tissues. *Dev. Camb. Engl.* 125, 1529–1539. <https://doi.org/10.1242/dev.125.8.1529>
- Drouet, V., Perrin, V., Hassig, R., Dufour, N., Auregan, G., Alves, S., Bonvento, G., Brouillet, E., Luthi-Carter, R., Hantraye, P., Déglon, N., 2009. Sustained effects of nonallele-specific Huntingtin silencing. *Ann. Neurol.* 65, 276–285. <https://doi.org/10.1002/ana.21569>

- Drouet, V., Ruiz, M., Zala, D., Feyeux, M., Auregan, G., Cambon, K., Troquier, L., Carpentier, J., Aubert, S., Merienne, N., Bourgois-Rocha, F., Hassig, R., Rey, M., Dufour, N., Saudou, F., Perrier, A.L., Hantraye, P., Déglon, N., 2014. Allele-specific silencing of mutant huntingtin in rodent brain and human stem cells. *PloS One* 9, e99341. <https://doi.org/10.1371/journal.pone.0099341>
- Duyao, M., Ambrose, C., Myers, R., Novelletto, A., Persichetti, F., Frontali, M., Folstein, S., Ross, C., Franz, M., Abbott, M., 1993. Trinucleotide repeat length instability and age of onset in Huntington's disease. *Nat. Genet.* 4, 387–392. <https://doi.org/10.1038/ng0893-387>
- Eckel-Passow, J.E., Lachance, D.H., Molinaro, A.M., Walsh, K.M., Decker, P.A., Sicotte, H., Pekmezci, M., Rice, T., Kosel, M.L., Smirnov, I.V., Sarkar, G., Caron, A.A., Kollmeyer, T.M., Praska, C.E., Chada, A.R., Halder, C., Hansen, H.M., McCoy, L.S., Bracci, P.M., Marshall, R., Zheng, S., Reis, G.F., Pico, A.R., O'Neill, B.P., Buckner, J.C., Giannini, C., Huse, J.T., Perry, A., Tihan, T., Berger, M.S., Chang, S.M., Prados, M.D., Wiemels, J., Wiencke, J.K., Wrensch, M.R., Jenkins, R.B., 2015. Glioma Groups Based on 1p/19q, IDH, and TERT Promoter Mutations in Tumors. *N. Engl. J. Med.* 372, 2499–2508. <https://doi.org/10.1056/NEJMoa1407279>
- Eddy, C.M., Rickards, H.E., 2015. Theory of mind can be impaired prior to motor onset in Huntington's disease. *Neuropsychology* 29, 792–798. <https://doi.org/10.1037/neu0000190>
- Ehrnhoefer, D.E., Sutton, L., Hayden, M.R., 2011. Small changes, big impact: posttranslational modifications and function of huntingtin in Huntington disease. *Neurosci. Rev. J. Bringing Neurobiol. Neurol. Psychiatry* 17, 475–492. <https://doi.org/10.1177/1073858410390378>
- El-Daher, M.-T., Hangen, E., Bruyère, J., Poizat, G., Al-Ramahi, I., Pardo, R., Bourg, N., Souquere, S., Mayet, C., Pierron, G., Lévêque-Fort, S., Botas, J., Humbert, S., Saudou, F., 2015. Huntingtin proteolysis releases non-polyQ fragments that cause toxicity through dynamin 1 dysregulation. *EMBO J.* 34, 2255–2271. <https://doi.org/10.15252/emj.201490808>
- Elias, S., McGuire, J.R., Yu, H., Humbert, S., 2015. Huntingtin Is Required for Epithelial Polarity through RAB11A-Mediated Apical Trafficking of PAR3-aPKC. *PLoS Biol.* 13, e1002142. <https://doi.org/10.1371/journal.pbio.1002142>
- Epping, E.A., Kim, J.-I., Craufurd, D., Brashers-Krug, T.M., Anderson, K.E., McCusker, E., Luther, J., Long, J.D., Paulsen, J.S., PREDICT-HD Investigators and Coordinators of the Huntington Study Group, 2016. Longitudinal Psychiatric Symptoms in Prodromal Huntington's Disease: A Decade of Data. *Am. J. Psychiatry* 173, 184–192. <https://doi.org/10.1176/appi.ajp.2015.14121551>
- Epping, E.A., Paulsen, J.S., 2011. Depression in the early stages of Huntington disease. *Neurodegener. Dis. Manag.* 1, 407–414. <https://doi.org/10.2217/nmt.11.45>
- Ernst, A., Alkass, K., Bernard, S., Salehpour, M., Perl, S., Tisdale, J., Possnert, G., Druid, H., Frisén, J., 2014. Neurogenesis in the striatum of the adult human brain. *Cell* 156, 1072–1083. <https://doi.org/10.1016/j.cell.2014.01.044>
- F, D., V, C., A, C., M, d'Angelo, 2023. Cell Rearrangement and Oxidant/Antioxidant Imbalance in Huntington's Disease. *Antioxid. Basel Switz.* 12. <https://doi.org/10.3390/antiox12030571>
- Faber, P.W., Barnes, G.T., Srinidhi, J., Chen, J., Gusella, J.F., MacDonald, M.E., 1998. Huntingtin interacts with a family of WW domain proteins. *Hum. Mol. Genet.* 7, 1463–1474. <https://doi.org/10.1093/hmg/7.9.1463>
- Fan, Q.-W., Cheng, C.K., Gustafson, W.C., Charron, E., Zipper, P., Wong, R.A., Chen, J., Lau, J., Knobbe-Thomsen, C., Weller, M., Jura, N., Reifenberger, G., Shokat, K.M.,

- Weiss, W.A., 2013. EGFR phosphorylates tumor-derived EGFRvIII driving STAT3/5 and progression in glioblastoma. *Cancer Cell* 24, 438–449. <https://doi.org/10.1016/j.ccr.2013.09.004>
- Fedele, V., Roybon, L., Nordström, U., Li, J.Y., Brundin, P., 2011. Neurogenesis in the R6/2 mouse model of Huntington's disease is impaired at the level of NeuroD1. *Neuroscience* 173, 76–81. <https://doi.org/10.1016/j.neuroscience.2010.08.022>
- Fontebasso, A.M., Schwartzenuber, J., Khuong-Quang, D.-A., Liu, X.-Y., Sturm, D., Korshunov, A., Jones, D.T.W., Witt, H., Kool, M., Albrecht, S., Fleming, A., Hadjadj, D., Busche, S., Lepage, P., Montpetit, A., Staffa, A., Gerges, N., Zakrzewska, M., Zakrzewski, K., Liberski, P.P., Hauser, P., Garami, M., Klekner, A., Bogner, L., Zadeh, G., Faury, D., Pfister, S.M., Jabado, N., Majewski, J., 2013. Mutations in SETD2 and genes affecting histone H3K36 methylation target hemispheric high-grade gliomas. *Acta Neuropathol. (Berl.)* 125, 659–669. <https://doi.org/10.1007/s00401-013-1095-8>
- Galli, R., Binda, E., Orfanelli, U., Cipelletti, B., Gritti, A., De Vitis, S., Fiocco, R., Foroni, C., Dimeco, F., Vescovi, A., 2004. Isolation and characterization of tumorigenic, stem-like neural precursors from human glioblastoma. *Cancer Res.* 64, 7011–7021. <https://doi.org/10.1158/0008-5472.CAN-04-1364>
- Gao, R., Chakraborty, A., Geater, C., Pradhan, S., Gordon, K.L., Snowden, J., Yuan, S., Dickey, A.S., Choudhary, S., Ashizawa, T., Ellerby, L.M., La Spada, A.R., Thompson, L.M., Hazra, T.K., Sarkar, P.S., 2019. Mutant huntingtin impairs PNKP and ATXN3, disrupting DNA repair and transcription. *eLife* 8, e42988. <https://doi.org/10.7554/eLife.42988>
- Gao, Y.-G., Yan, X.-Z., Song, A.-X., Chang, Y.-G., Gao, X.-C., Jiang, N., Zhang, Q., Hu, H.-Y., 2006. Structural insights into the specific binding of huntingtin proline-rich region with the SH3 and WW domains. *Struct. Lond. Engl.* 1993 14, 1755–1765. <https://doi.org/10.1016/j.str.2006.09.014>
- Garcia, A.D.R., Doan, N.B., Imura, T., Bush, T.G., Sofroniew, M.V., 2004. GFAP-expressing progenitors are the principal source of constitutive neurogenesis in adult mouse forebrain. *Nat. Neurosci.* 7, 1233–1241. <https://doi.org/10.1038/nn1340>
- Gauthier, L.R., Charrin, B.C., Borrell-Pagès, M., Dompierre, J.P., Rangone, H., Cordelières, F.P., De Mey, J., MacDonald, M.E., Lessmann, V., Humbert, S., Saudou, F., 2004. Huntingtin controls neurotrophic support and survival of neurons by enhancing BDNF vesicular transport along microtubules. *Cell* 118, 127–138. <https://doi.org/10.1016/j.cell.2004.06.018>
- Gervais, F.G., Singaraja, R., Xanthoudakis, S., Gutekunst, C.-A., Leavitt, B.R., Metzler, M., Hackam, A.S., Tam, J., Vaillancourt, J.P., Houtzager, V., Rasper, D.M., Roy, S., Hayden, M.R., Nicholson, D.W., 2002. Recruitment and activation of caspase-8 by the Huntingtin-interacting protein Hip-1 and a novel partner Hippi. *Nat. Cell Biol.* 4, 95–105. <https://doi.org/10.1038/ncb735>
- Gil Del Alcazar, C.R., Todorova, P.K., Habib, A.A., Mukherjee, B., Burma, S., 2016. Augmented HR Repair Mediates Acquired Temozolomide Resistance in Glioblastoma. *Mol. Cancer Res. MCR* 14, 928–940. <https://doi.org/10.1158/1541-7786.MCR-16-0125>
- Giuliano, P., De Cristofaro, T., Affaitati, A., Pizzulo, G.M., Feliciello, A., Criscuolo, C., De Michele, G., Filla, A., Avvedimento, E.V., Varrone, S., 2003. DNA damage induced by polyglutamine-expanded proteins. *Hum. Mol. Genet.* 12, 2301–2309. <https://doi.org/10.1093/hmg/ddg242>
- Godin, J.D., Colombo, K., Molina-Calavita, M., Keryer, G., Zala, D., Charrin, B.C., Dietrich, P., Volvert, M.-L., Guillemot, F., Dragatsis, I., Bellaïche, Y., Saudou, F., Nguyen, L.,

- Humbert, S., 2010a. Huntingtin is required for mitotic spindle orientation and mammalian neurogenesis. *Neuron* 67, 392–406.
<https://doi.org/10.1016/j.neuron.2010.06.027>
- Godin, J.D., Colombo, K., Molina-Calavita, M., Keryer, G., Zala, D., Charrin, B.C., Dietrich, P., Volvert, M.-L., Guillemot, F., Dragatsis, I., Bellaïche, Y., Saudou, F., Nguyen, L., Humbert, S., 2010b. Huntingtin is required for mitotic spindle orientation and mammalian neurogenesis. *Neuron* 67, 392–406.
<https://doi.org/10.1016/j.neuron.2010.06.027>
- Goldberg, Y.P., Nicholson, D.W., Rasper, D.M., Kalchman, M.A., Koide, H.B., Graham, R.K., Bromm, M., Kazemi-Esfarjani, P., Thornberry, N.A., Vaillancourt, J.P., Hayden, M.R., 1996. Cleavage of huntingtin by apopain, a proapoptotic cysteine protease, is modulated by the polyglutamine tract. *Nat. Genet.* 13, 442–449.
<https://doi.org/10.1038/ng0896-442>
- Golebiewska, A., Bougnaud, S., Stieber, D., Brons, N.H.C., Vallar, L., Hertel, F., Klink, B., Schröck, E., Bjerkvig, R., Niclou, S.P., 2013. Side population in human glioblastoma is non-tumorigenic and characterizes brain endothelial cells. *Brain J. Neurol.* 136, 1462–1475. <https://doi.org/10.1093/brain/awt025>
- Graham, R.K., Deng, Y., Slow, E.J., Haigh, B., Bissada, N., Lu, G., Pearson, J., Shehadeh, J., Bertram, L., Murphy, Z., Warby, S.C., Doty, C.N., Roy, S., Wellington, C.L., Leavitt, B.R., Raymond, L.A., Nicholson, D.W., Hayden, M.R., 2006. Cleavage at the caspase-6 site is required for neuronal dysfunction and degeneration due to mutant huntingtin. *Cell* 125, 1179–1191. <https://doi.org/10.1016/j.cell.2006.04.026>
- Guan, X., Hasan, M.N., Maniar, S., Jia, W., Sun, D., 2018. Reactive Astrocytes in Glioblastoma Multiforme. *Mol. Neurobiol.* 55, 6927–6938.
<https://doi.org/10.1007/s12035-018-0880-8>
- Guo, G., Gong, K., Wohlfeld, B., Hatanpaa, K.J., Zhao, D., Habib, A.A., 2015. Ligand-Independent EGFR Signaling. *Cancer Res.* 75, 3436–3441.
<https://doi.org/10.1158/0008-5472.CAN-15-0989>
- Guo, Q., Bin Huang, null, Cheng, J., Seefelder, M., Engler, T., Pfeifer, G., Oeckl, P., Otto, M., Moser, F., Maurer, M., Pautsch, A., Baumeister, W., Fernández-Busnadiego, R., Kochanek, S., 2018. The cryo-electron microscopy structure of huntingtin. *Nature* 555, 117–120. <https://doi.org/10.1038/nature25502>
- Hackam, A.S., Yassa, A.S., Singaraja, R., Metzler, M., Gutekunst, C.A., Gan, L., Warby, S., Wellington, C.L., Vaillancourt, J., Chen, N., Gervais, F.G., Raymond, L., Nicholson, D.W., Hayden, M.R., 2000. Huntingtin interacting protein 1 induces apoptosis via a novel caspase-dependent death effector domain. *J. Biol. Chem.* 275, 41299–41308.
<https://doi.org/10.1074/jbc.M008408200>
- Han, F., Hu, R., Yang, H., Liu, J., Sui, J., Xiang, X., Wang, F., Chu, L., Song, S., 2016. PTEN gene mutations correlate to poor prognosis in glioma patients: a meta-analysis. *OncoTargets Ther.* 9, 3485–3492. <https://doi.org/10.2147/OTT.S99942>
- Hanna, C., Kurian, K.M., Williams, K., Watts, C., Jackson, A., Carruthers, R., Strathdee, K., Cruickshank, G., Dunn, L., Erridge, S., Godfrey, L., Jefferies, S., McBain, C., Sleigh, R., McCormick, A., Pittman, M., Halford, S., Chalmers, A.J., 2020. Pharmacokinetics, safety, and tolerability of olaparib and temozolomide for recurrent glioblastoma: results of the phase I OPARATIC trial. *Neuro-Oncol.* 22, 1840–1850.
<https://doi.org/10.1093/neuonc/noaa104>
- Haremaki, T., Deglincerti, A., Brivanlou, A.H., 2015. Huntingtin is required for ciliogenesis and neurogenesis during early *Xenopus* development. *Dev. Biol.* 408, 305–315.
<https://doi.org/10.1016/j.ydbio.2015.07.013>

- Harjes, P., Wanker, E.E., 2003. The hunt for huntingtin function: interaction partners tell many different stories. *Trends Biochem. Sci.* 28, 425–433. [https://doi.org/10.1016/S0968-0004\(03\)00168-3](https://doi.org/10.1016/S0968-0004(03)00168-3)
- Hattula, K., Peränen, J., 2000. FIP-2, a coiled-coil protein, links Huntingtin to Rab8 and modulates cellular morphogenesis. *Curr. Biol. CB* 10, 1603–1606. [https://doi.org/10.1016/s0960-9822\(00\)00864-2](https://doi.org/10.1016/s0960-9822(00)00864-2)
- Henshall, T.L., Tucker, B., Lumsden, A.L., Nornes, S., Lardelli, M.T., Richards, R.I., 2009. Selective neuronal requirement for huntingtin in the developing zebrafish. *Hum. Mol. Genet.* 18, 4830–4842. <https://doi.org/10.1093/hmg/ddp455>
- Hirose, Y., Berger, M.S., Pieper, R.O., 2001. Abrogation of the Chk1-mediated G(2) checkpoint pathway potentiates temozolomide-induced toxicity in a p53-independent manner in human glioblastoma cells. *Cancer Res.* 61, 5843–5849.
- Hsu, E.J., Thomas, J., Maher, E.A., Youssef, M., Timmerman, R.D., Wardak, Z., Dan, T.D., Patel, T.R., Vo, D.T., 2022. Impact of CDKN2A/B, MTAP, and TERT Genetic Alterations on Survival in IDH Wild Type Glioblastomas. *Discov. Oncol.* 13, 126. <https://doi.org/10.1007/s12672-022-00590-2>
- Huang, B., Wei, W., Wang, G., Gaertig, M.A., Feng, Y., Wang, W., Li, X.-J., Li, S., 2015. Mutant huntingtin downregulates myelin regulatory factor-mediated myelin gene expression and affects mature oligodendrocytes. *Neuron* 85, 1212–1226. <https://doi.org/10.1016/j.neuron.2015.02.026>
- Huang, L.E., 2022. Impact of CDKN2A/B Homozygous Deletion on the Prognosis and Biology of IDH-Mutant Glioma. *Biomedicines* 10, 246. <https://doi.org/10.3390/biomedicines10020246>
- Hughes, A.C., Mort, M., Elliston, L., Thomas, R.M., Brooks, S.P., Dunnett, S.B., Jones, L., 2014. Identification of novel alternative splicing events in the huntingtin gene and assessment of the functional consequences using structural protein homology modelling. *J. Mol. Biol.* 426, 1428–1438. <https://doi.org/10.1016/j.jmb.2013.12.028>
- Humbert, S., Bryson, E.A., Cordelières, F.P., Connors, N.C., Datta, S.R., Finkbeiner, S., Greenberg, M.E., Saudou, F., 2002. The IGF-1/Akt pathway is neuroprotective in Huntington's disease and involves Huntingtin phosphorylation by Akt. *Dev. Cell* 2, 831–837. [https://doi.org/10.1016/s1534-5807\(02\)00188-0](https://doi.org/10.1016/s1534-5807(02)00188-0)
- Hunter, C., Smith, R., Cahill, D.P., Stephens, P., Stevens, C., Teague, J., Greenman, C., Edkins, S., Bignell, G., Davies, H., O'Meara, S., Parker, A., Avis, T., Barthorpe, S., Brackenbury, L., Buck, G., Butler, A., Clements, J., Cole, J., Dicks, E., Forbes, S., Gorton, M., Gray, K., Halliday, K., Harrison, R., Hills, K., Hinton, J., Jenkinson, A., Jones, D., Kosmidou, V., Laman, R., Lugg, R., Menzies, A., Perry, J., Petty, R., Raine, K., Richardson, D., Shepherd, R., Small, A., Solomon, H., Tofts, C., Varian, J., West, S., Widaa, S., Yates, A., Easton, D.F., Riggins, G., Roy, J.E., Levine, K.K., Mueller, W., Batchelor, T.T., Louis, D.N., Stratton, M.R., Futreal, P.A., Wooster, R., 2006. A hypermutation phenotype and somatic MSH6 mutations in recurrent human malignant gliomas after alkylator chemotherapy. *Cancer Res.* 66, 3987–3991. <https://doi.org/10.1158/0008-5472.CAN-06-0127>
- Iwamoto, N., Butler, D.C.D., Svrzikapa, N., Mohapatra, S., Zlatev, I., Sah, D.W.Y., Meena, null, Standley, S.M., Lu, G., Apponi, L.H., Frank-Kamenetsky, M., Zhang, J.J., Vargeese, C., Verdine, G.L., 2017. Control of phosphorothioate stereochemistry substantially increases the efficacy of antisense oligonucleotides. *Nat. Biotechnol.* 35, 845–851. <https://doi.org/10.1038/nbt.3948>
- Jain, K.K., 2018. A Critical Overview of Targeted Therapies for Glioblastoma. *Front. Oncol.* 8, 419. <https://doi.org/10.3389/fonc.2018.00419>

- Jeong, H., Then, F., Melia, T.J., Mazzulli, J.R., Cui, L., Savas, J.N., Voisine, C., Paganetti, P., Tanese, N., Hart, A.C., Yamamoto, A., Krainc, D., 2009. Acetylation targets mutant huntingtin to autophagosomes for degradation. *Cell* 137, 60–72. <https://doi.org/10.1016/j.cell.2009.03.018>
- Johansson, E., Grassi, E.S., Pantazopoulou, V., Tong, B., Lindgren, D., Berg, T.J., Pietras, E.J., Axelson, H., Pietras, A., 2017. CD44 Interacts with HIF-2 α to Modulate the Hypoxic Phenotype of Perinecrotic and Perivascular Glioma Cells. *Cell Rep.* 20, 1641–1653. <https://doi.org/10.1016/j.celrep.2017.07.049>
- Johnson, E.B., Ziegler, G., Penny, W., Rees, G., Tabrizi, S.J., Scahill, R.I., Gregory, S., 2021. Dynamics of Cortical Degeneration Over a Decade in Huntington’s Disease. *Biol. Psychiatry* 89, 807–816. <https://doi.org/10.1016/j.biopsych.2020.11.009>
- Juliano, R., n.d. Juliano, R. L., Ming, X., & Nakagawa, O. (2012). Cellular uptake and intracellular trafficking of antisense and siRNA oligonucleotides. *Bioconjugate Chemistry*, 23(2), 147-157.
- Jung, T., Shin, B., Tamo, G., Kim, H., Vijayvargia, R., Leitner, A., Marcaida, M.J., Astorga-Wells, J., Jung, R., Aebersold, R., Peraro, M.D., Hebert, H., Seong, I.S., Song, J.-J., 2020. The Polyglutamine Expansion at the N-Terminal of Huntingtin Protein Modulates the Dynamic Configuration and Phosphorylation of the C-Terminal HEAT Domain. *Struct. Lond. Engl.* 1993 28, 1035-1050.e8. <https://doi.org/10.1016/j.str.2020.06.008>
- Juratli, T.A., Schackert, G., Krex, D., 2013. Current status of local therapy in malignant gliomas--a clinical review of three selected approaches. *Pharmacol. Ther.* 139, 341–358. <https://doi.org/10.1016/j.pharmthera.2013.05.003>
- Kader, B.A., Distefano, R., West, K.L., West, A.G., 2021. EZH2 inhibition in glioblastoma stem cells increases the expression of neuronal genes and the neuronal developmental regulators ZIC2, ZNF423 and MAFB. <https://doi.org/10.1101/2021.11.22.469535>
- Kamal, M.M., Sathyan, P., Singh, S.K., Zinn, P.O., Marisetty, A.L., Liang, S., Gumin, J., El-Mesallamy, H.O., Suki, D., Colman, H., Fuller, G.N., Lang, F.F., Majumder, S., 2012. REST Regulates Oncogenic Properties of Glioblastoma Stem Cells. *STEM CELLS* 30, 405–414. <https://doi.org/10.1002/stem.1020>
- Kanda, M., Kasahara, Y., Shimizu, D., Miwa, T., Umeda, S., Sawaki, K., Nakamura, S., Koda, Y., Obika, S., 2020. Amido-Bridged Nucleic Acid-Modified Antisense Oligonucleotides Targeting SYT13 to Treat Peritoneal Metastasis of Gastric Cancer. *Mol. Ther. Nucleic Acids* 22, 791–802. <https://doi.org/10.1016/j.omtn.2020.10.001>
- Kandasamy, P., Liu, Y., Aduda, V., Akare, S., Alam, R., Andreucci, A., Boulay, D., Bowman, K., Byrne, M., Cannon, M., Chivatakarn, O., Shelke, J.D., Iwamoto, N., Kawamoto, T., Kumarasamy, J., Lamore, S., Lemaitre, M., Lin, X., Longo, K., Looby, R., Marappan, S., Metterville, J., Mohapatra, S., Newman, B., Paik, I.-H., Patil, S., Purcell-Estabrook, E., Shimizu, M., Shum, P., Standley, S., Taborn, K., Tripathi, S., Yang, H., Yin, Y., Zhao, X., Dale, E., Vargeese, C., 2022. Impact of guanidine-containing backbone linkages on stereopure antisense oligonucleotides in the CNS. *Nucleic Acids Res.* 50, 5401–5423. <https://doi.org/10.1093/nar/gkac037>
- Kegel, K.B., Kim, M., Sapp, E., McIntyre, C., Castaño, J.G., Aronin, N., DiFiglia, M., 2000. Huntingtin expression stimulates endosomal-lysosomal activity, endosome tubulation, and autophagy. *J. Neurosci. Off. J. Soc. Neurosci.* 20, 7268–7278. <https://doi.org/10.1523/JNEUROSCI.20-19-07268.2000>
- Keryer, G., Pineda, J.R., Liot, G., Kim, J., Dietrich, P., Benstaali, C., Smith, K., Cordelières, F.P., Spassky, N., Ferrante, R.J., Dragatsis, I., Saudou, F., 2011. Ciliogenesis is regulated by a huntingtin-HAP1-PCM1 pathway and is altered in Huntington disease. *J. Clin. Invest.* 121, 4372–4382. <https://doi.org/10.1172/JCI57552>

- Kim, M.W., Chelliah, Y., Kim, S.W., Otwinowski, Z., Bezprozvanny, I., 2009. Secondary structure of Huntingtin amino-terminal region. *Struct. Lond. Engl.* 17, 1205–1212. <https://doi.org/10.1016/j.str.2009.08.002>
- Kim, W., Lee, S., Seo, D., Kim, D., Kim, K., Kim, E., Kang, J., Seong, K.M., Youn, H., Youn, B., 2019. Cellular Stress Responses in Radiotherapy. *Cells* 8, 1105. <https://doi.org/10.3390/cells8091105>
- Kim, Y., Jo, M., Schmidt, J., Luo, X., Prakash, T.P., Zhou, T., Klein, S., Xiao, X., Post, N., Yin, Z., MacLeod, A.R., 2019. Enhanced Potency of GalNAc-Conjugated Antisense Oligonucleotides in Hepatocellular Cancer Models. *Mol. Ther. J. Am. Soc. Gene Ther.* 27, 1547–1557. <https://doi.org/10.1016/j.ymthe.2019.06.009>
- Kingwell, K., 2021. Double setback for ASO trials in Huntington disease. *Nat. Rev. Drug Discov.* 20, 412–413. <https://doi.org/10.1038/d41573-021-00088-6>
- Knizhnik, A.V., Roos, W.P., Nikolova, T., Quiros, S., Tomaszowski, K.-H., Christmann, M., Kaina, B., 2013. Survival and death strategies in glioma cells: autophagy, senescence and apoptosis triggered by a single type of temozolomide-induced DNA damage. *PLoS One* 8, e55665. <https://doi.org/10.1371/journal.pone.0055665>
- Kohl, Z., Regensburger, M., Aigner, R., Kandasamy, M., Winner, B., Aigner, L., Winkler, J., 2010. Impaired adult olfactory bulb neurogenesis in the R6/2 mouse model of Huntington's disease. *BMC Neurosci.* 11, 114. <https://doi.org/10.1186/1471-2202-11-114>
- Kondo, T., Setoguchi, T., Taga, T., 2004. Persistence of a small subpopulation of cancer stem-like cells in the C6 glioma cell line. *Proc. Natl. Acad. Sci. U. S. A.* 101, 781–786. <https://doi.org/10.1073/pnas.0307618100>
- Kordasiewicz, H.B., Stanek, L.M., Wancewicz, E.V., Mazur, C., McAlonis, M.M., Pytel, K.A., Artates, J.W., Weiss, A., Cheng, S.H., Shihabuddin, L.S., Hung, G., Bennett, C.F., Cleveland, D.W., 2012. Sustained therapeutic reversal of Huntington's disease by transient repression of huntingtin synthesis. *Neuron* 74, 1031–1044. <https://doi.org/10.1016/j.neuron.2012.05.009>
- Kremer, B., Goldberg, P., Andrew, S.E., Theilmann, J., Telenius, H., Zeisler, J., Squitieri, F., Lin, B., Bassett, A., Almqvist, E., 1994. A worldwide study of the Huntington's disease mutation. The sensitivity and specificity of measuring CAG repeats. *N. Engl. J. Med.* 330, 1401–1406. <https://doi.org/10.1056/NEJM199405193302001>
- Lara-Velazquez, M., Al-Kharboosh, R., Jeanneret, S., Vazquez-Ramos, C., Mahato, D., Tavanaiepour, D., Rahmathulla, G., Quinones-Hinojosa, A., 2017. Advances in Brain Tumor Surgery for Glioblastoma in Adults. *Brain Sci.* 7, 166. <https://doi.org/10.3390/brainsci7120166>
- Leavitt, B.R., Kordasiewicz, H.B., Schobel, S.A., 2020. Huntingtin-Lowering Therapies for Huntington Disease: A Review of the Evidence of Potential Benefits and Risks. *JAMA Neurol.* 77, 764–772. <https://doi.org/10.1001/jamaneurol.2020.0299>
- Lee, Joo Ho, Lee, J.E., Kahng, J.Y., Kim, S.H., Park, J.S., Yoon, S.J., Um, J.-Y., Kim, W.K., Lee, J.-K., Park, J., Kim, E.H., Lee, Ji-Hyun, Lee, Joon-Hyuk, Chung, W.-S., Ju, Y.S., Park, S.-H., Chang, J.H., Kang, S.-G., Lee, Jeong Ho, 2018. Human glioblastoma arises from subventricular zone cells with low-level driver mutations. *Nature* 560, 243–247. <https://doi.org/10.1038/s41586-018-0389-3>
- Li, F., Deng, Z., Zhang, L., Wu, C., Jin, Y., Hwang, I., Vladimirova, O., Xu, L., Yang, L., Lu, B., Dheekollu, J., Li, J.-Y., Feng, H., Hu, J., Vakoc, C.R., Ying, H., Paik, J., Lieberman, P.M., Zheng, H., 2019. ATRX loss induces telomere dysfunction and necessitates induction of alternative lengthening of telomeres during human cell immortalization. *EMBO J.* 38, e96659. <https://doi.org/10.15252/embj.201796659>

- Li, X., Sapp, E., Valencia, A., Kegel, K.B., Qin, Z.-H., Alexander, J., Masso, N., Reeves, P., Ritch, J.J., Zeitlin, S., Aronin, N., Difiglia, M., 2008. A function of huntingtin in guanine nucleotide exchange on Rab11. *Neuroreport* 19, 1643–1647. <https://doi.org/10.1097/WNR.0b013e328315cd4c>
- Li, Z., Bao, S., Wu, Q., Wang, H., Eyler, C., Sathornsumetee, S., Shi, Q., Cao, Y., Lathia, J., McLendon, R.E., Hjelmeland, A.B., Rich, J.N., 2009. Hypoxia-inducible factors regulate tumorigenic capacity of glioma stem cells. *Cancer Cell* 15, 501–513. <https://doi.org/10.1016/j.ccr.2009.03.018>
- Liu, C., Tu, Y., Yuan, J., Mao, X., He, S., Wang, L., Fu, G., Zong, J., Zhang, Y., 2012. Aberrant expression of N-methylpurine-DNA glycosylase influences patient survival in malignant gliomas. *J. Biomed. Biotechnol.* 2012, 760679. <https://doi.org/10.1155/2012/760679>
- Liu, J.-P., Zeitlin, S.O., 2011. The long and the short of aberrant ciliogenesis in Huntington disease. *J. Clin. Invest.* 121, 4237–4241. <https://doi.org/10.1172/JCI60243>
- Liu, Y.F., Deth, R.C., Devys, D., 1997. SH3 domain-dependent association of huntingtin with epidermal growth factor receptor signaling complexes. *J. Biol. Chem.* 272, 8121–8124. <https://doi.org/10.1074/jbc.272.13.8121>
- Lledo, P.-M., Alonso, M., Grubb, M.S., 2006. Adult neurogenesis and functional plasticity in neuronal circuits. *Nat. Rev. Neurosci.* 7, 179–193. <https://doi.org/10.1038/nrn1867>
- Lo Sardo, V., Zuccato, C., Gaudenzi, G., Vitali, B., Ramos, C., Tartari, M., Myre, M.A., Walker, J.A., Pistocchi, A., Conti, L., Valenza, M., Drung, B., Schmidt, B., Gusella, J., Zeitlin, S., Cotelli, F., Cattaneo, E., 2012. An evolutionary recent neuroepithelial cell adhesion function of huntingtin implicates ADAM10-Ncadherin. *Nat. Neurosci.* 15, 713–721. <https://doi.org/10.1038/nn.3080>
- Lombardi, G., De Salvo, G.L., Brandes, A.A., Eoli, M., Rudà, R., Faedi, M., Lolli, I., Pace, A., Daniele, B., Pasqualetti, F., Rizzato, S., Bellu, L., Pambuku, A., Farina, M., Magni, G., Indraccolo, S., Gardiman, M.P., Soffietti, R., Zagonel, V., 2019. Regorafenib compared with lomustine in patients with relapsed glioblastoma (REGOMA): a multicentre, open-label, randomised, controlled, phase 2 trial. *Lancet Oncol.* 20, 110–119. [https://doi.org/10.1016/S1470-2045\(18\)30675-2](https://doi.org/10.1016/S1470-2045(18)30675-2)
- Lopes, C., Aubert, S., Bourgois-Rocha, F., Barnat, M., Rego, A.C., Déglon, N., Perrier, A.L., Humbert, S., 2016. Dominant-Negative Effects of Adult-Onset Huntingtin Mutations Alter the Division of Human Embryonic Stem Cells-Derived Neural Cells. *PloS One* 11, e0148680. <https://doi.org/10.1371/journal.pone.0148680>
- Louis, D.N., Perry, A., Reifenberger, G., von Deimling, A., Figarella-Branger, D., Cavenee, W.K., Ohgaki, H., Wiestler, O.D., Kleihues, P., Ellison, D.W., 2016. The 2016 World Health Organization Classification of Tumors of the Central Nervous System: a summary. *Acta Neuropathol. (Berl.)* 131, 803–820. <https://doi.org/10.1007/s00401-016-1545-1>
- Lu, X.-H., Mattis, V.B., Wang, N., Al-Ramahi, I., van den Berg, N., Fratantoni, S.A., Waldvogel, H., Greiner, E., Osmand, A., Elzein, K., Xiao, J., Dijkstra, S., de Pril, R., Vinters, H.V., Faull, R., Signer, E., Kwak, S., Marugan, J.J., Botas, J., Fischer, D.F., Svendsen, C.N., Munoz-Sanjuan, I., Yang, X.W., 2014. Targeting ATM ameliorates mutant Huntingtin toxicity in cell and animal models of Huntington's disease. *Sci. Transl. Med.* 6, 268ra178. <https://doi.org/10.1126/scitranslmed.3010523>
- Luo, S., Vacher, C., Davies, J.E., Rubinsztein, D.C., 2005. Cdk5 phosphorylation of huntingtin reduces its cleavage by caspases: implications for mutant huntingtin toxicity. *J. Cell Biol.* 169, 647–656. <https://doi.org/10.1083/jcb.200412071>
- Maiuri, T., Bazan, C.B., Harding, R.J., Begeja, N., Kam, T.-I., Byrne, L.M., Rodrigues, F.B., Warner, M.M., Neuman, K., Mansoor, M., Badiee, M., Dasovich, M., Leung, A.K.L.,

- Andres, S.N., Wild, E.J., Dawson, T.M., Dawson, V.L., Arrowsmith, C.H., Truant, R., 2022. Poly ADP-Ribose Signaling is Dysregulated in Huntington's Disease Patients. <https://doi.org/10.1101/2022.11.23.517669>
- Maiuri, T., Mocle, A.J., Hung, C.L., Xia, J., van Roon-Mom, W.M.C., Truant, R., 2017. Huntingtin is a scaffolding protein in the ATM oxidative DNA damage response complex. *Hum. Mol. Genet.* 26, 395–406. <https://doi.org/10.1093/hmg/ddw395>
- Maiuri, T., Woloshansky, T., Xia, J., Truant, R., 2013. The huntingtin N17 domain is a multifunctional CRM1 and Ran-dependent nuclear and ciliary export signal. *Hum. Mol. Genet.* 22, 1383–1394. <https://doi.org/10.1093/hmg/dds554>
- Marampon, F., Gravina, G.L., Zani, B.M., Popov, V.M., Fratticci, A., Cerasani, M., Di Genova, D., Mancini, M., Ciccarelli, C., Ficorella, C., Di Cesare, E., Festuccia, C., 2014. Hypoxia sustains glioblastoma radioresistance through ERKs/DNA-PKcs/HIF-1 α functional interplay. *Int. J. Oncol.* 44, 2121–2131. <https://doi.org/10.3892/ijo.2014.2358>
- Marchesi, F., Turriziani, M., Tortorelli, G., Avvisati, G., Torino, F., De Vecchis, L., 2007. Triazene compounds: mechanism of action and related DNA repair systems. *Pharmacol. Res.* 56, 275–287. <https://doi.org/10.1016/j.phrs.2007.08.003>
- Marques Sousa, C., Humbert, S., 2013. Huntingtin: here, there, everywhere! *J. Huntingt. Dis.* 2, 395–403. <https://doi.org/10.3233/JHD-130082>
- Martin, D.D.O., Ladha, S., Ehrnhoefer, D.E., Hayden, M.R., 2015. Autophagy in Huntington disease and huntingtin in autophagy. *Trends Neurosci.* 38, 26–35. <https://doi.org/10.1016/j.tins.2014.09.003>
- McColgan, P., Tabrizi, S.J., 2018. Huntington's disease: a clinical review. *Eur. J. Neurol.* 25, 24–34. <https://doi.org/10.1111/ene.13413>
- McFarland, K.N., Huizenga, M.N., Darnell, S.B., Sangrey, G.R., Berezovska, O., Cha, J.-H.J., Outeiro, T.F., Sadri-Vakili, G., 2014. MeCP2: a novel Huntingtin interactor. *Hum. Mol. Genet.* 23, 1036–1044. <https://doi.org/10.1093/hmg/ddt499>
- McKinstry, S.U., Karadeniz, Y.B., Worthington, A.K., Hayrapetyan, V.Y., Ozlu, M.I., Serafin-Molina, K., Risher, W.C., Ustunkaya, T., Dragatsis, I., Zeitlin, S., Yin, H.H., Eroglu, C., 2014. Huntingtin is required for normal excitatory synapse development in cortical and striatal circuits. *J. Neurosci. Off. J. Soc. Neurosci.* 34, 9455–9472. <https://doi.org/10.1523/JNEUROSCI.4699-13.2014>
- Mendell, J.R., Khan, N., Sha, N., Eliopoulos, H., McDonald, C.M., Goemans, N., Mercuri, E., Lowes, L.P., Alfano, L.N., Eteplirsen Study Group, 2021. Comparison of Long-term Ambulatory Function in Patients with Duchenne Muscular Dystrophy Treated with Eteplirsen and Matched Natural History Controls. *J. Neuromuscul. Dis.* 8, 469–479. <https://doi.org/10.3233/JND-200548>
- Meyerson, M., Counter, C.M., Eaton, E.N., Ellisen, L.W., Steiner, P., Caddle, S.D., Ziaugra, L., Beijersbergen, R.L., Davidoff, M.J., Liu, Q., Bacchetti, S., Haber, D.A., Weinberg, R.A., 1997. hEST2, the putative human telomerase catalytic subunit gene, is up-regulated in tumor cells and during immortalization. *Cell* 90, 785–795. [https://doi.org/10.1016/s0092-8674\(00\)80538-3](https://doi.org/10.1016/s0092-8674(00)80538-3)
- Miller, K.D., Ostrom, Q.T., Kruchko, C., Patil, N., Tihan, T., Cioffi, G., Fuchs, H.E., Waite, K.A., Jemal, A., Siegel, R.L., Barnholtz-Sloan, J.S., 2021. Brain and other central nervous system tumor statistics, 2021. *CA. Cancer J. Clin.* 71, 381–406. <https://doi.org/10.3322/caac.21693>
- Ming, G.-L., Song, H., 2011. Adult neurogenesis in the mammalian brain: significant answers and significant questions. *Neuron* 70, 687–702. <https://doi.org/10.1016/j.neuron.2011.05.001>

- Miranda-Gonçalves, V., Bezerra, F., Costa-Almeida, R., Freitas-Cunha, M., Soares, R., Martinho, O., Reis, R.M., Pinheiro, C., Baltazar, F., 2017. Monocarboxylate transporter 1 is a key player in glioma-endothelial cell crosstalk. *Mol. Carcinog.* 56, 2630–2642. <https://doi.org/10.1002/mc.22707>
- Mogilevsky, M., Shimshon, O., Kumar, S., Mogilevsky, A., Keshet, E., Yavin, E., Heyd, F., Karni, R., 2018. Modulation of MKNK2 alternative splicing by splice-switching oligonucleotides as a novel approach for glioblastoma treatment. *Nucleic Acids Res.* 46, 11396–11404. <https://doi.org/10.1093/nar/gky921>
- Molero, A.E., Arteaga-Bracho, E.E., Chen, C.H., Gulinello, M., Winchester, M.L., Pichamoorthy, N., Gokhan, S., Khodakhah, K., Mehler, M.F., 2016. Selective expression of mutant huntingtin during development recapitulates characteristic features of Huntington’s disease. *Proc. Natl. Acad. Sci. U. S. A.* 113, 5736–5741. <https://doi.org/10.1073/pnas.1603871113>
- Molina-Calavita, M., Barnat, M., Elias, S., Aparicio, E., Piel, M., Humbert, S., 2014. Mutant huntingtin affects cortical progenitor cell division and development of the mouse neocortex. *J. Neurosci. Off. J. Soc. Neurosci.* 34, 10034–10040. <https://doi.org/10.1523/JNEUROSCI.0715-14.2014>
- Moreira Sousa, C., McGuire, J.R., Thion, M.S., Gentien, D., de la Grange, P., Tezenas du Montcel, S., Vincent-Salomon, A., Durr, A., Humbert, S., 2013. The Huntington disease protein accelerates breast tumour development and metastasis through ErbB2/HER2 signalling. *EMBO Mol. Med.* 5, 309–325. <https://doi.org/10.1002/emmm.201201546>
- Murnyák, B., Kouhsari, M.C., Hershkovitch, R., Kálmán, B., Marko-Varga, G., Klekner, Á., Hortobágyi, T., 2017. PARP1 expression and its correlation with survival is tumour molecular subtype dependent in glioblastoma. *Oncotarget* 8, 46348–46362. <https://doi.org/10.18632/oncotarget.18013>
- Myers, R.H., 2004. Huntington’s disease genetics. *NeuroRx J. Am. Soc. Exp. Neurother.* 1, 255–262. <https://doi.org/10.1602/neurorx.1.2.255>
- Nasir, J., Floresco, S.B., O’Kusky, J.R., Diewert, V.M., Richman, J.M., Zeisler, J., Borowski, A., Marth, J.D., Phillips, A.G., Hayden, M.R., 1995. Targeted disruption of the Huntington’s disease gene results in embryonic lethality and behavioral and morphological changes in heterozygotes. *Cell* 81, 811–823. [https://doi.org/10.1016/0092-8674\(95\)90542-1](https://doi.org/10.1016/0092-8674(95)90542-1)
- Neveklovská, M., Clabough, E.B.D., Steffan, J.S., Zeitlin, S.O., 2012. Deletion of the huntingtin proline-rich region does not significantly affect normal huntingtin function in mice. *J. Huntingt. Dis.* 1, 71–87. <https://doi.org/10.3233/JHD-2012-120016>
- Nygren, H., Eksborg, S., 2012. Stability of temozolomide in solutions aimed for oral treatment prepared from a commercially available powder for infusion. *Pharm. Methods* 3, 1–3. <https://doi.org/10.4103/2229-4708.97700>
- Obernier, K., Alvarez-Buylla, A., 2019. Neural stem cells: origin, heterogeneity and regulation in the adult mammalian brain. *Dev. Camb. Engl.* 146, dev156059. <https://doi.org/10.1242/dev.156059>
- Obernier, K., Cebrian-Silla, A., Thomson, M., Parraguez, J.I., Anderson, R., Guinto, C., Rodas Rodriguez, J., Garcia-Verdugo, J.-M., Alvarez-Buylla, A., 2018. Adult Neurogenesis Is Sustained by Symmetric Self-Renewal and Differentiation. *Cell Stem Cell* 22, 221–234.e8. <https://doi.org/10.1016/j.stem.2018.01.003>
- Ochaba, J., Lukacsovich, T., Csikos, G., Zheng, S., Margulis, J., Salazar, L., Mao, K., Lau, A.L., Yeung, S.Y., Humbert, S., Saudou, F., Klionsky, D.J., Finkbeiner, S., Zeitlin, S.O., Marsh, J.L., Housman, D.E., Thompson, L.M., Steffan, J.S., 2014. Potential

- function for the Huntingtin protein as a scaffold for selective autophagy. *Proc. Natl. Acad. Sci. U. S. A.* 111, 16889–16894. <https://doi.org/10.1073/pnas.1420103111>
- Ohanian, M., Tari Ashizawa, A., Garcia-Manero, G., Pemmaraju, N., Kadia, T., Jabbour, E., Ravandi, F., Borthakur, G., Andreeff, M., Konopleva, M., Lim, M., Pierce, S., O'Brien, S., Alvarado, Y., Verstovsek, S., Wierda, W., Kantarjian, H., Cortes, J., 2018. Liposomal Grb2 antisense oligodeoxynucleotide (BP1001) in patients with refractory or relapsed haematological malignancies: a single-centre, open-label, dose-escalation, phase 1/1b trial. *Lancet Haematol.* 5, e136–e146. [https://doi.org/10.1016/S2352-3026\(18\)30021-8](https://doi.org/10.1016/S2352-3026(18)30021-8)
- Ohgaki, H., Kleihues, P., 2013. The definition of primary and secondary glioblastoma. *Clin. Cancer Res. Off. J. Am. Assoc. Cancer Res.* 19, 764–772. <https://doi.org/10.1158/1078-0432.CCR-12-3002>
- Opoku-Darko, M., Amuah, J.E., Kelly, J.J.P., 2018. Surgical Resection of Anterior and Posterior Butterfly Glioblastoma. *World Neurosurg.* 110, e612–e620. <https://doi.org/10.1016/j.wneu.2017.11.059>
- Orr, B.A., Clay, M.R., Pinto, E.M., Kesserwan, C., 2020. An update on the central nervous system manifestations of Li-Fraumeni syndrome. *Acta Neuropathol. (Berl.)* 139, 669–687. <https://doi.org/10.1007/s00401-019-02055-3>
- Ostermann, S., Csajka, C., Buclin, T., Leyvraz, S., Lejeune, F., Decosterd, L.A., Stupp, R., 2004. Plasma and cerebrospinal fluid population pharmacokinetics of temozolomide in malignant glioma patients. *Clin. Cancer Res. Off. J. Am. Assoc. Cancer Res.* 10, 3728–3736. <https://doi.org/10.1158/1078-0432.CCR-03-0807>
- Ostrom, Q.T., Patil, N., Cioffi, G., Waite, K., Kruchko, C., Barnholtz-Sloan, J.S., 2020. CBTRUS Statistical Report: Primary Brain and Other Central Nervous System Tumors Diagnosed in the United States in 2013-2017. *Neuro-Oncol.* 22, iv1–iv96. <https://doi.org/10.1093/neuonc/noaa200>
- Pal, A., Severin, F., Lommer, B., Shevchenko, A., Zerial, M., 2006. Huntingtin-HAP40 complex is a novel Rab5 effector that regulates early endosome motility and is up-regulated in Huntington's disease. *J. Cell Biol.* 172, 605–618. <https://doi.org/10.1083/jcb.200509091>
- Palidwor, G.A., Shcherbinin, S., Huska, M.R., Rasko, T., Stelzl, U., Arumughan, A., Foulle, R., Porras, P., Sanchez-Pulido, L., Wanker, E.E., Andrade-Navarro, M.A., 2009. Detection of alpha-rod protein repeats using a neural network and application to huntingtin. *PLoS Comput. Biol.* 5, e1000304. <https://doi.org/10.1371/journal.pcbi.1000304>
- Pan, Y., Daito, T., Sasaki, Y., Chung, Y.H., Xing, X., Pondugula, S., Swamidass, S.J., Wang, T., Kim, A.H., Yano, H., 2016. Inhibition of DNA Methyltransferases Blocks Mutant Huntingtin-Induced Neurotoxicity. *Sci. Rep.* 6, 31022. <https://doi.org/10.1038/srep31022>
- Park, S.H., Kim, M.J., Jung, H.H., Chang, W.S., Choi, H.S., Rachmilevitch, I., Zadicario, E., Chang, J.W., 2020. One-Year Outcome of Multiple Blood-Brain Barrier Disruptions With Temozolomide for the Treatment of Glioblastoma. *Front. Oncol.* 10, 1663. <https://doi.org/10.3389/fonc.2020.01663>
- Passani, L.A., Bedford, M.T., Faber, P.W., McGinnis, K.M., Sharp, A.H., Gusella, J.F., Vonsattel, J.P., MacDonald, M.E., 2000. Huntingtin's WW domain partners in Huntington's disease post-mortem brain fulfill genetic criteria for direct involvement in Huntington's disease pathogenesis. *Hum. Mol. Genet.* 9, 2175–2182. <https://doi.org/10.1093/hmg/9.14.2175>
- Pawson, T., Gish, G.D., 1992. SH2 and SH3 domains: from structure to function. *Cell* 71, 359–362. [https://doi.org/10.1016/0092-8674\(92\)90504-6](https://doi.org/10.1016/0092-8674(92)90504-6)

- Perazzoli, G., Prados, J., Ortiz, R., Caba, O., Cabeza, L., Berdasco, M., González, B., Melguizo, C., 2015. Temozolomide Resistance in Glioblastoma Cell Lines: Implication of MGMT, MMR, P-Glycoprotein and CD133 Expression. *PloS One* 10, e0140131. <https://doi.org/10.1371/journal.pone.0140131>
- Phillips, H.S., Kharbanda, S., Chen, R., Forrest, W.F., Soriano, R.H., Wu, T.D., Misra, A., Nigro, J.M., Colman, H., Soroceanu, L., Williams, P.M., Modrusan, Z., Feuerstein, B.G., Aldape, K., 2006. Molecular subclasses of high-grade glioma predict prognosis, delineate a pattern of disease progression, and resemble stages in neurogenesis. *Cancer Cell* 9, 157–173. <https://doi.org/10.1016/j.ccr.2006.02.019>
- Phillips, J.J., Aranda, D., Ellison, D.W., Judkins, A.R., Croul, S.E., Brat, D.J., Ligon, K.L., Horbinski, C., Venneti, S., Zadeh, G., Santi, M., Zhou, S., Appin, C.L., Sioletic, S., Sullivan, L.M., Martinez-Lage, M., Robinson, A.E., Yong, W.H., Cloughesy, T., Lai, A., Phillips, H.S., Marshall, R., Mueller, S., Haas-Kogan, D.A., Molinaro, A.M., Perry, A., 2013. PDGFRA amplification is common in pediatric and adult high-grade astrocytomas and identifies a poor prognostic group in IDH1 mutant glioblastoma. *Brain Pathol. Zurich Switz.* 23, 565–573. <https://doi.org/10.1111/bpa.12043>
- Pirro, V., Alfaro, C.M., Jarmusch, A.K., Hattab, E.M., Cohen-Gadol, A.A., Cooks, R.G., 2017. Intraoperative assessment of tumor margins during glioma resection by desorption electrospray ionization-mass spectrometry. *Proc. Natl. Acad. Sci. U. S. A.* 114, 6700–6705. <https://doi.org/10.1073/pnas.1706459114>
- Pollard, S.M., Yoshikawa, K., Clarke, I.D., Danovi, D., Stricker, S., Russell, R., Bayani, J., Head, R., Lee, M., Bernstein, M., Squire, J.A., Smith, A., Dirks, P., 2009. Glioma stem cell lines expanded in adherent culture have tumor-specific phenotypes and are suitable for chemical and genetic screens. *Cell Stem Cell* 4, 568–580. <https://doi.org/10.1016/j.stem.2009.03.014>
- Pompos, A., Foote, R.L., Koong, A.C., Le, Q.T., Mohan, R., Paganetti, H., Choy, H., 2022. National Effort to Re-Establish Heavy Ion Cancer Therapy in the United States. *Front. Oncol.* 12, 880712. <https://doi.org/10.3389/fonc.2022.880712>
- Portnow, J., Badie, B., Chen, M., Liu, A., Blanchard, S., Synold, T.W., 2009. The neuropharmacokinetics of temozolomide in patients with resectable brain tumors: potential implications for the current approach to chemoradiation. *Clin. Cancer Res. Off. J. Am. Assoc. Cancer Res.* 15, 7092–7098. <https://doi.org/10.1158/1078-0432.CCR-09-1349>
- Qiao, M.-Y., Cui, H.-T., Zhao, L.-Z., Miao, J.-K., Chen, Q.-X., 2021. Efficacy and Safety of Levetiracetam vs. Phenobarbital for Neonatal Seizures: A Systematic Review and Meta-Analysis. *Front. Neurol.* 12, 747745. <https://doi.org/10.3389/fneur.2021.747745>
- Quan, A.L., Barnett, G.H., Lee, S.-Y., Vogelbaum, M.A., Toms, S.A., Staugaitis, S.M., Prayson, R.A., Peereboom, D.M., Stevens, G.H.J., Cohen, B.H., Suh, J.H., 2005. Epidermal growth factor receptor amplification does not have prognostic significance in patients with glioblastoma multiforme. *Int. J. Radiat. Oncol. Biol. Phys.* 63, 695–703. <https://doi.org/10.1016/j.ijrobp.2005.03.051>
- Rao, D.S., Hyun, T.S., Kumar, P.D., Mizukami, I.F., Rubin, M.A., Lucas, P.C., Sanda, M.G., Ross, T.S., 2002. Huntingtin-interacting protein 1 is overexpressed in prostate and colon cancer and is critical for cellular survival. *J. Clin. Invest.* 110, 351–360. <https://doi.org/10.1172/JCI15529>
- Rasper, M., Schäfer, A., Piontek, G., Teufel, J., Brockhoff, G., Ringel, F., Heindl, S., Zimmer, C., Schlegel, J., 2010. Aldehyde dehydrogenase 1 positive glioblastoma cells show brain tumor stem cell capacity. *Neuro-Oncol.* 12, 1024–1033. <https://doi.org/10.1093/neuonc/noq070>

- Ratovitski, T., Chighladze, E., Arbez, N., Boronina, T., Herbrich, S., Cole, R.N., Ross, C.A., 2012. Huntingtin protein interactions altered by polyglutamine expansion as determined by quantitative proteomic analysis. *Cell Cycle Georget. Tex* 11, 2006–2021. <https://doi.org/10.4161/cc.20423>
- Ravikumar, B., Vacher, C., Berger, Z., Davies, J.E., Luo, S., Oroz, L.G., Scaravilli, F., Easton, D.F., Duden, R., O’Kane, C.J., Rubinsztein, D.C., 2004. Inhibition of mTOR induces autophagy and reduces toxicity of polyglutamine expansions in fly and mouse models of Huntington disease. *Nat. Genet.* 36, 585–595. <https://doi.org/10.1038/ng1362>
- Reiner, A., Dragatsis, I., Zeitlin, S., Goldowitz, D., 2003. Wild-type huntingtin plays a role in brain development and neuronal survival. *Mol. Neurobiol.* 28, 259–276. <https://doi.org/10.1385/MN:28:3:259>
- Relizani, K., Griffith, G., Echevarría, L., Zarrouki, F., Facchinetti, P., Vaillend, C., Leumann, C., Garcia, L., Goyenvalle, A., 2017. Efficacy and Safety Profile of Tricyclo-DNA Antisense Oligonucleotides in Duchenne Muscular Dystrophy Mouse Model. *Mol. Ther. Nucleic Acids* 8, 144–157. <https://doi.org/10.1016/j.omtn.2017.06.013>
- Reuss, D., von Deimling, A., 2009. Hereditary tumor syndromes and gliomas. *Recent Results Cancer Res. Fortschritte Krebsforsch. Progres Dans Rech. Sur Cancer* 171, 83–102. https://doi.org/10.1007/978-3-540-31206-2_5
- Rey, S., Schito, L., Koritzinsky, M., Wouters, B.G., 2017. Molecular targeting of hypoxia in radiotherapy. *Adv. Drug Deliv. Rev.* 109, 45–62. <https://doi.org/10.1016/j.addr.2016.10.002>
- Reynolds, B.A., Weiss, S., 1992. Generation of neurons and astrocytes from isolated cells of the adult mammalian central nervous system. *Science* 255, 1707–1710. <https://doi.org/10.1126/science.1553558>
- Rice, M.A., Ishteiwy, R.A., Magani, F., Udayakumar, T., Reiner, T., Yates, T.J., Miller, P., Perez-Stable, C., Rai, P., Verdun, R., Dykxhoorn, D.M., Burnstein, K.L., 2016. The microRNA-23b/-27b cluster suppresses prostate cancer metastasis via Huntingtin-interacting protein 1-related. *Oncogene* 35, 4752–4761. <https://doi.org/10.1038/onc.2016.6>
- Richichi, C., Osti, D., Del Bene, M., Fornasari, L., Patanè, M., Pollo, B., DiMeco, F., Pelicci, G., 2016. Tumor-initiating cell frequency is relevant for glioblastoma aggressiveness. *Oncotarget* 7, 71491–71503. <https://doi.org/10.18632/oncotarget.11600>
- Rinaldi, C., Wood, M.J.A., 2018. Antisense oligonucleotides: the next frontier for treatment of neurological disorders. *Nat. Rev. Neurol.* 14, 9–21. <https://doi.org/10.1038/nrneurol.2017.148>
- Roberts, T.C., Langer, R., Wood, M.J.A., 2020. Advances in oligonucleotide drug delivery. *Nat. Rev. Drug Discov.* 19, 673–694. <https://doi.org/10.1038/s41573-020-0075-7>
- Rosas, H.D., Salat, D.H., Lee, S.Y., Zaleta, A.K., Hevelone, N., Hersch, S.M., 2008. Complexity and heterogeneity: what drives the ever-changing brain in Huntington’s disease? *Ann. N. Y. Acad. Sci.* 1147, 196–205. <https://doi.org/10.1196/annals.1427.034>
- Rosenberg, T., Aaberg-Jessen, C., Petterson, S.A., Kristensen, B.W., 2018. Heterogenic expression of stem cell markers in patient-derived glioblastoma spheroid cultures exposed to long-term hypoxia. *CNS Oncol.* 7, CNS15. <https://doi.org/10.2217/cns-2017-0034>
- Rubinsztein, D.C., Leggo, J., Coles, R., Almqvist, E., Biancalana, V., Cassiman, J.J., Chotai, K., Connarty, M., Crauford, D., Curtis, A., Curtis, D., Davidson, M.J., Differ, A.M., Dode, C., Dodge, A., Frontali, M., Ranen, N.G., Stine, O.C., Sherr, M., Abbott, M.H., Franz, M.L., Graham, C.A., Harper, P.S., Hedreen, J.C., Hayden, M.R., 1996.

- Phenotypic characterization of individuals with 30-40 CAG repeats in the Huntington disease (HD) gene reveals HD cases with 36 repeats and apparently normal elderly individuals with 36-39 repeats. *Am. J. Hum. Genet.* 59, 16–22.
- Rui, Y.-N., Xu, Z., Patel, B., Chen, Z., Chen, D., Tito, A., David, G., Sun, Y., Stimming, E.F., Bellen, H.J., Cuervo, A.M., Zhang, S., 2015. Huntingtin functions as a scaffold for selective macroautophagy. *Nat. Cell Biol.* 17, 262–275.
<https://doi.org/10.1038/ncb3101>
- Ruzo, A., Ismailoglu, I., Popowski, M., Haremaki, T., Croft, G.F., Deglincerti, A., Brivanlou, A.H., 2015. Discovery of novel isoforms of huntingtin reveals a new hominid-specific exon. *PloS One* 10, e0127687. <https://doi.org/10.1371/journal.pone.0127687>
- Sanai, N., Nguyen, T., Ihrie, R.A., Mirzadeh, Z., Tsai, H.-H., Wong, M., Gupta, N., Berger, M.S., Huang, E., Garcia-Verdugo, J.-M., Rowitch, D.H., Alvarez-Buylla, A., 2011. Corridors of migrating neurons in the human brain and their decline during infancy. *Nature* 478, 382–386. <https://doi.org/10.1038/nature10487>
- Sanai, N., Tramontin, A.D., Quiñones-Hinojosa, A., Barbaro, N.M., Gupta, N., Kunwar, S., Lawton, M.T., McDermott, M.W., Parsa, A.T., Manuel-García Verdugo, J., Berger, M.S., Alvarez-Buylla, A., 2004. Unique astrocyte ribbon in adult human brain contains neural stem cells but lacks chain migration. *Nature* 427, 740–744.
<https://doi.org/10.1038/nature02301>
- Sandrine humbert, frederic saudou, 2016. The biology of huntingtin.
<https://doi.org/10.1016/j.neuron.2016.02.003>
- Sarah J Ross, E.L., n.d. Differential uptake, kinetics and mechanisms of intracellular trafficking of next-generation antisense oligonucleotides across human cancer cell lines. <https://doi.org/10.1093/nar/gkz214>
- Saudou, F., Finkbeiner, S., Devys, D., Greenberg, M.E., 1998. Huntingtin acts in the nucleus to induce apoptosis but death does not correlate with the formation of intranuclear inclusions. *Cell* 95, 55–66. [https://doi.org/10.1016/s0092-8674\(00\)81782-1](https://doi.org/10.1016/s0092-8674(00)81782-1)
- Saudou, F., Humbert, S., 2016a. The Biology of Huntingtin. *Neuron* 89, 910–926.
<https://doi.org/10.1016/j.neuron.2016.02.003>
- Saudou, F., Humbert, S., 2016b. The Biology of Huntingtin. *Neuron* 89, 910–926.
<https://doi.org/10.1016/j.neuron.2016.02.003>
- Scheer, M., Leisz, S., Sorge, E., Storozhuk, O., Prell, J., Ho, I., Harder, A., 2021. Neurofibromatosis Type 1 Gene Alterations Define Specific Features of a Subset of Glioblastomas. *Int. J. Mol. Sci.* 23, 352. <https://doi.org/10.3390/ijms23010352>
- Scherer, H.J., 1940. A CRITICAL REVIEW: THE PATHOLOGY OF CEREBRAL GLIOMAS. *J. Neurol. Psychiatry* 3, 147–177. <https://doi.org/10.1136/jnnp.3.2.147>
- Schilling, B., Gafni, J., Torcassi, C., Cong, X., Row, R.H., LaFevre-Bernt, M.A., Cusack, M.P., Ratovitski, T., Hirschhorn, R., Ross, C.A., Gibson, B.W., Ellerby, L.M., 2006. Huntingtin phosphorylation sites mapped by mass spectrometry. Modulation of cleavage and toxicity. *J. Biol. Chem.* 281, 23686–23697.
<https://doi.org/10.1074/jbc.M513507200>
- Schüz, J., Pirie, K., Reeves, G.K., Floud, S., Beral, V., 2022. Response to Moskowitz and Birnbaum, Taylor, Baldwin, et al. *J. Natl. Cancer Inst.* 114, 1555–1556.
<https://doi.org/10.1093/jnci/djac111>
- Seervai, R.N.H., Jangid, R.K., Karki, M., Tripathi, D.N., Jung, S.Y., Kearns, S.E., Verhey, K.J., Cianfrocco, M.A., Millis, B.A., Tyska, M.J., Mason, F.M., Rathmell, W.K., Park, I.Y., Dere, R., Walker, C.L., 2020. The Huntingtin-interacting protein SETD2/HYPB is an actin lysine methyltransferase. *Sci. Adv.* 6, eabb7854.
<https://doi.org/10.1126/sciadv.abb7854>

- Seong, I.S., Woda, J.M., Song, J.-J., Lloret, A., Abeyrathne, P.D., Woo, C.J., Gregory, G., Lee, J.-M., Wheeler, V.C., Walz, T., Kingston, R.E., Gusella, J.F., Conlon, R.A., MacDonald, M.E., 2010. Huntingtin facilitates polycomb repressive complex 2. *Hum. Mol. Genet.* 19, 573–583. <https://doi.org/10.1093/hmg/ddp524>
- Shen, M., Xie, S., Rowicki, M., Michel, S., Wei, Y., Hang, X., Wan, L., Lu, X., Yuan, M., Jin, J.F., Jaschinski, F., Zhou, T., Klar, R., Kang, Y., 2021. Therapeutic Targeting of Metadherin Suppresses Colorectal and Lung Cancer Progression and Metastasis. *Cancer Res.* 81, 1014–1025. <https://doi.org/10.1158/0008-5472.CAN-20-1876>
- Shirasaki, D.I., Greiner, E.R., Al-Ramahi, I., Gray, M., Boonthueung, P., Geschwind, D.H., Botas, J., Coppola, G., Horvath, S., Loo, J.A., Yang, X.W., 2012. Network organization of the huntingtin proteomic interactome in mammalian brain. *Neuron* 75, 41–57. <https://doi.org/10.1016/j.neuron.2012.05.024>
- Siddiqui, A., Rivera-Sánchez, S., Castro, M. del R., Acevedo-Torres, K., Rane, A., Torres-Ramos, C.A., Nicholls, D.G., Andersen, J.K., Ayala-Torres, S., 2012. Mitochondrial DNA damage is associated with reduced mitochondrial bioenergetics in Huntington’s disease. *Free Radic. Biol. Med.* 53, 1478–1488. <https://doi.org/10.1016/j.freeradbiomed.2012.06.008>
- Silva, A.C., Ferreira, I.L., Hayden, M.R., Ferreira, E., Rego, A.C., 2018. Characterization of subventricular zone-derived progenitor cells from mild and late symptomatic YAC128 mouse model of Huntington’s disease. *Biochim. Biophys. Acta Mol. Basis Dis.* 1864, 34–44. <https://doi.org/10.1016/j.bbadis.2017.09.009>
- Simeone, P., Trerotola, M., Urbanella, A., Lattanzio, R., Ciavardelli, D., Di Giuseppe, F., Eleuterio, E., Sulpizio, M., Eusebi, V., Pession, A., Piantelli, M., Alberti, S., 2014. A unique four-hub protein cluster associates to glioblastoma progression. *PloS One* 9, e103030. <https://doi.org/10.1371/journal.pone.0103030>
- Singh, S.K., Hawkins, C., Clarke, I.D., Squire, J.A., Bayani, J., Hide, T., Henkelman, R.M., Cusimano, M.D., Dirks, P.B., 2004. Identification of human brain tumour initiating cells. *Nature* 432, 396–401. <https://doi.org/10.1038/nature03128>
- Soeda, A., Park, M., Lee, D., Mintz, A., Androutsellis-Theotokis, A., McKay, R.D., Engh, J., Iwama, T., Kunisada, T., Kassam, A.B., Pollack, I.F., Park, D.M., 2009. Hypoxia promotes expansion of the CD133-positive glioma stem cells through activation of HIF-1 α . *Oncogene* 28, 3949–3959. <https://doi.org/10.1038/onc.2009.252>
- Son, M.J., Woolard, K., Nam, D.-H., Lee, J., Fine, H.A., 2009. SSEA-1 is an enrichment marker for tumor-initiating cells in human glioblastoma. *Cell Stem Cell* 4, 440–452. <https://doi.org/10.1016/j.stem.2009.03.003>
- Song, Z., Pan, Y., Ling, G., Wang, S., Huang, M., Jiang, X., Ke, Y., 2017. Escape of U251 glioma cells from temozolomide-induced senescence was modulated by CDK1/survivin signaling. *Am. J. Transl. Res.* 9, 2163–2180.
- SongTao, Q., Lei, Y., Si, G., YanQing, D., HuiXia, H., XueLin, Z., LanXiao, W., Fei, Y., 2012. IDH mutations predict longer survival and response to temozolomide in secondary glioblastoma. *Cancer Sci.* 103, 269–273. <https://doi.org/10.1111/j.1349-7006.2011.02134.x>
- Southwell, A.L., Kordasiewicz, H.B., Langbehn, D., Skotte, N.H., Parsons, M.P., Villanueva, E.B., Caron, N.S., Østergaard, M.E., Anderson, L.M., Xie, Y., Cengio, L.D., Findlay-Black, H., Doty, C.N., Fittsimmons, B., Swayze, E.E., Seth, P.P., Raymond, L.A., Frank Bennett, C., Hayden, M.R., 2018. Huntingtin suppression restores cognitive function in a mouse model of Huntington’s disease. *Sci. Transl. Med.* 10, eaar3959. <https://doi.org/10.1126/scitranslmed.aa3959>
- Southwell, A.L., Skotte, N.H., Kordasiewicz, H.B., Østergaard, M.E., Watt, A.T., Carroll, J.B., Doty, C.N., Villanueva, E.B., Petoukhov, E., Vaid, K., Xie, Y., Freier, S.M.,

- Swayze, E.E., Seth, P.P., Bennett, C.F., Hayden, M.R., 2014. In vivo evaluation of candidate allele-specific mutant huntingtin gene silencing antisense oligonucleotides. *Mol. Ther. J. Am. Soc. Gene Ther.* 22, 2093–2106. <https://doi.org/10.1038/mt.2014.153>
- Steffan, J.S., Agrawal, N., Pallos, J., Rockabrand, E., Trotman, L.C., Slepko, N., Illes, K., Lukacsovich, T., Zhu, Y.-Z., Cattaneo, E., Pandolfi, P.P., Thompson, L.M., Marsh, J.L., 2004. SUMO modification of Huntingtin and Huntington's disease pathology. *Science* 304, 100–104. <https://doi.org/10.1126/science.1092194>
- Stoyanov, G.S., Dzhankov, D.L., 2018. On the Concepts and History of Glioblastoma Multiforme - Morphology, Genetics and Epigenetics. *Folia Med. (Plovdiv)* 60, 48–66. <https://doi.org/10.1515/folmed-2017-0069>
- Strobel, H., Baisch, T., Fitzel, R., Schilberg, K., Siegelin, M.D., Karpel-Massler, G., Debatin, K.-M., Westhoff, M.-A., 2019. Temozolomide and Other Alkylating Agents in Glioblastoma Therapy. *Biomedicines* 7, 69. <https://doi.org/10.3390/biomedicines7030069>
- Stupp, R., Hegi, M.E., Mason, W.P., van den Bent, M.J., Taphoorn, M.J.B., Janzer, R.C., Ludwin, S.K., Allgeier, A., Fisher, B., Belanger, K., Hau, P., Brandes, A.A., Gijtenbeek, J., Marosi, C., Vecht, C.J., Mokhtari, K., Wesseling, P., Villa, S., Eisenhauer, E., Gorlia, T., Weller, M., Lacombe, D., Cairncross, J.G., Mirimanoff, R.-O., European Organisation for Research and Treatment of Cancer Brain Tumour and Radiation Oncology Groups, National Cancer Institute of Canada Clinical Trials Group, 2009. Effects of radiotherapy with concomitant and adjuvant temozolomide versus radiotherapy alone on survival in glioblastoma in a randomised phase III study: 5-year analysis of the EORTC-NCIC trial. *Lancet Oncol.* 10, 459–466. [https://doi.org/10.1016/S1470-2045\(09\)70025-7](https://doi.org/10.1016/S1470-2045(09)70025-7)
- Stupp, R., Mason, W.P., van den Bent, M.J., Weller, M., Fisher, B., Taphoorn, M.J.B., Belanger, K., Brandes, A.A., Marosi, C., Bogdahn, U., Curschmann, J., Janzer, R.C., Ludwin, S.K., Gorlia, T., Allgeier, A., Lacombe, D., Cairncross, J.G., Eisenhauer, E., Mirimanoff, R.O., European Organisation for Research and Treatment of Cancer Brain Tumor and Radiotherapy Groups, National Cancer Institute of Canada Clinical Trials Group, 2005. Radiotherapy plus concomitant and adjuvant temozolomide for glioblastoma. *N. Engl. J. Med.* 352, 987–996. <https://doi.org/10.1056/NEJMoa043330>
- Stupp, R., Taillibert, S., Kanner, A., Read, W., Steinberg, D., Lhermitte, B., Toms, S., Idbaih, A., Ahluwalia, M.S., Fink, K., Di Meo, F., Lieberman, F., Zhu, J.-J., Stragliotto, G., Tran, D., Brem, S., Hottinger, A., Kirson, E.D., Lavy-Shahaf, G., Weinberg, U., Kim, C.-Y., Paek, S.-H., Nicholas, G., Bruna, J., Hirte, H., Weller, M., Palti, Y., Hegi, M.E., Ram, Z., 2017. Effect of Tumor-Treating Fields Plus Maintenance Temozolomide vs Maintenance Temozolomide Alone on Survival in Patients With Glioblastoma: A Randomized Clinical Trial. *JAMA* 318, 2306–2316. <https://doi.org/10.1001/jama.2017.18718>
- Tabrizi, S.J., Langbehn, D.R., Leavitt, B.R., Roos, R.A., Durr, A., Craufurd, D., Kennard, C., Hicks, S.L., Fox, N.C., Scahill, R.I., Borowsky, B., Tobin, A.J., Rosas, H.D., Johnson, H., Reilmann, R., Landwehrmeyer, B., Stout, J.C., TRACK-HD investigators, 2009. Biological and clinical manifestations of Huntington's disease in the longitudinal TRACK-HD study: cross-sectional analysis of baseline data. *Lancet Neurol.* 8, 791–801. [https://doi.org/10.1016/S1474-4422\(09\)70170-X](https://doi.org/10.1016/S1474-4422(09)70170-X)
- Tabrizi, S.J., Leavitt, B.R., Landwehrmeyer, G.B., Wild, E.J., Saft, C., Barker, R.A., Blair, N.F., Craufurd, D., Priller, J., Rickards, H., Rosser, A., Kordasiewicz, H.B., Czech, C., Swayze, E.E., Norris, D.A., Baumann, T., Gerlach, I., Schobel, S.A., Paz, E., Smith, A.V., Bennett, C.F., Lane, R.M., Phase 1–2a IONIS-HTTRx Study Site Teams, 2019.

- Targeting Huntingtin Expression in Patients with Huntington's Disease. *N. Engl. J. Med.* 380, 2307–2316. <https://doi.org/10.1056/NEJMoa1900907>
- Tabrizi, S.J., Schobel, S., Gantman, E.C., Mansbach, A., Borowsky, B., Konstantinova, P., Mestre, T.A., Panagoulas, J., Ross, C.A., Zauderer, M., Mullin, A.P., Romero, K., Sivakumaran, S., Turner, E.C., Long, J.D., Sampaio, C., Huntington's Disease Regulatory Science Consortium (HD-RSC), 2022. A biological classification of Huntington's disease: the Integrated Staging System. *Lancet Neurol.* 21, 632–644. [https://doi.org/10.1016/S1474-4422\(22\)00120-X](https://doi.org/10.1016/S1474-4422(22)00120-X)
- Tamimi, A.F., Juweid, M., 2017. Epidemiology and Outcome of Glioblastoma, in: De Vleeschouwer, S. (Ed.), *Glioblastoma*. Codon Publications, Brisbane (AU).
- Tebbenkamp, A.T.N., Crosby, K.W., Siemienski, Z.B., Brown, H.H., Golde, T.E., Borchelt, D.R., 2012. Analysis of proteolytic processes and enzymatic activities in the generation of huntingtin n-terminal fragments in an HEK293 cell model. *PLoS One* 7, e50750. <https://doi.org/10.1371/journal.pone.0050750>
- Thion, M.S., Humbert, S., 2018. Cancer: From Wild-Type to Mutant Huntingtin. *J. Huntingt. Dis.* 7, 201–208. <https://doi.org/10.3233/JHD-180290>
- Thion, M.S., McGuire, J.R., Sousa, C.M., Fuhrmann, L., Fitamant, J., Leboucher, S., Vacher, S., du Montcel, S.T., Bièche, I., Bernet, A., Mehlen, P., Vincent-Salomon, A., Humbert, S., 2015. Unraveling the Role of Huntingtin in Breast Cancer Metastasis. *J. Natl. Cancer Inst.* 107, djv208. <https://doi.org/10.1093/jnci/djv208>
- Thion, M.S., Tézenas du Montcel, S., Golmard, J.-L., Vacher, S., Barjhoux, L., Sornin, V., Cazeneuve, C., Bièche, I., Sinilnikova, O., Stoppa-Lyonnet, D., Durr, A., Humbert, S., 2016. CAG repeat size in Huntingtin alleles is associated with cancer prognosis. *Eur. J. Hum. Genet. EJHG* 24, 1310–1315. <https://doi.org/10.1038/ejhg.2016.13>
- Tong, Y., Ha, T.J., Liu, L., Nishimoto, A., Reiner, A., Goldowitz, D., 2011. Spatial and temporal requirements for huntingtin (Htt) in neuronal migration and survival during brain development. *J. Neurosci. Off. J. Soc. Neurosci.* 31, 14794–14799. <https://doi.org/10.1523/JNEUROSCI.2774-11.2011>
- Tourette, C., Li, B., Bell, R., O'Hare, S., Kaltenbach, L.S., Mooney, S.D., Hughes, R.E., 2014. A large scale Huntingtin protein interaction network implicates Rho GTPase signaling pathways in Huntington disease. *J. Biol. Chem.* 289, 6709–6726. <https://doi.org/10.1074/jbc.M113.523696>
- Turcan, S., Rohle, D., Goenka, A., Walsh, L.A., Fang, F., Yilmaz, E., Campos, C., Fabius, A.W.M., Lu, C., Ward, P.S., Thompson, C.B., Kaufman, A., Guryanova, O., Levine, R., Heguy, A., Viale, A., Morris, L.G.T., Huse, J.T., Mellinghoff, I.K., Chan, T.A., 2012. IDH1 mutation is sufficient to establish the glioma hypermethylator phenotype. *Nature* 483, 479–483. <https://doi.org/10.1038/nature10866>
- Uckun, F.M., Qazi, S., Hwang, L., Trieu, V.N., 2019. Recurrent or Refractory High-Grade Gliomas Treated by Convection-Enhanced Delivery of a TGFβ2-Targeting RNA Therapeutic: A Post-Hoc Analysis with Long-Term Follow-Up. *Cancers* 11, 1892. <https://doi.org/10.3390/cancers11121892>
- Uhrbom, L., Dai, C., Celestino, J.C., Rosenblum, M.K., Fuller, G.N., Holland, E.C., 2002. Ink4a-Arf loss cooperates with KRas activation in astrocytes and neural progenitors to generate glioblastomas of various morphologies depending on activated Akt. *Cancer Res.* 62, 5551–5558.
- Unified Huntington's Disease Rating Scale: reliability and consistency. Huntington Study Group, 1996. *Mov. Disord. Off. J. Mov. Disord. Soc.* 11, 136–142. <https://doi.org/10.1002/mds.870110204>
- Unmack Larsen, I., Vinther-Jensen, T., Gade, A., Nielsen, J.E., Vogel, A., 2015. Assessing impairment of executive function and psychomotor speed in premanifest and manifest

- Huntington's disease gene-expansion carriers. *J. Int. Neuropsychol. Soc. JINS* 21, 193–202. <https://doi.org/10.1017/S1355617715000090>
- Valdor, R., García-Bernal, D., Bueno, C., Ródenas, M., Moraleda, J.M., Macian, F., Martínez, S., 2017. Glioblastoma progression is assisted by induction of immunosuppressive function of pericytes through interaction with tumor cells. *Oncotarget* 8, 68614–68626. <https://doi.org/10.18632/oncotarget.19804>
- Vanderburg, D.G., Batar, E., Fogel, I., Kremer, C.M.E., 2009. A pooled analysis of suicidality in double-blind, placebo-controlled studies of sertraline in adults. *J. Clin. Psychiatry* 70, 674–683. <https://doi.org/10.4088/jcp.07m04004>
- Verhaak, R.G.W., Hoadley, K.A., Purdom, E., Wang, V., Qi, Y., Wilkerson, M.D., Miller, C.R., Ding, L., Golub, T., Mesirov, J.P., Alexe, G., Lawrence, M., O'Kelly, M., Tamayo, P., Weir, B.A., Gabriel, S., Winckler, W., Gupta, S., Jakkula, L., Feiler, H.S., Hodgson, J.G., James, C.D., Sarkaria, J.N., Brennan, C., Kahn, A., Spellman, P.T., Wilson, R.K., Speed, T.P., Gray, J.W., Meyerson, M., Getz, G., Perou, C.M., Hayes, D.N., Cancer Genome Atlas Research Network, 2010. Integrated genomic analysis identifies clinically relevant subtypes of glioblastoma characterized by abnormalities in PDGFRA, IDH1, EGFR, and NF1. *Cancer Cell* 17, 98–110. <https://doi.org/10.1016/j.ccr.2009.12.020>
- Vescovi, A.L., Galli, R., Reynolds, B.A., 2006. Brain tumour stem cells. *Nat. Rev. Cancer* 6, 425–436. <https://doi.org/10.1038/nrc1889>
- Vijayvargia, R., Epand, R., Leitner, A., Jung, T.-Y., Shin, B., Jung, R., Lloret, A., Singh Atwal, R., Lee, H., Lee, J.-M., Aebersold, R., Hebert, H., Song, J.-J., Seong, I.S., 2016. Huntingtin's spherical solenoid structure enables polyglutamine tract-dependent modulation of its structure and function. *eLife* 5, e11184. <https://doi.org/10.7554/eLife.11184>
- Virlogeux, A., Moutaux, E., Christaller, W., Genoux, A., Bruyère, J., Fino, E., Charlot, B., Cazorla, M., Saudou, F., 2018. Reconstituting Corticostriatal Network on-a-Chip Reveals the Contribution of the Presynaptic Compartment to Huntington's Disease. *Cell Rep.* 22, 110–122. <https://doi.org/10.1016/j.celrep.2017.12.013>
- Virrey, J.J., Dong, D., Stiles, C., Patterson, J.B., Pen, L., Ni, M., Schönthal, A.H., Chen, T.C., Hofman, F.M., Lee, A.S., 2008. Stress chaperone GRP78/BiP confers chemoresistance to tumor-associated endothelial cells. *Mol. Cancer Res. MCR* 6, 1268–1275. <https://doi.org/10.1158/1541-7786.MCR-08-0060>
- Vitet, H., Brandt, V., Saudou, F., 2020. Traffic signaling: new functions of huntingtin and axonal transport in neurological disease. *Curr. Opin. Neurobiol.* 63, 122–130. <https://doi.org/10.1016/j.conb.2020.04.001>
- Vonsattel, J.P., DiFiglia, M., 1998. Huntington disease. *J. Neuropathol. Exp. Neurol.* 57, 369–384. <https://doi.org/10.1097/00005072-199805000-00001>
- Wang, J.Y.J., Edelmann, W., 2006. Mismatch repair proteins as sensors of alkylation DNA damage. *Cancer Cell* 9, 417–418. <https://doi.org/10.1016/j.ccr.2006.05.013>
- Wang, S., Allen, N., Vickers, T.A., Revenko, A.S., Sun, H., Liang, X.-H., Crooke, S.T., 2018. Cellular uptake mediated by epidermal growth factor receptor facilitates the intracellular activity of phosphorothioate-modified antisense oligonucleotides. *Nucleic Acids Res.* 46, 3579–3594. <https://doi.org/10.1093/nar/gky145>
- Warby, S.C., Doty, C.N., Graham, R.K., Carroll, J.B., Yang, Y.-Z., Singaraja, R.R., Overall, C.M., Hayden, M.R., 2008. Activated caspase-6 and caspase-6-cleaved fragments of huntingtin specifically colocalize in the nucleus. *Hum. Mol. Genet.* 17, 2390–2404. <https://doi.org/10.1093/hmg/ddn139>

- Watkin, E.E., Arbez, N., Waldron-Roby, E., O’Meally, R., Ratovitski, T., Cole, R.N., Ross, C.A., 2014. Phosphorylation of mutant huntingtin at serine 116 modulates neuronal toxicity. *PLoS One* 9, e88284. <https://doi.org/10.1371/journal.pone.0088284>
- Weiss, S., Dunne, C., Hewson, J., Wohl, C., Wheatley, M., Peterson, A.C., Reynolds, B.A., 1996. Multipotent CNS stem cells are present in the adult mammalian spinal cord and ventricular neuroaxis. *J. Neurosci. Off. J. Soc. Neurosci.* 16, 7599–7609. <https://doi.org/10.1523/JNEUROSCI.16-23-07599.1996>
- Weller, M., Le Rhun, E., 2020. How did lomustine become standard of care in recurrent glioblastoma? *Cancer Treat. Rev.* 87, 102029. <https://doi.org/10.1016/j.ctrv.2020.102029>
- Wellington, C.L., Ellerby, L.M., Gutekunst, C.-A., Rogers, D., Warby, S., Graham, R.K., Loubser, O., van Raamsdonk, J., Singaraja, R., Yang, Y.-Z., Gafni, J., Bredesen, D., Hersch, S.M., Leavitt, B.R., Roy, S., Nicholson, D.W., Hayden, M.R., 2002. Caspase cleavage of mutant huntingtin precedes neurodegeneration in Huntington’s disease. *J. Neurosci. Off. J. Soc. Neurosci.* 22, 7862–7872. <https://doi.org/10.1523/JNEUROSCI.22-18-07862.2002>
- Wiatr, K., Szlachcic, W.J., Trzeciak, M., Figlerowicz, M., Figiel, M., 2018. Huntington Disease as a Neurodevelopmental Disorder and Early Signs of the Disease in Stem Cells. *Mol. Neurobiol.* 55, 3351–3371. <https://doi.org/10.1007/s12035-017-0477-7>
- Woda, J.M., Calzonetti, T., Hilditch-Maguire, P., Duyao, M.P., Conlon, R.A., MacDonald, M.E., 2005. Inactivation of the Huntington’s disease gene (*Hdh*) impairs anterior streak formation and early patterning of the mouse embryo. *BMC Dev. Biol.* 5, 17. <https://doi.org/10.1186/1471-213X-5-17>
- Xiao, Z.-Z., Wang, Z.-F., Lan, T., Huang, W.-H., Zhao, Y.-H., Ma, C., Li, Z.-Q., 2020. Carmustine as a Supplementary Therapeutic Option for Glioblastoma: A Systematic Review and Meta-Analysis. *Front. Neurol.* 11, 1036. <https://doi.org/10.3389/fneur.2020.01036>
- Yi, J., Wang, L., Hu, G.-S., Zhang, Y.-Y., Du, J., Ding, J.-C., Ji, X., Shen, H.-F., Huang, H.-H., Ye, F., Liu, W., 2023. CircPVT1 promotes ER-positive breast tumorigenesis and drug resistance by targeting *ESR1* and *MAVS*. *EMBO J.* 42, e112408. <https://doi.org/10.15252/embj.2022112408>
- Yip, S., Miao, J., Cahill, D.P., Iafrate, A.J., Aldape, K., Nutt, C.L., Louis, D.N., 2009. *MSH6* mutations arise in glioblastomas during temozolomide therapy and mediate temozolomide resistance. *Clin. Cancer Res. Off. J. Am. Assoc. Cancer Res.* 15, 4622–4629. <https://doi.org/10.1158/1078-0432.CCR-08-3012>
- Yuan, H., Han, Y., Wang, Xuege, Li, N., Liu, Q., Yin, Y., Wang, H., Pan, L., Li, L., Song, K., Qiu, T., Pan, Q., Chen, Q., Zhang, G., Zang, Y., Tan, M., Zhang, J., Li, Q., Wang, Xiaoming, Jiang, J., Qin, J., 2020. *SETD2* Restricts Prostate Cancer Metastasis by Integrating *EZH2* and *AMPK* Signaling Pathways. *Cancer Cell* 38, 350-365.e7. <https://doi.org/10.1016/j.ccell.2020.05.022>
- Yuan, X., Curtin, J., Xiong, Y., Liu, G., Waschmann-Hogiu, S., Farkas, D.L., Black, K.L., Yu, J.S., 2004. Isolation of cancer stem cells from adult glioblastoma multiforme. *Oncogene* 23, 9392–9400. <https://doi.org/10.1038/sj.onc.1208311>
- Zannini, L., Delia, D., Buscemi, G., 2014. *CHK2* kinase in the DNA damage response and beyond. *J. Mol. Cell Biol.* 6, 442–457. <https://doi.org/10.1093/jmcb/mju045>
- Zeitlin, S., Liu, J.P., Chapman, D.L., Papaioannou, V.E., Efstratiadis, A., 1995. Increased apoptosis and early embryonic lethality in mice nullizygous for the Huntington’s disease gene homologue. *Nat. Genet.* 11, 155–163. <https://doi.org/10.1038/ng1095-155>

- Zhang, D., Wu, B., Wang, P., Wang, Y., Lu, P., Nechiporuk, T., Floss, T., Grealley, J.M., Zheng, D., Zhou, B., 2017. Non-CpG methylation by DNMT3B facilitates REST binding and gene silencing in developing mouse hearts. *Nucleic Acids Res.* 45, 3102–3115. <https://doi.org/10.1093/nar/gkw1258>
- Zhang, H., Tang, J., Li, C., Kong, J., Wang, J., Wu, Y., Xu, E., Lai, M., 2015. MiR-22 regulates 5-FU sensitivity by inhibiting autophagy and promoting apoptosis in colorectal cancer cells. *Cancer Lett.* 356, 781–790. <https://doi.org/10.1016/j.canlet.2014.10.029>
- Zhang, Q., Yang, L., Liu, Y.H., Wilkinson, J.E., Krainer, A.R., 2023. Antisense oligonucleotide therapy for H3.3K27M diffuse midline glioma. *Sci. Transl. Med.* 15, eadd8280. <https://doi.org/10.1126/scitranslmed.add8280>
- Zhao, J.C., Saleh, A., Crooke, S.T., 2023. SIDT2 Inhibits Phosphorothioate Antisense Oligonucleotide Activity by Regulating Cellular Localization of Lysosomes. *Nucleic Acid Ther.* 33, 108–116. <https://doi.org/10.1089/nat.2022.0055>
- Zhao, Y., Zurawel, A.A., Jenkins, N.P., Duennwald, M.L., Cheng, C., Kettenbach, A.N., Supattapone, S., 2018. Comparative Analysis of Mutant Huntingtin Binding Partners in Yeast Species. *Sci. Rep.* 8, 9554. <https://doi.org/10.1038/s41598-018-27900-5>
- Zheng, S., Clabough, E.B.D., Sarkar, S., Futter, M., Rubinsztein, D.C., Zeitlin, S.O., 2010. Deletion of the huntingtin polyglutamine stretch enhances neuronal autophagy and longevity in mice. *PLoS Genet.* 6, e1000838. <https://doi.org/10.1371/journal.pgen.1000838>
- Zuccato, C., Tartari, M., Crotti, A., Goffredo, D., Valenza, M., Conti, L., Cataudella, T., Leavitt, B.R., Hayden, M.R., Timmusk, T., Rigamonti, D., Cattaneo, E., 2003. Huntingtin interacts with REST/NRSF to modulate the transcription of NRSE-controlled neuronal genes. *Nat. Genet.* 35, 76–83. <https://doi.org/10.1038/ng1219>